Surveillance of novel infectious diseases: from the development of diagnostic methods to biological-based statistical and mathematical modelling of SARS CoV-2

Kumulative Habilitationsschrift

vorgelegt von

Dr. rer. nat. Noemi Castelletti

(2024)

Diese Arbeit ist meinem Mann Klemens und meiner Familie gewidmet.

Table of Contents

I

Summary of the habilitation project

Surveillance of novel infectious diseases: from the development of diagnostic methods to biological-based statistical and mathematical modelling of SARS-CoV-2

Table of contents

Surveillance of novel infectious diseases: from the development of diagnostic methods to biological-based statistical and mathematical modelling of SARS-CoV-2

This habilitation project delineates the strategy employed by the Division of Infectious Diseases and Tropical Medicine to monitor the emergence of the novel infectious disease, SARS-CoV-2. The project encompasses the evolution of innovative diagnostic techniques and their utilization in antibody surveillance within a prospective cohort representative of Munich. This endeavour has also led to the establishment of a novel data analysis unit. Furthermore, an overview of ongoing projects and areas of analysis currently being pursued within the data analysis unit will be provided in the outlook session.

1. Introduction

Starting point: the spread of the novel infectious disease SARS-CoV-2

The novel coronavirus disease (COVID-19) was initially identified in December 2019 in Wuhan, China. Since then, it has rapidly spread across the globe and was declared a global emergency by the World Health Organization (WHO) in early 2020 [1]. The first case of COVID-19 in Germany was confirmed in January 2020 at our institute, the Division of Infectious Diseases and Tropical Medicine, LMU University Hospital Munich [2, 3]. Despite implementing contact tracing and isolating affected individuals to break the chain of transmission, the virus managed to spread to 13 out of 16 federal states within a month due to German tourists returning from high-risk areas in northern Italy and a carnival celebration in the district of Heinsberg (located 60 km west of Cologne) [4].

With concerns that healthcare systems would become overwhelmed and potentially collapse, and due to the absence of vaccines and specific treatment options, the German government implemented public health measures. These measures included isolating confirmed patients, placing their contacts in quarantine, using personal protective equipment, practicing social distancing (which involved closing schools), and closure of the country's borders [5, 6]. However, although these actions were aimed at saving lives, it was anticipated that social distancing measures could have a severe impact on both national and global economies, healthcare systems, individuals' and families' incomes (especially those in precarious employment situations), education (particularly affecting disadvantaged groups), and the overall psychological and social well-being of the population [7, 8].

In early 2020, when the pandemic began, we encountered a challenge regarding the accurate determination of the number of confirmed cases. This was because it relied on factors such as access to healthcare, availability of laboratory testing, and the criteria used to select individuals for testing. As a result, estimating the basic and effective reproduction numbers became a rough approximation, and confirming hospitalization and mortality rates remained pending. During that period, it was already recognized that individuals infected with SARS-CoV-2, even if asymptomatic or with mild symptoms, could transmit the disease. However, quantifying the magnitude of the infection was not feasible [4, 9-11].

In order to monitor and manage the spread of the epidemic in Munich, our institute made the decision to establish the prospective COVID-19 cohort Munich, called KoCo19. Community cohorts are more effective in assessing the overall infection spread within the population. By doing so, we can obtain more accurate estimates of the basic and effective reproduction numbers, evaluate the impact on the healthcare system, and measure the effectiveness of public health interventions [11].

Outline of the habilitation project

The objective of this habilitation project is to provide a comprehensive overview of the analytical process delineated at the Division of Infectious Diseases and Tropical Medicine in monitoring the emergence and spread of the novel infectious disease, SARS-CoV-2. I joined the institute after the conception of the analysed cohort, but became the principal statistician afterwards. In the materials presented here, I was responsible for managing the entire data flow process, from the laboratory to the data analysts. Furthermore, I performed the analysis of laboratory-related publications, and later on also the conduction/coordination of epidemiological analyses. Given the substantial scope of the project, it involved collaboration with multiple partners from the Helmholtz Center Munich, the University of Bonn, and the University of Bielefeld. I coordinated both the formal and scientific collaboration among these institutions. A visual representation of the project's activities is illustrated in **Figure 1**.
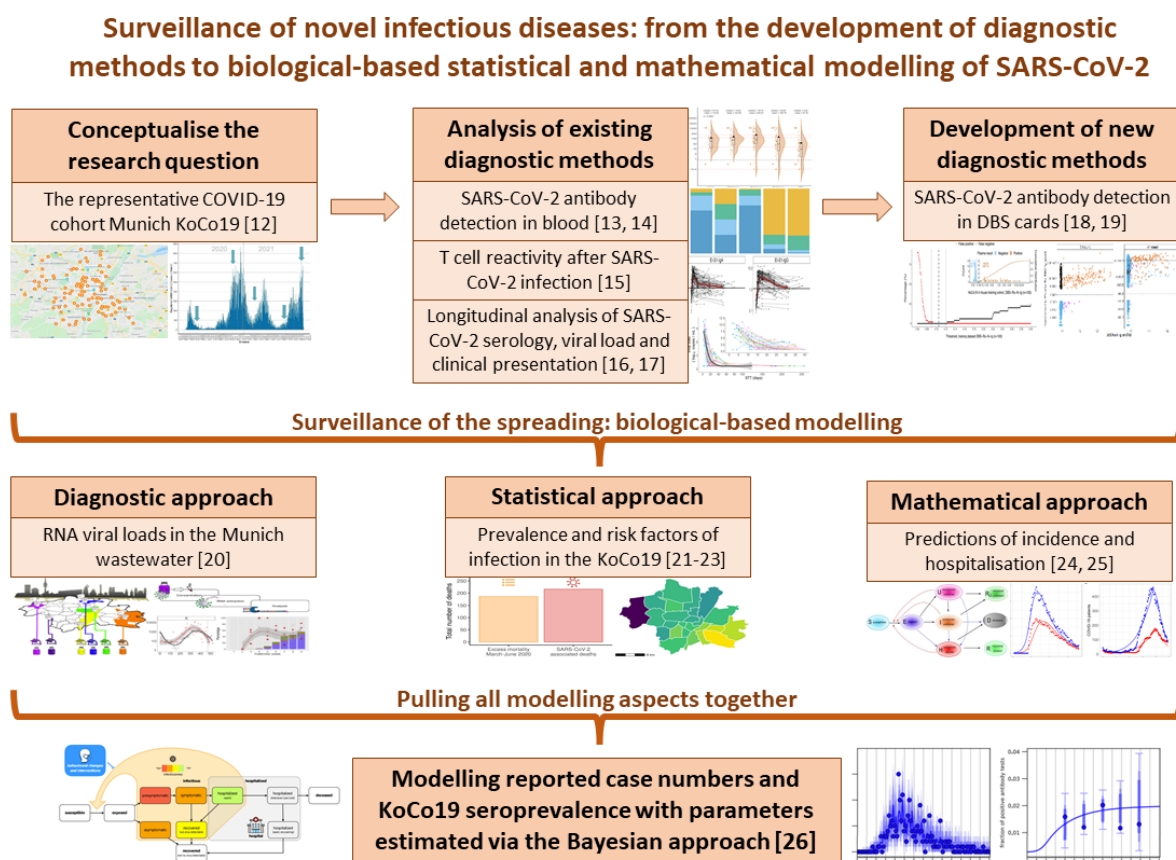

Figure 1: Outline of the habilitation project. First row: Introduction of the prospective COVID-19 cohort in Munich, known as KoCo19 (left). We then proceed with an analysis and comparison of the diagnostic methods available at the start of the pandemic for detecting antibodies post-SARS-CoV-2 infection (middle) and the development of innovative diagnostic methods for detecting antibodies using dried blood spots (DBS) on filter papers (right). Second row: Application of the knowledge gained in the process described in the first row to establish biological-based models for monitoring the pandemic within the population. In the diagnostic approach (left), we measure RNA viral loads in wastewater to predict the current incidence of infections. The statistical/epidemiological approach (middle) involves analysing infection prevalence and identifying risk factors in the KoCo19 and therefore in the city of Munich. In the mathematical approach (right), we combine data on incidence and hospitalization from the Robert Koch Institute (RKI) with information from the IVENA framework to create a compartmental biological-based model that simulates the epidemic's spread in the population, enabling predictions of potential future scenarios. Third row: Integration of all the aspects analysed in the previous sections. We fit reported cases and KoCo19 seroprevalence data into a single comprehensive model, with parameters estimated using a Bayesian approach. This approach provides a unified and coherent understanding of the pandemic's dynamics and the prevalence of antibodies in the population.

Following the rapid and alarming transmission of SARS-CoV-2 in Germany, particularly in Munich, the team recognized the urgent need to take action and improve the situation through social policy changes. Consequently, the prospective COVID-19 cohort Munich (KoCo19) was established with the primary objective to assess the prevalence and incidence of SARS-CoV-2 antibodies in the population of the city [12]. To achieve this, the team swiftly examined existing diagnostic methods for detecting SARS-CoV-2 antibodies in the blood following infection [13, 14]. Lab antibody results from the pre pandemic times were also obtained to exclude cross-reactions with cold or flu. Additionally, we focused on studying the T cell immune response after infection [15]. A specific subgroup of KoCo19, comprised of healthcare workers, was visited on a weekly basis for over a year, allowing for the longitudinal monitoring of serological values in their blood [16, 17].

Following the initial visit of KoCo19, it became evident that physically visiting all participants of the entire cohort multiple times would be burden on limited medical resources available. Consequently, new diagnostic methods were developed to measure SARS-CoV-2 antibodies using dried blood spots (DBS) on filter cards, as an alternative to traditional blood samples. Participants receive DBS filter cards by mail, can perform a self-prick procedure (refer to https://www.youtube.com/watch?v=vpZUzuQV10E&feature=emb_title), and subsequently send the samples back to the laboratory via mail [18, 19].

Now that the KoCo19 cohort and the diagnostic methods used to track it are well-documented, an evaluation of the disease's spread can be conducted by employing biological-based modelling techniques that focus on various aspects:

- Diagnostic Approach: This involves measuring RNA viral loads in Munich's wastewater. By comparing the reported incidence data provided by the municipality of Munich with the viral loads detected in the water, conclusions can be drawn regarding the "real" infection numbers in the city [20].
- Statistical Approach: Analysing data from KoCo19, we predict the actual seroprevalence in Munich. This analysis often reveals a significant gap between the real infection numbers and those reported officially. Furthermore, this approach allows for the identification and quantification of risk factors and symptoms following SARS-CoV-2 infection [21-23].
- Mathematical Approach: This approach involves combining Robert Koch Institute (RKI) data on incidence and hospitalization with data from the IVENA framework. These combined datasets are then used in a compartmental biological-based model designed to mimic the epidemic's spread within the population. The objective is to make predictions about the number of infections and hospitalizations under different scenarios of public health interventions [24, 25].

It is essential to clarify that by using the term "mathematical approach," we specifically refer to biological-based models described by stochastic or deterministic ordinary differential equations. While statistical models also have mathematical foundations, they are distinct in their application within a statistical context.

The statistical and mathematical approaches are two of the most crucial branches of modelling. The statistical approach involves testing and quantifying dependencies between variables. On the other hand, the mathematical approach aims to replicate real-world processes. Defining a mathematical model, however, is more challenging, and statistical models are employed to support idea generation. These distinct schools of thought are often competitive, each possessing its own strengths and weaknesses. This discussion leads to the final part of this work: a mathematical model that simulates the spread of SARS-CoV-2 in Munich, combining the reported cases from the municipality of Munich

and KoCo19 seroprevalence data. The data is integrated into a single model, and parameters are estimated using the statistical Bayesian approach [26].

Among the key insights gained from this project, which has paved the way for my habilitation, is a deep appreciation for the importance of diverse perspectives within the framework of modelling and analysis. As a result, a productive research endeavour necessitates the harmonious integration of these distinct schools of thought. This aspect holds utmost importance in achieving increasingly impactful outcomes in the realm of medicine and biology as applied in my institute. This stands as my personal research objective, one that I am committed to implementing within the data analysis group I have established and I am presently overseeing.

2.   The prospective COVID-19 cohort Munich: KoCo19

In this chapter, we present a concise summary of the KoCo19 cohort. More detailed and comprehensive information regarding the study design, setting, and population can be found in the previously published works by Radon *et al.* [12] and Pritsch *et al.* [21]. I assumed responsibility for managing the dataflow, preparing the foundational serological data and contributed to the analysis plan.

Between 5th April and 12th June 2020, we selected a random sample of 100 out of 755 Munich constituencies (refer to **Figure 2A**) to accurately represent the Munich population. To achieve this, fieldworkers utilized a "random walk" method [27] starting from the geographic centre of each constituency, selecting approximately 30 households per constituency. Ultimately, we successfully included 2994 households in 368 of the 755 constituencies, encompassing a total of 5325 household members aged 14 years or older (as illustrated in **Figure 2B** and **D**). When dealing with multi-party houses, we requested the inclusion of one household per floor to study the transmission dynamics within buildings. The number of households recruited per house varied between 1 and 7 across constituencies (as depicted in **Figure 2C**).

The primary questions that KoCo19 aims to address during the baseline visit were as follows [12]:

- What is the prevalence of SARS-CoV-2 antibodies in the Munich general population?
- How many of the individuals with positive antibody results have previously undergone PCR testing (pharyngeal swab and nucleic acid amplification) with positive or negative outcomes, and have they experienced symptoms suggestive of COVID-19?
- What is the distribution of symptom severity?
- What is the risk of infection for other members of the same household when one person is infected, and can household risk factors be identified?
- What is the risk of infection for other residents of the same apartment building when one person is infected?
- What are the risk factors associated with SARS-CoV-2 infections?

To address most of these questions, detailed information about the household and their members is necessary. This information was collected through three types of web-based questionnaires [12]:

- Household questionnaire: This covers the living situation (type of housing, number of bedrooms, apartment size), the number of inhabitants (including date of birth and sex), the highest level of education, employment situation, household income, exposure to second-hand smoke, the work of household members in potentially high-risk jobs for SARS-CoV-2 infections, and past pharyngeal swab testing for SARS-CoV-2 in household members, including the test results.

- Individual baseline questionnaire: This includes date of birth, sex, level of education, employment situation, smoking history, general health, pregnancy status, recent influenza vaccination, pre-existing medical conditions, symptoms suggestive of COVID-19 in the 14 days prior to the study, past PCR testing of nasopharyngeal samples for SARS-CoV-2, including test results, use of respiratory masks, and work in potentially high-risk jobs for SARS-CoV-2 infection.
- Diary: This records symptoms suggestive of COVID-19, social contacts, whereabouts, and use of public transport in the past 24 hours, as well as the psychosocial and economic situation (perceived health status, behavioural aspects, employment, and income, which will be collected periodically, e.g., once a week).
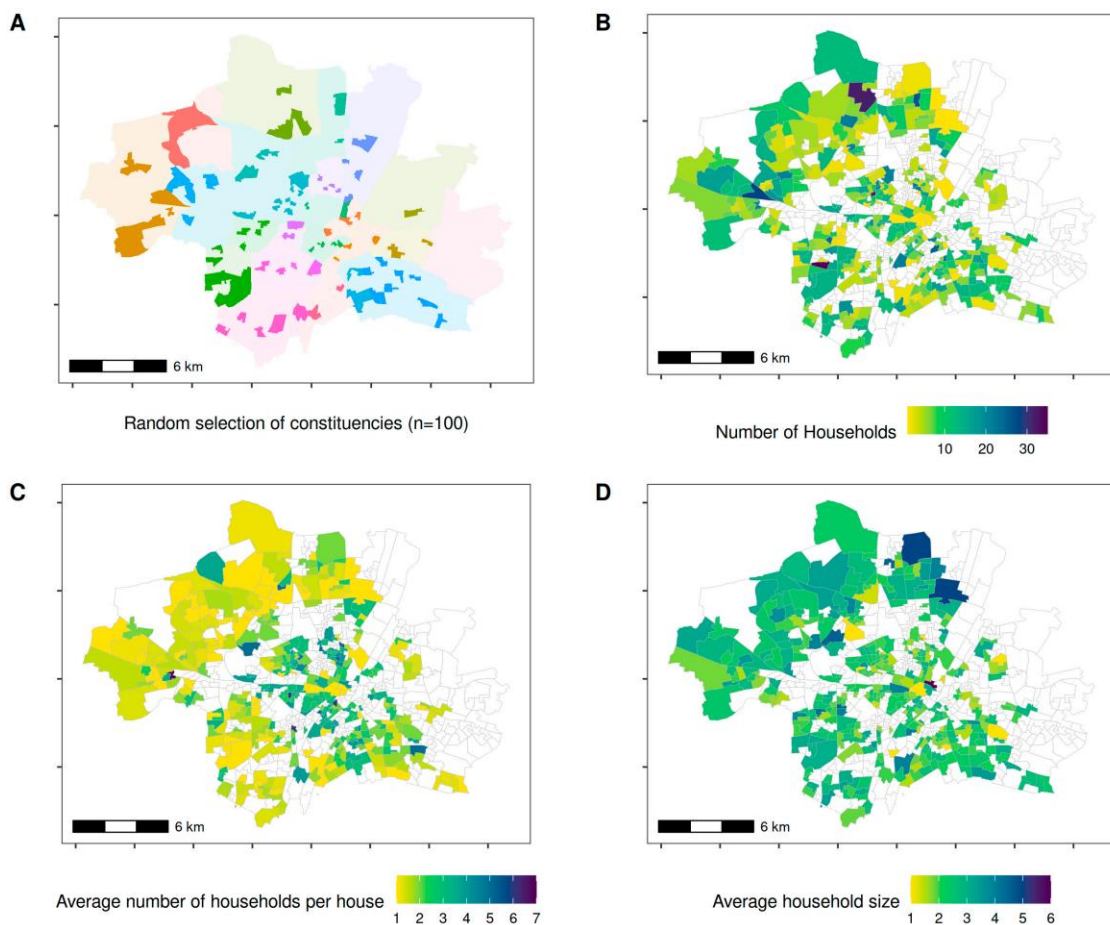

Figure 2: Geospatial distribution of the KoCO19. (A) The districts of the municipality of Munich distinguished by colours. (B) Distribution of the 2994 household in their respective 368 constituencies. (C) Average number of KoCo19-households per building in their constituencies. (D) Average number of members per KoCo19 household in their constituencies. Reproduced from [21].

To estimate seroprevalence and seroincidence over time, households were requested to provide new blood sample every three to six months, with the frequency adjusted based on current requirements of predicted models.

The primary topics to investigate during follow-up visits are as follows [12, 21]:

- Is there a change in antibody titres in individuals who initially tested positive, which might be necessary to differentiate from cross-reactivity with other coronaviruses?
- How long are SARS-CoV-2-specific antibodies detectable after infections of varying severity?

6

- How does the spread of the disease develop, and what impact do public health measures have on the incidence?
- What is the influence of individual behaviour on the incidence of infection?
- Which risk factors are associated with SARS-CoV-2 incidence?
- What is the socio-economic impact of the pandemic and the measures taken to combat it, especially on employment and psychosocial aspects?

Sampling was done at different times over the course of the pandemic (compare **Figure 3**):

1) May 2020 at the peak of the first infection wave in Germany,
2) December 2020, at the beginning of the second wave,
3) March 2021, at the peak of the third wave and at the beginning of the vaccination campaign for the general population,
4) August 2021, at the end of the third wave with around 68% of the general population 14 years or older being vaccinated against SARS-CoV-2,
5) November 2021, in the middle of the fourth wave and before the spread of the Omicron variant started in Germany.
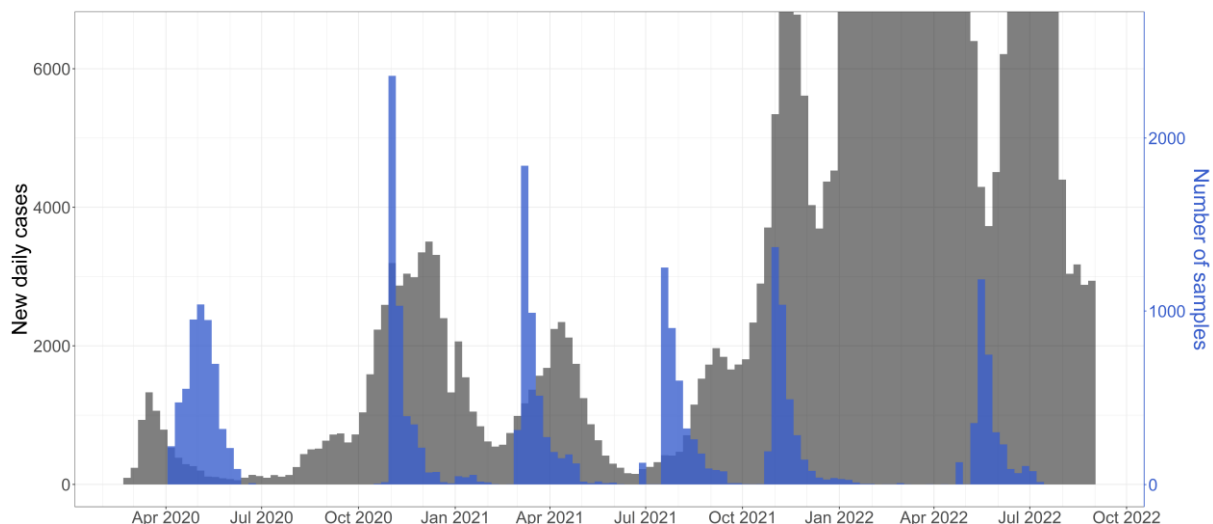6) Mai 2022, the end of the fifth wave in spring, at the beginning of the sixth one.

Figure 3: Epidemic evolution in Munich with description of the sample collection. *Black: number of new daily SARS-CoV-2 cases officially reported by the Robert Koch Institute (RKI). Blue: number of blood/DBS samples of the KoCo19 collected daily. Reproduced from [23].*

To the best of our knowledge, KoCo19 is the SARS-CoV-2 cohort with the longest follow-up time in the world. On December 1st, 2020, the KoCo19 cohort joined the ORCHESTRA (Connecting European Cohorts to Increase Common and Effective Response to SARS-CoV-2 Pandemic) project. During the whole pandemic, KoCo19 results were used to advise political decision making.

The KoCo19 baseline recruitment served as the foundation for all subsequent work. The laboratory aspect involved investigating the potential of existing diagnostic methods to determine seroincidence and prevalence from the collected blood samples. Additionally, the statistical and mathematical aspects involved planning and developing various types of models, which will be elaborated on in the following chapters.

Evaluation of the existing diagnostic methods

The baseline blood samples of KoCo19 were analysed using seven distinct diagnostic tests that were already available on the market (refer to **Table 1**) [13]:

- Euroimmun Anti-S1- SARS-CoV-2-ELISA-IgA (EI-S1-IgA; Euroimmun, Lübeck, Germany)
- Euroimmun Anti-S1- SARS-CoV-2-ELISA-IgG (EI-S1-IgG; Euroimmun, Lübeck, Germany)
- Elecsys Anti-SARSCoV-2 Roche N pan–Ig (Ro-Ig-N; Roche, Mannheim, Germany)
- Micro-virus neutralisation (NT)
- GeneScriptcPass (GS-cPass; GenScript, Piscataway, New Jersey, USA)
- Mikrogen-recomLine-RBD IgG line immunoassay (MG-S1, MG-N, MG-RBD; Mikrogen, Neuried, Germany))
- VIRAMED-SARS-CoV-2 ViraChip microarray (VC-N-IgA/IgM/ IgG; VC-S1-IgA/IgM/IgG; VC-S2-IgA/IgM/IgG; VIRAMED Biotech AG, Planegg, Germany).

Table 1: Evaluation of diagnostic accuracy of serological test. Optimised cut-off, sensitivity, specificity and overall accuracy of primary tests (Euroimmun Anti-S1- SARS-CoV-2-ELISA-IgA and -IgG, EI-S1-IgA and –IgG in the following, and Elecsys Anti-SARSCoV-2 Roche N pan–Ig, RO-N-Ig in the following) were conducted from 193 true-positive samples (samples of PCR positive individuals) and 1073 true-negatives (samples of blood donors prior the COVID-10 era). Reproduced from [13].

Sample composition True pos. / true neg.	Test	Manuf.'s cut-off	Optimised cut-off [CI]	Sensitivity [%] (Manuf's / Optim. cut-off)	Specificity [%] (Manuf's / Optim. cut-off)	Overall accuracy [%] (Manuf's / Optim. cut-off)
193/1073	EI-S1-IgA	1.100	1.085 [0.855; 1.705]	64.77/64.77	93.29/92.64	88.94/88.39
193/1073	EI-S1-IgG	1.100	1.015 [0.850; 1.395]	77.20/79.79	98.04/97.76	94.87/95.02
193/1073	Ro-N-Ig	1.000	0.422 [0.295; 0.527]	85.49/88.60	99.81/99.72	97.63/98.03
107/106	NT	–	5.0*	- / 73.83	- / 100.00	- / 86.85
108/106	GS-cPass	20.000	20.538 [13.768; 24.241]	96.30/96.30	100.00/99.06	98.13/97.66
108/111	VC-N-IgG	100.000	18.500 [13.500; 23.000]	39.81/93.52	99.10/91.89	69.86/92.69
108/111	VC-S1-IgG	100.000	10.000 [10.000; 10.000]	65.74/95.37	100.00/100.00	83.11/97.72
108/111	VC-S2-IgG	100.000	10.000 [10.000; 10.000]	17.59/63.89	100.00/99.10	59.36/81.74
78/106	MG-N	1.000	1.000 [1.000; 1.600]	94.87/94.87	98.11/98.11	96.74/96.74
78/106	MG-RBD	1.000	1.000 [1.000; 1.000]	94.87/94.87	100.00/100.00	97.83/97.83
78/106	MG-S1	1.000	1.000 [1.000; 1.000]	96.15/96.15	100.00/100.00	98.37/98.37
193/1073	Random Forest	–	–	88.60†	99.81†	98.10†
193/1073	Support Vector Machine	–	–	84.46†	99.91†	97.47†

*For NT, dilutions starting at 1:5 were used; see Methods.
†The random forest and the support vector machine combine all three primary tests, the accuracy measures thus do not relate to specific cut-offs.

The first three methods served as primary tests to screen samples for infection. The remaining tests were used to confirm the results. Within our facility, we were able to conduct measurements for the first five assays. Among these five tests, Ro-N-Ig and GS-cPass demonstrated the best performance (refer to **Table 1**).

Additionally, we conducted measurements for two quantitative assays: the Euroimmun Anti-SARS-CoV-2 QuantiVac enzyme-linked immunosorbent assay (EI-S1-IgG-quant) and the Roche Elecsys Anti-SARS-CoV-2 S (Ro-RBD-Ig-quant). These assays were compared with each other and with confirmatory tests [14]. Ro-RBD-Ig-quant effectively distinguished between true-positive and true-negative results, exhibiting lower non-specific reactivity compared to EI-S1-IgG-quant.

A value above the specified thresholds in the Ro-N-Ig test indicates a previous infection, while the EI assays and Ro-RBD-Ig-quant may also suggest vaccination. These analyses have verified that both the

Roche Elecsys® serological assays are suitable for conducting sero-surveillance of KoCo19. We could therefore proceed with the follow-ups.

I was responsible for managing the entire dataflow in the publications [13, 14]. This included preparing the dataset, conducting initial analysis on the data, and planning and coordinating the analyses to be performed by the other data analysts, as well as determining the appropriate types of graphical presentation of the observed data and statistical estimates to be used.

3. Development of new diagnostic methods

After the initial baseline visit, we realized that the effort required to personally visit each household would exceed our available resources. Therefore, in order to achieve a sufficient sample size, we needed alternatives to venous blood sampling that did not rely on medical personnel or cold-chains. While dried-blood-spots (DBS) on filter-cards have been used in various studies, they have not been commonly used for serology. As a result, we developed a semi-automated protocol for SARS-CoV-2 serology using self-sampled DBS [18, 19]. At that time, as the principal statistician, I was closely collaborating with the laboratory staff to comprehend the appropriate methods for measuring and examining the paired samples of both blood and DBS. To begin with, we applied this protocol to measure Ro-N-Ig and validated it in a cohort consisting of both DBS and venous blood samples (n = 1710). The feasibility of the method was demonstrated in two large sero-surveys involving 10,247 company employees and 4,465 participants from a population cohort. The sensitivity and specificity of the DBS method were 99.20% and 98.65%, respectively, compared to whole blood testing (**Figure 4**) [18]. Subsequently, we further developed the DBS method to measure Ro-RBD-Ig-quant antibodies and validated it in a cohort with matched DBS and venous blood samples (n = 825) [19]. The sensitivity and specificity of this method were found to be 96.63% and 97.81%, respectively, compared to the same test performed with paired venous blood samples.
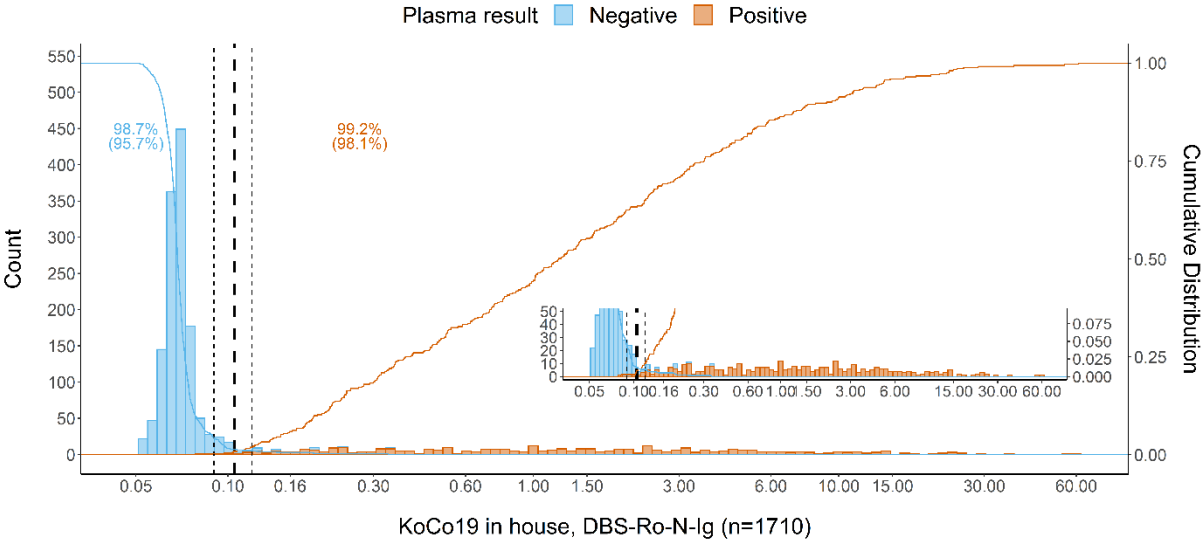

Figure 4: Frequency distribution of Ro-N-Ig antibody titres detected in DBS. For this analysis, we used 1710 samples of the KoCo19. The dashed vertical lines: the empirically determined cut-off value (bold) for result classification with its boundary values (light). The insert at the bottom right represents a zoom-in on the y-axis to allow visualization of the lower frequency positive values. Reproduced from [18].

The importance of the Ro-RBD-Ig-quant test was most pronounced during the onset of the vaccination campaign. At that time, questions regarding the number of vaccinated individuals within the population and the potential occurrence of breakthrough infections (infections that transpired after

complete vaccination) became a major point of discussion. With the Ro-N-Ig and Ro-RBD-Ig-quant tests, we are capable of distinguishing between prior infections and immune responses induced by vaccination (see **Figure 5**). This is achievable because the Ro-RBD-Ig test identifies antibodies after both infection and vaccination, while the Ro-N-Ig test discerns between antibodies resulting from infection (both anti-S and anti-N present) and those arising from vaccination (only anti-S present). The Ro-N-Ig test can ascertain whether an individual had a previous infection but does not provide information about the exact date of the infection.

We observed that at the onset of the vaccination campaign in early 2021 (**Figure 5A left**), approximately 5.5% of the participants tested positive for anti-S but negative for anti-N, which aligns with a vaccination response and roughly represents the proportion of people eligible for full vaccinations at that time. Around 4.1% of the analysed samples exhibited the pattern expected in infected individuals, with both values showing positive for anti-S and anti-N, while 0.4% only showed positivity for anti-N. This last group could either be individuals who did not produce an anti-S response after infection or may have false positive values for anti-N. Of note, most of these raw values are very low as compared to the anti-N values seen in the double positive group, so it may as well be individuals shortly after acute infection which are not yet positive in anti-S but already show a beginning low anti-N reactivity. This is also supported by the fact that all but one of those individuals were found to be anti-N and anti-S positive in the subsequent later sampling round. Approximately 90.0% of the participants had not received either SARS-CoV-2 vaccination or contracted the infection.

A significant vertical upward shift of the data points was observed in follow-up three compared to the results of follow-up two (**Figure 5A right**). Between July and September 2021, the vaccination campaign had been ongoing for a considerable period in the Munich population. As a result, 88.9% of the samples received during this round exhibited the expected pattern in vaccinated individuals (anti-S positive, anti-N negative). During the summer, with low SARS-CoV-2 spread and minimal losses due to titre drop after infections, the rate of double positives increased slightly to 4.9%. These increased anti-S values were a result of a combination of vaccination and infection. Simultaneously, the population that was anti-N positive but anti-S negative disappeared, moving into the double positive fraction. This supports the notion that these subjects were at the early stage of their seroconversion and developed their anti-S titre after follow-up two. The percentage of participants still unexposed to both SARS-CoV-2 vaccination and infection decreased to 6.2%.

In follow-up four (**Figure 5B right**) after the summer of 2021, the proportion of vaccinated individuals further increased to 91.6%. The number of infected subjects also slightly rose to 6.4%, with 50 out of 193 (25.9%) being newly infected. Among these 50 participants, 5 (10.0%) experienced breakthrough infections, as they became infected after vaccination (transitioning from S+N- in follow-up three to S+N+ in follow-up four, denoted in black). Only one participant was anti-N positive but had not yet seroconverted to anti-S.

In the fifth follow-up (**Figure 5C right**), all participants except one completed anti-S seroconversion. With the emergence of Omicron, the proportion of anti-N positives dramatically increased to 42.6%, with 86.3% (1118/1295) representing newly positive cases (96.2% (1075/1118) of these were breakthrough infections, indicated by pink dots). The one participant who was positive for anti-N but negative for anti-S in follow-up four also converted to anti-N, suggesting an early infection with the development of the anti-S titre after the follow-up.

With the effective performance of the DBS methods, it became feasible to continue the KoCo19 surveillance and acquire significant insights into the SARS-CoV-2 pandemic. Having established the cohort and diagnostic methods, we are now able to move forward with outlining the techniques employed for pandemic surveillance.
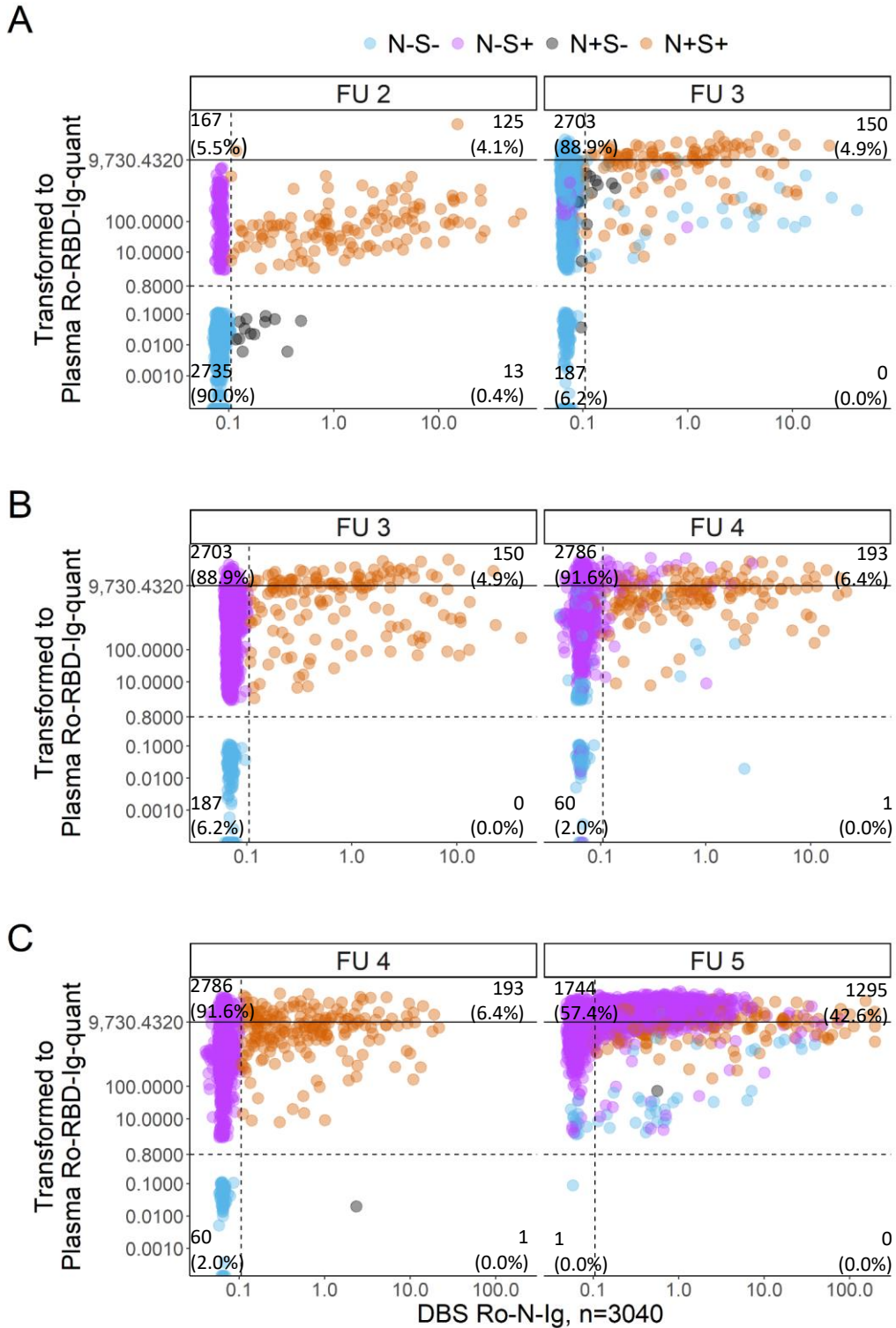
Figure 5: Scatterplot of four follow-ups of the KoCo19 cohort for people that participated in all rounds (n=3040). The Ro-N-Ig measurement from DBS is abbreviated with "N", Ro-RBD-Ig-quant from the same DBS is abbreviated "S". Positivity is represented with "+", negative, below cut-off with "-". The colour code is defined by the status of the respective subject in the (A) second, (B) third and (C) fourth follow-up respectively (represented by "FU"). Blue dots represent N-S-, orange dots represent N+S+, grey spots are N+S- and pink dots are N-S+, considering the left column as reference for colour-coding. Samples above the nonlinear range of Ro-RBD-Ig-quant (solid black line at 9730.4 for back calculated plasma BAU/ml) were not diluted. (A) Evolution from second to third follow-up. Left: Second follow-up sampled between March and April 2021; right: Third follow-up sampled between July and September 2021. (B) Evolution from third to fourth follow-up, sampled between October and December 2021 and (C) evolution from the fourth to the fifth follow-up, sampled between May and July 2022. Reproduced from [19].

4. Epidemic surveillance

The statistical approach

In conjunction with the laboratory samples, questionnaire data was also collected throughout the various rounds of our study. The combination of these two datasets culminated in the publication of three papers concerning the analysis of risk factors associated with SARS-CoV-2 and the assessment of underreporting bias over time [21-23]. For the first two papers, I assumed responsibility for the laboratory data and curated the final dataset utilized for the analysis. I also coordinated communication among the different institutions involved in the research. As for the last paper, I assumed the additional role of conducting the analysis, conceptualizing, and composing the core sections of the paper. In this presentation, I present only the primary findings of our analyses. For a comprehensive explanation of the technical aspects, please refer to the respective publications.

The baseline data analysis revealed limited evidence of a strong connection between anti-N seropositivity and the various factors under investigation, as illustrated in Figure 4 of reference [21]. Notably, the loss of the sense of smell or taste during the study period was linked to the outcome. However, it's important to note that this association was characterized by a wide confidence interval (odds ratio (OR) 41.3; 95% CI 6.7 – 231.0) when employing a conventional generalized linear mixed model (GLMM). Furthermore, respiratory allergies (OR 3.3; 95% CI 1.1 – 10.3) displayed a statistically significant association with anti-N seropositivity. Factors such as occupation in a high-risk job, household type, and residential area per inhabitant also exhibited a weak connection with the likelihood of infection. It is worth noting that all these variables were incorporated into the final GLMM analysis, even though the loss of the sense of smell or taste was considered a symptom of the outcome rather than a true risk factor. However, none of these associations reached statistical significance. Similar outcomes were obtained through sensitivity analyses, utilizing a Bayesian GLMM with imputed missing values, as shown in **Figure 6**.
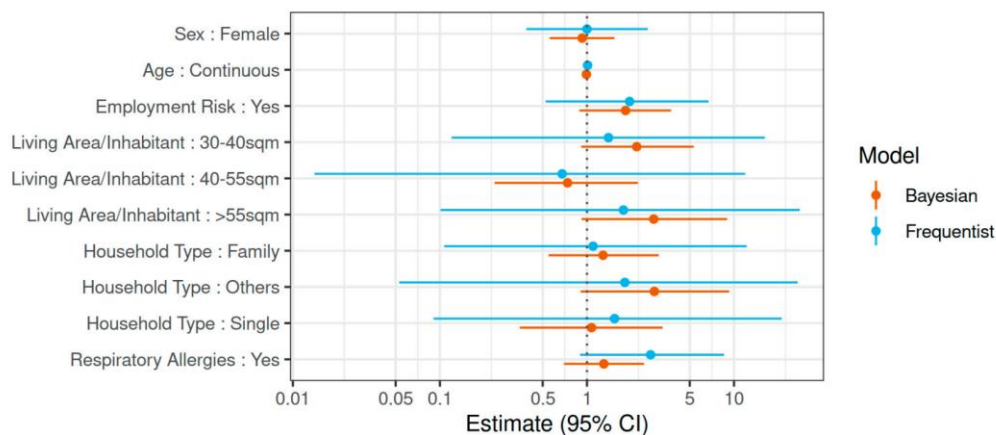

Figure 6: Multivariate risk factor analysis for SARS¬CoV-2 seropositivity in the KoCo19 baseline round. The multivariate risk factor analysis is mutually adjusted for all variables in the figure. OR: odds ratio; 95% CI: 95% credible interval (Bayesian analyses)/95% confidence interval (frequentist GLMM). Reproduced from [21].

In the first follow-up, the seroprevalence, which had been weighted and adjusted for specificity and sensitivity, exhibited an increase from 1.8% (95% CI 1.3 – 3.4%) at the baseline to 3.6% (95% CI 2.9 – 4.3%) during the follow-up period [22]. Notably, 91% of the participants who tested positive at the outset retained their antibody-positive status during the follow-up. While cases tended to cluster within households, there was no statistically significant evidence of geospatial clustering across the city of Munich (see **Figure 7**). Groups at the highest risk were identified as men and participants aged

between 20 and 34, taking baseline results and the duration to follow-up into consideration. To elucidate these effects, a sensitivity analysis was conducted, revealing that differences could be attributed to health-risk behaviours, the number of personal contacts, and leisure-time activities (refer to **Figure 8**).
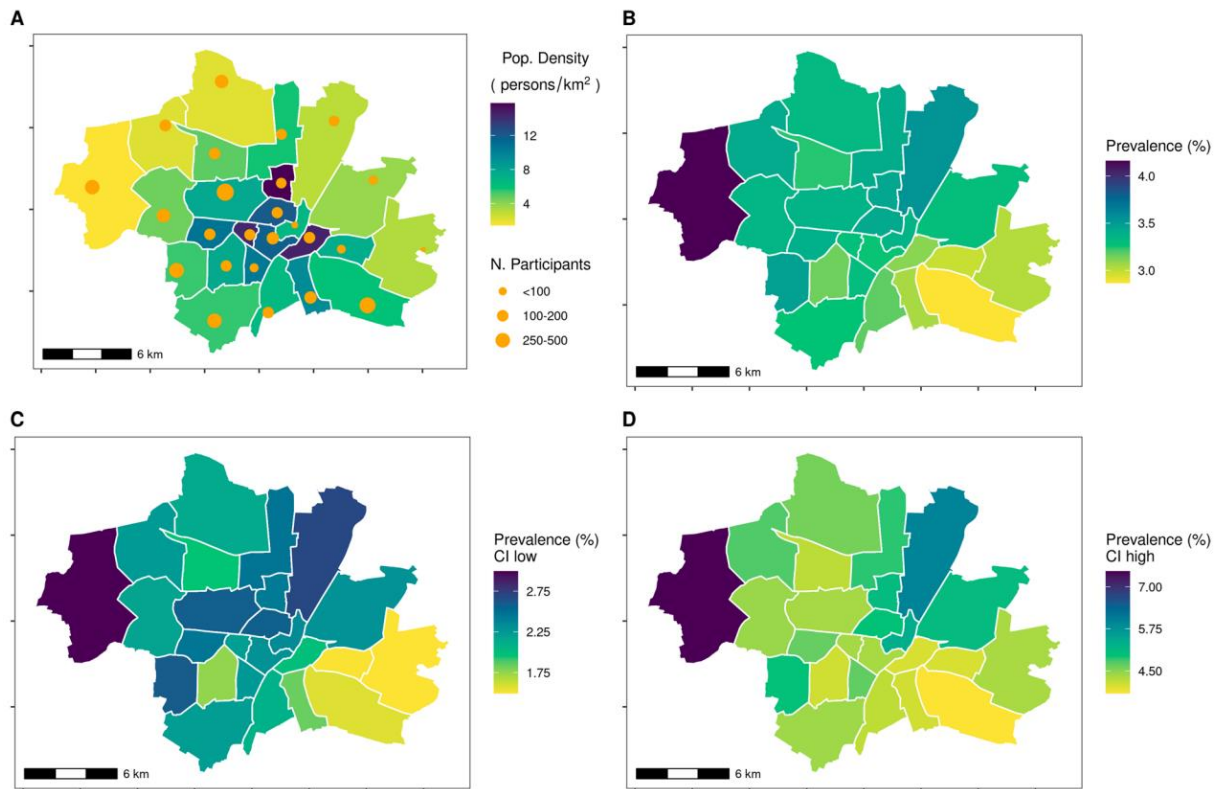

*Figure 7: Geospatial distribution of the prevalence in the Munich constituencies. (**A**) The Munich population density (taken from https://simple. wikipedia.org/wiki/Boroughs_of_Munich, as background colour) and number of participants in each constituency (yellow dots). (**B**) Weighted seroprevalence. (**C**) Lower 95% confidence bounds of the weighted seroprevalence. (**D**) Upper 95% confidence bounds of the weighted seroprevalence. The seropositivity varied slightly across constituencies, however, not reaching statistical significance. Reproduced from [22].*

The final analysis presented in this section focuses on the follow-ups two to four. The blue estimate in **Figure 9A** shows the calibrated seroprevalence (adjusted for sensitivity and specificity) in private households for the Munich population aged 14 years and older:

- Baseline: 1.6% (1.1 – 2.1%)
- Follow-up 1: 4.1% (3.3 – 4.9%), and after adjustment for vaccination status
- Follow-up 2: 7.3% (6.1 – 8.5%),
- Follow-up 3: 12.4% (10.7 – 14.1%),
- Follow-up 4: 14.5% (12.7 – 16.2%).

As expected, the seroprevalence is increasing over time. The official number of positive cases is reported in pink for the general population of Munich, which includes institutions like nursing homes and potential reinfections. Given that the KoCo19 cohort is limited to private households and the estimated seroprevalence does not account for multiple infections, comparing this estimate with the official number over time allows us to estimate a lower bound for the underreporting factor. The estimated underreporting factor varies across the rounds:

- Baseline: 3.4 (2.4 – 4.4),

13

- Follow-up 1: 1.3 (1.0 – 1.6),
- Follow-up 2: 1.8 (1.5 – 2.1),
- Follow-up 3: 2.3 (2.0 – 2.6) and
- Follow-up 4: 2.2 (2.0 – 2.5).

To gain a better understanding of the impact of the vaccination campaign, the calibrated cumulative seroprevalence was analysed separately for vaccinated and non-vaccinated individuals (**Figure 9C**):

- Follow-up 2: 3.1% (0.5 – 5.6%) versus 7.8% (6.6 – 9.1%),
- Follow-up 3: 8.5% (6.6 – 10.4%) versus 20.6% (16.2 – 25.0%) and
- Follow-up 4: 11.8% (9.8 – 13.8%) versus 22.9% (18.5 – 27.4%).
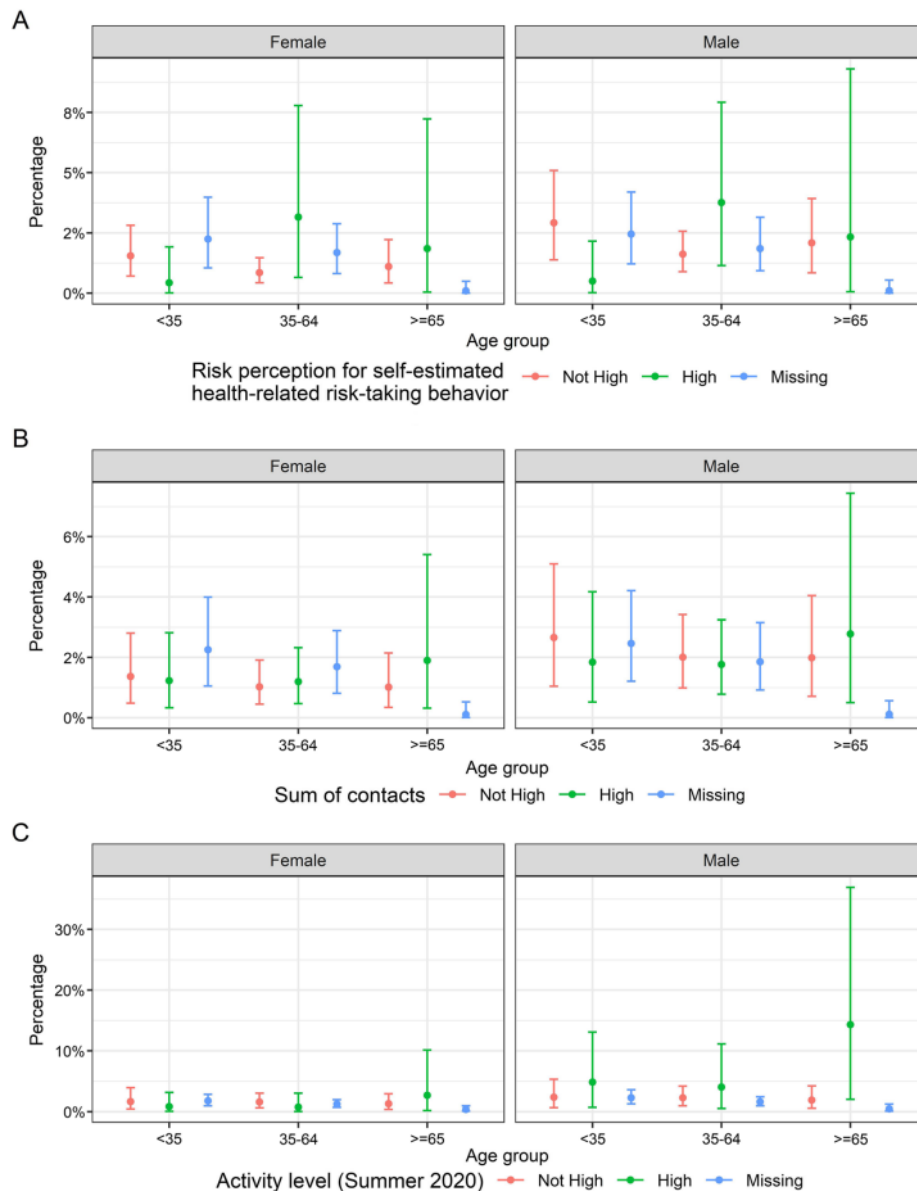
Figure 8: Seroincidence between baseline and follow-up. (A) From the participant self-estimated health-related risk-taking behaviour. (B) Sum of contacts. (C) Leisure time activities in summer 2020 stratified for sex and age group. Reproduced from [22].

The seroprevalence of the vaccinated group is lower compared to the non-vaccinated group. In **Figure 9D**, we compare the adjusted (for sensitivity and specificity) incidence rates for breakthrough

infections (BTIs, infections occurring after complete vaccination coverage) versus infections in naïve subjects (INS) over the rounds:

- Follow-up 3: 1.3% (0 – 3.7%) versus 3.3% (2.6 – 4%) and
- Follow-up 4: 1.8% (0.6 – 2.9%) versus 4.1% (2.3 – 5.9%).

In August and November 2021, the incidence rates of INS were greater than the ones of BTI. Despite the cumulative seroprevalence appearing higher among the non-vaccinated population compared to the vaccinated population (**Figure 9C** and **D**), BTIs relevantly contributed to community spread, considering that the population of vaccinated individuals was much larger than the non-vaccinated one during the last rounds of investigation (**Figure 9E**). **Figure 9F** provides a more detailed illustration of this effect, showing that the proportion of vaccinated and infected individuals increased over time, becoming significantly greater than the proportion of infected and non-vaccinated individuals by follow-up four.
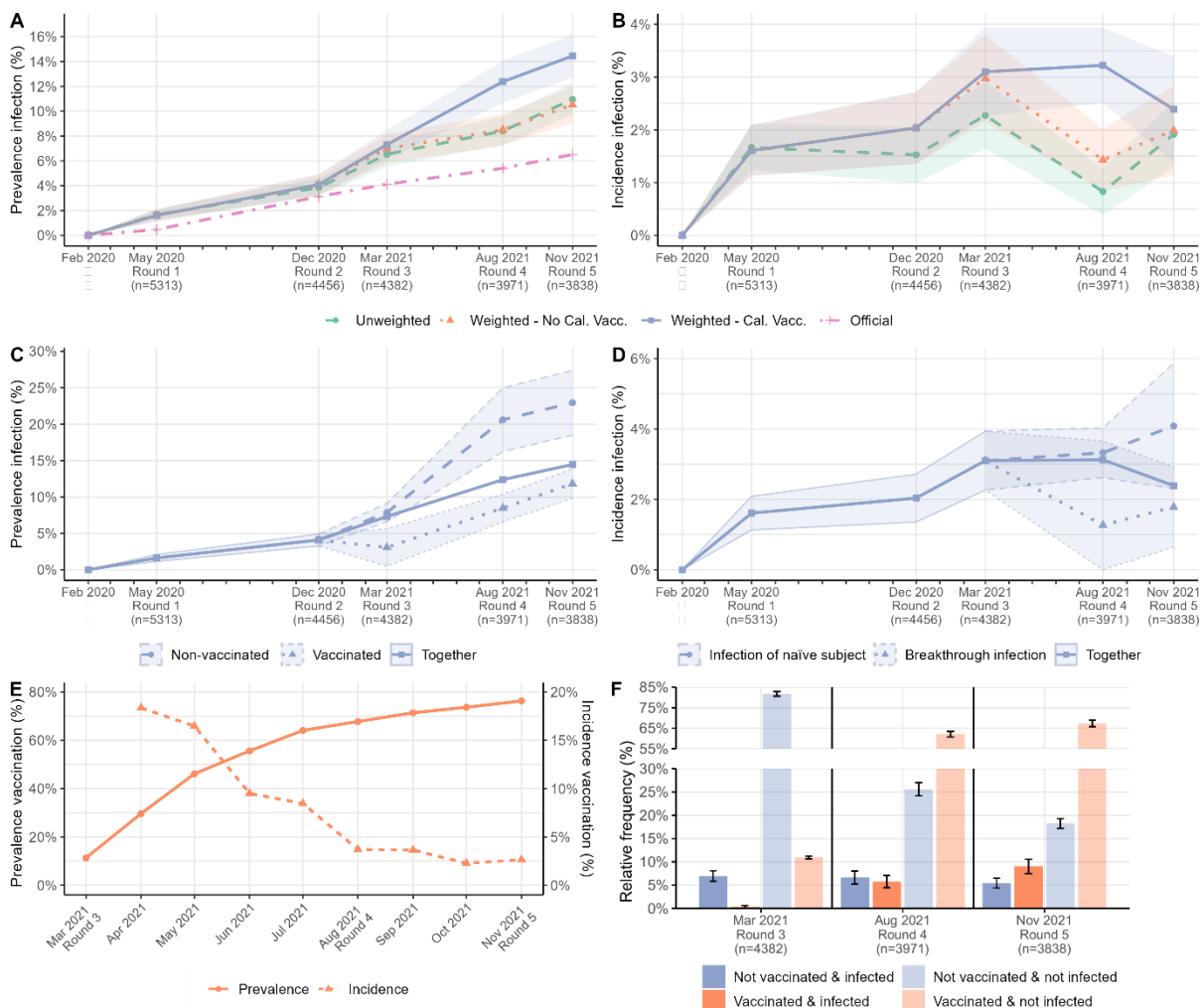
Figure 9: (A) Cumulative anti-N seroprevalence, both weighted and unweighted, in private households compared to official cases reports by the authorities for the Munich population aged 13 and older. (B) Anti-N sero-incidence, both weighted and unweighted. (C) Estimates of Seroprevalence for Anti-N Antibodies, Adjusted Based on the Number of Vaccinated Individuals, Segmented by Their Vaccination Status in the Same Round. (D) Calibrated estimates for infections of naïve subjects and breakthrough infections. (E) Prevalence and incidence of vaccination in Munich (official numbers). (F) Relative frequencies based on infection and vaccination status.
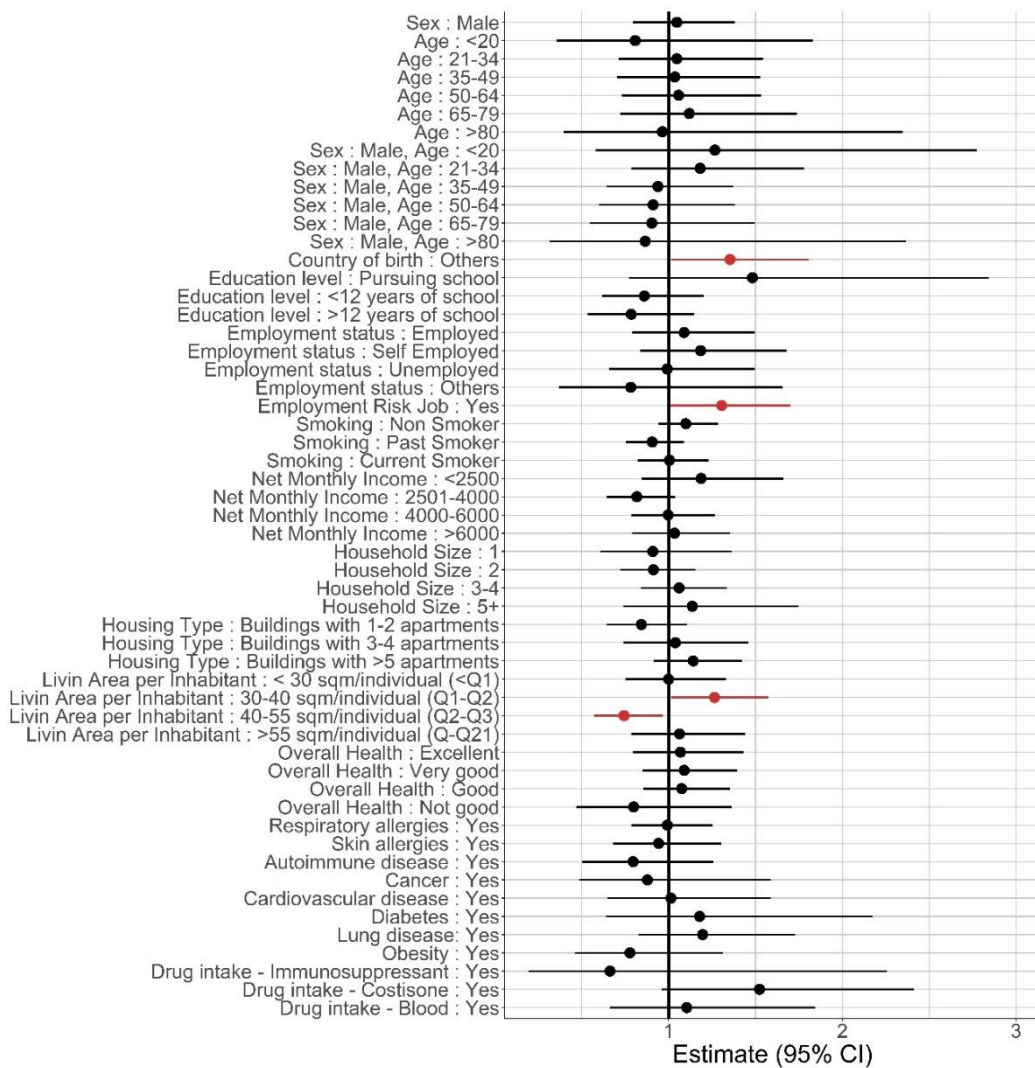
Figure 10: Association between potential risk factors and SARS-CoV-2 sero-positivity while accounting for the time gap between baseline assessment and Follow-up four. The data is this right-censored, and the results are generated using multiple imputation.

The results of the risk factor analysis can be found in **Figure 10**. The extended Cox regression model indicated certain factors being associated with an increased risk of SARS-CoV-2 sero-positivity. Specifically, being born outside Germany (hazard ratio (HR) 1.36, 95% CI $1.01 - 1.85$) and holding a job with a high potential for contact with COVID-19 cases (HR 1.31, 95% CI $1.00 - 1.70$) were identified as risk factors. Additionally, residing in an area with $30 - 40$ square meters per inhabitant slightly elevated the risk of infection (HR 1.27, 95% CI $1.01 - 1.59$), while for areas with $40 - 55$ square meters per inhabitant, the risk decreased (HR 0.74, 95% CI $0.57 - 0.97$), in comparison to the average hazard across all living area categories. Notably, none of the other socio-demographic variables (such as sex, age, level of education, employment status, building type, household income) or health-related factors (including smoking status, general health status, various diseases, and medication intake) were identified as risk factors for infection.

The mathematical approach

The mathematical models presented in this chapter aim to replicate the stages of the COVID-19 outbreak in Germany and Munich, considering the potential effects of both existing and hypothetical non-pharmaceutical interventions [24, 25]. These models simulate the transmission of the SARS-CoV-2 virus among various population groups by utilizing systems of differential equations to describe

16

interactions between individuals. In the first publication, I was responsible for curating the data, contributed to the conceptualization of the analysis, and coordinated collaboration with external groups. In the second publication I conceived the project, obtained various datasets, conducted data cleaning, and supervised the work of a master's student. Additionally, I authored a substantial portion of the paper.

The proposed approaches extend the known S-E-I-R (susceptible-exposed-infected-recovered) model for disease dynamics. In particular a distinction is made between individuals who have been exposed to the virus but are not yet infectious, asymptomatic infectives, infectives with mild or influenza-like symptoms (not reported as SARS-CoV-2 infections) and reported SARS-CoV-2 infectives. Infected individuals without SARS-CoV-2 diagnosis are assumed to unlikely die of the virus-induced disease. These models cannot take into account the number of unreported and unknown cases.

The work presented in Barbarossa *et al.* [24] was among the initial models introduced at the beginning of the pandemic, focusing on different strategies to mitigate the current outbreak. The results suggest that a partial and gradual easing of control measures could become feasible if accompanied by increased testing, strict isolation of detected cases, and reduced contact with at-risk groups (**Figure 11**).
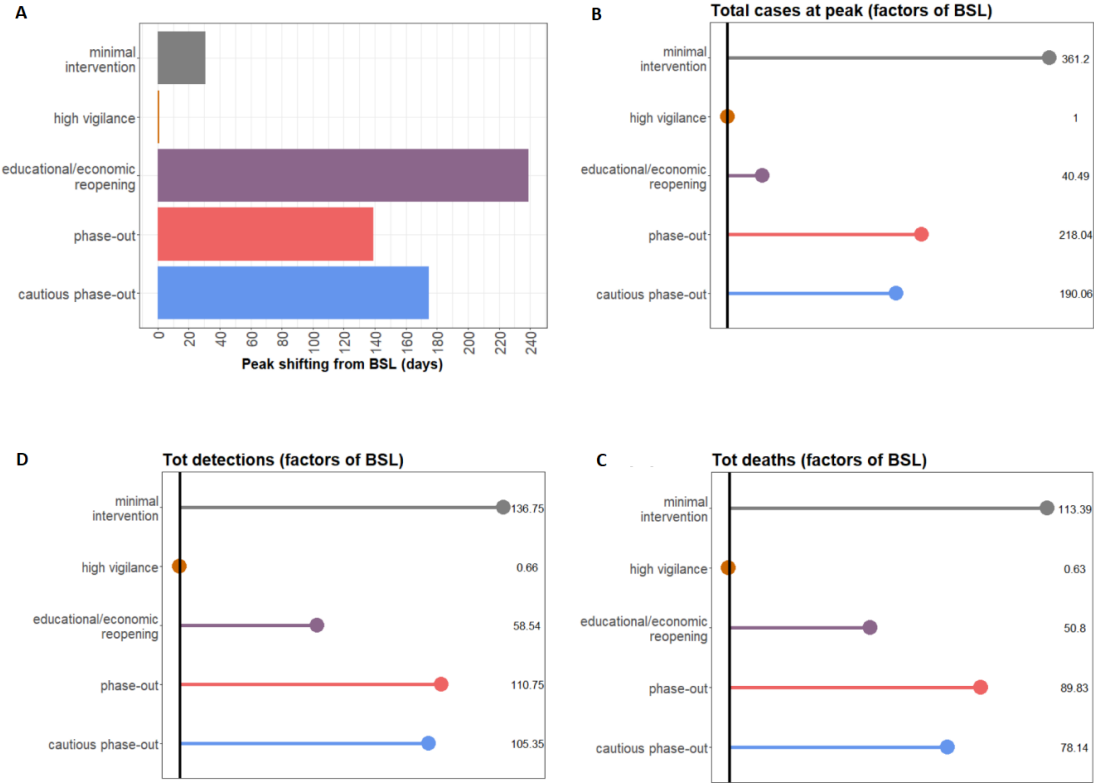

Figure 11: Differences between the baseline model output scenario (BSL) and the considered possible alternatives. (A) Peak shifting (in days) compared to BSL. (B) Differences in reported cases (factor) at the day of the peak. (C) Differences in total detected cases (factor); (D) Differences in total deaths (factor). For all rollback scenarios, results refer to the second peak of the outbreak in Germany. Reproduced from [24].

Fuderer *et al.* [25] considered in their analysis not only the reported incidence numbers but also hospitalizations. The models are similar, but the focus now shifts to hospital occupancy, which became more crucial after successful vaccination campaigns. The model encompasses data from the pandemic's early days to mid-October 2021. Predictions for the second half of the fourth wave are presented based on data from the first months of the fourth wave until October 15, 2021, to fit the

model's parameters and predict the number of new COVID-19 cases. Various scenarios were considered for predicting future developments:

- Optimal: Vaccination rate and contact rate remain constant from October 15, 2021.
- Severe: Vaccination continues from October 15, 2021, but at lower rates while contact rate continues to increase.
- Extreme: Vaccination is entirely stopped from October 15, 2021, and the number of contacts continues to increase rapidly.

The results, shown in **Figure 12**, indicate that even with a significant portion of the population already vaccinated, the number of new COVID-19 cases will increase with rising contact rates and decreasing willingness to vaccinate. A rapid reopening combined with a stop in vaccination could lead to an extreme fourth wave, with a significantly higher incidence than the previous waves. However, despite the higher incidence during the fourth wave in the extreme scenario compared to the second wave, the number of COVID-19 patients in regular hospital wards is considerably lower. This suggests that an increasing number of fully vaccinated individuals is associated with a decrease in the hospitalization rate.
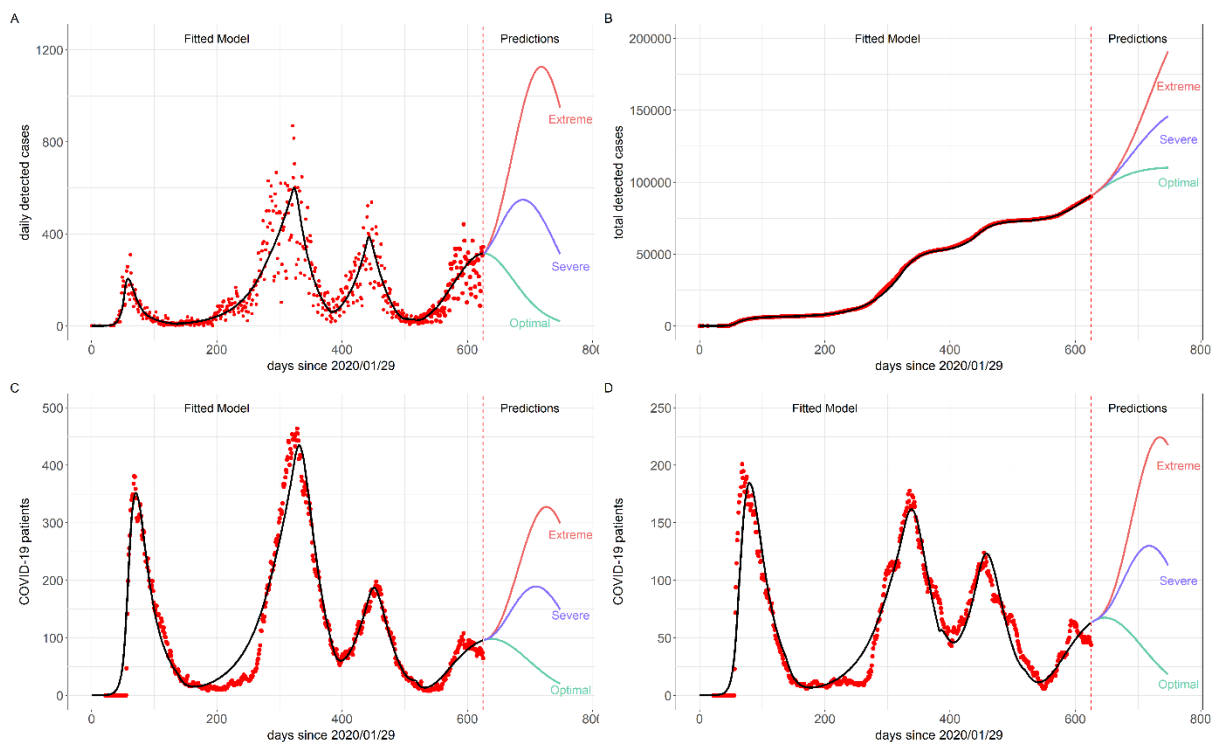

Figure 12: Data description and model results. Detected COVID-19 cases in Munich reported by the RKI (A) daily and (B) cumulative. Hospitalized COVID-19 cases in Munich for the normal ward stations (c) and intensive care units (d). The solid black lines denote the results of (A)-(B) the preferred model and (C)-(D) the hospitalization model. For first and second wave no vaccination compartments were needed. Reproduced from [25].

Comparing the model predictions with **Figure 3** we can observe that the detected infection cases indeed increased exponentially. The rise, however, can be attributed not only to the lower-than-expected vaccination rate or to the relaxation of social distances measures, but also to the emergence of a new variant of the virus. It is imperative to adjust mathematical models in response to any alterations in the biological circumstances. Fortunately, these adjustments are relatively straightforward to implement, as demonstrated in this analysis.

5. Merging biological-based mathematical models and statistical approaches

The statistical models presented in the preceding chapters do not mimic or explain the underlying biological mechanisms driving the infection. However, they do offer improved quantification of the "true" number of infections and different risk factors associated with infection. On the other hand, mathematical models can simulate the process and make predictions under specific conditions. However, these models have weaker parameter estimates and fail to account for the impact of unreported and unknown cases.

To address this limitation, we combined all the information into a mechanistic model [26]. For this analysis I oversaw delineating the underlining mathematical model, describing the equations, and delivering the KoCo19 and hospital data. As many studies rely solely on officially reported case numbers (as demonstrated in the previous chapter), we first assessed the reliability of such an approach. We evaluated the predictive accuracy by comparing the predicted seroprevalence derived from the posterior samples with the independent KoCo19 data, which were not used for fitting the model. The model's predictions for the total number of cases exhibit wide confidence intervals (**Figure 13**), indicating that relying solely on officially reported case numbers, even with prior knowledge, does not adequately predict the actual number of COVID-19 infections during an epidemic with sufficient confidence. By incorporating representative data, the model's uncertainties are reduced. To measure the added value of the KoCo19 prevalence data, we expanded the dataset with time-dependent prevalence reported by KoCo19 and repeated the Bayesian parameter estimation process. The inclusion of seroprevalence data substantially reduces the uncertainty related to the hidden states of the model, particularly for the total number of cases (which is closely linked to seroprevalence levels) and for the number of asymptomatic cases. This demonstrates the effectiveness of seroprevalence data in reducing uncertainty. Additionally, it becomes evident that the actual number of infections is significantly higher than the number of reported cases, underscoring the limitations of publicly reported case counts.

6. Outlook

In this habilitation thesis, I presented a strategy for monitoring pandemics. I commenced by introducing the prospective COVID-19 cohort, KoCo19, which is representative of the Munich population. To analyse the spread of the pandemic, a serological approach was adopted, focusing on detecting antibodies produced either due to infection with SARS-CoV-2 or vaccination against it. Consequently, various commercially available plasma tests were scrutinized and compared. The findings revealed that the Roche Elecsys® Anti-SARS-CoV-2 anti-N and anti-S assays outperformed others. Subsequently, it became logistically challenging to collect in-person samples from all participants. To overcome this, a method to measure these antibodies using DBS filter papers was devised. This innovation enabled to conduct six follow-up assessments of the cohort. Concurrently, several statistical and mathematical analyses related to infection risk factors, vaccination campaign, underreporting, and the population-wide dynamics of the pandemic are conducted. Notably, the KoCo19 cohort remains the longest standing and the only ongoing COVID-related cohort. The KoCo19 cohort remains the longest standing COVID-related cohort. This work, alongside collaboration with the laboratory, is a unique contribution to the literature and has facilitated a comprehensive understanding of the dark number and of the trajectory of the pandemic in the Munich population.

Building on this foundation, I established a biometrics research group. A key insight from this multidisciplinary project is the recognition of the vital role that diverse perspectives by multiple stakeholders played such as laboratory, medical expertise, biological knowledge, and data analysis to name a major few. In my view, fruitful research endeavours demand the seamless integration of these

distinct disciplines. This principle underpins my personal research objective, which I am committed to implement within the biometrics group that I am currently leading.
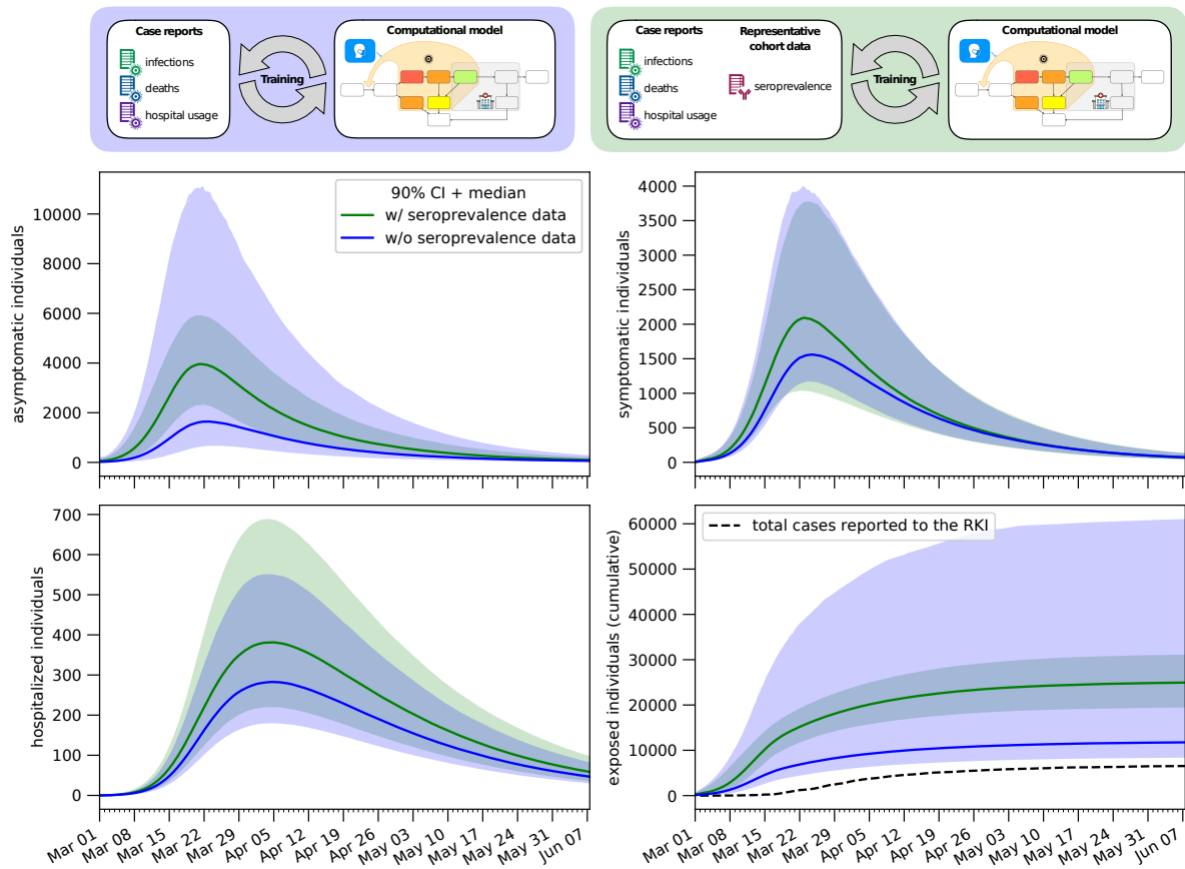

Figure 13: The dynamics of the epidemic. Model fits taking into account the KoCo19 seroprevalence data are plotted in green. Model fits without cohort information in blue. In the bottom-right panel the cumulative number of cases detected by the healthcare authorities is also plotted for reference. The bands correspond to 90% posterior credible intervals, while the solid line denotes the median value. Reproduced from [26].

To end, the group comprises experts in various domains, such as development of lab techniques, epidemiology, statistical and mathematical modelling, and machine learning. Collaborative engagement with other groups within the institute is essential to our success. Our ongoing projects encompass Tuberculosis research, where we are exploring improved diagnostic methods for both children and adults and investigating long-term sequelae following infection in multi-centre cohorts in Africa. We are also engaged in HIV-related projects, focusing on understanding of mother to newborn-child infection transmission and prevention. Additionally, we concentrate on the development of rapid detection methods for emerging infectious diseases.

The essence of the group is collaboration, working closely with medical doctors and biologists to co-create projects. This ensures that analysis is not merely an endpoint but intersects with the initial project ideas, generating new concepts from the outset. While we have experts in specific areas, our greatest strength lies in the versatility of potential analyses we can undertake.

The publications presented previously, and this entire habilitation project represents my approach to research and leadership within an analytical role, set within a robust medical and biological context.

List of Figures and Tables

Bibliography

1.   Sohrabi, C., et al., *World Health Organization declares global emergency: A review of the 2019 novel coronavirus (COVID-19).* Int J Surg, 2020. **76**: p. 71-76.

2.   Rothe, C., et al., *Transmission of 2019-nCoV Infection from an Asymptomatic Contact in Germany.* N Engl J Med, 2020. **382**(10): p. 970-971.

3.   Wolfel, R., et al., *Virological assessment of hospitalized patients with COVID-2019.* Nature, 2020. **581**(7809): p. 465-469.

4.   *COVID-19: Fallzahlen in Deutschland und weltweit. [Available from: https://www.rki.de/DE/Content/InfAZ/N/Neuartiges_Coronavirus/Fallzahlen.html. Accessed 28 April 2022]*. Robert Koch Institut.

5.   Wu, J.T., K. Leung, and G.M. Leung, *Nowcasting and forecasting the potential domestic and international spread of the 2019-nCoV outbreak originating in Wuhan, China: a modelling study.* Lancet, 2020. **395**(10225): p. 689-697.

6.   Ferguson NM, L.D., Nedjati-Gilani G, Imai N, Baguelin M, Bhatia S, *Report 9: impact of non-pharmaceutical interventions (NPIs) to reduce COVID-19 mortality and healthcare demand. London: Imperial College; 2020.*

7.   Venkatesh, A. and S. Edirappuli, *Social distancing in covid-19: what are the mental health implications?* BMJ, 2020. **369**: p. m1379.

8.   Gupta, M., et al., *COVID-19 and economy.* Dermatol Ther, 2020. **33**(4): p. e13329.

9.   Park, M., et al., *A Systematic Review of COVID-19 Epidemiology Based on Current Evidence.* J Clin Med, 2020. **9**(4).

10.   Khafaie, M.A. and F. Rahim, *Cross-Country Comparison of Case Fatality Rates of COVID-19/SARS-COV-2.* Osong Public Health Res Perspect, 2020. **11**(2): p. 74-80.

11.   Lipsitch, M., D.L. Swerdlow, and L. Finelli, *Defining the Epidemiology of Covid-19 - Studies Needed.* N Engl J Med, 2020. **382**(13): p. 1194-1196.

12.   Radon, K., et al., *Protocol of a population-based prospective COVID-19 cohort study Munich, Germany (KoCo19).* BMC Public Health, 2020. **20**(1): p. 1036.

13.   Olbrich, L., et al., *Head-to-head evaluation of seven different seroassays including direct viral neutralisation in a representative cohort for SARS-CoV-2.* J Gen Virol, 2021. **102**(10).

14.   Rubio-Acero, R., et al., *In Search of the SARS-CoV-2 Protection Correlate: Head-to-Head Comparison of Two Quantitative S1 Assays in Pre-characterized Oligo-/Asymptomatic Patients.* Infect Dis Ther, 2021: p. 1-14.

15.   Brand, I., et al., *Broad T Cell Targeting of Structural Proteins After SARS-CoV-2 Infection: High Throughput Assessment of T Cell Reactivity Using an Automated Interferon Gamma Release Assay.* Front Immunol, 2021. **12**: p. 688436.

16.   Puchinger, K., et al., *The interplay of viral loads, clinical presentation, and serological responses in SARS-CoV-2 - Results from a prospective cohort of outpatient COVID-19 cases.* Virology, 2022. **569**: p. 37-43.

17.   Kroidl, I., et al., *Studying temporal titre evolution of commercial SARS-CoV-2 assays reveals significant shortcomings of using BAU standardization for comparison.* Virol J, 2023. **20**(1): p. 200.

18.   Beyerl, J., et al., *A dried blood spot protocol for high throughput analysis of SARS-CoV-2 serology based on the Roche Elecsys anti-N assay.* EBioMedicine, 2021. **70**: p. 103502.

19.   Castelletti, N., et al., *Manuscript: A Dried Blood Spot Protocol for high-throughput quantitative analysis of SARS-CoV-2 RBD Serology based on the Roche Elecsys System.* In preparation for submission in Lancet Global Health, 2022.

20.   Rubio-Acero, R., et al., *Spatially resolved qualified sewage spot sampling to track SARS-CoV-2 dynamics in Munich - One year of experience.* Sci Total Environ, 2021. **797**: p. 149031.

21.   Pritsch, M., et al., *Prevalence and Risk Factors of Infection in the Representative COVID-19 Cohort Munich.* Int J Environ Res Public Health, 2021. **18**(7).

22.   Radon, K., et al., *From first to second wave: follow-up of the prospective COVID-19 cohort (KoCo19) in Munich (Germany).* BMC Infect Dis, 2021. **21**(1): p. 925.

23. Le Gleut, R., et al., *The representative COVID-19 cohort Munich (KoCo19): from the beginning of the pandemic to the Delta virus variant.* BMC Infect Dis, 2023. **23**(1): p. 466.

24. Barbarossa, M.V., et al., *Modeling the spread of COVID-19 in Germany: Early assessment and possible scenarios.* PLoS One, 2020. **15**(9): p. e0238559.

25. Fuderer, S., et al., *Data suggested hospitalization as pandemic-indicator already at early stages of the COVID-19 pandemic.* Mathematical Biosciences and Engineering, 2022.

26. Contento, L., et al., *Manuscript: Integrative modelling of reported case numbers and seroprevalence reveals time-dependent test efficiency and infectious contacts.* Submitted in Epidemics, 2022.

27. Lemeshow, S. and D. Robinson, *Surveys to measure programme coverage and impact: a review of the methodology used by the expanded programme on immunization.* World Health Stat Q, 1985. **38**(1): p. 65-75.

II
Complete list of publications

Original works as first or last author

1. *Risk of lung adenocarcinoma from smoking and radiation arises in distinct molecular pathways*,
Noemi Castelletti, Jan Christian Kaiser, Cristoforo Simonetto, Kyoji Furukawa, Helmut Küchenhoff, Georgios T Stathopoulos;
Carcinogenesis, Oct 2019, IF 4.944

2. *Deterministic approaches for head lice infestations and treatments*,
Noemi Castelletti, Maria Vittoria Barbarossa;
Infectious Disease Modelling, Jun 2020, IF 2.318

3. *Integrative modelling of reported case numbers and seroprevalence reveals time-dependent test efficiency and infectious contacts*,
Lorenzo Contento*, **Noemi Castelletti***, Elba Raimúndez, Ronan Le Gleut, Yannik Schälte, Paul Stapor, Ludwig Christian Hinske, Michael Hoelscher, Andreas Wieser+, Katja Radon+, Christiane Fuchs+, Jan Hasenauer+ and KoCo19 study group;
Epidemics, March 2023, IF 3.239
*Shared first authorship.

4. *Data suggested hospitalization as pandemic-indicator already at early stages of the COVID-19 pandemic*,
Stefanie Fuderer, Christina Kuttler, Michael Hoelscher, Ludwig Christian Hinske and **Noemi Castelletti**;
Mathematical Biosciences and Engineering, Dec 2022, IF 2.080

5. *Studying temporal titre evolution of commercial SARS-CoV-2 assays reveals significant shortcomings of using BAU standardization for comparison,*
Inge Kroidl*, Simon Winter*, Raquel Rubio-Acero, Abhishek Bakuli, Christof Geldmacher, Tabea M. Eser, Flora Déak, Sacha Horn, Anna Zielke, Mohamed I. M. Ahmed, Paulina Diepers, Jessica Guggenbühl, Jonathan Frese, Jan Bruger, Kerstin Puchinger, Jakob Reich, Philine Falk, Alisa Markgraf, Heike Fensterseifer, Ivana Paunovic, Angelika Thomschke, Michael Pritsch, Friedrich Riess, Elmar Saathoff, Michael Hoelscher, Laura Olbrich+, **Noemi Castelletti+**, Andreas Wieser+ and KoCo19/ORCHESTRA study group;
Virology Journal, August 2023, IF 5.916
+Shared last authorship.

6. *The representative COVID-19 Cohort Munich (KoCo19): from the beginning of the pandemic to the Delta virus variant*,
Ronan Le Gleut*, Michael Plank*, Peter Pütz, Katja Radon, Abhishek Bakuli, Raquel Rubio-Acero, Ivana Paunovic, Friedrich Rieß, Simon Winter, Christina Reinkemeyer, Yannik Schälte, Laura Olbrich, Marlene Hannes, Inge Kroidl, Ivan Noreña, Christian Janke, Andreas Wieser+, Michael Hoelscher+, Christiane Fuchs+, **Noemi Castelletti+** and the KoCo19 study group;
BMC Infectious Diseases, July 2023, IF 3.670
+Shared last authorship.

7. *Head-to-head evaluation of seven different seroassays including direct viral neutralisation in a representative cohort for SARS-CoV-2*,
Laura Olbrich*, **Noemi Castelletti***, Yannik Schälte*, Mercè Garí*, Peter Pütz, Abhishek Bakuli, Michael Pritsch, Inge Kroidl, Elmar Saathoff, Jessica Michelle Guggenbuehl Noller, Volker Fingerle, Ronan Le Gleut, Leonard Gilberg, Isabel Brand, Philine Falk, Alisa Markgraf, Flora Deák, Friedrich Riess, Max Diefenbach, Tabea Eser, Franz Weinauer, Silke Martin, Ernst-Markus Quenzel, Marc Becker, Jürgen Durner, Philipp Girl, Katharina Müller, Katja Radon, Christiane Fuchs, Roman Wölfel+, Jan Hasenauer+, Michael Hoelscher+, Andreas Wieser+, On Behalf Of The KoCo-Study Group;
Journal of General Virology, Oct 2021, IF 3.891
*Shared first authorship.

8. *The interplay of viral loads, clinical presentation, and serological responses in SARS-CoV-2 – Results from a prospective cohort of outpatient COVID-19 cases*,
Kerstin Puchinger*, **Noemi Castelletti***, Raquel Rubio-Acero, Christof Geldmacher, Tabea M. Eser, Flora Deák, Ivana Paunovic, Abhishek Bakuli, Elmar Saathoff, Alexander von Meyer, Alisa Markgraf, Philline Falk, Jakob Reich, Friedrich Riess, Philipp Girl, Katharina Müller, Katja Radon, Jessica Michelle Guggenbuehl Noller, Roman Wölfel, Michael Hoelscher, Inge Kroidl+, Andreas Wieser+, Laura Olbrich+, KoCo19 study team;
Virology, Feb 2022, IF 3.513
*Shared first authorship.

9. *The Prospective COVID-19 Post-Immunization Serological Cohort in Munich (KoCo-Impf): Risk Factors and Determinants of Immune Response in Healthcare Workers,*
Christina Reinkemeyer*, Yeganeh Khazaei*, Maximilian Weigert, Marlene Hannes, Ronan Le Gleut, Michael Plank, Simon Winter, Ivan Noreña, Theresa Meier, Lisa Xu, Raquel Rubio-Acero, Simon Wiegrebe, Thu Giang Le Thi, Christiane Fuchs, Katja Radon, Ivana Paunovic, Christian Janke, Andreas Wieser, Helmut Küchenhoff, Michael Hoelscher, **Noemi Castelletti** and KoCo-Impf/ORCHESTRA working group;
Viruses, July 2023, IF 5.818

10. *In Search of the SARS-CoV-2 Protection Correlate: Head-to-Head Comparison of Two Quantitative S1 Assays in Pre-characterized Oligo-/Asymptomatic Patients*,
Raquel Rubio-Acero*, **Noemi Castelletti***, Volker Fingerle, Laura Olbrich, Abhishek Bakuli, Roman Wölfel, Philipp Girl, Katharina Müller, Simon Jochum, Matthias Strobl, Michael Hoelscher, Andreas Wieser+, KoCo19 study team;
Infectious Disease and Therapy, Sep 2021, IF 6.119
*Shared first authorship.

Original works as co-author

1. *Impact of Omicron Variant Infection on Assessment of Spike-Specific Immune Responses Using the EUROIMMUN Quan-T-Cell SARS-CoV-2 Assay and Roche Elecsys Anti-SARS-CoV-2-S*,
Mohamed I. M. Ahmed*, Michael Plank*, **Noemi Castelletti**, Paulina Diepers, Tabea M. Eser, Raquel Rubio-Acero, Ivan Noreña, Christina Reinkemeyer, Dorinja Zapf, Michael Hoelscher, Christian Janke, Andreas Wieser+, Christof Geldmacher+ and on behalf of the KoCo19/ORCHESTRA Study Group;
Diagnostics, March 2023, IF 3.992

2. *Modeling the spread of COVID-19 in Germany: Early assessment and possible scenarios*,
   Maria Vittoria Barbarossa, Jan Fuhrmann, Jan H Meinke, Stefan Krieg, Hridya Vinod Varma,
   Noemi Castelletti, Thomas Lippert;
   PLoS One, Sep 2020, IF 3.752

3. *A dried blood spot protocol for high throughput analysis of SARS-CoV-2 serology based on the Roche Elecsys anti-N assay*,
   Jessica Beyerl*, Raquel Rubio-Acero*, **Noemi Castelletti**, Ivana Paunovic, Inge Kroidl, Zohaib N Khan, Abhishek Bakuli, Andreas Tautz, Judith Oft, Michael Hoelscher, Andreas Wieser and the KoCo19 Study group;
   EBioMedicine, Aug 2021, IF 8.143

4. *Broad T Cell Targeting of Structural Proteins After SARS-CoV-2 Infection: High Throughput Assessment of T Cell Reactivity Using an Automated Interferon Gamma Release Assay*,
   Isabel Brand*, Leonard Gilberg*, Jan Bruger*, Mercè Garí, Andreas Wieser, Tabea M Eser, Jonathan Frese, Mohamed I M Ahmed, Raquel Rubio-Acero, Jessica M Guggenbuehl Noller, **Noemi Castelletti**, Jana Diekmannshemke, Sophie Thiesbrummel, Duc Huynh, Simon Winter, Inge Kroidl, Christiane Fuchs, Michael Hoelscher+, Julia Roider+, Sebastian Kobold+, Michael Pritsch+, Christof Geldmacher+;
   Frontiers in Immunology, May 2021, IF 8.786

5. *Determinants of anti-S immune response at 6 months after COVID-19 vaccination in a multicentric European cohort of healthcare workers – ORCHESTRA project*,
   Giulia Collatuzzo, Giovanni Visci, Francesco S. Violante, Stefano Porru, Gianluca Spiteri, Maria Grazia Lourdes Monaco, Francesca Larese Fillon, Corrado Negro, Christian Janke, **Noemi Castelletti**, Giuseppe De Palma, Emanuele Sansone, Dana Mates, Silvia Teodorescu, Eleonóra Fabiánová, Jana Béresová, Luigi Vimercati, Silvio Tafuri, Mahsa Abedini, Giorgia Ditano, Shuffield S. Asafo, Paolo Boffetta, and Orchestra WP5 Working Group;
   Frontiers in Immunology, Sep 2022, IF 8.786

6. *Determinants of anti-S immune response at 9 months after COVID-19 vaccination in a multicentric European cohort of healthcare workers - ORCHESTRA project*,
   Giulia Collatuzzo, Vittorio Lodi, Daniela Feola, Giuseppe De Palma, Emanuele Sansone, Emma Sala, Christian Janke, **Noemi Castelletti**, Stefano Porru, Gianluca Spiteri, Maria Grazia Lourdes Monaco, Francesca Larese Filon, Corrado Negro, Luca Cegolon, Jana Beresova, Eleonora Fabianova, Lucia A. Carrasco-Ribelles, Pere Toràn-Monserrat, Marta Maria Rodriguez-Suarez, Guillermo Fernandez-Tardon, Shuffield S. Asafo, Giorgia Ditano, Mahsa Abedini and Paolo Boffetta;
   Viruses, Nov 2022, IF 3.513

7. *Prediction of surface area size in orbital floor and medial orbital wall fractures based on topographical subregions*,
   Carl-Peter Cornelius, Tobias Stiebler, Peter Mayer, Wenko Smolka, Christoph Kunz, Beat Hammer, Claude Jaquiéry C, Carlos Buitrago-Téllez, Christoph Sebastian Leiggener, Marc Christian Metzger, Frank Wilde, Laurent Audigé, Monika Probst, Edward Bradley Strong, **Noemi Castelletti**, Joachim Prein, Florian Andreas Probst;
   Journal of Craniomaxillofacial Surgery, Jul 2021, IF 2.933

8. *Enhanced Spike-specific, but attenuated Nucleocapsid-specific T cell responses upon SARS-CoV-2 breakthrough versus non-breakthrough infections*,
   Mohamed Ibraheem Mahmoud Ahmed*, Paulina Diepers*, Christian Janke, Michael Plank, Tabea M Eser, Raquel Rubio-Acero, Anna Fuchs, Olga Baranov, **Noemi Castelletti**, Inge Kroidl, Laura Olbrich, Bernadette Bauer, Danni Wang, Martina Prelog, Johannes G Liese, Christina

Reinkemeyer, Michael Hoelscher, Philipp Steininger, Klaus Überla, Andreas Wieser, Christof Geldmacher;
Frontiers in Immunology, Dec 2022, IF 8.786

9. *Early Nucleocapsid-specific T cell responses correlate with SARS-CoV-2 control in the upper airways and reduced systemic inflammation before seroconversion*,
Tabea M. Eser, Olga Baranov, Manuel Huth, Mohammed I.M. Ahmed, Flora Deák, Kathrin Held, Kami Pekayvez, Alexander Leunig, Nicolai Leo, Georgios Pollakis, Raquel Rubio-Acero, Jakob Reich, Philine Falk, Alissa Markgraf, Kerstin Puchinger, **Noemi Castelletti**, Laura Olbrich, Kanika Vanshylla, Florian Klein, Andreas Wieser, Jan Hasenauer, Inge Kroidl, Michael Hoelscher and Christof Geldmacher;
Nature Communications, Feb 2023, IF 17.694

10. *Comparison of signalment, clinical, laboratory and radiographic parameters in cats with feline asthma and chronic bronchitis*,
Maike Grotheer, Johannes Hirschberger, Katrin Hartmann, **Noemi Castelletti**, Bianka Schulz;
Journal Feline Medicine and Surgery, Jul 2020, IF 2.162

11. *Clinical relevance of intradermal test results in atopic dogs*,
Stefanie Mallmann, Christoph J Klinger, Janine Claßen, Iris Wagner, Andre Klima, **Noemi Castelletti**, Ralf S Müller;
Tierarztl Prax Ausg K Kleintiere Heimtiere, Oct 2021, 0.29

12. *Socioeconomic and risk-related drivers of compliance with measures to prevent SARS- CoV-2 infection: evidence from the Munich-based KoCo19 study*,
Sara Pedron, Michael Laxya, Katja Radon, Ronan Le Gleut, **Noemi Castelletti**, Jessica Michelle Guggenbüehl Noller, Maximilian Nikolaus Diefenbach, Michael Hölscher, Reiner Leidl+, Lars Schwettmann+ and the KoCo19 collaboration group;
BMC, April 2023, IF 11.806

13. *Prevalence and Risk Factors of Infection in the Representative COVID-19 Cohort Munich*,
Michael Pritsch*, Katja Radon*, Abhishek Bakuli*, Ronan Le Gleut*, Laura Olbrich, Jessica Michelle Guggenbüehl Noller, Elmar Saathoff, Noemi Castelletti, Mercè Garí, Peter Pütz, Yannik Schälte, Turid Frahnow, Roman Wölfel, Camilla Rothe, Michel Pletschette, Dafni Metaxa, Felix Forster, Verena Thiel, Friedrich Rieß, Maximilian Nikolaus Diefenbach, Günter Fröschl, Jan Bruger, Simon Winter, Jonathan Frese, Kerstin Puchinger, Isabel Brand, Inge Kroidl, Jan Hasenauer+, Christiane Fuchs+, Andreas Wieser+, Michael Hoelscher+, On Behalf Of The **KoCo Study Group**;
Internation Journal of Environmental Research and Public Health, Mar 2021, IF 2.849

14. *Protocol of a population-based prospective COVID-19 cohort study Munich, Germany (KoCo19)*,
Katja Radon*, Elmar Saathoff*, Michael Pritsch, Jessica Michelle Guggenbühl Noller, Inge Kroidl, Laura Olbrich, Verena Thiel, Max Diefenbach, Friedrich Riess, Felix Forster, Fabian Theis+, Andreas Wieser+, Michael Hoelscher+, and the **KoCo19 collaboration group**;
BMC Public Health, Jun 2020, IF 3.980

15. *From first to second wave: follow-up of the prospective COVID-19 cohort (KoCo19) in Munich (Germany)*,
Katja Radon*, Abhishek Bakuli*, Peter Pütz*, Ronan Le Gleut*, Jessica Michelle Guggenbuehl Noller, Laura Olbrich, Elmar Saathoff, Mercè Garí, Yannik Schälte, Turid Frahnow, Roman Wölfel, Michael Pritsch, Camilla Rothe, Michel Pletschette, Raquel Rubio-Acero, Jessica Beyerl, Dafni Metaxa, Felix Forster, Verena Thiel, **Noemi Castelletti**, Friedrich Rieß, Maximilian N Diefenbach, Günter Fröschl, Jan Bruger, Simon Winter, Jonathan Frese, Kerstin Puchinger, Isabel Brand, Inge Kroidl, Andreas Wieser+, Michael Hoelscher+, Jan Hasenauer+, Christiane Fuchs+, KoCo19 study group;

BMC Infectious Diseases, Sep 2021, IF 3.670

16. *Spatially resolved qualified sewage spot sampling to track SARS-CoV-2 dynamics in Munich - One year of experience*,
Raquel Rubio-Acero*, Jessica Beyerl*, Maximilian Muenchhoff*, Marc Sancho Roth, **Noemi Castelletti**, Ivana Paunovic, Katja Radon, Bernd Springer, Christian Nagel, Bernhard Boehm, Merle M Böhmer, Alexander Graf, Helmut Blum, Stefan Krebs, Oliver T Keppler, Andreas Osterman, Zohaib Nisar Khan, Michael Hoelscher, Andreas Wieser, KoCo19-Study Group;
Science of the Total Environment, Nov 2021, IF 10.753

17. *Estimating long-term health risks after breast cancer radiotherapy: merging evidence from low and high doses*,
Cristoforo Simonetto, Daniel Wollschläger, Pavel Kundrát, Alexander Ulanowski, Janine Becker, **Noemi Castelletti**, Denise Güthlin, Elena Shemiakina, Markus Eidemüller;
Radiation and Environment Biophysics, Aug 2021, IF 1.925

III

Reprints of publications with first and last authorships

Publication 1:

Studying temporal titre evolution of commercial SARS-CoV-2 assays reveals significant shortcomings of using BAU standardization for comparison

Inge Kroidl*, Simon Winter*, Raquel Rubio-Acero, Abhishek Bakuli, Christof Geldmacher, Tabea M. Eser, Flora Déak, Sacha Horn, Anna Zielke, Mohamed I. M. Ahmed, Paulina Diepers, Jessica Guggenbühl, Jonathan Frese, Jan Bruger, Kerstin Puchinger, Jakob Reich, Philine Falk, Alisa Markgraf, Heike Fensterseifer, Ivana Paunovic, Angelika Thomschke, Michael Pritsch, Friedrich Riess, Elmar Saathoff, Michael Hoelscher, Laura Olbrich+, **Noemi Castelletti+**, Andreas Wieser+ and KoCo19/ORCHESTRA study group

Check for updates

Studying temporal titre evolution of commercial SARS-CoV-2 assays reveals significant shortcomings of using BAU standardization for comparison

Inge Kroidl[1,2†], Simon Winter[1†], Raquel Rubio-Acero[1,3], Abhishek Bakuli[1], Christof Geldmacher[1,2], Tabea M. Eser[1,2], Flora Déak[1], Sacha Horn[1], Anna Zielke[1], Mohamed I. M. Ahmed[1,2], Paulina Diepers[1], Jessica Guggenbühl[1], Jonathan Frese[1], Jan Bruger[1], Kerstin Puchinger[1], Jakob Reich[1], Philine Falk[1], Alisa Markgraf[1], Heike Fensterseifer[1], Ivana Paunovic[1,3,4], Angelika Thomschke[1], Michael Pritsch[1], Friedrich Riess[1], Elmar Saathoff[1], Michael Hoelscher[1,2,4,5], Laura Olbrich[1,2†], Noemi Castelletti[1,4,6†] and Andreas Wieser[1,2,3,4*†] on behalf of KoCo19/ORCHESTRA Study Group

Abstract

Background Measuring specific anti-SARS-CoV-2 antibodies has become one of the main epidemiological tools to survey the ongoing SARS-CoV-2 pandemic, but also vaccination response. The WHO made available a set of well-characterized samples derived from recovered individuals to allow normalization between different quantitative anti-Spike assays to defined Binding Antibody Units (BAU).

Methods To assess sero-responses longitudinally, a cohort of ninety-nine SARS-CoV-2 RT-PCR positive subjects was followed up together with forty-five vaccinees without previous infection but with two vaccinations. Sero-responses were evaluated using a total of six different assays: four measuring anti-Spike proteins (converted to BAU), one measuring anti-Nucleocapsid proteins and one SARS-CoV-2 surrogate virus neutralization. Both cohorts were evaluated using the Euroimmun Anti-SARS-CoV-2-ELISA anti-S1 IgG and the Roche Elecsys Anti-SARS-CoV-2 anti-S1 assay.

Results In SARS-CoV-2-convalesce subjects, the BAU-sero-responses of Euroimmun Anti-SARS-CoV-2-ELISA anti-S1 IgG and Roche Elecsys Anti-SARS-CoV-2 anti-S1 peaked both at 47 (43–51) days, the first assay followed by a slow decay thereafter (> 208 days), while the second assay not presenting any decay within one year. Both assay values in BAUs are only equivalent a few months after infection, elsewhere correction factors up to 10 are necessary. In contrast, in infection-naive vaccinees the assays perform similarly.

Conclusion The results of our study suggest that the establishment of a protective correlate or vaccination booster recommendation based on different assays, although BAU-standardised, is still challenging. At the moment

---

†Inge Kroidl and Simon Winter share first authorship.

†Laura Olbrich, Noemi Castelletti and Andreas Wieser share last authorship.

*Correspondence:
Andreas Wieser
Andreas.Wieser@lmu.de
Full list of author information is available at the end of the article

the characteristics of the available assays used are not related, and the BAU-standardisation is unable to correct for that.

Keywords Antibody, COVID-19, Nucleocapsid, RBD, SARS-CoV-2, Serology, Spike, Binding antibody units

Background

Since the surge of the SARS Corona Virus 2 (SARS-CoV-2) pandemic, considerable progress has been made regarding diagnosis, treatment and prevention of COVID-19. Although by mid-2022, more than 545 million people have been infected and more than 6 million died, serological responses following infection or vaccination are still not fully understood and a correlate of protection has not been identified yet [1, 2].

Describing the natural course of the disease in detail may be key to understanding the immune mechanisms and subsequent protection, either through previous infection or vaccination, or both. Natural infection with SARS-CoV-2 reduces the risk of subsequent infections with the wild-type virus by 82–89% for at least 6 months [3, 4]. In addition, SARS-CoV-2 vaccines protection against symptomatic COVID-19 disease was reported to be 95% for BNT162b2, 94% for mRNA 1273, 70% for ChAdOx1 and 50% for Sinovac [5–9]. The difference in the estimated protective effect of the vaccines correlates with the elicited immune responses, which have been considerably higher in the mRNA vaccines compared to vector-based products [10]. The longevity of this protective effect however, is a matter of debate.

In addition, viral variants of SARS-CoV-2 have emerged since and acquired immune protection was found to be reduced [11]. Large studies have now demonstrated breakthrough infections in vaccinated individuals even during the peak of the antibody response, i.e., weeks or months after completion of the vaccination course [12–15]. A waning of the immune response against SARS CoV-2 was suggested by Mizrahi et al. [14], demonstrating a 1.5 times increased risk for breakthrough infections with the Delta-variant 6 month after vaccination with BioNTech/Pfizer, compared to a 3 month time lag. In an in-house study in early 2022 we observed many breakthrough infections with the Omicron variant regardless of vaccination status or previous infections, including recent infection with the Delta-variant.

Several serological studies have tried to estimate the duration and dynamics of antibody responses following SARS-CoV-2 infection, yielding ambiguous results. Long et al. [16] reported rapid waning of nucleocapsid antibodies in the first 3 months after infection [16, 17]. Similarly, Ibarrondo et al. [18] described a half-life of antibodies against the receptor binding domain (RBD)

of 36 days. In contrast, Dan et al. [19], Flehmig et al. [20] and Ripperger et al. [21] reported that immunity against RBD and the anti-Spike domain persisted for at least 7 months. The reasons for these different reports may be e.g. heterogeneity of population, assays used etc.

Several studies highlighted considerable differences in the readout of serological assays, indicating a hampered cross-comparison. In a report by Harris et al. [22], anti-nucleocapsid antibodies measured with the SARS-CoV-2 IgG Assay from Abbott (Abbott Diagnostic, IL, USA), or anti S1 antibodies measured with the Euroimmun Anti-SARS- CoV-2 ELISA IgG (Euroimmun, Lubeck, Germany) were declining within few months. Similarly, plasma from the same subjects measured for anti-nucleocapsid or anti RBD antibodies respectively using the Elecsys Anti-SARS-CoV-2 Roche assays (Roche, Mannheim, Germany), demonstrated stable values over the same time [22, 23].

To improve standardization of serological anti-spike measurements, the WHO made available a set of well-characterized samples deriving from SARS-CoV-2-recovered individuals and shipped by late 2020/early 2021 to laboratories requesting it [24]. These samples were subsequently used to normalize results of different quantitative anti-Spike test systems to standardized units termed "BAU" (Binding Antibody Units) [25]. Many different manufacturers have since published correction factors or formulas to calculate BAU values from their quantitative anti-Spike assays [26]. In addition, laboratories have provided SARS-CoV-2 serology results in BAU to patients and physicians in routine care [27, 28]. Of note, the use of this WHO standard was encouraged to cross validate internal standards, effectively generating a chain of standards [29].

Following the suggested approach, we compared anti-spike antibody titres quantitatively at defined and standardized time points spanning over 18 months after infection using different commercially available test kits. Therefore, we used samples derived from ninety-nine SARS-CoV-2-infected individuals and from forty-five participants with no history of previous infection but with two vaccinations. The anti-spike quantitative responses were calculated to BAU units as suggested by the manufacturers and compared. Two assays reacting only to infection were added to the analysis.

Kroidl *et al. Virology Journal*   (2023) 20:200

Page 3 of 12

Methods

Cohort members: patients and vaccinees

From April to December 2020, 66 households were included in the study with all household members, irrespective of a SARS-CoV-2 infection (Fig. 1A). A total of 145 non-vaccinated participants were enrolled, including 102 members infected with SARS CoV-2. For the three children below the age of 14, no venous blood draw was performed, for the remaining ninety-nine patients venous blood was drawn as soon as possible after the first positive RT-PCR and at multiple time points thereafter.

Additionally, it was possible to recruit forty-five participants with no history of previous infection but with two vaccinations (Fig. 1B). A possible previous infection was excluded with all the following criteria: (i) no past positive RT-PCR for SARS-CoV-2, (ii) past COVID-19 like symptoms had to be followed by a negative RT-PCR, (iii) negative serology deriving from infection (Roche Elecsys Anti-SARS-CoV-2 anti-N, see next paragraph for details), and (iv) negative SARS-CoV-2 surrogate virus neutralization test (GenScript®, see next paragraph for details). The latest performed only at recruitment, end of follow-up and at sporadic time-points.

Sample collection was performed as previously presented [30].

On December 1st 2020, this cohort joined the ORCHESTRA (Connecting European Cohorts to Increase Common and Effective Response to SARS-CoV-2 Pandemic) project but was not previously published.

Laboratory analysis

Serologic assays were performed using EDTA-plasma samples and were conducted as previously published [23, 30, 31]. The serological assays used were chosen if: available in large quantities, performable with semi-automated workup, acceptable pricing, licensed for the use in Europe, and well-described in performance [23]. The manufacturer's instructions were followed for all assays. For sample time-points of PCR-positive participants the following assays were performed: Euroimmun Anti-SARS-CoV-2-ELISA anti-S1 IgA/IgG (hereafter called EI-S1-IgA/EI-S1-IgG; Euroimmun, Lübeck, Germany), Quantitative Euroimmun Anti-SARS-CoV-2-QuantiVac ELISA (IgG) (hereafter called EI-S1-IgG-quant;
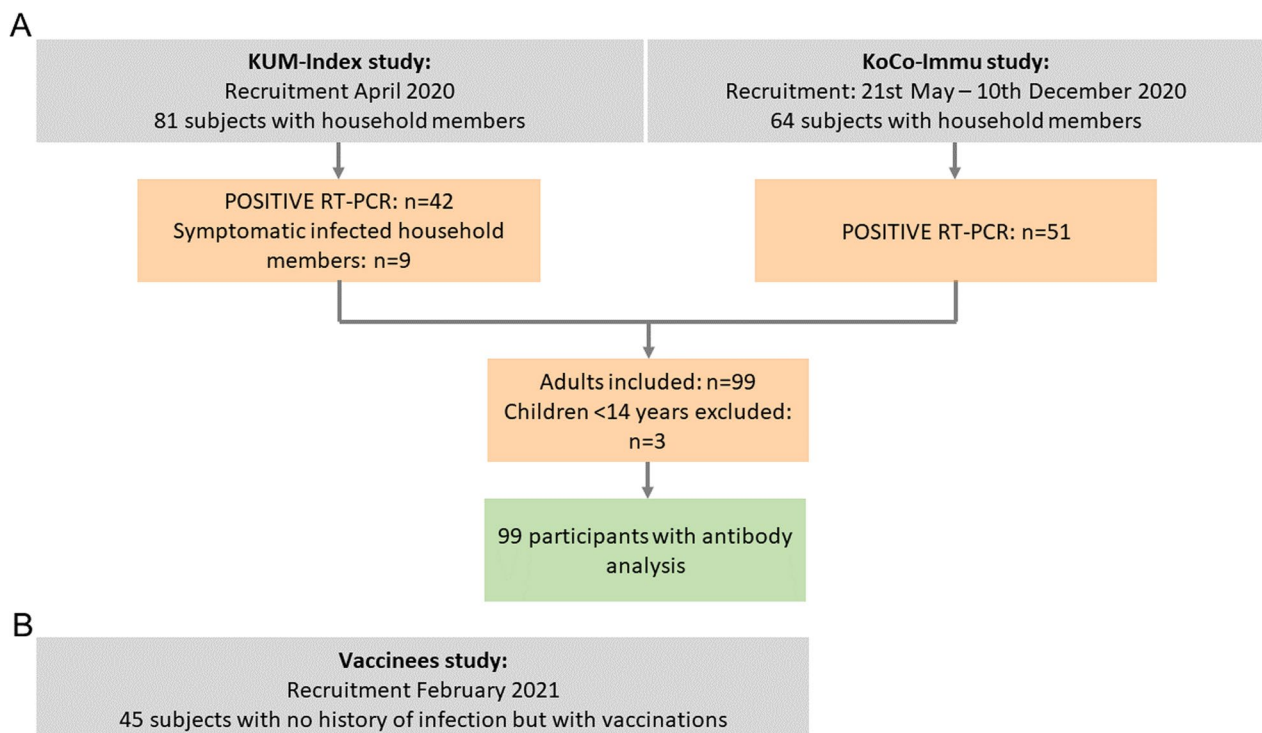
Fig. 1 Cohort flow chart. **A** Cohort of non-vaccinated SARS-CoV-2 RT-PCR positive subjects. Two recruitment strategies were used: fifty-one participants, who had a SARS CoV-2 infection in February/March 2020 were recruited in April 2020 together with their household members (KUM-Index-study). Forty-two of them had a positive PCR and additional 9 household members developed SARS CoV-2 specific antibodies. From 21 May till 10 December 2020 another fifty-one SARS-CoV-2 infected individuals were recruited as early as possible after their first positive RT-PCR (Koco19-Immu-Study). **B** Cohort of vaccinees. Forty-five participants with no history of infection but with two vaccinations were recruited

Kroidl *et al. Virology Journal*   (2023) 20:200

Page 4 of 12

Euroimmun, Lübeck, Germany), Roche Elecsys Anti-SARS-CoV-2 anti-N and Elecsys Anti-SARS-CoV-2 S anti-S1 (hereafter called Ro-N-Ig and Ro-RBD-Ig-quant, respectively; Roche, Mannheim, Germany) and GenScript® (hereafter called GS-cPass, Piscataway, New Jersey, USA). For sample time-points of vaccinees two assays were performed: Ro-RBD-Ig-quant and Quantitative Euroimmun Anti-SARS-CoV-2-QuantiVac ELISA (IgG) (hereafter called EI-S1-IgG-quant; Euroimmun, Lübeck, Germany). Values of EI-S1-IgG-quant and Ro-RBD-Ig-quant could be obtained in BAUs.

Multiple measurements of the same sample (operational replicates) were performed on different days with different operators and lots to control the intra-variability of all the assays. The very good intra-variability of EI-S1-IgG and Ro-N-Ig was already published [23]. For GS-cPass and Ro-RBD-Ig-quant evaluation was performed with in house samples and similar results as for the published assays were obtained (data now shown here).The World Health Organization (WHO) reference sera (National Institute for Biological Standards and Control [NIBSC] code 20/268) were measured on the assays EI-S1-IgG, EI-S1-IgG-quant, Ro-N-Ig and Ro-RBD-Ig-quant in replicates (n=3) to standardize the results [31]. In this analysis we present only the mean value.

Data analysis

Prior to analysis, the data was cleaned and locked, so that no new measurements can be included after review. For operational replicates, the first measurement of EI-S1-IgG was used, since small losses compared to fresh samples were found. In the case of Ro-N-Ig and GS-cPass the latest measurement was included, while for Ro-RBD-Ig-quant the most diluted value still within the linear range was selected to calculate the true unit count. The software R, 4.0.5 (https://cloud.r-project.org/) was used to perform statistical analysis and visualisation. Longitudinal serological dynamics were analysed applying the LOESS (locally estimated scatterplot smoothing or local regression) method with the 95% CI.

Results

Cohort description

After recruitment of 190 individuals, a total of 144 participants were included in the analysis, 69% (99/144) of which were oligo-symptomatic non-vaccinated SARS-CoV-2 RT-PCR positives and the remaining were subjects with no history of previous infection but with two vaccinations (hereafter called vaccinees).

For the non-vaccinated RT-PCR positive individuals a total of 438 study visits were conducted, between 1 and 8 per participant. The median age at enrollment was 37.8 years; 61% (60/99) of the participants were females. For

the vaccinees (29/45, 64.4% females) 250 blood samples were collected, 92 (36.8%) before and 158 (63.2%) after the second vaccination. The time of collection after the second vaccination varied between 1 and 236 days (mean=43.57 days and median=6 days). In the first vaccination the vaccines used were Biontech Pfizer (27/45, 60.0%), AstraZeneca (11/45, 24.4%) and Johnson & Johnson (6/45, 13.3%), while for the second vaccine dose, it changed to Biontech Pfizer (37/45, 82.2%), Moderna (5/45, 11.1%) and AstraZeneca (1/45, 2.2%).

Premedical history and symptoms during infection

A small percentage of the non-vaccinated PCR-positive participants reported chronic medical conditions (diabetes mellitus, heart disease or hypertension, 13%) and an additional 5% reported known allergies. During the initial phase of the SARS CoV-2 infection, symptoms were recorded and classified according to the WHO classification (Additional file 1: Fig. S1) [29, 30]. In total, 7% (7/99) of the participants were classified as WHO-category 1, 44% (43/99) as WHO-category 2 and 48% (47/99) as WHO-category 3. One third (14/43) of the WHO-category 2 patients reported clinically significant involvement of the lower respiratory tract, while for WHO-category 3 patients the proportion rose to two thirds (30/47). Additionally, two participants had to be hospitalized due to the severity of the symptoms. For further analysis, we divided the participants in two groups, WHO 1–2 and WHO ≥ 3. Analysis of WHO-classification can be found in the Additional file 1.

Sero-positivity at baseline measurements after SARS-CoV-2 infection

The longitudinal serological dynamics of non-vaccinated SARS-CoV-2 RT-PCR positive individuals was followed using five assays for head-to-head comparison (Fig. 2). The baseline measurements yielded positive sero-responses in 57% (56/99) of the samples for EI-S1-IgA, 44% (43/99) for EI-S1-IgG, 33% (32/99) for Ro-RBD-Ig-quant, 53% (52/99) for Ro-N-Ig, and 83% (81/99) for GS-cPass. 31% (30/99) of the cohort was seroconverted in all assays, while negative results in all assays were recorded in 16% (16/99). Over time, 79% (78/99) of participants seroconverted as detected by all assays while 9% (9/99) did not develop any or solely very low antibody titres (GS-cPass or GS-cPass and Ro-N-Ig/EI-S1-IgA/G positive). For three subjects, a potentially false positive RT-PCR test result was discussed due to complete lack of any clinical symptoms or other signs for SARS-CoV-2 infection. The remaining 12% (12/99) of participants had a measurable sero-response in at least three of the five assays used.

Kroidl *et al. Virology Journal*   (2023) 20:200

Page 5 of 12
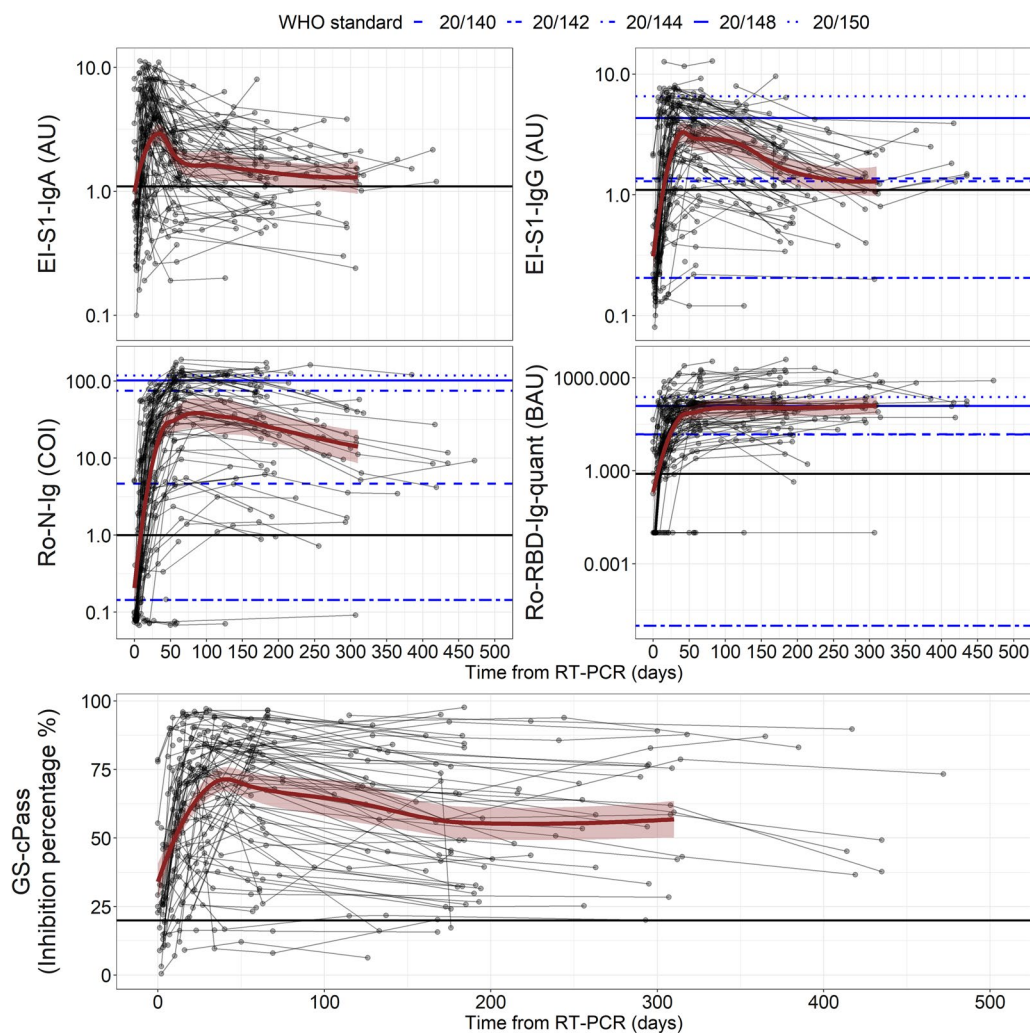
Fig. 2 Longitudinal serological dynamics of SARS-CoV-2 RT-PCR positive cohort. Solid black horizontals line denote the cut-off for positivity. Blue lines represent the WHO reference panel for anti-SARS-CoV-2 immunoglobulin (NIBSC code 20/268). Each line represents one subject, the dots represent the individual samples. All assays were performed from the same sample in a head-to-head comparison. Top left: Euroimmun Anti Spike IgA; top right: Euroimmun Anti-Spike IgG; middle left: Roche Anti-Nucleocapsid; middle right: Roche Anti Spike/RBD; bottom: GenScript neutralization surrogate test

Time to seroconversion was determined in those participants with initial negative readouts. Here, mean EI-S1-IgA positivity was detected 20 days (min = 8 days, max = 69 days) after symptom onset, EI-S1-IgG positivity after 31 days (min = 14 days, max = 118 days), Ro-RBD-Ig-quant positivity after 20 days (min = 7 days, max = 133 days), positive Ro-N-Ig reaction after 30 days (min = 10 days, max = 118 days), and GS-cPass-positivity after 16 days (min = 11 days, max = 31 days).

Longitudinal serological dynamics after SARS-CoV-2 infection

Subsequently, we compared the quantitative reactivity of the test systems over time (Fig. 2). For the anti-S1/anti-RBD tests, the EI-S1-IgA peaked fastest (35, 31–39 days) and declined rapidly at first, followed by a phase of slower decay at > 86 days. Using the same antigen but measuring IgG, we saw the peak/slope change much later (47, 43–51 days) and a subsequent slower decay (> 208 days). Values obtained by the Ro-RBD-Ig-quant test rose similarly fast (47, 43–51 days), however, without any decline over time as observed in both EI-S1-IgG and IgA assays. Comparing the results with GS-cPass we observed an initial peak reached after 43 (39–47) days which was similar to the dynamics measured by EI-S1-IgG and Ro-RBD-Ig-quant. Afterwards, the inhibition declines and plateaus at a level of about 55.5% (55–56%). The sero-response of the Ro-N-Ig assay peaks later (75,

Kroidl *et al. Virology Journal*   (2023) 20:200

Page 6 of 12

71–78 days) compared to EI-S1-IgG and subsequently declined almost linearly (122, 118–126 days).

In a second step, we aimed to compare the non-quantitative readouts of EI-S1-Ig with the quantitative readouts of Ro-RBD-Ig-quant. For this purpose non-quantitative EI-S1-Ig values were transformed into quantitative EI-S1-Ig-quant (called EI-S1-Ig-quant-trafo). Details on the procedure are outlined in the Additional file 1 and the longitudinal analysis is presented in Fig. 3A. After standardization for BAU, the paired values of EI-S1-IgG-quant-trafo and Ro-RBD-Ig-quant were compared (Fig. 3B). The EI-S1-IgG-quant-trafo peaked at day 43 (40–47) with a

mean value of 147.04 (116.88–184.98) BAU, while Ro-RBD-Ig-quant reached its maximum at day 47 (43–51) with a mean value of 100.20 (65.09–154.26) BAU.

EI-S1-IgG-quant-trafo and Ro-RBD-Ig-quant assays after SARS-CoV-2 infection

In order to examine in more depth the differences between the assays EI-S1-IgG-quant-trafo and Ro-RBD-Ig-quant, three time bands for time since symptom onset were defined: (i) short time (0–20 days, increase phase of antibody titres), (ii) intermediate time (70–150 days, plateaued antibody titers) and (iii) long time (170–250 days,
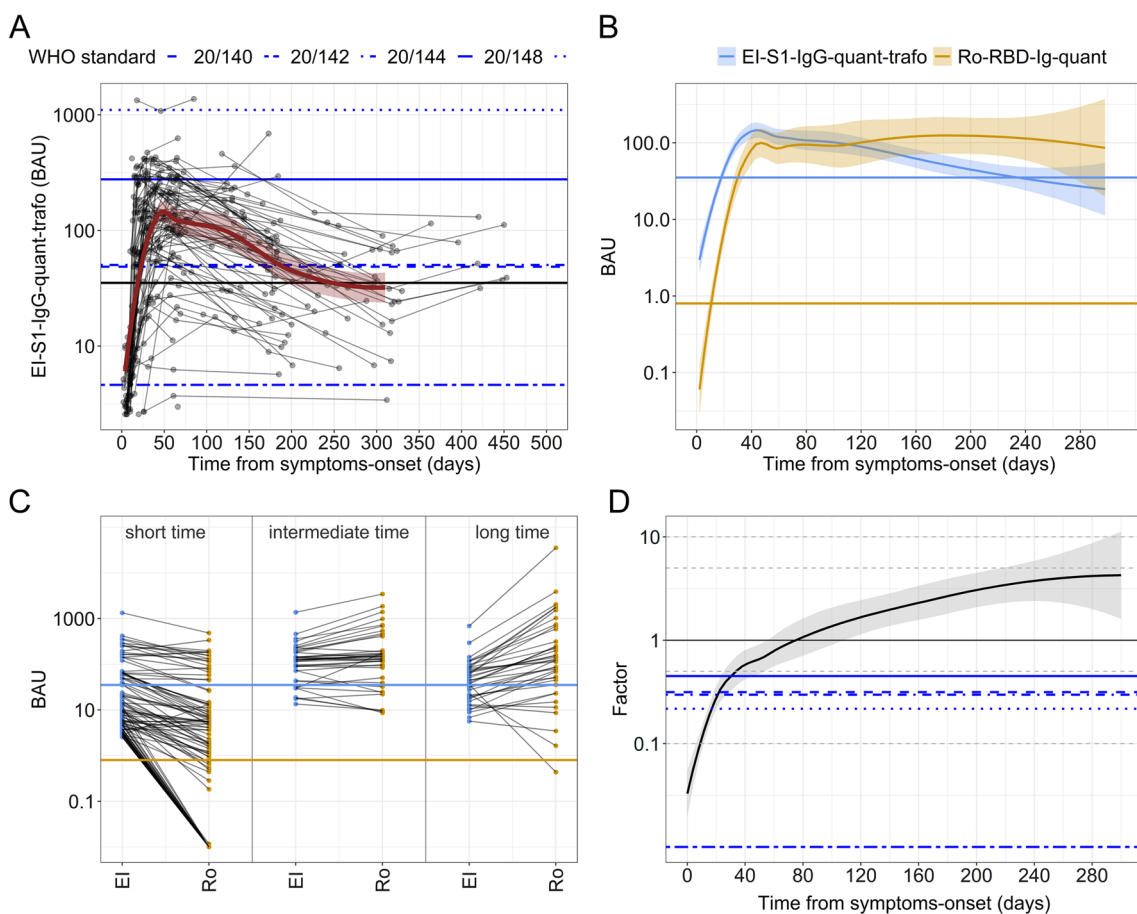
Fig. 3 Comparison of quantitative serology of individual patients (PCR-positive cohort) over time for EI-S1-IgG-quant-trafo and Ro-RBD-Ig-quant. When assays are compared, the EI-S1-IgG-quant-trafo is represented in blue while Ro-RBD-Ig-quant in yellow. Blue lines represent the WHO reference panel for anti-SARS-CoV-2 immunoglobulin (NIBSC code 20/268). Solid horizontal lines represent the cut-off for positivity. **A** Longitudinal EI-S1-IgG-quant-trafo serology data over time. Each line represents one subject, the dots represent the individual samples. The red solid line shows the LOESS (locally estimated scatterplot smoothing or local regression) estimations with CI in translucent red. **B** Aggregated BAU value curves of the subjects over time for the two tests. EI-S1-IgG-quant-trafo rises faster, reaches similar values than Ro-RBD-Ig-quant between days 70 and 150 after infection and then drops to about 1/10th of the value observed in Ro-RBD-Ig-quant after one year (please note that here almost half of the samples measured in EI-S1-IgG-quant-trafo are already below the positivity threshold). **C** Parallel coordinate plot dividing the time from symptom onset into three intervals: short (0–20 days), intermediate (70–150 days) and long (170–250 days). EI denotes the EI-S1-IgG-quant-trafo assay while Ro represents the Ro-RBD-Ig-quant assay. **D** The Quotient of the two BAU values depicted in log10 scale over time (Ro-RBD-Ig-quant/EI-S1-IgG-quant-trafo). At the Factor Value of 1, the BAU values are identical. This occurs only in a short timeframe about 80 days post symptom onset

Kroidl *et al. Virology Journal*   (2023) 20:200

Page 7 of 12

decrease phase of antibody titres). Time intervals are not equally long and there are gaps in the timeline to better define the three phases of the serological dynamic.

The parallel coordinate plot (Fig. 3C) demonstrates that the two assays yielded differing results and were only similar in the intermediate time band. Subsequently, the quotient between the measured BAU values was calculated in an effort to quantify the differences observed, whereby a factor of 1 implied the same readout in both tests. This, however, was only observed at day 80 after symptom onset with values differing greatly before and after (Fig. 3D). Shortly after infection, multiplication by factor 0.1 was necessary to obtain similar values of EI-S1-IgG-quant-trafo compared to Ro-RBD-Ig-quant, whereas after 250 days the factor was 5. In addition, the differences are likely to be underestimated, as a correction was no longer possible if one test dropped below

detection limit. This occurred in almost half (48.65%; 18/37) of the EI-S1-IgG-quant-trafo values and only in less than 5% (2/41) in the Ro-RBD-Ig-quant at the 250 day mark. The WHO reference panel for anti-SARS-CoV-2 immunoglobulin (NIBSC code 20/268) resulted to have higher values in EI-S1-IgG-quant-trafo compared to Ro-RBD-Ig-quant in all samples (Fig. 3D, quotient smaller than 1).

EI-S1-IgG-quant-trafo and Ro-RBD-Ig-quant assays after twice vaccination against SARS-CoV-2

Serological dynamics, assay readouts, and BAU values from the non-vaccinated SARS-CoV-2 infected cohort were compared to healthy controls vaccinated twice against SARS-CoV-2. Therefore, EI-S1-IgG-quant and Ro-RBD-Ig-quant assays were measured in blood samples before and after second vaccination (Fig. 4A).
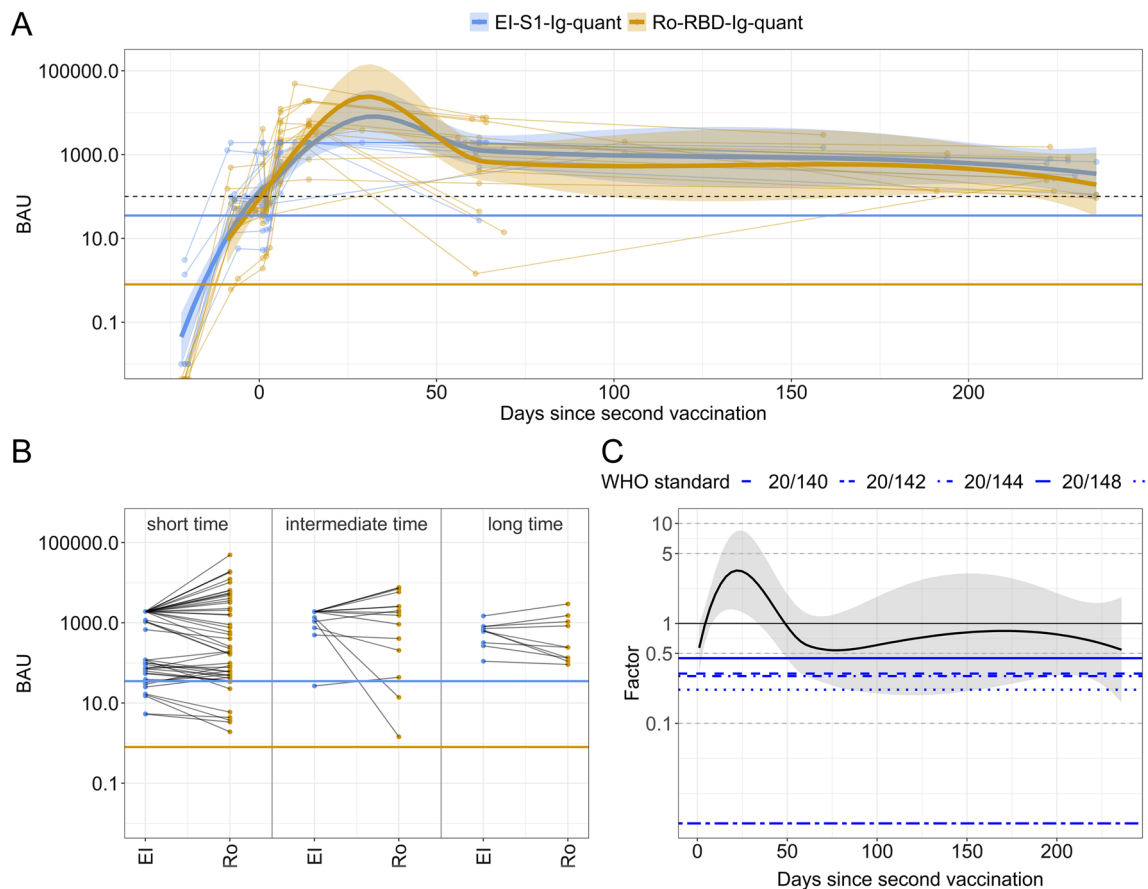
Fig. 4 Comparison of individual Anti-S1 BAU values of vaccinees over time for EI-S1-IgG-quant and Ro-RBD-Ig-quant, respectively. The time zero denotes the day of the second vaccination. The EI-S1-IgG-quant is represented in blue while Ro-RBD-Ig-quant in yellow. Solid horizontal lines represent the cut-off for positivity. **A** Longitudinal serology data of subjects over time. Each line represents one subject, the dots represent the individual samples. The solid lines show the LOESSs (locally estimated scatterplot smoothing or local regressions) estimations with CI as a shadowed region. The dashed black lines denotes 250 BUS/mL. **B** Parallel coordinate plot dividing the time from symptom onset into three intervals: short (0–20 days), intermediate (70–150 days) and long (170–250 days). EI denotes the EI-S1-IgG-quant assay while RO the Ro-RBD-Ig-quant assay. **C** Quotient of the two BAU values depicted in log10 scale over time (Ro-RBD-Ig-quant/EI-S1-IgG-quant-trafo); at 1, the BAU values are identical. Blue lines represent the WHO reference panel for anti-SARS-CoV-2 immunoglobulin (NIBSC code 20/268)

Kroidl *et al. Virology Journal*   (2023) 20:200

Page 8 of 12

Serological dynamics and temporal evolution of the titers measured by EI-S1-IgG-quant and Ro-RBD-Ig-quant differed considerably in naturally infected individuals, this was not the case for vaccinated individuals. As Fig. 4B and C demonstrate, parallel coordinate plots were less divergent and the ratio of the two assays showed to be closer to 1. After a first increase phase (from day 0 to day 34 (30–37) for EI-S1-IgG-quant and to day 31 (28–34) for Ro-RBD-Ig-quant), the median peak was reached with a level of 8069.21 (1912.37–34,047.96) BAU for EI-S1-IgG-quant and 23,988.33 (4073.80–144,543.98) BAU for Ro-RBD-Ig-quant. Both serological dynamics then decrease rapidly until day 63 (60–66) or 62 (59–65) for EI-S1-IgG-quant or Ro-RBD-Ig-quant, respectively. Thereafter, the slopes of the decrease reduce greatly.

Natural infection versus double SARS-CoV-2 vaccination

In our study, antibody-titers in fully vaccinated (i.e., twice) non-infected individuals were considerably higher compared to the naturally infected participants. For EI-S1-IgG-quant, the difference between the maximum value for vaccinated vs. naturally infected was 7.92217 BAU, while for Ro-RBD-Ig-quant the difference increased to 13.96833. In total, 93.75% of the vaccinees reached a maximum value over 1000 BAU, while only 69.7% of the vaccination naive infected subjects reached a value over 100 BAU.

In contrast to natural infections, vaccinated individuals exhibited a sharp decline in antibody titers as determined by Ro-RBD-Ig-quant, limited to approximately 60 days after the second vaccination followed by a plateau of titer (Fig. 3B compared to Fig. 4A). EI-S1-IgG-quant presented a similar profile, but in this assay a sharp decrease was also observed after natural infection. After vaccination however, the observed velocity of decrease seems to reduce. In mean, both assays yield positive readouts over the period analyzed, with values of the EI-S1-IgG-quant assay being closer to the positivity threshold compared to the ones as determined by Ro-RBD-Ig-quant.

Discussion

In this study, we compared serological dynamics using samples from ninety-nine non-vaccinated PCR-positive participants and from forty-five participants with no history of previous infection but with two vaccinations against SARS-CoV-2. Serum samples were analyzed with a total of six different assays. To follow infection, assay readouts of Ro-N-Ig and GS-cPass were performed from the same sample in a head-to-head comparison. Participants showed positive antibodies against these assays for at least 400 days. The remaining four assays detect responses to both infection and vaccination. In previous studies the EI-S1-IgA showed to be less reliable [23] and

was therefore performed only for samples of the PCR-positive participants. The EI-S1-IgG assay is per manufacturer's definition non-quantitative and its quantitative version is defined by the EI-S1-IgG-quant assay [31]. It was possible to measure samples of the PCR-positive participants only with the non-quantitative version. Measurements were hence transformed to quantitative values using paired samples presented in [31]. A comparison with the vaccinees was possible thereafter, together with direct readouts of the Ro-RBD-Ig-quant for both cohorts. As a results, the longitudinal dynamics of EI-S1-IgG-quant and Ro-RBD-Ig-quant in the PCR-positive cohort present completely different trends, while for vaccinees the trends a very similar.

Duration and magnitude of serological responses in relation to different testing systems and antigen-target has been subject to dissent. Harris et al. [22] demonstrated a rapid decline of anti-N antibodies using the ELISA from Abbot, with only 51% of SARS-CoV-2 infected individuals having a sero-response after 6 months. In contrast, Favresse et al. [32] showed a positivity rate of 94% after 10 months but using the Ro-N-Ig test. Muecksch et al. [33] compared four different assays: the Ro-N-Ig and the Abbott SARS-CoV-2 immunoglobulin (Ig) G assay for anti-N detection, and the DiaSorin SARS-CoV-2 IgG together with the Siemens SARS-CoV-2 RBD assay for anti-S comparisons. Similarly to our analysis, the shapes of the curves strongly differ between assays. Dan et al. [19] described a half-life of binding anti-S antibodies of 103 days. In contrast Ibarrondo et al. [18] described a rapid decay of anti-RBD antibodies with a half-life of only 36 days.

In our cohort of non-vaccinated SARS-CoV-2 RT-PCR-positive individuals direct readout values are coherent to previous published literature, comparing the same testing platform [33]. If compared to other assays, same discrepancies as in the rest of the literature appear. In addition, clinical characteristics of the underlying cohorts differed greatly. Several authors described a correlation between magnitude of antibody responses and degree of clinical symptoms in SARS-CoV-2 infected individuals [16, 17, 32, 34–38]. This was replicated in our cohort, where we could observe a trend towards higher antibodies titers in individuals with more severe symptoms. As we solely enrolled oligo-symptomatic participants, these findings did not reach statistical significance. Of importance, exactly that group of oligo-symptomatic patients is the overwhelming majority of the population which might be subject to serological testing for different reasons.

A correlate of protection of SARS-CoV-2 has not been established yet and it is still debated whether the protection after natural infection is different or perhaps even superior to vaccination [39]. Natural infection is likely

to elicit a broader response against more epitopes of the virus [40]. However, several studies describe the immune response after vaccination to be characterized by higher antibody levels compared to natural infections, especially following vaccination with mRNA- based vaccines [5, 7, 9, 33, 41]. Recent reports describe waning protection already shortly after the second dose and the decay seems more pronounced than after a natural infection [42–45]. Similarly, when comparing naturally infected to vaccinated participants, we observed pronouncedly higher antibody levels in the latter compared to the former. Antibody levels remained positive for at least seven months after vaccination.

Initial reports on SARS-CoV-2 infected cohorts declared a high level of protection of 82–89% for approximately 6 months against the wild type virus [3]. Similarly, data from Israel suggested a high level of protection after vaccinating with Pfizer-BioNTech [46]. Since the surge of new virus variants protection against Delta and Omicron variants was reduced [14]. Mizrahi et al. [14] described a 1.5 times increased risk for breakthrough infections with Delta variant for subjects 6 months after vaccination with Pfizer-BioNTech compared to subjects 3 months after vaccination. Shrotri et al. [42] compared protection of vaccinated individuals with anti-RBD antibodies above and below 500 BAU (ELYSYS Ro-Ig) and found significantly more infected participants with antibodies below 500 BAU. However, our data suggests that an antibody lever of 500 BAU is usually not reached after natural infection. Our SARS-CoV-2 RT-PCR-positive cohort only included participants infected with the original wild type strain. A comparison between variants is therefore not possible, but would also only generate data unclear to compare, as the vaccines and the antigens used in the tests are all also wild type.

Modelling the temporal evolution of the antibody levels, the serological dynamics of the vaccinated cohort is completely different than that of the PCR-positive vaccine naive infected participants. After vaccination, we observed a short initial peak phase, followed by a very slow decline of antibody levels in both quantitative tests EI-S1-Ig-quant and Ro-RBD-Ig. All measurements were above the positivity threshold even seven months after the second dose. The curves representing the antibody dynamics of both quantitative tests were very similar. This is in contrast to our observations in the SARS-CoV-2 RT-PCR-positive cohort described here. The ELISA-based Euroimmun test suggested a rapid decline of antibodies with more than 50% of the samples dropping below the threshold for positivity within less than one year while the Ro-RBD-Ig assay yielded positive readouts after 200 days almost without declining. An explanation for the slow EI-S1-Ig-quant antibody decrease in vaccinated

versus the steady state suggested by Ro-RBD-Ig readout in the RT-PCR-positive cohort could be the rise in avidity as also described by Scheiblauer et al. [47]. The authors hypothesized that two vaccine doses lead to an antibody response dominated by highly specific and highly avid IgG directed against the S-protein. Thus, the antibody-signal dynamics over time reflect the overall amount of antibodies in both tests. In contrast, natural infection will likely elicit a much broader response which maturates over time [47], including detection of the RBD-domain which in turn might lead to an increase in avidity, while the overall antibody amount is dropping [47]. Those two opposing effects may compensate each other at different rates depending on the assay format. The Ro-RBD-Ig assay reportedly detects the binding of few antibodies but favors high avidity [47], potentially resulting in a persistently high assay readout, while the ELISA-based Euroimmun assay values are biased towards whole antibody binding and thus decline. Persisting non-declining Roche RBD-antibodies detectable for more than 300 days after natural infection have been repetitively described with a level of ~ 100 BAU [32, 47].

Summarising, we present the results of a well-characterized cohort to investigate dynamics in serological responses to non-vaccinated SARS-CoV-2 infected individuals compared to vaccinated healthy controls. For quantitative anti-Spike assays, we used BAU standardization which is provided by the manufacturer.

However, we observe distinct differences both in the magnitude and dynamics of the measured antibody response, although BAU standardization for anti-S1/RBD tests was used. Interestingly, these differences were negligible for samples taken two months after symptom onset. The standardization however is less accurate before and after this time period, resulting in differences of up to one order of magnitude in supposedly standardized and comparable values. These differences disappeared in the vaccinated cohort. One potential explanation could be the fact that the assays measure different targets. While the EI-S1-IgG detects the overall amount of binding antibodies in an ELISA-format, Ro-RBD-Ig-quant is an ELECSYS based double-antigen sandwich-test, detecting highly avid antibodies [47]. Importantly, the BAU-standard provided by the WHO is derived from a group of donors relatively shortly after the infection. Subsequently, standardization performed for an assay will likely be accurate for tests with a similar profile of antibodies, regarding both subclass as well as avidity, hence only in individuals few months after natural infection [25]. Therefore, it is not be the best standard for clinical cohorts, including samples from individuals very early or late after the infection, or after vaccination.

Kroidl *et al. Virology Journal*   (2023) 20:200

Page 10 of 12

Conclusion

The data presented here suggest that the establishment of a protective correlate or vaccination booster recommendation based on BAU might be hampered. Also, comparisons of individual patient values between different laboratories will be unreliable even if reported in BAU. The characteristics of the individual test systems employed need to be considered and should be corrected for, as the differences are likely to be high especially in subjects with small amounts of highly avid antibodies.

Supplementary Information

The online version contains supplementary material available at https://doi.org/10.1186/s12985-023-02167-z.

Additional file 1: Figure S1 WHO grading of symptoms (from [29]). **Figure S2** Longitudinal serology data of patients (PCR-positive cohort) over time colored by WHO symptom grade. Each line represents one subject, the dots represent the individual sample. All assays were performed from the same sample in a head-to-head comparison. The blue and red solid lines show the LOESS (locally estimated scatterplot smoothing or local regression) estimations with CI. Top left: Euroimmun Anti Spike IgA; Top right: Euroimmun Anti-Spike IgG; Middle left: Roche Anti-Nucleocapsid; Middle right: Roche Anti Spike/RBD; Bottom: GenScript neutralization surrogate test. Patients with lighter symptoms tend to have lower antibodies titre. The two groups do however not significantly differ, since the 95% confidence intervals overlap. **Figure S3** Bivariate comparisons shown as scatter plot for non-quantitative EI-S1-IgG vs quantitative EI-S1-IgG-quant. Dashed lines represent manufacturers' cut-off values. The red solid line shows the LOESS (locally estimated scatterplot smoothing or local regression) estimation with CI. The black solid line with CI is a linear regression given for comparison. Square root R of coefficients of determination is given for association among continuous variables. Data presented in Rubio-Acero et al. [31].

Author contributions

MH and IK are the principal investigator and obtained funds. AW, MH, IK and LO designed the study and experimental setup with input from NC and SW. The clinical work and study design of KoCo19 was led by IK and LO, with support by SW and TME. Serological testing was designed and conducted with AW, RRA, HF, IP and AT. Data was cleaned and prepared by NC. Statistical analysis was performed by NC, with support by AB and SW. The manuscript was primarily written by NC, AW, IK and SW with substantial contributions from LO. All authors revised and approved the final version of this manuscript.

Availability of data and materials

Data and code are accessible subject to data protection regulations upon reasonable request to the corresponding author.

Declarations

Ethics approval and consent to participate

KUM-Index was approved as sub-study 1 of the Koco19-study under project number 20-275-V and Koco19-Immu under 20-371 by the Ethics Commission of the Faculty of Medicine at LMU Munich, Munich.

Competing interests

AW and MH report personal fees and non-financial support from Roche Diagnostics, LO reports non-financial support from Roche Diagnostics. AW, MH and LO report non-financial support from Euroimmun, non-financial support from Viramed, non-financial support from Mikrogen. AW, MH, LO report grants, non-financial support and other from German Centre for Infection Research DZIF, grants and non-financial support from Government of Bavaria, non-financial support from BMW, non-financial support from Munich Police, nonfinancial support and other from Accenture. MH and AW report personal fees and nonfinancial support from Dr. Box-Betrobox, non-financial support from Dr.

Kroidl *et al. Virology Journal*   (2023) 20:200

Page 11 of 12

Author details
[1]Division of Infectious Diseases and Tropical Medicine, Medical Center of the University of Munich (LMU), Munich, Germany. [2]German Center for Infection Research (DZIF), Partner Site Munich, Munich, Germany. [3]Max-von-Pettenkofer Institute, LMU Munich, Munich, Germany. [4]Fraunhofer Institute for Translational Medicine and Pharmacology ITMP, Immunology, Infection and Pandemic Research, Türkenstraße 87, 80799 Munich, Germany. [5]Center for International Health (CIH), University Hospital, LMU Munich, 80336 Munich, Germany. [6]Institute of Radiation Medicine, Helmholtz Zentrum München, 85764 Neuherberg, Germany.

References

1. WHO. Coronavirus disease (COVID-19) pandemic. 01 July 2022. https://www.who.int/emergencies/diseases/novel-coronavirus-2019.
2. CSSE. Center for Systems Science and Engineering (CSSE) at Johns Hopkins University (JHU) COVID-19 dashboard. 01 July 2022 https://coronavirus.jhu.edu/map.html.
3. Lumley SF, et al. Antibody status and incidence of SARS-CoV-2 infection in health care workers. N Engl J Med. 2021;384(6):533–40.
4. Letizia AG, et al. SARS-CoV-2 seropositivity and subsequent infection risk in healthy young adults: a prospective cohort study. Lancet Respir Med. 2021;9(7):712–20.
5. Polack FP, et al. Safety and efficacy of the BNT162b2 mRNA Covid-19 vaccine. N Engl J Med. 2020;383(27):2603–15.
6. Dagan N, et al. BNT162b2 mRNA Covid-19 vaccine in a nationwide mass vaccination setting. N Engl J Med. 2021;384(15):1412–23.
7. Baden LR, et al. Efficacy and safety of the mRNA-1273 SARS-CoV-2 vaccine. N Engl J Med. 2021;384(5):403–16.
8. Voysey M, et al. Safety and efficacy of the ChAdOx1 nCoV-19 vaccine (AZD1222) against SARS-CoV-2: an interim analysis of four randomised controlled trials in Brazil, South Africa, and the UK. Lancet. 2021;397(10269):99–111.
9. Kim JH, Marks F, Clemens JD. Looking beyond COVID-19 vaccine phase 3 trials. Nat Med. 2021;27(2):205–11.
10. Barros-Martins J, et al. Immune responses against SARS-CoV-2 variants after heterologous and homologous ChAdOx1 nCoV-19/BNT162b2 vaccination. Nat Med. 2021;27(9):1525–9.
11. Caniels TG, et al. Emerging SARS-CoV-2 variants of concern evade humoral immune responses from infection and vaccination. Sci Adv. 2021;7(36):eabj5365.
12. Kroidl I, et al. Vaccine breakthrough infection and onward transmission of SARS-CoV-2 Beta (B.1.351) variant, Bavaria, Germany, February to March 2021. Euro Surveill. 2021;26(30):2100673.
13. Hacisuleyman E, et al. Vaccine Breakthrough Infections with SARS-CoV-2 Variants. N Engl J Med. 2021;384(23):2212–8.
14. Mizrahi B, et al. Correlation of SARS-CoV-2-breakthrough infections to time-from-vaccine. Nat Commun. 2021;12(1):6379.
15. Bergwerk M, et al. Covid-19 breakthrough infections in vaccinated health care workers. N Engl J Med. 2021;385(16):1474–84.
16. Long QX, et al. Antibody responses to SARS-CoV-2 in patients with COVID-19. Nat Med. 2020;26(6):845–8.
17. Long QX, et al. Clinical and immunological assessment of asymptomatic SARS-CoV-2 infections. Nat Med. 2020;26(8):1200–4.
18. Ibarrondo FJ, et al. Rapid decay of Anti-SARS-CoV-2 antibodies in persons with mild Covid-19. N Engl J Med. 2020;383(11):1085–7.
19. Dan JM, et al. Immunological memory to SARS-CoV-2 assessed for up to 8 months after infection. Science. 2021;371(6529):eabf4063.
20. Flehmig B, et al. Persisting neutralizing activity to SARS-CoV-2 over months in sera of COVID-19 patients. Viruses. 2020;12(12):1357.
21. Ripperger TJ, et al. Orthogonal SARS-CoV-2 serological assays enable surveillance of low-prevalence communities and reveal durable humoral immunity. Immunity. 2020;53(5):925–33.
22. Harris RJ, et al. Serological surveillance of SARS-CoV-2: six-month trends and antibody response in a cohort of public health workers. J Infect. 2021;82(5):162–9.
23. Olbrich L, et al. (2021) Head-to-head evaluation of seven different seroassays including direct viral neutralisation in a representative cohort for SARS-CoV-2. J Gen Virol. 2021;102(10):001653.
24. Kristiansen PA, et al. WHO International Standard for anti-SARS-CoV-2 immunoglobulin. Lancet. 2021;397(10282):1347–8.
25. WHO. WHO/BS.2020.2403 Establishment of the WHO International Standard and reference panel for anti-SARS-CoV-2 antibody. 04 July 2022 https://www.who.int/publications/m/item/WHO-BS-2020.2403.
26. Ag EML. Quantitativer Nachweis von Antikörpern gegen SARS-CoV-2. 2021 https://www.coronavirus-diagnostik.de/documents/Indications/Infections/Coronavirus/EI_2606_I_DE_B.pdf.
27. Nordlab L. Testumstellung für den Nachweis von Anti-SARS-CoV-2 IgG. https://www.nordlab.de/index.php/de/21-aktuelles/272-testumstellung-fuer-den-nachweis-von-anti-sars-cov-2-igg.
28. BV MDB. https://www.mediphos.be/en/news/who-standardized-igg-antibody-determination-against-whole-spike-sars-cov-2.
29. Characterisation WHOWGotC, Management of C-I. A minimal common outcome measure set for COVID-19 clinical research. Lancet Infect Dis. 2020; 20(8): e192–7.
30. Puchinger K, et al. The interplay of viral loads, clinical presentation, and serological responses in SARS-CoV-2: results from a prospective cohort of outpatient COVID-19 cases. Virology. 2022;569:37–43.
31. Rubio-Acero R, et al. In search of the SARS-CoV-2 protection correlate: head-to-head comparison of two quantitative S1 assays in pre-characterized oligo-/asymptomatic patients. Infect Dis Ther. 2021;7:491.
32. Favresse J, et al. Persistence of anti-SARS-CoV-2 antibodies depends on the analytical kit: a report for up to 10 months after infection. Microorganisms. 2021;9(3):556.
33. Muecksch F, et al. Longitudinal serological analysis and neutralizing antibody levels in coronavirus disease 2019 convalescent patients. J Infect Dis. 2021;223(3):389–98.
34. Chen X, et al. Disease severity dictates SARS-CoV-2-specific neutralizing antibody responses in COVID-19. Signal Transduct Target Ther. 2020;5(1):180.
35. Figueiredo-Campos P, et al. Seroprevalence of anti-SARS-CoV-2 antibodies in COVID-19 patients and healthy volunteers up to 6 months post disease onset. Eur J Immunol. 2020;50(12):2025–40.
36. Seow J, et al. Longitudinal observation and decline of neutralizing antibody responses in the three months following SARS-CoV-2 infection in humans. Nat Microbiol. 2020;5(12):1598–607.
37. Gudbjartsson DF, et al. Humoral immune response to SARS-CoV-2 in Iceland. N Engl J Med. 2020;383(18):1724–34.
38. Roltgen K, et al. Defining the features and duration of antibody responses to SARS-CoV-2 infection associated with disease severity and outcome. Sci Immunol. 2020;5(54):eabe0240.
39. Krammer F. A correlate of protection for SARS-CoV-2 vaccines is urgently needed. Nat Med. 2021;27(7):1147–8.
40. Feng S, et al. Correlates of protection against symptomatic and asymptomatic SARS-CoV-2 infection. Nat Med. 2021;27(11):2032–40.
41. Haas EJ, et al. Impact and effectiveness of mRNA BNT162b2 vaccine against SARS-CoV-2 infections and COVID-19 cases, hospitalisations, and deaths following a nationwide vaccination campaign in Israel: an observational study using national surveillance data. Lancet. 2021;397(10287):1819–29.
42. Shrotri M, et al. Spike-antibody waning after second dose of BNT162b2 or ChAdOx1. Lancet. 2021;398(10298):385–7.
43. Tang P, et al. BNT162b2 and mRNA-1273 COVID-19 vaccine effectiveness against the SARS-CoV-2 Delta variant in Qatar. Nat Med. 2021;27(12):2136–43.
44. Levin EG, et al. Waning immune humoral response to BNT162b2 Covid-19 vaccine over 6 months. N Engl J Med. 2021;385(24):e84.
45. Chemaitelly H, et al. Waning of BNT162b2 vaccine protection against SARS-CoV-2 infection in Qatar. N Engl J Med. 2021;385(24):e83.

Kroidl *et al. Virology Journal* (2023) 20:200

Page 12 of 12

46. Feikin DR, et al. Duration of effectiveness of vaccines against SARS-CoV-2 infection and COVID-19 disease: results of a systematic review and meta-regression. Lancet. 2022;399(10328):924–44.
47. Scheiblauer H, et al. Antibody response to SARS-CoV-2 for more than one year: kinetics and persistence of detection are predominantly determined by avidity progression and test design. J Clin Virol. 2022;146:105052.

Publisher's Note

Publication 2:

The Prospective COVID-19 Post-Immunization Serological Cohort in Munich (KoCo-Impf): Risk Factors and Determinants of Immune Response in Healthcare Workers

Christina Reinkemeyer*, Yeganeh Khazaei*, Maximilian Weigert, Marlene Hannes, Ronan Le Gleut, Michael Plank, Simon Winter, Ivan Noreña, Theresa Meier, Lisa Xu, Raquel Rubio-Acero, Simon Wiegrebe, Thu Giang Le Thi, Christiane Fuchs, Katja Radon, Ivana Paunovic, Christian Janke, Andreas Wieser, Helmut Küchenhoff, Michael Hoelscher, **Noemi Castelletti** and KoCo-Impf/ORCHESTRA working group

The Prospective COVID-19 Post-Immunization Serological Cohort in Munich (KoCo-Impf): Risk Factors and Determinants of Immune Response in Healthcare Workers

Christina Reinkemeyer [1,†], Yeganeh Khazaei [2,†], Maximilian Weigert [2,3], Marlene Hannes [1], Ronan Le Gleut [4,5], Michael Plank [1], Simon Winter [1], Ivan Noreña [1], Theresa Meier [2], Lisa Xu [2], Raquel Rubio-Acero [1], Simon Wiegrebe [2,6], Thu Giang Le Thi [7], Christiane Fuchs [4,5,8,9], Katja Radon [10,11,12], Ivana Paunovic [1], Christian Janke [1], Andreas Wieser [1,13,14,15], Helmut Küchenhoff [2], Michael Hoelscher [1,11,13,14] and Noemi Castelletti [1,14,16,*,‡] on behalf of the KoCo-Impf/ORCHESTRA working group

[1] Division of Infectious Diseases and Tropical Medicine, LMU University Hospital, LMU Munich, 80802 Munich, Germany; christina.reinkemeyer@med.uni-muenchen.de (C.R.); marlene.hannes@med.uni-muenchen.de (M.H.); michael.plank@med.uni-muenchen.de (M.P.); simon.winter@med.uni-muenchen.de (S.W.); ivan.norena@lrz.uni-muenchen.de (I.N.); raquel.rubio@med.uni-muenchen.de (R.R.-A.); ivana.paunovic@med.uni-muenchen.de (I.P.); christian.janke@lrz.uni-muenchen.de (C.J.); wieser@mvp.lmu.de (A.W.); hoelscher@lrz.uni-muenchen.de (M.H.)
[2] Statistical Consulting Unit StaBLab, Department of Statistics, LMU Munich, Ludwigstraße 33, 80539 Munich, Germany; yeganeh.khazaei@stat.uni-muenchen.de (Y.K.); maximilian.weigert@stat.uni-muenchen.de (M.W.); theresa.meier@stablab.stat.uni-muenchen.de (T.M.); lisa-xu@gmx.at (L.X.); simon.wiegrebe@stat.uni-muenchen.de (S.W.); kuechenhoff@stat.uni-muenchen.de (H.K.)
[3] Munich Center for Machine Learning (MCML), 80539 Munich, Germany
[4] Institute of Computational Biology, Helmholtz Munich, 85764 Neuherberg, Germany; ronan.legleut@helmholtz-munich.de (R.L.G.); christiane.fuchs@helmholtz-munich.de (C.F.)
[5] Core Facility Statistical Consulting, Helmholtz Munich, 85764 Neuherberg, Germany
[6] Department of Genetic Epidemiology, University of Regensburg, 93053 Regensburg, Germany
[7] Department of Pediatrics, Dr. von Hauner Children's Hospital, University Hospital, LMU Munich, Lindwurmstrasse 4, 80337 Munich, Germany; tlethi@med.lmu.de
[8] Faculty of Business Administration and Economics, Bielefeld University, 33615 Bielefeld, Germany
[9] Center for Mathematics, Technische Universität München, 85748 Garching, Germany
[10] Institute and Outpatient Clinic for Occupational, Social and Environmental Medicine, University Hospital, LMU Munich, 80336 Munich, Germany; katja.radon@med.uni-muenchen.de
[11] Center for International Health (CIH), University Hospital, LMU Munich, 80336 Munich, Germany
[12] Comprehensive Pneumology Center (CPC) Munich, German Center for Lung Research (DZL), 89337 Munich, Germany
[13] German Center for Infection Research (DZIF), Partner Site Munich, 80802 Munich, Germany
[14] Fraunhofer Institute for Translational Medicine and Pharmacology ITMP, Immunology, Infection and Pandemic Research, 80799 Munich, Germany
[15] Max von Pettenkofer Institute, Faculty of Medicine, LMU Munich, 80336 Munich, Germany
[16] Institute of Radiation Medicine, Helmholtz Zentrum München, 85764 Neuherberg, Germany
*   Correspondence: noemi.castelletti@med.uni-muenchen.de
†   These authors contributed equally to this work.
‡   Members are listed in the Acknowledgements section.

Abstract: Antibody studies analyze immune responses to SARS-CoV-2 vaccination and infection, which is crucial for selecting vaccination strategies. In the KoCo-Impf study, conducted between 16 June and 16 December 2021, 6088 participants aged 18 and above from Munich were recruited to monitor antibodies, particularly in healthcare workers (HCWs) at higher risk of infection. Roche Elecsys® Anti-SARS-CoV-2 assays on dried blood spots were used to detect prior infections (anti-Nucleocapsid antibodies) and to indicate combinations of vaccinations/infections (anti-Spike antibodies). The anti-Spike seroprevalence was 94.7%, whereas, for anti-Nucleocapsid, it was only 6.9%. HCW status and contact with SARS-CoV-2-positive individuals were identified as infection risk factors, while vaccination and current smoking were associated with reduced risk. Older age

correlated with higher anti-Nucleocapsid antibody levels, while vaccination and current smoking decreased the response. Vaccination alone or combined with infection led to higher anti-Spike antibody levels. Increasing time since the second vaccination, advancing age, and current smoking reduced the anti-Spike response. The cumulative number of cases in Munich affected the anti-Spike response over time but had no impact on anti-Nucleocapsid antibody development/seropositivity. Due to the significantly higher infection risk faced by HCWs and the limited number of significant risk factors, it is suggested that all HCWs require protection regardless of individual traits.

1. Introduction

The first report of the severe acute respiratory syndrome Coronavirus 2 (SARS-CoV-2) causing COVID-19 was on 31 December 2019 in the city of Wuhan (Hubei province, China) [1]. The World Health Organization (WHO) declared COVID-19 as a pandemic on 11 March 2020, after more than 118,000 cases in 114 countries and 4291 deaths occurred [2]. Since then, there have been outbreaks worldwide, with approximately 767 million confirmed cases and more than 6.9 million deaths as of June 2023 [3]. The first COVID-19 cases in Germany were observed in the municipality of Munich in late January 2020 [4]. Several vaccines were promptly developed and have been available in Germany since 27 December 2020 [5]. The first individuals to receive vaccinations were healthcare workers (HCW: people engaged in work actions whose primary intent is to improve health [6]) (HCWs), the elderly, and those who were at a high risk of severe illness to prevent the healthcare system from collapsing from overwhelming case numbers or lack of personnel [6–9]. HCWs are of particular interest and require careful investigation regarding SARS-CoV-2 infections. As vaccine protection diminishes over time, receiving an early vaccination reduces the risk of early infection but may increase the risk of later infection. This has been noted in several studies [9–11].

Many cohort studies have been set up since the beginning of the pandemic to analyze risk factors for infection before and after vaccination in both the general population [12–16] and HCWs [17,18].

Considering the role of antibody levels in protection against infection, most studies also analyze antibody titers over time. Anti-nucleocapsid (anti-N) antibodies develop only after natural infection (or vaccination with nucleocapsid-containing vaccines not commonly used in the Western world), while anti-spike (anti-S) antibodies develop after natural infection or/and vaccination [19].

Collatuzzo et al. [17] analyzed the predictors for a longer duration of the anti-S immune response at 9 months after the first COVID-19 vaccination in a multicentric European cohort of HCWs. A part of these data was fed into their analysis following the European-wide Consortium ORCHESTRA (Connecting European Cohorts to Increase Common and Effective Response to SARS-CoV-2 Pandemic). Female gender, young age, a previous infection, two vaccine doses, and mRNA and heterologous vaccination were found to determine higher anti-S antibody levels.

Moncunill et al. [20] analyzed determinants of antibody responses to COVID-19 mRNA vaccines in a cohort of exposed and naïve HCWs. Comparing previously SARS-CoV-2 infected versus uninfected individuals, the first ones were found to have higher anti-S IgA, IgG, and IgM levels, independently of the brand of the vaccine. At the same time, non-infected individuals developed significantly higher antibodies, depending on the brand of the vaccine. Interestingly, despite the clear impact of SARS-CoV-2 exposure on vaccine response, time since infection did not have a major effect on antibody response. Moreover, age and sex were not significantly associated with anti-S IgG levels in multivariable models.

Notarte et al. [21,22] analyzed determinants of antibody responses after COVID-19 mRNA vaccines in different populations. Regardless of the vaccine brand used, older age, male sex, seronegative status prior to vaccination, and presence of major comorbidities were associated with lower antibody titers (total antibodies, IgG, and/or IgA), supporting the findings of Yang [23].

Other factors leading to lower anti-S antibody titers were smoking [20,24] and homologous vaccination schemes [25–27].

In April 2020, the prospective Munich COVID-19 cohort (KoCo19) began to better evaluate the true case numbers [12,28,29]. Latest results show that vaccination prevents infection: anti-N seroprevalence was greater in the non-vaccinated population compared to the vaccinated one. At the same time, anti-N seroconversion rates (incidence) among vaccinated subjects did not show any statistical difference compared to the non-vaccinated group. Breakthrough infections (BTIs) may thus contribute relevantly to community spread, also considering the fact that the vaccinated population is much larger than the non-vaccinated population. The sub-cohort with jobs having a high contact risk with COVID-19 cases (e.g., HCWs) was found to have an increased risk for infection [30].

In May 2021, a new longitudinal cohort named KoCo-Impf (Prospective COVID-19 post-immunization Serological Cohort in Munich—Determination of immune response in vaccinated subjects) was established at the Division of Infectious Diseases and Tropical Medicine, comprising mostly HCWs with high contact risk with the SARS-CoV-2 virus. The analysis presented here aimed to identify risk factors for infection among HCWs, factors that influence the immune response following infection or vaccination, and differences between HCWs and the general population. The analysis utilized multivariable logistic regression analysis to identify risk factors for infection based on qualitative anti-N antibody results. Additionally, multivariable generalized linear models (GLM) were employed to determine the factors that raise antibody titers following infection and/or vaccination, using quantitative anti-N and anti-S antibody values.

The KoCo-Impf study was recruited concurrently with the third and fourth follow-ups of KoCo19 in Munich. This allowed for a comparison of the general population of Munich (KoCo19) with their HCWs. Although the crude rates for anti-N seroprevalence were similar, a direct comparison was challenging. However, it was confirmed in both the KoCo19 and the KoCo-Impf that HCWs had a higher risk of infection. Sex, age, household size, and intake of immune-suppressing drugs were not found to be significant risk factors for infection in either cohort, but being a current smoker was.

2. Materials and Methods

2.1. The KoCo-Impf Cohort: Cohort Design, Inclusion Criteria, and Setting

The objective of KoCo-Impf is to investigate the short-, medium- and long-term immune response to SARS-CoV-2 vaccination. This study is funded by the European Union's Horizon 2020 research and innovation program, as part of ORCHESTRA (Connecting European Cohorts to increase common and Effective SARS-CoV-2 Response), and also by the Division of Infectious Diseases and Tropical Medicine's own resources [31].

Between 16 June and 16 December 2021, a total of 6467 participants aged 18 years or older, who had received at least one COVID-19 vaccination, were recruited for this study from the Munich municipality and surrounding areas. The recruitment campaign was carried out through three different paths (Figure 1, top):
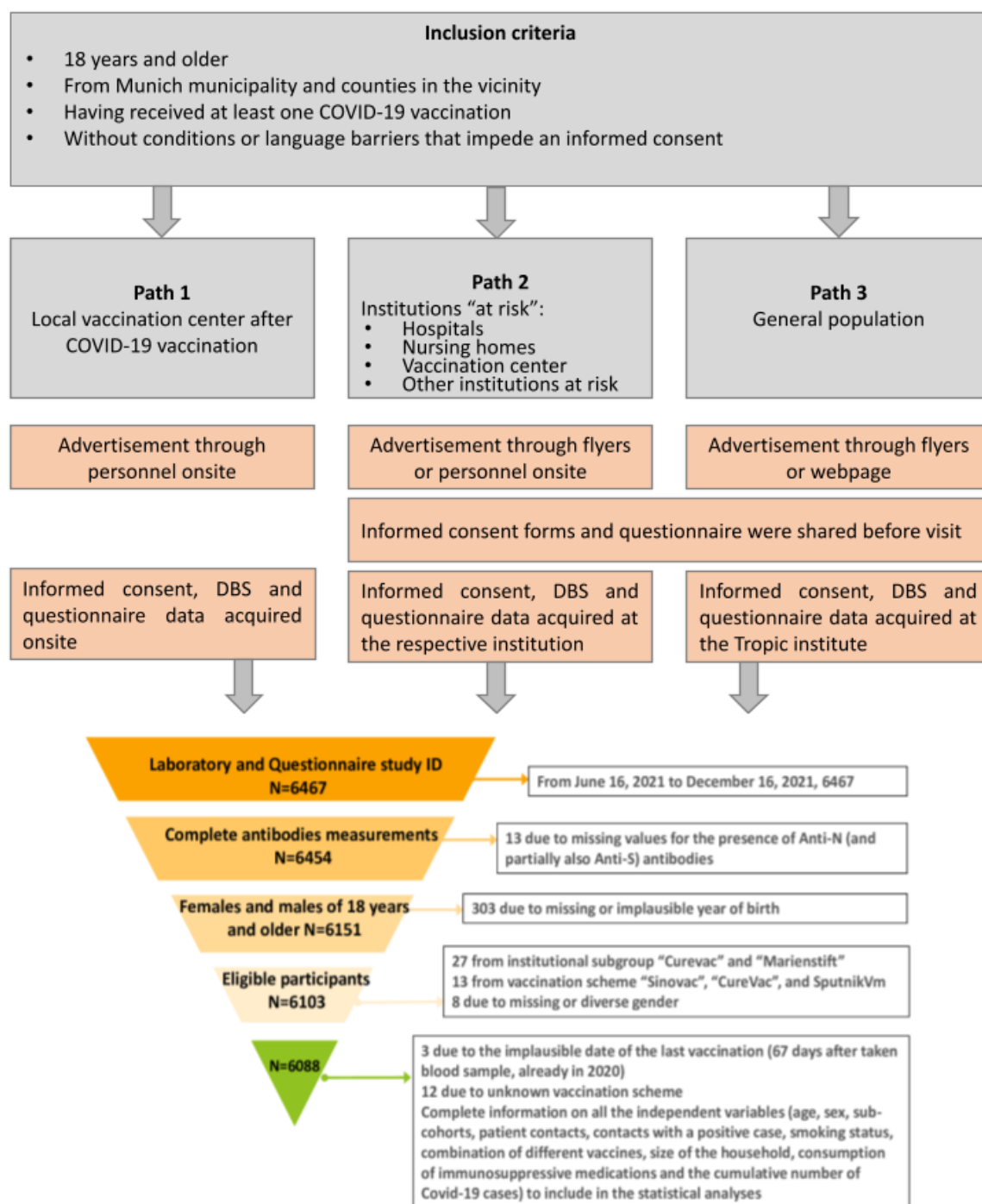
Figure 1. Recruitment paths and criteria for inclusion into the analysis. Gray boxes: inclusion criteria and places of recruitment. Orange boxes: information on advertisement modalities for recruiting participants; modalities of the acquisition of informed consent, questionnaire data, and capillary blood samples (acquired in person by study personnel). A triangle diagram describing the exclusion criteria and the final information of the analyzed participants.

Path 1: At the local vaccination center Riem, where individuals were approached with this study's information after their vaccination,

Path 2: At hospitals and nursing homes in the Munich area, targeting particularly exposed or vulnerable individuals (HCWs), and

Path 3: Via brochures and on the website of the Division of Infectious Diseases and Tropical Medicine for the general population.

Participants with language barriers (insufficient knowledge of the German language) or inability to provide informed consent were excluded.

Recruitment strategy, acquisition of informed consent, capillary blood samples, and questionnaire data occurred in different ways depending on the recruitment pathway:

Path 1: Directly after vaccination,

Path 2: By study teams making appointments on specific days to visit the sites, catching participants in the building during their working time, and

Path 3: Posting advertisements on the webpage of the Division of Infectious Diseases and Tropical Medicine, Klinikum der Universität München; participants could make an appointment for a personal visit via a hotline.

After data cleaning, 6088 participants were included in the analysis (Figure 1, bottom). Capillary blood samples were taken from participants to determine their antibody status, and questionnaire data were collected to obtain information on participants' characteristics. The recruitment of employees from the University Hospital of Munich (LMU) was conducted simultaneously with the RisCoin HCWs cohort study, which studies risk factors for COVID-19 vaccine failure among HCWs [32].

2.2. Specimen Collection and Laboratory Analyses

Teams of trained field workers collected capillary blood samples (also known as a dry blood spot or DBS) following proper infectious disease control and blood sampling procedures to conduct laboratory analysis. The process for analyzing a DBS is explained in detail [33]. Two types of assays were used: the Roche Elecsys® Anti-SARS-CoV-2 assay anti-Spike (anti-S) test, referred to as Ro-RBD-Ig, and the Roche Elecsys® Anti-SARS-CoV-2 anti-Nucleocapsid (anti-N) test, referred to as Ro-N-Ig. The Ro-RBD-Ig detects antibodies after infection and vaccination, while the Ro-N-Ig test is used to differentiate between antibodies resulting from infection (both anti-S and anti-N present) and those due to vaccination (only anti-S present). The Ro-N-Ig test determines if an individual has previously had an infection but cannot provide information on the infection date. The Ro-RBD-Ig test has a cut-off value of 0.115 for DBS-seropositivity, while the Ro-N-Ig test has a cut-off value of 0.105. For both assays, a cross-reaction with viral infections predating the COVID-19 era could be excluded. This was achieved by analyzing samples obtained from blood donors prior to the emergence of COVID-19 [34,35].

2.3. Questionnaire Data

This study used questionnaires to gather information from participants about

- recruitment (institutional subgroup; recruitment date);
- demographic (date/year of birth; sex; level of education; household size);
- health-related behavior (smoking status; pre-existing medical conditions; medication scheme (intake of immunosuppressive drugs; others));
- employment-related behavior (occupational status; working conditions);
- COVID-19-related health status (vaccination status such as the date and type of first, second, and third vaccination if applicable; infection status, only Polymerase chain reaction (PCR)-confirmed COVID-19-diagnosis; diagnosis period; diagnosis date, month, and year; diagnosis in relation to vaccination and immunization status; diagnosis date after first vaccination; diagnosis date after full immunization (Two doses of Comirnaty, Spikevax or Vaxzevria or one dose of Jcovden at the time of data collection); severity of SARS-CoV-2-infection; previous contact with SARS-CoV-2 infected person; testing frequency; symptoms suggestive for COVID-19).

In the course of this study, three different versions of the questionnaire were used: Questionnaire 1 was provided on paper and used at the beginning of this study. Questionnaire 2 (used after 15 October 2021) was also provided on paper and included questions about the possibility of a third COVID-19 vaccination, as well as additional information that had emerged as potentially relevant during the course of this study (e.g., educational attainment, occupation, the presence of pre-existing conditions, and the course of COVID-19

disease). Questionnaire 3 was completed online by LMU employee hospital participants and requested the same information as Questionnaires 1 and 2.

Participants in Path 1 received Questionnaire 1 on the day of recruitment and filled it out during the recruitment procedures. Participants in Paths 2 and 3 were given the option to fill out Questionnaires 1 and 2 beforehand and bring them to the recruitment session or to fill them out on the day of recruitment. Participants in Path 2 also received Questionnaire 3 on the day of recruitment and were asked to fill it out during the recruitment procedures or as soon as possible thereafter.

Paper-based questionnaires were digitized using the software FormPro (version 3.1, OCR System GmbH, Leipzig, Germany, 2021).

2.4. Variables Definition

The variables that were used for the analysis are described in Table 1 and were selected following medical relevance. While most of the variables were obtained directly from the questionnaire, some of them were derived from other variables. The latter includes the vaccination scheme, time since the second vaccination, the occurrence of BTIs, time since infection, and the combination of the vaccination scheme and former infection, which is referred to as "immunity" hereafter. The recruitment process for KoCo-Impf was unique as it took place at various institutions over a period of seven months during the pandemic. Since a positive anti-N antibody level indicates a past infection, which could have occurred a long time ago, it is essential to take the different waves of the pandemic into account and correct for the different times at risk. Therefore, the cumulative number of new COVID-19 cases from the beginning of the pandemic to each date of recruitment was added as a covariate based on a weekly rolling window. A time lag of two weeks was applied, as anti-N and anti-S antibodies often need two weeks to develop after infection. [36,37].

Unlike most studies, we defined a SARS-CoV-2 infection by looking at anti-N antibody positivity instead of just considering PCR-positive tests. This approach ensures that asymptomatic and previously undiagnosed infections are more likely to be detected. Infection and vaccination by those vaccines used in our cohorts can be differentiated by serology, detecting both anti-S and anti-N antibodies. This analysis neglects information on symptoms. This choice was made due to the fact that many infections resulted in being asymptomatic, and the severity of symptoms does not necessarily indicate a different change in the antibody response.

2.5. Statistical Analyses

Before conducting statistical analysis, data were cleaned and secured. Categorical variables are presented as frequencies and percentages, while continuous variables are presented as mean values and standard deviations (SD). Mean values, SDs, and crude associations were calculated for all quantities and are presented in Table 2.

Table 1. Variables description with color-coded allocation to the three statistical models used in the analysis. Covariables of: all three models, green; only anti-N qualitative model, pink; only anti-S quantitative model, gray; anti-N quantitative model and anti-S quantitative model, blue; anti-N qualitative model; anti-N quantitative model, gold.

Variable Name	Definition (Type of Variable)
Quantitative anti-N/S	The detected amount of Ro-N-Ig/Ro-RBD-Ig from DBS (continuous)
Qualitative anti-N/S	A positive anti-N/S result is defined when the amount of Ro-N-Ig/Ro-RBD-Ig is $\geq$0.105/0.115 (positive/negative)
Age ****	Age of participants in years (continuous)
Cumulative cases	Cumulative number of COVID-19 cases from the beginning of the pandemic till the recruitment date (continuous)
Intake of immunosuppressive drugs ****	Current intake of medications that may suppress the immune system (yes, no)
Sex ****	Sex of the participant (male, female)
Smoking status ****	Current smoking status (never smoker, current smoker, past smoker)
Contact with patients ****	Direct contact with patients (yes, no)
Contact with positives ****	Previous contact with COVID-19 affected/SARS-CoV-2 infected person (yes, no, or unwittingly)
Household size ****	Number of household members including participant (1, 2, 3, 4, 5, >5)
Institutional subgroup	Categorization according to the institution of recruitment (Hospitals *: Medical center of LMU, Tropical Institute **, MK Bogenhausen, MK Harlaching, MK Neuperlach, MK Schwabing, MK Thalkirchner Straße, Barmherzige Brüder, Seefeld, Institutions of long-term care: Eichenau, MS Heilig Geist, MS Rümannstraße, Obersendling Others: Vaccination center Riem, Friedenheimer Brücke, General population ***)
Breakthrough Infection (BTI) ****	An infection happened at least 2 weeks after the second dose (yes, no, not applicable)
Time since infection ****	Time between the sampling date and the positive PCR (infected in less than 3 months, infected between 3 and 6 months, infected between 6 and 12 months, infected after 12 months, no infection)
Combination of vaccination scheme and former infection (immunity)	A composite variable containing information on the previous infection (based on anti-N result) and the undergone vaccination scheme (infection yes, not vaccinated, infection yes + one vaccination, infection yes + two vaccinations, infection yes + three vaccinations, infection no + one vaccination, infection no + two vaccinations, infection no + three vaccinations)
Time since second vaccination ****	Time between the second vaccination and the sampling date (continuous)
Vaccination scheme ****	A combination of types of vaccination and number of vaccinations, including BioNTech/Pfizer, Moderna, AstraZeneca, Johnson & Johnson/Janssen (no vaccination, one vaccination, two vaccinations, three vaccinations)

* Includes study participants from Path 2. ** Division of Infectious Diseases and Tropical Medicine of LMU. *** Includes study participants from Path 1 and Path 3. **** Based on self-reported questionnaire data.

Table 2. Cohort description with data before imputation.

Covariate	Category	Number of Participants N (%)	Qualitative Anti-N N (%)		Qualitative Anti-S N (%)		Quantitative Anti-N Mean Value (SD)		Quantitative Anti-S Mean Value (SD)	
			Positive	Negative	Positive	Negative	Positive	Negative	Positive	Negative
Overall cohort		6088 (100.0)	424 (6.9)	5664 (93.1)	5767 (94.8)	321 (5.2)	0.94 (1.52)	0.06 (0.01)	83.54 (200.35)	0.03 (0.02)
Sex	Female	4379 (72.0)	296 (6.7)	4083 (93.3)	4199 (95.9)	180 (4.1)	0.88 (1.33)	0.06 (0.01)	82.39 (199.08)	0.03 (0.02)
	Male	1709 (28.0)	128 (7.4)	1581 (92.6)	1568 (91.8)	141 (8.2)	1.10 (1.86)	0.06 (0.01)	86.68 (204.17)	0.03 (0.02)
Institutional subgroup	Barmherzige Brüder	188 (3.0)	40 (21.2)	148 (78.8)	187 (99.5)	1 (0.5)	0.98 (1.04)	0.07 (0.008)	55.02 (106.23)	0.06 (NA)
	Eichenau	34 (0.5)	5 (14.7)	29 (85.3)	34 (100.0)	0 (0.0)	1.59 (2.00)	0.07 (0.004)	447.20 (427.47)	- *
	Friedenheimer Brücke	34 (0.5)	1 (2.9)	33 (97.1)	34 (100.0)	0 (0.0)	0.88 (NA)	0.08 (0.006)	82.45 (122.71)	-
	General population	671 (11.0)	50 (7.5)	621 (92.5)	366 (54.6)	306 (45.4)	1.33 (2.25)	0.07 (0.02)	43.84 (121.03)	0.03 (0.02)
	Medical Center of LMU	3689 (60.6)	213 (5.7)	3476 (94.3)	3680 (99.8)	9 (0.2)	0.86 (1.53)	0.06 (0.01)	85.62 (205.49)	0.04 (0.04)
	MK, Bogenhausen	238 (3.9)	23 (9.6)	215 (90.4)	238 (100.0)	0 (0.0)	1.42 (1.78)	0.07 (0.01)	62.67 (172.21)	-
	MK, Harlaching	154 (2.5)	14 (9.1)	140 (90.9)	154 (100.0)	0 (0.0)	0.87 (1.19)	0.07 (0.006)	43.20 (60.97)	-
	MK, Neuperlach	112 (1.8)	5 (4.4)	107 (95.6)	112 (100.0)	0 (0.0)	0.45 (0.38)	0.07 (0.005)	33.44 (32.95)	-
	MK, Schwabing	281 (4.6)	13 (4.7)	268 (95.3)	281 (100.0)	0 (0.0)	0.36 (0.35)	0.07 (0.009)	48.08 (128.11)	-
	MK, Thalkirchner Straße	67 (1.1)	4 (5.9)	63 (94.1)	67 (100.0)	0 (0.0)	2.15 (2.27)	0.07 (0.006)	40.60 (46.19)	-
	MS, Heilig Geist	60 (0.9)	14 (23.3)	46 (76.7)	60 (100.0)	0 (0.0)	0.61 (0.69)	0.06 (0.02)	140.81 (380.16)	-

Table 2. *Cont.*

Covariate	Category	Number of Participants N (%)	Qualitative Anti-N N (%)		Qualitative Anti-S N (%)		Quantitative Anti-N Mean Value (SD)		Quantitative Anti-S Mean Value (SD)	
			Positive	Negative	Positive	Negative	Positive	Negative	Positive	Negative
	MS, Rümannstraße	36 (0.5)	2 (5.5)	34 (94.5)	36 (100.0)	0 (0.0)	0.58 (0.67)	0.06 (0.005)	531.93 (574.09)	-
	Obersendling	27 (0.4)	4 (14.8)	23 (85.2)	27 (100.0)	0 (0.0)	0.88 (0.66)	0.08 (0.004)	54.03 (113.73)	-
	Seefeld	83 (1.3)	5 (6.1)	78 (93.9)	83 (100.0)	0 (0.0)	1.26 (0.52)	0.06 (0.01)	138.71 (285.03)	-
	Tropical Institute	48 (0.8)	2 (4.1)	46 (95.9)	46 (95.9)	2 (4.1)	0.16 (0.05)	0.07 (0.01)	78.37 (115.27)	0.05 (0.02)
	Vaccination center Riem	366 (6.0)	29 (7.9)	337 (92.1)	363 (99.2)	3 (0.8)	0.76 (0.85)	0.07 (0.007)	101.04 (148.18)	0.06 (0.04)
Contact with patients	Yes	3505 (57.5)	261 (7.4)	3244 (92.6)	3493 (99.7)	12 (0.3)	0.90 (1.42)	0.06 (0.01)	94.39 (227.33)	0.03 (0.03)
	No	1833 (30.2)	111 (6.1)	1722 (93.9)	1647 (89.9)	186 (10.1)	0.89 (1.39)	0.06 (0.02)	65.44 (140.44)	0.03 (0.02)
	Unknown **	750 (12.3)	52 (6.8)	698 (93.2)	627 (83.8)	123 (16.2)	1.26 (2.09)	0.07 (0.02)	70.64 (167.82)	0.03 (0.02)
Contact with positives	Yes	2804 (45.9)	278 (9.9)	2526 (90.1)	2747 (97.9)	57 (2.1)	1.00 (1.62)	0.06 (0.01)	89.99 (215.54)	0.03 (0.02)
	No or unwittingly	3284 (54.1)	146 (4.4)	3138 (95.6)	3020 (91.9)	264 (8.1)	0.84 (1.28)	0.06 (0.01)	77.70 (185.37)	0.03 (0.02)
Smoking status	Never smoker	4177 (68.5)	315 (7.5)	3862 (92.5)	3967 (94.9)	210 (5.1)	0.96 (1.57)	0.06 (0.02)	86.29 (205.12)	0.03 (0.02)
	Current smoker	1062 (17.5)	49 (4.6)	1013 (95.4)	1009 (95.1)	53 (4.9)	0.52 (0.61)	0.06 (0.01)	73.95 (188.65)	0.03 (0.02)
	Past smoker	798 (13.1)	56 (7.1)	742 (92.9)	740 (92.8)	58 (7.2)	1.20 (1.71)	0.07 (0.01)	82.21 (190.29)	0.03 (0.02)
	Unknown	51 (0.9)	4 (7.8)	47 (92.2)	51 (100.0)	0 (0.0)	0.91 (0.65)	0.06 (0.007)	80.02 (201.80)	-

Table 2. *Cont.*

Covariate	Category	Number of Participants N (%)	Qualitative Anti-N N (%)		Qualitative Anti-S N (%)		Quantitative Anti-N Mean Value (SD)		Quantitative Anti-S Mean Value (SD)	
			Positive	Negative	Positive	Negative	Positive	Negative	Positive	Negative
Vaccination scheme	No vacc. ***	353 (5.7)	40 (11.3)	313 (88.7)	53 (15.0)	300 (85.0)	1.65 (2.64)	0.07 (0.02)	13.25 (50.72)	0.03 (0.02)
	One vaccination	380 (6.1)	123 (32.5)	257 (67.5)	367 (96.6)	13 (3.4)	1.15 (1.53)	0.07 (0.01)	98.05 (226.56)	0.04 (0.04)
	Two vaccinations	5001 (82.2)	245 (4.9)	4756 (95.1)	4997 (99.9)	4 (0.1)	0.75 (1.23)	0.06 (0.01)	55.40 (136.23)	0.06 (0.03)
	Three vaccinations	354 (5.8)	16 (4.4)	338 (95.6)	350 (98.9)	4 (1.1)	0.79 (1.07)	0.06 (0.01)	480.65 (416.65)	0.04 (0.04)
Household size	One person	1586 (25.9)	117 (7.3)	1469 (92.7)	1477 (93.2)	109 (6.8)	1.01 (1.57)	0.06 (0.01)	80.86 (197.26)	0.03 (0.02)
	2 people	2219 (36.5)	140 (6.3)	2079 (93.7)	2107 (94.9)	112 (5.1)	1.08 (1.65)	0.06 (0.01)	84.91 (209.09)	0.03 (0.02)
	3 people	969 (15.8)	68 (7.1)	901 (92.9)	924 (95.4)	45 (4.6)	0.89 (1.53)	0.06 (0.01)	82.79 (172.72)	0.04 (0.03)
	4 people	890 (14.8)	67 (7.6)	823 (92.4)	859 (96.6)	31 (3.4)	0.70 (1.13)	0.06 (0.01)	83.94 (213.37)	0.02 (0.02)
	5 people or more	331 (5.4)	23 (6.9)	308 (93.1)	314 (94.9)	17 (5.1)	0.50 (0.67)	0.06 (0.01)	92.08 (205.55)	0.04 (0.03)
	Unknown	93 (1.5)	9 (8.8)	84 (91.2)	86 (93.2)	7 (6.8)	1.15 (2.29)	0.07 (0.01)	68.55 (163.15)	0.04 (0.03)
Intake of immunosuppressive drugs	Yes	178 (2.9)	11 (6.1)	167 (93.9)	166 (93.3)	12 (6.7)	1.09 (1.21)	0.06 (0.02)	103.35 (234.73)	0.03 (0.02)
	No	5855 (96.0)	406 (6.9)	5449 (93.1)	5550 (94.8)	305 (5.2)	0.94 (1.53)	0.06 (0.01)	82.39 (199.94)	0.03 (0.02)
	Unknown	55 (1.1)	7 (10.9)	48 (89.1)	51 (93.8)	4 (6.2)	0.81 (0.64)	0.06 (0.008)	144.25 (233.67)	0.01 (0.01)

Table 2. *Cont.*

Covariate	Category	Number of Participants N (%)	Qualitative Anti-N N (%)		Qualitative Anti-S N (%)		Quantitative Anti-N Mean Value (SD)		Quantitative Anti-S Mean Value (SD)	
			Positive	Negative	Positive	Negative	Positive	Negative	Positive	Negative
Time since infection	Less than three months ago	11 (0.1)	7 (63.6)	4 (36.4)	10 (90.9)	1 (9.1)	0.74 (1.53)	0.03 (0.03)	835.43 (653.70)	0.04 (NA)
	Three to less than six months ago	10 (0.1)	3 (30.0)	7 (70.0)	10 (100.0)	0 (0.0)	0.74 (1.00)	0.05 (0.03)	184.22 (387.26)	-
	Six to twelve months ago	81 (1.3)	57 (70.3)	24 (29.7)	81 (100.0)	0 (0.0)	1.04 (1.75)	0.06 (0.03)	357.00 (500.08)	-
	More than twelve months ago	118 (1.9)	71 (59.6)	47 (40.4)	116 (98.4)	2 (1.6)	0.76 (1.10)	0.06 (0.02)	221.56 (301.96)	0.05 (0.05)
	No infection	5582 (91.8)	0 (0.0)	5582 (100.0)	5268 (94.4)	314 (5.6)	-	0.06 (0.01)	67.39 (166.41)	0.03 (0.02)
	Unknown	286 (4.8)	286 (100.0)	0 (0.0)	282 (98.7)	4 (1.3)	0.98 (1.56)	-	220.78 (323.30)	0.05 (0.03)
Breakthrough Infection (BTI)	Yes	63 (1.1)	28 (46.4)	35 (53.6)	62 (98.6)	1 (1.4)	0.58 (0.85)	0.05 (0.03)	546.24 (532.41)	0.09 (NA)
	No	6018 (98.8)	396 (6.5)	5622 (93.5)	5698 (94.8)	320 (5.2)	0.97 (1.55)	0.06 (0.01)	78.58 (187.13)	0.03 (0.02)
	Not applicable	7 (0.1)	0 (0.0)	7 (100.0)	7 (100.0)	0 (0.0)	-	0.07 (0.02)	21.87 (19.57)	-
Vaccination scheme and infection (immunity)	Infection yes, not vaccinated	40 (0.7)	40 (100.0)	0 (0.0)	36 (90.0)	4 (10.0)	1.65 (2.64)	-	18.30 (60.95)	0.05 (0.03)
	Infection yes + one vaccination	123 (2.0)	123 (100.0)	0 (0.0)	123 (100.0)	0 (0.0)	1.15 (1.53)	-	238.20 (341.43)	-
	Infection yes + two vaccinations	245 (4.0)	245 (100.0)	0 (0.0)	245 (100.0)	0 (0.0)	0.75 (1.23)	-	294.99 (398.29)	-
	Infection yes + three vaccinations	16 (0.3)	16 (100.0)	0 (0.0)	16 (100.0)	0 (0.0)	0.79 (1.07)	-	437.20 (462.30)	-

Table 2. *Cont.*

Covariate	Category	Number of Participants N (%)	Qualitative Anti-N N (%)		Qualitative Anti-S N (%)		Quantitative Anti-N Mean Value (SD)		Quantitative Anti-S Mean Value (SD)	
			Positive	Negative	Positive	Negative	Positive	Negative	Positive	Negative
	Infection no, not vaccinated	313 (5.1)	0 (0.0)	313 (100.0)	17 (5.5)	296 (94.5)	-	0.06 (0.02)	2.56 (7.37)	0.03 (0.02)
	Infection no + one vaccination	257 (4.1)	0 (0.0)	257 (100.0)	244 (94.9)	13 (5.1)	-	0.07 (0.01)	27.40 (62.10)	0.04 (0.03)
	Infection no + two vaccinations	4756 (78.3)	0 (0.0)	4756 (100.0)	4752 (99.9)	4 (0.1)	-	0.06 (0.01)	43.06 (90.88)	0.06 (0.02)
	Infection no + three vaccinations	338 (5.5)	0 (0.0)	338 (100.0)	334 (98.9)	4 (1.1)	-	0.06 (0.01)	482.71 (414.94)	0.03 (0.04)

* (-) indicates NA(NA); ** The values for the "unknown" category of the corresponding variables have been imputed for the modeling process; *** These participants were vaccinated on the day of blood sampling and thus considered as "not vaccinated".

To evaluate the risk of infection (anti-N seropositivity) based on qualitative binary anti-N results, a multivariable logistic regression model was used. Odds ratios (OR), 95% confidence intervals (CI), and *p*-values were computed. For the quantitative analyses, only participants with positive anti-N/S antibody values were included since the negative region is just affected by noise measurement and has no biological meaning. Two multivariable generalized linear models (GLM) with gamma distribution were fitted, with exponentiated coefficients representing the expected multiplicative changes in anti-N/S antibodies, 95% CIs, and *p*-values as output. To stabilize the anti-N model, fitting values greater than 10 were set to 10 (5 participants).

The covariate representing the cumulative number of COVID-19 cases detected in Munich (log-transformed to address the skewed distribution) was incorporated into all three models. This adjustment considered the different durations of potential exposure during the recruitment period. The covariables used in the three models are listed in Table 1, color-coded by model affiliation, and selected based on medical relevance. The missingness in the covariables was corrected by multiple imputations with m = 5 iterations. The response variables were also used in the multiple imputation procedure to obtain unbiased regression coefficients [38]. The total variance of the coefficient estimates over the repeated analyses was computed using Rubin's rules [39]. The model evaluation was performed using (i) the area under the receiver operating characteristic curve (AUC) value obtained from a ten-fold cross-validation for the qualitative analysis of binary anti-N and (ii) diagnostics plots for the quantitative analyses (Supplemental Figure S1).

All statistical analyses and visualization were performed using the R software (version 4.1.1, R Development Core Team, 2021). The models were estimated using the R package mgcv [40], and the visualization was conducted using the package APCtools [41].

3. Results

3.1. Cohort Description

Of a total of 6467 participants who were recruited for this study, 379 had to be excluded because of

- missing or incomplete antibody measurements (*n* = 13);
- missing or implausible self-reported year of birth (*n* = 303);
- participation in clinical vaccination trials or recruitment after 16 December 2021 *n* = 27);
- vaccination with brands not authorized in Germany (*n* = 13);
- missing or diverse information on sex (*n* = 8);
- implausible vaccination dates (*n* = 3)
- unknown vaccination scheme (*n* = 12).

The final dataset that was analyzed included 6088 participants who were enrolled in 16 different institutional subgroups. All of these participants had complete measurements of anti-S/anti-N antibodies and self-reported questionnaire data (as shown in Figure 1). In total, 6088 participants were included in the qualitative binary anti-N model, 424 participants in the quantitative anti-N model, and 5750 participants in the quantitative anti-S model.

A description of the final cohort can be found in Table 2. Participants were aged from 18 to 96 years, with a mean/median age of 41.8/41.0. Thereof, 72.0% (4379/6088) were female, and 28.0% (1709/6088) male. The majority of study participants were HCWs in hospitals (79.8%, 4860/6088) or of other HC institutions (9.1%, 557/6088), while 11.0% (671/6088) were non-HCWs but from the general population. A total of 94.8% (5676/6088) of the participants were anti-S positive, while only 6.9% (424/6088) were anti-N positive. When the analysis was limited to HCWs, 6.9% (374/5417) were found to be anti-N positive.

3.2. Risk Factor Analysis for Anti-N Seropositivity

To determine the risk factors for contracting SARS-CoV-2, the qualitative anti-N serology test was used in conjunction with different covariables in a multivariable logistic regression model. The variables were selected following medical relevance and are described in Table 1. The results are presented in both Figure 2, where they are displayed as ORs, and in Supplemental Table S1, where they are displayed as logarithms of the ORs.
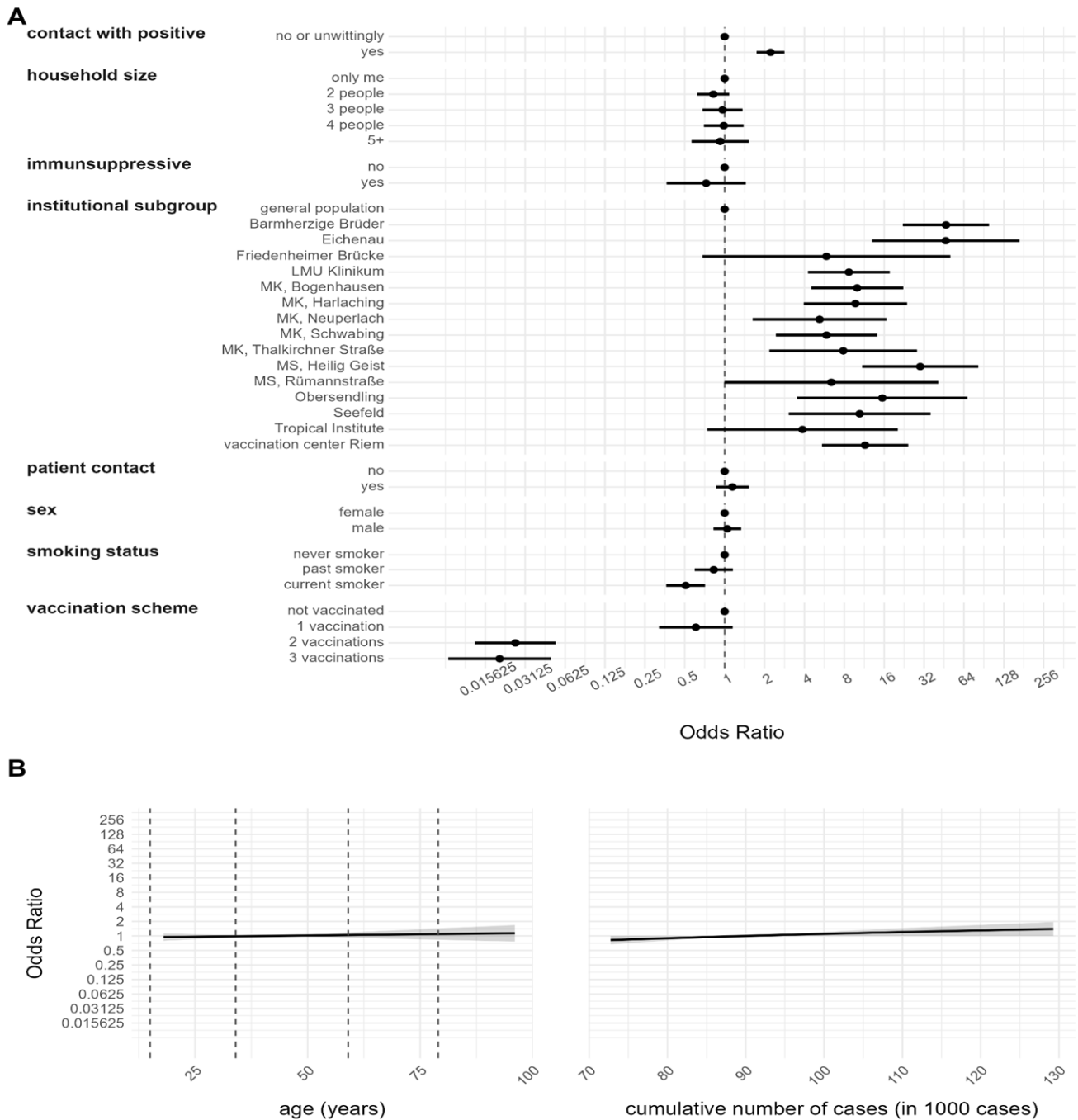

Figure 2. Risk factor analysis for SARS-CoV-2 infection, based on positive anti-N serology. Results are based on a logistic regression model and are given as ORs with a 95% CI. The obtained value of model evaluation using pooled AUC was 0.7398. (**A**) Estimates for categorical variables. (**B**) Estimates for continuous variables with 95% CI represented by the grey shadowed region.

The results indicate that compared to the general population, there is a statistically significant positive association between being an HCW employed in a hospital and an increased risk of contracting the virus (Barmherzige Brüder 46.8 [22.1, 99.1], LMU Klinikum 8.6 [4.2, 17.6], MK Bogenhausen 10.0 [4.4, 22.2], MK Harlaching 9.7 [3.9, 23.8], MK Neuperlach 5.2 [1.6, 16.6], MK Schwabing 5.8 [2.4, 14.1], MK Thalkirchner Straße 7.8 [2.1, 28.3], MS Rümannstraße (6.3 [1.0, 40.9] and Seefeld 10.4 [3.0, 35.8]). This was also the case for HCWs employed in institutions of long-term care (Eichenau 46.6 [12.9, 168.3], MS Heilig Geist 29.9 [10.9, 82.1] and Obersendling 15.4 [3.5, 67.9]) and for HCWs employed in the vaccination center Riem (11.4 [5.4, 24.2]). Interestingly, two centers did not show a statistically significant association between being an HCW and an increased risk of infection (Tropical Institute (3.8 [0.7, 20.2]) and Friedenheimer Brücke (5.8 [0.6, 50.5]). The vaccination scheme analysis revealed a strong negative association for individuals vaccinated with two (0.03 [0.01, 0.05]) or three (0.02 [0.008, 0.04]) doses compared to unvaccinated individuals. Compared to non-vaccinated participants (353 individuals), no significant effect for a vaccination with one dose (380 individuals) could be found (0.6 [0.3, 1.1]). Participants reporting a past known contact with SARS-CoV-2-positives demonstrated a strong positive association with anti-N antibody seropositivity (2.2 [1.7, 2.8]) compared to those having none or unwitting contact. Interestingly, compared to non-smokers, a strong negative association could be detected only for current smokers (0.5 [0.3, 0.7]) (former smokers not significant 0.8 [0.5, 1.1]). Age (1.0 [0.9, 1.0]), sex (male 1.0 [0.8, 1.3]), household size (2 people 0.8 [0.6, 1.0], 3 people 0.9 [0.6, 1.3], 4 people 0.9 [0.6, 1.3], 5 people or more 0.9 [0.5, 1.5], intake of immunosuppressive drugs (yes 0.7 [0.3, 1.4]) and having had contact with patients (yes 1.1 [0.8, 1.5]) were not statistically significant associated with anti-N seropositivity. The cumulative cases in the Munich municipality, indicating the development of the pandemic, were also shown to be non-significant (2.5 [0.8, 7.5]).

3.3. Determinants of Antibody Response after SARS-CoV-2 Infection

To identify the factors that influence antibody responses following infection with SARS-CoV-2, the quantitative anti-N serology was associated with different covariables in a multivariable GLM with gamma distribution. The variables were selected following medical relevance and are described in Table 1. The findings of this analysis are presented in Figure 3 as the expected multiplicative changes in anti-N/S antibodies (exponentiated coefficients) and in Supplemental Table S2 as coefficients of the model. The vaccination scheme analysis revealed that individuals with two (0.4 [0.2, 0.9]) and three vaccination doses (0.3 [0.1, 0.9]) had lower anti-N antibody levels compared to unvaccinated ones. No significant effect was found for participants with one vaccination dose (0.6 [0.3, 1.2]). A negative association could be detected for current smokers (0.6 [0.4, 1.0]), compared to non-smokers (former smokers not significant 1.1 [0.7, 1.7]). Age as a continuous variable was found to be a significant determinant, with older participants demonstrating higher anti-N antibody levels compared to younger ones (1.0 [1.003, 1.02]). Sex (male 1.2 [0.9, 1.6]), intake of immunosuppressive drugs (yes 1.1 [0.4, 2.8]), time since infection (three to less than six months ago 1.9 [0.1, 36.2], six to twelve months ago 1.3 [0.5, 3.2], more than twelve months ago 0.9 [0.3, 2.5]), BTI (yes 0.9 [0.4, 1.9]) and cumulative cases (1.9 [0.5, 6.9]) were not significant.

Figure 3. Anti-N antibody level after infection. Association between quantitative anti-N serology and determinants of antibody response. Results are based on a GLM with gamma distribution and are given as the expected multiplicative changes in anti-N/S antibodies (exponentiated coefficients) with a 95% CI. (**A**) Estimates for categorical variables. (**B**) Estimates for continuous variables with 95% CI represented by the grey shadowed region.

3.4. Determinants of Antibody Response after SARS-CoV-2 Vaccination and/or Infection

To ascertain the determinants that impact the antibody response after SARS-CoV-2 vaccination and infection, the quantitative anti-S serology was associated with different covariables in a multivariable GLM with gamma distribution. The results are presented in Figure 4 as the expected multiplicative changes in anti-N/S antibodies (exponentiated coefficients) and Supplemental Table S3 as coefficients of the model. Compared to unvaccinated but infected individuals, a strong positive association could be found for participants who were vaccinated one (4.4 [1.6, 12.2]), two (23.4 [8.4, 64.8]), or three (469.5 [162.9, 1352.8]) times but did not undergo an infection. An even stronger positive association was found for participants who were vaccinated one (15.9 [6.3, 40.0]) or two (51.0 [20.9, 124.8]) times and underwent an infection. The group that received three vaccinations in addition to a past infection had a lower estimate (81.9 [20.6, 325.0]) compared to the group with three vaccinations but no previous infection. However, the estimate was still higher than the group that had received two vaccinations and had a history of infection. Moreover, days since the second vaccination and thus completion of the primary vaccination schedule revealed a high negative association (0.994 [0.993, 0.995]). Participants with BTI (infection occurring two weeks after the second vaccination) demonstrated a positive association compared to non-BTI infections (infection prior to or within two weeks after the second vaccination) (4.0 [2.2, 7.4]). Interestingly, the cumulative cases in the Munich municipality, indicating the development of the pandemic, were also shown to be significant (2.5 [1.6, 3.8]). Age was found to be a significant determinant, with older participants demonstrating a negative association with anti-S antibody quantity compared to younger participants (0.987 [0.983, 0.992]). Compared to non-smokers, a negative association could be detected for

current smokers (0.8 [0.6, 0.9]) (former smokers not significant 1.0 [0.8, 1.1]). Time since infection (three to less than six months ago 0.7 [0.2, 2.6], six to twelve months ago 1.5 [0.6, 3.8], more than twelve months ago 1.3 [0.5, 3.4], no infection 0.4 [0.1, 1.2]), as well as sex (male 0.9 [0.8, 1.0]) and intake of immunosuppressive drugs (yes 1.1 [0.8, 1.5]) were not statistically significantly associated with quantitative anti-S serology.
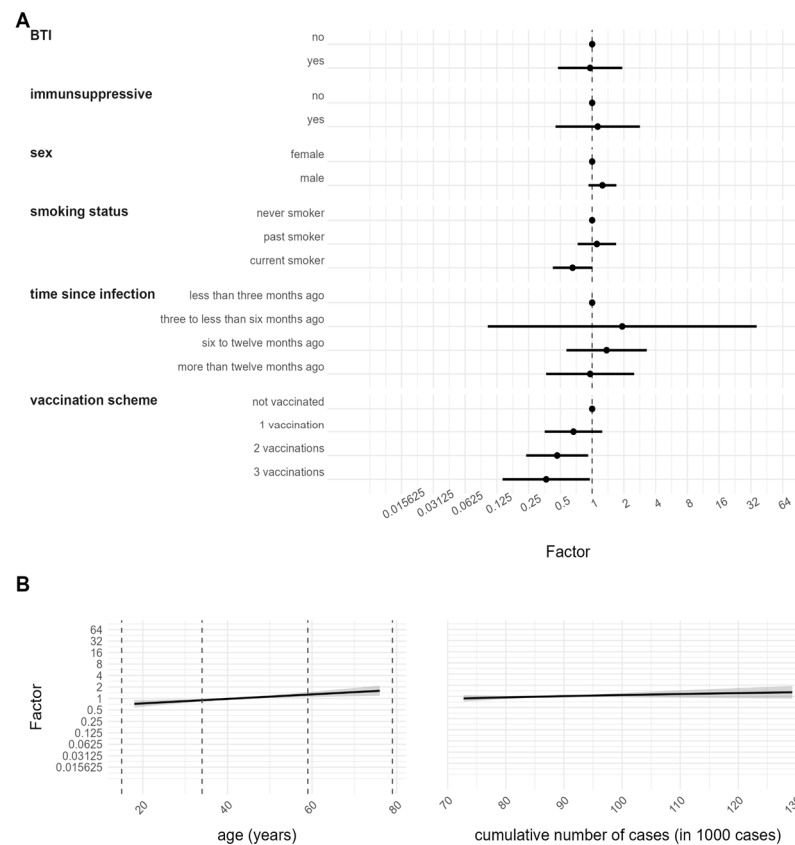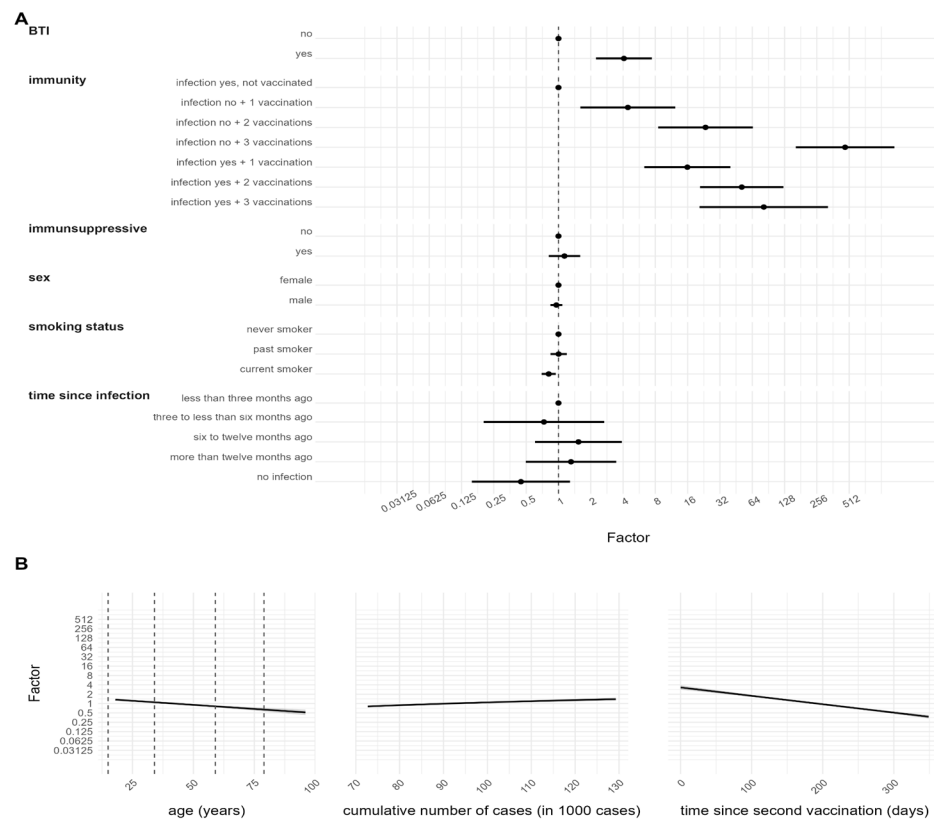

Figure 4. Anti-S antibody level after infection and vaccination. Association between quantitative anti-S serology and determinants of antibody response. Results are based on a GLM with gamma distribution and are given as the expected multiplicative changes in anti-N/S antibodies (exponentiated coefficients) with a 95% CI. (**A**) Estimates for categorical variables. (**B**) Estimates for continuous variables with 95% CI represented by the grey shadowed region.

4. Discussion

In this study, we explore the factors contributing to COVID-19 infections in a cohort comprising both the general population and HCWs, who face an increased risk of exposure to the SARS-CoV-2 virus. We utilized capillary blood samples to detect the presence of SARS-CoV-2 antibodies, which are indicative of previous infections, including both symptomatic and asymptomatic cases, as well as vaccination history. Moreover, our analysis aimed to identify factors that influence the immune response following infection or vaccination.

The recruitment process for KoCo-Impf took place over a period of seven months during the waves of the pandemic. To consider the changing time under risk, we included the overall cumulative number of cases in Munich at the respective recruitment time as a continuous covariate in our analysis. Our analysis showed that this variable has a positive though not significant, effect on anti-N seropositivity, indicating that HCWs were only weakly affected by the infection waves of the general population. One possible explanation is that since most of the reported infections occurred between six and twelve months prior to blood sampling, they mostly occurred in the first half of 2021. As a result, any association between the cumulative number of cases and anti-N seropositivity in the second half of 2021 may not be evident. Another reason could be that localized outbreaks within

specific institutions strongly influence the observed differences. This could potentially overshadow the effects of broader waves occurring within the general population. Other reasons could be that there was increasing availability of personal protective equipment (PPE) [42] and changes in risk behavior in 2021 [43]. In Bavaria, wearing protective FFP2 masks became mandatory in January 2021. Additionally, restrictions on access to public life were introduced in August 2021, based on vaccination, infection, and testing status, to reduce transmission rates [43]. As PPE has been shown to reduce the risk of infection [44], the increasing use of PPE may have compensated for any emerging outbreaks in 2021. In contrast, we found that the cumulative cases had an impact on anti-S antibody response, which could be explained by the different immune solicitations during the different waves. The dominant virus variant in Germany changed from alpha to delta in June 2021 [45], and a heterologous vaccination scheme was recommended from July 2021 onward [25–27,46,47]. Vaccination with Comirnaty rather than Spikevax was recommended for individuals younger than 30 years in November 2021 [48].

Age was found to be a statistically significant factor in anti-N immune response, with older participants showing higher levels after infection compared to younger ones. This is consistent with previous research that found a correlation between higher levels of the anti-N antibody and older age, male gender, ethnicity, and prior symptom history [49–51]. This suggests that infections in elderly individuals could lead to a more severe course of the disease and higher production of antibodies. In contrast to the anti-N immune response, our study showed that older age results in a decreased anti-S immune response, which is consistent with previous studies [21,22,52,53]. This suggests that the stimulation caused by vaccinations is more effective in younger individuals when compared to older ones.

Another aspect to consider when examining the pattern of higher anti-N levels after infection but generally lower anti-S levels in non-infected individuals of higher age is the longitudinal development of the immune response in relation to the time since vaccination. Since older individuals are considered a "high-risk" group, they were vaccinated earlier than younger individuals [6–8]. Considering that anti-S antibodies follow a pattern of rising, peaking, falling, and eventually reaching a plateau [53], the earlier timing of vaccination could have led to a decrease in the anti-S antibody titer at the time of blood collection, resulting in a lower overall level. Consequently, the protection against a second infection is considered to be lower in this group, posing an increased risk of SARS-CoV-2 infection and a stronger immune response against the N protein compared to younger individuals who were recently vaccinated and had a higher anti-S antibody titer shortly after vaccination.

However, it is worth noting that a systematic review and meta-analysis conducted by Cheng et al. (2022) focused on prime-boost immunization with the COVID-19 vaccine but only analyzed studies with non-infected participants [27]. Subgroup analyses by age did not find a significant difference in antibody concentrations between young and old populations. Nevertheless, this finding may be attributed to the selection bias of only analyzing non-infected individuals. Young and elderly people who were most affected by the pandemic were excluded, and the definition of non-infected might vary between studies (RT-PCR and serology).

Our analysis has shown that individuals who currently smoke have a lower prevalence of anti-N SARS-CoV-2 antibodies compared to those who never smoked. It is important to note that the current smoker group in our cohort had significantly fewer participants compared to the non-smoker group (1 to 4 ratio). This discrepancy in sample size raises concerns about the comparability of the two groups, as the underrepresentation of current smokers may introduce bias to the results. However, the lower risk of infection among current smokers aligns with similar findings from the analysis of the KoCo19 cohort [30]. Additionally, a recent study by Günther et al. (2022) supports these findings, as it demonstrated that current smokers were nearly half as likely to test positive for SARS-CoV-2 antibodies compared to non-smokers [54]. That study did not observe any differences in antibody levels between smokers and non-smokers who had been infected with or vaccinated against SARS-CoV-2, suggesting that the lower prevalence of antibodies in

smokers may be attributed to lower infection rates rather than reduced antibody response. In contrast, our results show a significantly reduced response to both the anti-S and anti-N antibodies in current smokers compared to non-smokers, consistent with previous studies by Reusch (2023), Ferrara (2022), and Moncunill (2022) [20,24,52]. Smoking may induce an immunosuppressive effect, as reported by Haddad (2021) and Sopori (2002) [55,56]. The lower anti-N antibody levels in current smokers compared to never-smokers may indicate not only a reduced development of antibodies but also a faster seroconversion to negative levels. Therefore, the anti-N seropositivity in current smokers may not be directly comparable to the never-smoker group, assuming a similar decrease and subsequent non-detection of past cases. It is also worth considering that smoking has been identified and communicated through the media as a risk factor for severe COVID-19 infections, leading to increased morbidity and mortality. Hence, it cannot be excluded that current smokers may have taken more precautions to avoid contact compared to non-smokers. The effect of current smoking on the risk of infection remains controversial and should be interpreted with caution [57].

The risk factor analysis showed that HCWs had an increased risk of infection compared to the general population, which is interestingly consistent with previous research on the KoCo19 cohort and other studies that have identified HCWs as a vulnerable group for infection [30,44,54]. However, the use of PPE has been shown to reduce the risk of infection [44], possibly leading to a change in the risk of infection in HCWs over time. Since our definition of infection is based only on positive anti-N, which remains positive for a long period of time [58], this baseline analysis of our study is not designed to detect this aspect. Recent research by Vivaldi et al. (2022) identified a change in the risk of infection due to time and vaccination status, with HCWs being at a higher risk of infection before vaccination but a reduced risk of breakthrough infection after primary vaccination [14]. Since the inclusion criteria for the KoCo-Impf study required at least one vaccination, it is impossible to correct this effect here. However, a follow-up analysis with the KoCo19 and the KoCo-Impf cohort may provide more insight into this aspect.

Another approach to determining whether HCWs have an increased risk of SARS-CoV-2 infection than the general population is by comparing anti-N seropositivities. In November 2021, the KoCo19 cohort, which represents the general Munich population, conducted its fourth follow-up in parallel with the KoCo-Impf recruitment. To compare the anti-N seroprevalence of both cohorts, we focused on the estimates for vaccinated persons in the KoCo19 cohort. The seropositivity was estimated to be 11.8% (9.8–13.8%) [30]. When we restricted the KoCo-Impf analysis to only HCWs, we observed a seroprevalence of 6.9% (6.2–7.6%), which is considerably lower than the seroprevalence of the vaccinated KoCo19 participants at the same time point. However, it is important to note that while the KoCo19 cohort is population-based and representative of the Munich population after statistical weighting, the KoCo-Impf cohort can be considered a convenience sample since it was not randomly selected. Therefore, it might be very complicated to compare both seroprevalences. This further emphasizes the importance of representative study designs. As the risk factor analysis for both KoCo19 and KoCo-Impf indicated a statistically significant higher risk of infections among HCWs, the lower seroprevalence in KoCo-Impf could be attributed to variations in infection and vaccination timing compared to the general population. Due to their higher risk, it is possible that HCWs were infected more frequently during the period when the general population was receiving their first two vaccinations. As HCWs, they had better access to testing facilities, which allowed them to become aware of their infection and receive vaccinations later in accordance with vaccination policies. On the other hand, in the general population, it is likely that more individuals were unknowingly infected and still received vaccinations despite their recent infection. The relatively lower underreporting probability among HCWs likely resulted in fewer cases where individuals were vaccinated despite having been recently infected, leading to lower seroprevalence among HCWs.

The risk of SARS-CoV-2 anti-N seropositivity was found to be higher among all HCWs except for those working in two specific institutions: Friedenheimer Brücke and Tropical Institute. While HCWs at Friedenheimer Brücke and the Tropical Institute have regular patient interactions, their work environment differs from that of HCWs in hospitals and long-term care facilities. Friedenheimer Brücke specializes in prenatal diagnostics, while the Tropical Institute primarily focuses on travel counseling and vaccinations. As a result, both facilities have a smaller patient population, and if symptomatic, these patients can choose to stay at home, thereby reducing the risk of infection for the personnel. The analysis did not find a significant effect of patient contact on SARS-CoV-2 anti-N seropositivity, suggesting that the increased risk of infection may be due to occupational activities and the working environment. This is consistent with recent research identifying occupational activities (tracheal intubation) as a risk factor for HCWs [44]. In addition, differences in infection frequency and spread between institutions can lead to variations in seropositivity rates.

As the institutional subgroup was found to have the strongest effect as a covariate, a sensitivity analysis was performed to evaluate how it impacted the overall risk factor analysis (Supplemental Table S4). However, no remarkable difference was observed.

Upon studying the kinetics of the anti-S antibody response, we found that the level increases with the number of COVID-19 vaccinations but decreases after days since the second vaccination. These results are consistent with previously published studies [52]. When individuals with one or two doses of vaccination were additionally infected, our analysis showed that they presented significantly higher anti-S values compared to only vaccinated individuals. Interestingly, with three vaccinations, the effect was reversed. While other studies with one or two vaccinations have shown similar behavior, we could not find comparable studies in the literature on the analysis of three vaccinations [21,22,52,53]. The combination of three vaccinations and one infection suggests that either the infection occurred in the early phases of the pandemic or recently (an infection between the vaccination scheme can be excluded in the time before Omicron), but the effect might be smaller due to the passage of time or ongoing immune response. This can be confirmed by the similarities with the estimate of two vaccinations with or without infection.

Our findings also indicate that the sequence of the triggers is important, with BTIs showing higher anti-S antibody titers but a non-significant tendency towards lower anti-N. This is in line with the other literature where the interpretation is that the immune system is solicited with vaccination (higher anti-S) so that a severe disease can be prevented (lower anti-N, since less reaction is needed) [59–61].

It is interesting to note that even though SARS-CoV-2 infection clearly affects the anti-S immune response, the duration since infection did not have a significant effect in any of our models. This finding is consistent with results that have already been published [20]. Numerous studies have demonstrated that the longitudinal development of both anti-N and anti-S antibodies follows a pattern of increasing, peaking, decreasing, and ultimately plateauing [53,62,63]. In our data, most of the reported infections occurred between six and twelve months prior to blood sampling, during which time most participants had already reached the plateau phase. Therefore, the lack of statistical significance is likely due to the fact that the only trajectory that can be fitted to these data is the plateau phase.

The analysis presented in this study encompasses the time period starting from the onset of the pandemic until December 2021. Therefore, the conclusions derived from this analysis specifically pertain to SARS-CoV-2 infections caused by the wild-type to delta variants of concern. A follow-up was carried out in May 2022 to include the circulation of the omicron variant of concern. A follow-up manuscript will present the findings of this follow-up study and compare them with the results obtained from the initial analysis.

The number of individuals who tested positive for anti-N antibodies but were unvaccinated (40) is lower than the number of individuals who tested positive for anti-S antibodies (53), even though their antibody response can only be attributed to a natural infection. This difference of 13 samples is likely due to the recruitment process rather than the assays them-

selves. Our cohort recruitment includes individuals at various stages of infection (recently infected, infected long ago, etc.) and at different time points of vaccination. Consequently, it is possible that a recently infected individual may only exhibit one type of antibody since their development requires time. On the other hand, someone who was infected a long time ago may have already seroconverted back, although not completely for both antibodies. Furthermore, information regarding vaccination status relies on self-reported questionnaire data, which may be influenced by bias or incomplete responses. Therefore, the discrepancy in this small number of samples is likely a combination of these factors.

After more than a year since the onset of the pandemic, we established the KoCo-Impf cohort to examine antibody development following vaccination and infection. Considering the significant findings already observed with KoCo19, we primarily focused on recruiting HCWs who face a specific risk of infection due to their frequent contact with multiple individuals, some of whom may be infected. It is important to note that our study population represents a convenience sample consisting solely of non-randomly selected vaccinated individuals. This aspect makes it more challenging to compare our results directly with those of the general population. However, the unique combination of our definition of seropositivity (based on anti-N and anti-S values) and the large sample size with detailed vaccination information makes our cohort unique in the world. We also found that vaccination protects against infection, but elderly people tend to have weaker immune responses and present higher anti-N but lower anti-S values compared to younger participants. Interestingly, smokers had a decreased risk of infection and lower immune responses after both vaccination and infection. HCWs were found to have a higher risk of SARS-CoV-2 infection in both the KoCo19 and the KoCo-Impf studies. However, only a few risk factors, such as age, vaccination status, contact with SARS-CoV-2 positive cases, and smoking status, were found to be statistically significant. As a result, no specific subgroups of HCWs requiring greater protection were identified. Instead, it is crucial to ensure the protection of all HCWs regardless of individual characteristics.

5. Conclusions

HCWs had a higher risk of SARS-CoV-2 infection in both the KoCo19 and KoCo-Impf studies. Multiple vaccinations and diverse vaccination schedules reduced infection risk while influencing the anti-N and anti-S immune response. Age impacted immune response, with older individuals exhibiting differences compared to younger ones. Interestingly, smokers had a lower infection risk, but their immune response weakened after vaccination and infection. The limited number of significant risk factors indicates that no specific HCW subgroups require heightened protection but that the protection of all HCWs remains crucial, regardless of individual characteristics.

Author Contributions: Conceptualization, M.H. (Michael Hoelscher), C.J., A.W. and N.C.; Methodology, N.C., C.R., S.W. (Simon Wiegrebe) and H.K.; Software, M.W., T.M., Y.K. and C.R.; Validation, C.R. and N.C.; Formal Analysis, M.W., T.M., C.R., Y.K., R.L.G. and N.C.; Investigation, M.H. (Michael

Hoelscher), N.C. and A.W.; Resources, M.P., I.N., S.W. (Simon Winter), R.R.-A., I.P. and M.H. (Marlene Hannes); Data Curation, C.R., M.H. (Marlene Hannes), M.W., T.M., L.X. and Y.K.; Writing—Original Draft Preparation, C.R., N.C. and Y.K.; Writing—Reviewing and Editing, C.R., N.C., H.K., Y.K., K.R., R.L.G., C.F., A.W. and T.G.L.T.; Visualization, M.W., T.M., Y.K., C.R. and N.C.; Supervision, N.C., H.K., C.J., A.W. and M.H. (Michael Hoelscher); Project Administration, C.J., C.R., M.P., I.N., S.W. (Simon Winter) and M.H. (Marlene Hannes); Funding Acquisition, M.H. (Michael Hoelscher). All authors have read and agreed to the published version of the manuscript.

Institutional Review Board Statement: This study was conducted in accordance with the Declaration of Helsinki and approved by the Ethics Committee of the LMU München (protocol code 21-0569 of 18 May 2021).

Informed Consent Statement: Informed consent was obtained from all subjects involved in this study.

Data Availability Statement: Data are subject to data protection regulations and can be made available upon reasonable request to the corresponding author. To facilitate reproducibility and reuse, the code used to perform the analyses and generate the figures was made available in an open-source GitHub repository (https://gitlab.lrz.de/tropi-data-analysis-team/koco/kocoimpf-data.git (accessed on 11 July 2023)).

Conflicts of Interest: In addition to the funding disclosed in the funding section, AW and MH report personal fees and non-financial support from Roche Diagnostics, non-financial support from Euroimmun, non-financial support from Viramed, and non-financial support from Mikrogen. AW and MH report grants, non-financial support and other from German Centre for Infection Research DZIF, grants and non-financial support from Government of Bavaria, non-financial support from BMW, non-financial support from Munich Police, non-financial support and other from Accenture. MH and AW report personal fees and non-financial support received from Box-Betrobox and non-financial support from Becker MVZ during the conduction of this study. AW is involved in other different patents and companies, not in relation to the serology of SARS-CoV-2. AW reports personal fees and others from Haeraeus Sensors and non-financial support from Bruker Daltonics, all of which are outside the submitted work and non-related to SARS-CoV-2. The funders had no role in this study's design, data collection, data analyses, data interpretation, writing, or submission of this manuscript.

References

1. Lai, C.C.; Shih, T.P.; Ko, W.C.; Tang, H.J.; Hsueh, P.R. Severe acute respiratory syndrome coronavirus 2 (SARS-CoV-2) and coronavirus disease-2019 (COVID-19): The epidemic and the challenges. *Int. J. Antimicrob. Agents.* **2020**, *55*, 105924. [CrossRef]
2. WHO Director-General's Opening Remarks at the Media Briefing on COVID-19—11 March 2020. Available online: https://www.who.int/director-general/speeches/detail/who-director-general-s-opening-remarks-at-the-media-briefing-on-covid-19{-}{-}-11-march-2020 (accessed on 13 April 2023).
3. WHO Coronavirus (COVID-19) Dashboard. Available online: https://covid19.who.int/ (accessed on 13 April 2023).
4. RKI. Table Showing Current COVID-19 Infections per Day as Time Series. Available online: https://npgeo-corona-npge-de.hub.arcgis.com/datasets/dd4580c810204019a7b8eb3e0b329dd6_0/explore (accessed on 16 October 2022).
5. RKI. Tabelle mit den Gemeldeten Impfungen nach Bundesländern und Impfquoten nach Altersgruppen. Available online: https://www.rki.de/DE/Content/InfAZ/N/Neuartiges_Coronavirus/Daten/Impfquotenmonitoring (accessed on 16 September 2021).
6. World Health Organization. Guidance on Developing a National Deployment and Vaccination Plan for COVID-19 Vaccines: Interim Guidance, 16 November 2020. Available online: https://apps.who.int/iris/handle/10665/336603?search-result=true&query=Guidance+on+developing+a+national+deployment+and+vaccination+plan+for+COVID-19+vaccines%3A+interim+guidance&scope=&rpp=10&sort_by=score&order=desc (accessed on 11 July 2023).
7. World Health Organization. Guidance on Developing a National Deployment and Vaccination Plan for COVID-19 Vaccines: Interim Guidance, 1 June 2021. Available online: https://apps.who.int/iris/handle/10665/341564?search-result=true&query=Guidance+on+developing+a+national+deployment+and+vaccination+plan+for+COVID-19+vaccines%3A+interim+guidance&scope=&rpp=10&sort_by=score&order=desc (accessed on 11 July 2023).
8. RKI. Positionspapier der STIKO, Leopoldina und des Deutschen Ethikrats zur Verteilung eines COVID-19-Impfstoffes. Available online: https://www.rki.de/DE/Content/Infekt/Impfen/ImpfungenAZ/COVID-19/Positionspapier.html (accessed on 12 January 2023).
9. Ledda, C.; Costantino, C.; Motta, G.; Cunsolo, R.; Stracquadanio, P.; Liberti, G.; Maltezou, H.C.; Rapisarda, V. SARS-CoV-2 mRNA Vaccine Breakthrough Infections in Fully Vaccinated Healthcare Personnel: A Systematic Review. *Trop. Med. Infect. Dis.* **2022**, *7*, 9. [CrossRef]
10. Petráš, M.; Máčalík, R.; Janovská, D.; Čelko, A.M.; Dáňová, J.; Selinger, E.; Doleček, J.; Neradová, S.; Franklová, M.; Dlouhý, P.; et al. Risk factors affecting COVID-19 vaccine effectiveness identified from 290 cross-country observational studies until February 2022: A meta-analysis and meta-regression. *BMC Med.* **2022**, *20*, 461. [CrossRef] [PubMed]
11. Mizrahi, B.; Lotan, R.; Kalkstein, N.; Peretz, A.; Perez, G.; Ben-Tov, A.; Chodick, G.; Gazit, S.; Patalon, T. Correlation of SARS-CoV-2-breakthrough infections to time-from-vaccine. *Nat. Commun.* **2021**, *12*, 6379. [CrossRef] [PubMed]
12. Radon, K.; Saathoff, E.; Pritsch, M.; Guggenbühl Noller, J.M.; Kroidl, I.; Olbrich, L.; Thiel, V.; Diefenbach, M.; Riess, F.; Forster, F.; et al. Protocol of a population-based prospective COVID-19 cohort study Munich, Germany (KoCo19). *BMC Public Health* **2020**, *20*, 1036. [CrossRef]
13. Warszawski, J.; Beaumont, A.L.; Seng, R.; de Lamballerie, X.; Rahib, D.; Lydié, N.; Slama, R.; Durrleman, S.; Raynaud, P.; Sillard, P.; et al. Prevalence of SARS-Cov-2 antibodies and living conditions: The French national random population-based EPICOV cohort. *BMC Infect. Dis.* **2022**, *22*, 41. [CrossRef] [PubMed]
14. Vivaldi, G.; Jolliffe, D.A.; Holt, H.; Tydeman, F.; Talaei, M.; Davies, G.A.; Lyons, R.A.; Griffiths, C.J.; Kee, F.; Sheikh, A.; et al. Risk factors for SARS-CoV-2 infection after primary vaccination with ChAdOx1 nCoV-19 or BNT162b2 and after booster vaccination with BNT162b2 or mRNA-1273: A population-based cohort study (COVIDENCE UK). *Lancet Reg. Health Eur.* **2022**, *22*, 100501. [CrossRef]
15. Einhauser, S.; Peterhoff, D.; Beileke, S.; Günther, F.; Niller, H.H.; Steininger, P.; Knöll, A.; Korn, K.; Berr, M.; Schütz, A.; et al. Time Trend in SARS-CoV-2 Seropositivity, Surveillance Detection- and Infection Fatality Ratio until Spring 2021 in the Tirschenreuth County-Results from a Population-Based Longitudinal Study in Germany. *Viruses* **2022**, *14*, 1168. [CrossRef]
16. Wagner, R.; Peterhoff, D.; Beileke, S.; Günther, F.; Berr, M.; Einhauser, S.; Schütz, A.; Niller, H.H.; Steininger, P.; Knöll, A.; et al. Estimates and Determinants of SARS-CoV-2 Seroprevalence and Infection Fatality Ratio Using Latent Class Analysis: The Population-Based Tirschenreuth Study in the Hardest-Hit German County in Spring 2020. *Viruses* **2021**, *13*, 1118. [CrossRef]
17. Collatuzzo, G.; Visci, G.; Violante, F.S.; Porru, S.; Spiteri, G.; Monaco, M.G.L.; Larese Fillon, F.; Negro, C.; Janke, C.; Castelletti, N.; et al. Determinants of anti-S immune response at 6 months after COVID-19 vaccination in a multicentric European cohort of healthcare workers—ORCHESTRA project. *Front. Immunol.* **2022**, *13*, 986085. [CrossRef]
18. Porru, S.; Monaco, M.G.L.; Spiteri, G.; Carta, A.; Pezzani, M.D.; Lippi, G.; Gibellini, D.; Tacconelli, E.; Dalla Vecchia, I.; Sala, E.; et al. SARS-CoV-2 Breakthrough Infections: Incidence and Risk Factors in a Large European Multicentric Cohort of Health Workers. *Vaccines* **2022**, *10*, 1193. [CrossRef] [PubMed]
19. Inchingolo, A.D.; Malcangi, G.; Ceci, S.; Patano, A.; Corriero, A.; Vimercati, L.; Azzollini, D.; Marinelli, G.; Coloccia, G.; Piras, F.; et al. Effectiveness of SARS-CoV-2 Vaccines for Short- and Long-Term Immunity: A General Overview for the Pandemic Contrast. *Int. J. Mol. Sci.* **2022**, *23*, 8485. [CrossRef] [PubMed]
20. Moncunill, G.; Aguilar, R.; Ribes, M.; Ortega, N.; Rubio, R.; Salmerón, G.; Molina, M.J.; Vidal, M.; Barrios, D.; Mitchell, R.A.; et al. Determinants of early antibody responses to COVID-19 mRNA vaccines in a cohort of exposed and naïve healthcare workers. *EBioMedicine* **2022**, *75*, 103805. [CrossRef] [PubMed]

21. Notarte, K.I.; Guerrero-Arguero, I.; Velasco, J.V.; Ver, A.T.; Santos de Oliveira, M.H.; Catahay, J.A.; Khan, M.S.R.; Pastrana, A.; Juszczyk, G.; Torrelles, J.B.; et al. Characterization of the significant decline in humoral immune response six months post-SARS-CoV-2 mRNA vaccination: A systematic review. *J. Med. Virol.* **2022**, *94*, 2939–2961. [CrossRef]

22. Notarte, K.I.; Ver, A.T.; Velasco, J.V.; Pastrana, A.; Catahay, J.A.; Salvagno, G.L.; Yap, E.P.H.; Martinez-Sobrido, L.B.; Torrelles, J.; Lippi, G.; et al. Effects of age, sex, serostatus, and underlying comorbidities on humoral response post-SARS-CoV-2 Pfizer-BioNTech mRNA vaccination: A systematic review. *Crit. Rev. Clin. Lab. Sci.* **2022**, *59*, 373–390. [CrossRef]

23. Yang, S.L.; Mat Ripen, A.; Leong, C.T.; Lee, J.V.; Yen, C.H.; Chand, A.K.; Koh, K.; Abdul Rahim, N.A.B.; Gokilavanan, V.; Mohamed, N.; et al. COVID-19 breakthrough infections and humoral immune response among BNT162b2 vaccinated healthcare workers in Malaysia. *Emerg. Microbes Infect.* **2022**, *11*, 1262–1271. [CrossRef]

24. Ferrara, P.; Gianfredi, V.; Tomaselli, V.; Polosa, R. The Effect of Smoking on Humoral Response to COVID-19 Vaccines: A Systematic Review of Epidemiological Studies. *Vaccines* **2022**, *10*, 303. [CrossRef]

25. Deng, J.; Ma, Y.; Liu, Q.; Du, M.; Liu, M.; Liu, J. Comparison of the Effectiveness and Safety of Heterologous Booster Doses with Homologous Booster Doses for SARS-CoV-2 Vaccines: A Systematic Review and Meta-Analysis. *Int. J. Environ. Res. Public Health* **2022**, *19*, 10752. [CrossRef]

26. Lv, J.; Wu, H.; Xu, J.; Liu, J. Immunogenicity and safety of heterologous versus homologous prime-boost schedules with an adenoviral vectored and mRNA COVID-19 vaccine: A systematic review. *Infect. Dis. Poverty* **2022**, *11*, 53. [CrossRef]

27. Cheng, H.; Peng, Z.; Si, S.; Alifu, X.; Zhou, H.; Chi, P.; Zhuang, Y.; Mo, M.; Yu, Y. Immunogenicity and Safety of Homologous and Heterologous Prime-Boost Immunization with COVID-19 Vaccine: Systematic Review and Meta-Analysis. *Vaccines* **2022**, *10*, 798. [CrossRef]

28. Pritsch, M.; Radon, K.; Bakuli, A.; Le Gleut, R.; Olbrich, L.; Guggenbüehl Noller, J.M.; Saathoff, E.; Castelletti, N.; Garí, M.; Pütz, P.; et al. Prevalence and Risk Factors of Infection in the Representative COVID-19 Cohort Munich. *Int. J. Environ. Res. Public Health* **2021**, *18*, 3572. [CrossRef] [PubMed]

29. Radon, K.; Bakuli, A.; Pütz, P.; Le Gleut, R.; Guggenbuehl Noller, J.M.; Olbrich, L.; Saathoff, E.; Garí, M.; Schälte, Y.; Frahnow, T.; et al. From first to second wave: Follow-up of the prospective COVID-19 cohort (KoCo19) in Munich (Germany). *BMC Infect. Dis.* **2021**, *21*, 925. [CrossRef] [PubMed]

30. Le Gleut, R.; Pütz, P.; Radon, K.; Reinkemeyer, C.; Castelletti, N. The Representative COVID-19 Cohort Munich (KoCo19): From the Beginning of the Pandemic to the Delta Virus Variant. *BMC Infect. Dis.* **2023**, *23*, 466. [CrossRef] [PubMed]

31. Orchestra. Available online: https://orchestra-cohort.eu/ (accessed on 19 January 2023).

32. Paul-Ehrlich-Institut. Nicht-interventionelle Studie (Anwendungsbeobachtung) NIS-Nr.: 619. Available online: https://www.pei.de/SharedDocs/awb/nis-0601-0700/0619.html?nn=173154] (accessed on 5 June 2023).

33. Beyerl, J.; Rubio-Acero, R.; Castelletti, N.; Paunovic, I.; Kroidl, I.; Khan, Z.N.; Bakuli, A.; Tautz, A.; Oft, J.; Hoelscher, M.; et al. A dried blood spot protocol for high throughput analysis of SARS-CoV-2 serology based on the Roche Elecsys anti-N assay. *EBioMedicine* **2021**, *70*, 103502. [CrossRef]

34. Rubio-Acero, R.; Castelletti, N.; Fingerle, V.; Olbrich, L.; Bakuli, A.; Wölfel, R.; Girl, P.; Müller, K.; Jochum, S.; Strobl, M.; et al. In Search of the SARS-CoV-2 Protection Correlate: Head-to-Head Comparison of Two Quantitative S1 Assays in Pre-characterized Oligo-/Asymptomatic Patients. *Infect. Dis. Ther.* **2021**, *10*, 1505–1518. [CrossRef]

35. Olbrich, L.; Castelletti, N.; Schälte, Y.; Garí, M.; Pütz, P.; Bakuli, A.; Pritsch, M.; Kroidl, I.; Saathoff, E.; Guggenbuehl Noller, J.M.; et al. Head-to-head evaluation of seven different seroassays including direct viral neutralisation in a representative cohort for SARS-CoV-2. *J. Gen Virol.* **2021**, *102*, 001653. [CrossRef]

36. Brochot, E.; Demey, B.; Touzé, A.; Belouzard, S.; Dubuisson, J.; Schmit, J.L.; Duverlie, G.; Francois, C.; Castelain, S.; Helle, F. Anti-spike, Anti-nucleocapsid and Neutralizing Antibodies in SARS-CoV-2 Inpatients and Asymptomatic Individuals. *Front. Microbiol.* **2020**, *11*, 584251. [CrossRef]

37. Borremans, B.; Gamble, A.; Prager, K.C.; Helman, S.K.; McClain, A.M.; Cox, C.; Savage, V.; Lloyd-Smith, J.O. Quantifying antibody kinetics and RNA detection during early-phase SARS-CoV-2 infection by time since symptom onset. *Elife* **2020**, *7*, 9. [CrossRef]

38. Moons, K.G.; Donders, R.A.; Stijnen, T.; Harrell, F.E., Jr. Using the outcome for imputation of missing predictor values was preferred. *J. Clin. Epidemiol.* **2006**, *59*, 1092–1101. [CrossRef]

39. Rubin, D.B. *Multiple Imputation for Nonresponse in Surveys*; John Wiley & Sons: Hoboken, NJ, USA, 2004; Volume 81.

40. Wood, S.N. *Generalized Additive Models: An Introduction with R*, 2nd ed.; Chapman and Hall/CRC: New York, NJ, USA, 2017.

41. Bauer, A.; Weigert, M.; Jalal, H. APCtools: Descriptive and Model-based Age-Period-Cohort Analysis. *J. Open Source Softw.* **2022**, *7*, 4056. [CrossRef]

42. Bayerisches Staatsministerium für Gesundheit und Pflege. *Verordnung zur Änderung der Elften Bayerischen Infektionsschutzmaßnahmenverordnung*; Bayerisches Staatsministerium für Gesundheit und Pflege: Munich, Germany, 2021; p. 34.

43. Bayerisches Staatsministerium für Gesundheit und Pflege. *Verordnung zur Änderung der Dreizehnten Bayerischen Infektionsschutzmaßnahmenverordnung*; Bayerisches Staatsministerium für Gesundheit und Pflege: Munich, Germany, 2021; p. 584.

44. Dzinamarira, T.; Nkambule, S.J.; Hlongwa, M.; Mhango, M.; Iradukunda, P.G.; Chitungo, I.; Dzobo, M.; Mapingure, M.P.; Chingombe, I.; Mashora, M.; et al. Risk Factors for COVID-19 Infection Among Healthcare Workers. A First Report from a Living Systematic Review and meta-Analysis. *Saf. Health Work* **2022**, *13*, 263–268. [CrossRef] [PubMed]

45. RKI. Wöchentlicher Lagebericht des RKI zur Coronavirus-Krankheit-2019 (COVID-19). Available online: https://www.rki.de/DE/Content/InfAZ/N/Neuartiges_Coronavirus/Situationsberichte/Wochenbericht/Wochenbericht_2022-01-06.pdf?__blob=publicationFile (accessed on 6 January 2022).

46. Nah, E.H.; Cho, S.; Park, H.; Kim, S.; Noh, D.; Kwon, E.; Cho, H.I. Antibody response after two doses of homologous or heterologous SARS-CoV-2 vaccines in healthcare workers at health promotion centers: A prospective observational study. *J. Med. Virol.* **2022**, *94*, 4719–4726. [CrossRef] [PubMed]

47. STIKO. *Mitteilung der STIKO zur COVID-19-Impfung: Impfabstand und heterologes Impfschema nach Erstimpfung mit Vaxzevria*; STIKO: Berlin, Germany, 2021.

48. STIKO. *Pressemitteilung der STIKO zur COVID-19-Impfung mit mRNA-Impfstoff bei Personen unter 30 Jahren*; STIKO: Berlin, Germany, 2021.

49. Paul, G.; Strnad, P.; Wienand, O.; Krause, U.; Plecko, T.; Effenberger-Klein, A.; Giel, K.E.; Junne, F.; Galante-Gottschalk, A.; Ehehalt, S.; et al. The humoral immune response more than one year after SARS-CoV-2 infection: Low detection rate of anti-nucleocapsid antibodies via Euroimmun ELISA. *Infection* **2023**, *51*, 83–90. [CrossRef] [PubMed]

50. Lumley, S.F.; Wei, J.; O'Donnell, D.; Stoesser, N.E.; Matthews, P.C.; Howarth, A.; Hatch, S.B.; Marsden, B.D.; Cox, S.; James, T.; et al. The Duration, Dynamics, and Determinants of Severe Acute Respiratory Syndrome Coronavirus 2 (SARS-CoV-2) Antibody Responses in Individual Healthcare Workers. *Clin. Infect. Dis.* **2021**, *73*, e699–e709. [CrossRef]

51. Van Elslande, J.; Oyaert, M.; Ailliet, S.; Van Ranst, M.; Lorent, N.; Vande Weygaerde, Y.; André, E.; Lagrou, K.; Vandendriessche, S.; Vermeersch, P. Longitudinal follow-up of IgG anti-nucleocapsid antibodies in SARS-CoV-2 infected patients up to eight months after infection. *J. Clin. Virol.* **2021**, *136*, 104765. [CrossRef]

52. Reusch, J.; Wagenhäuser, I.; Gabel, A.; Eggestein, A.; Höhn, A.; Lâm, T.T.; Frey, A.; Schubert-Unkmeir, A.; Dölken, L.; Frantz, S.; et al. Influencing factors of anti-SARS-CoV-2-spike-IgG antibody titers in healthcare workers: A cross-section study. *J. Med. Virol.* **2023**, *95*, e28300. [CrossRef]

53. Sarrigeorgiou, I.; Moschandreou, D.; Dimitriadis, A.; Tsinti, G.; Sotiropoulou, E.; Ntoukaki, E.; Eliadis, P.; Backovic, M.; Labropoulou, S.; Escriou, N.; et al. Combined monitoring of IgG and IgA anti-Spike and anti-Receptor binding domain long term responses following BNT162b2 mRNA vaccination in Greek healthcare workers. *PLoS ONE* **2022**, *17*, e0277827. [CrossRef]

54. Günther, F.; Einhauser, S.; Peterhoff, D.; Wiegrebe, S.; Niller, H.H.; Beileke, S.; Steininger, P.; Burkhardt, R.; Küchenhoff, H.; Gefeller, O.; et al. Higher Infection Risk among Health Care Workers and Lower Risk among Smokers Persistent across SARS-CoV-2 Waves-Longitudinal Results from the Population-Based TiKoCo Seroprevalence Study. *Int. J. Environ. Res. Public Health* **2022**, *19*, 16996. [CrossRef]

55. Haddad, C.; Bou Malhab, S.; Sacre, H.; Salameh, P. Smoking and COVID-19: A scoping review. *Tob. Use Insights* **2021**, *14*, 1179173X21994612. [CrossRef]

56. Sopori, M. Effects of cigarette smoke on the immune system. *Nat. Rev. Immunol.* **2002**, *2*, 372–377. [CrossRef]

57. Usman, M.S.; Siddiqi, T.J.; Khan, M.S.; Patel, U.K.; Shahid, I.; Ahmed, J.; Kalra, A.; Michos, E.D. Is there a smoker's paradox in COVID-19? *BMJ Evid.-Based Med.* **2021**, *26*, 279–284. [CrossRef] [PubMed]

58. Kroidl, I.; Rubio-Acero, R.; Olbrich, L.; Castelletti, N.; Wieser, A. *Studying Temporal Titre Evolution of Commercial SARS-CoV-2 Assays Reveals Significant Shortcomings of Using BAU Standardization for Comparison*; LMU Munich: Munich, Germany, 2023.

59. Whitaker, H.J.; Gower, C.; Otter, A.D.; Simmons, R.; Kirsebom, F.; Letley, L.; Quinot, C.; Ireland, G.; Linley, E.; Ribeiro, S. Nucleocapsid antibody positivity as a marker of past SARS-CoV-2 infection in population serosurveillance studies: Impact of variant, vaccination, and choice of assay cut-off. *MedRxiv* **2021**. [CrossRef]

60. Plumb, I.D.; Fette, L.M.; Tjaden, A.H.; Feldstein, L.; Saydah, S.; Ahmed, A.; Link-Gelles, R.; Wierzba, T.F.; Berry, A.A.; Friedman-Klabanoff, D. Estimated COVID-19 vaccine effectiveness against seroconversion from SARS-CoV-2 Infection, March–October, 2021. *Vaccine* **2023**, *41*, 2596–2604. [CrossRef]

61. Yu, H.; Guan, F.; Miller, H.; Lei, J.; Liu, C. The role of SARS-CoV-2 nucleocapsid protein in antiviral immunity and vaccine development. *Emerg. Microbes Infect.* **2023**, *12*, 2164219. [CrossRef]

62. Lo Sasso, B.; Agnello, L.; Giglio, R.V.; Gambino, C.M.; Ciaccio, A.M.; Vidali, M.; Ciaccio, M. Longitudinal analysis of anti-SARS-CoV-2 S-RBD IgG antibodies before and after the third dose of the BNT162b2 vaccine. *Sci. Rep.* **2022**, *12*, 8679. [CrossRef] [PubMed]

63. Choi, M.J.; Heo, J.Y.; Seo, Y.B.; Yoon, Y.K.; Sohn, J.W.; Noh, J.Y.; Cheong, H.J.; Kim, W.J.; Choi, J.Y.; Kim, H.J.; et al. Six-month longitudinal immune kinetics after mRNA-1273 vaccination: Correlation of peak antibody response with long-term, cross-reactive immunity. *Front. Immunol.* **2022**, *13*, 1035441. [CrossRef] [PubMed]

Publication 3:

The representative COVID-19 Cohort Munich (KoCo19): from the beginning of the pandemic to the Delta virus variant

Ronan Le Gleut*, Michael Plank*, Peter Pütz, Katja Radon, Abhishek Bakuli, Raquel Rubio-Acero, Ivana Paunovic, Friedrich Rieß, Simon Winter, Christina Reinkemeyer, Yannik Schälte, Laura Olbrich, Marlene Hannes, Inge Kroidl, Ivan Noreña, Christian Janke, Andreas Wieser+, Michael Hoelscher+, Christiane Fuchs+, **Noemi Castelletti+** and the KoCo19 study group

RESEARCH

Open Access

The representative COVID-19 cohort Munich (KoCo19): from the beginning of the pandemic to the Delta virus variant

Ronan Le Gleut[1,2†], Michael Plank[3†], Peter Pütz[4], Katja Radon[5,6,7], Abhishek Bakuli[3], Raquel Rubio-Acero[3], Ivana Paunovic[3], Friedrich Rieß[3], Simon Winter[3], Christina Reinkemeyer[3], Yannik Schälte[1,8,9], Laura Olbrich[3], Marlene Hannes[3], Inge Kroidl[3], Ivan Noreña[3], Christian Janke[3], Andreas Wieser[3,10,11,12†], Michael Hoelscher[3,6,10,11†], Christiane Fuchs[1,2,8,13†], Noemi Castelletti[3,11,14*†] and the KoCo19/ORCHESTRA-study group

Abstract

Background Population-based serological studies allow to estimate prevalence of SARS-CoV-2 infections despite a substantial number of mild or asymptomatic disease courses. This became even more relevant for decision making after vaccination started. The KoCo19 cohort tracks the pandemic progress in the Munich general population for over two years, setting it apart in Europe.

Methods Recruitment occurred during the initial pandemic wave, including 5313 participants above 13 years from private households in Munich. Four follow-ups were held at crucial times of the pandemic, with response rates of at least 70%. Participants filled questionnaires on socio-demographics and potential risk factors of infection. From Follow-up 2, information on SARS-CoV-2 vaccination was added. SARS-CoV-2 antibody status was measured using the Roche Elecsys® Anti-SARS-CoV-2 anti-N assay (indicating previous infection) and the Roche Elecsys® Anti-SARS-CoV-2 anti-S assay (indicating previous infection and/or vaccination). This allowed us to distinguish between sources of acquired antibodies.

Results The SARS-CoV-2 estimated cumulative sero-prevalence increased from 1.6% (1.1-2.1%) in May 2020 to 14.5% (12.7-16.2%) in November 2021. Underreporting with respect to official numbers fluctuated with testing policies and capacities, becoming a factor of more than two during the second half of 2021. Simultaneously, the vaccination campaign against the SARS-CoV-2 virus increased the percentage of the Munich population having antibodies, with 86.8% (85.5-87.9%) having developed anti-S and/or anti-N in November 2021. Incidence rates for infections after (BTI) and without previous vaccination (INS) differed (ratio INS/BTI of 2.1, 0.7-3.6). However, the prevalence of infections was higher in the non-vaccinated population than in the vaccinated one. Considering the whole follow-up time, being born outside Germany, working in a high-risk job and living area per inhabitant were identified as risk

*Correspondence:
Noemi Castelletti
noemi.castelliti@med.uni-muenchen.de
Full list of author information is available at the end of the article

Le Gleut *et al. BMC Infectious Diseases*   (2023) 23:466

Page 2 of 15

factors for infection, while other socio-demographic and health-related variables were not. Although we obtained significant within-household clustering of SARS-CoV-2 cases, no further geospatial clustering was found.

Conclusions Vaccination increased the coverage of the Munich population presenting SARS-CoV-2 antibodies, but breakthrough infections contribute to community spread. As underreporting stays relevant over time, infections can go undetected, so non-pharmaceutical measures are crucial, particularly for highly contagious strains like Omicron.

Keywords COVID-19, SARS-CoV-2, Population-based cohort study, Sero-prevalence, Sero-incidence, Vaccination status, Breakthrough infections, ORCHESTRA

Background

SARS-CoV-2 became pandemic mid-March 2020, within three months after the first report on 31st of December, 2019 in the city of Wuhan, Hubei province, China [1, 2]. In Germany, the first COVID-19 cases were observed in the municipality of Munich in late January 2020 [3]. Since then, the number of infections has been one of the predominant topics for political and social life [4, 5]. Looking at the pandemic in Munich in the time-frame between February 2020 and April 2022, four waves of infection can be identified (Fig. 1A):

– First wave: late January – mid June 2020
– Second wave: mid June 2020 – mid February 2021;
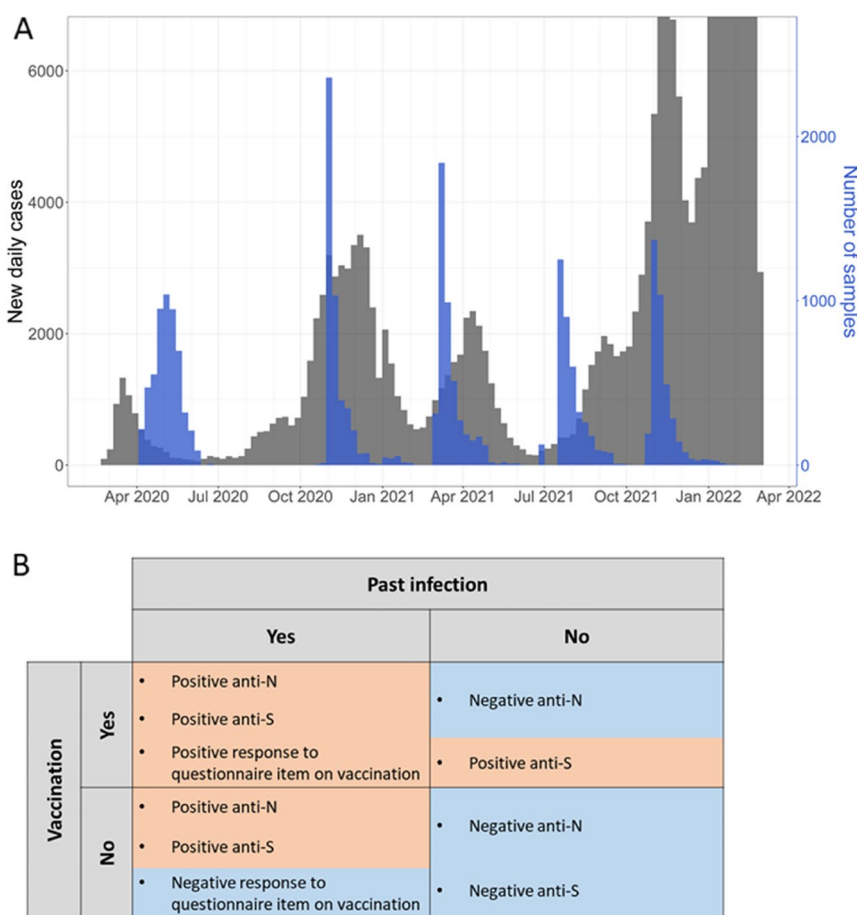
Fig. 1 Epidemic evolution in Munich with description of the sample analysis. **A** Black: number of new daily SARS-CoV-2 cases officially reported by the Robert Koch Institute (RKI). Blue: number of blood/DBS samples of the KoCo19 collected daily. **B** Description of the lab analysis. With anti-N, anti-S and the response to the questionnaire item on vaccination it was possible to define the participants as: infected and vaccinated, infected and non-vaccinated, non-infected and vaccinated and non-infected and non-vaccinated. Blue shaded regions denote a negative response while orange regions a positive one

Le Gleut *et al. BMC Infectious Diseases*   (2023) 23:466

Page 3 of 15

– Third wave: mid February 2021 – end July 2021;
– Fourth wave: end of July 2021 – after the end of the analysed period.

In the first wave, the main non-pharmaceutical interventions applied were to reduce contacts in the whole city of Munich followed by a lifting of the restrictions with still severe contact reductions. During this early phase of the pandemic, PCR tests were scarce good, and we suspect that only few chance finds entered the official statistics. In the second wave, contacts between people were reduced from June to October 2020, followed by stronger regulations, including FFP2 mask obligation. At the end of December 2020, only twelve months after the start of the pandemic, effective vaccines were introduced in Germany [6], preventing infection or at least reducing symptoms [7]. In parallel, the test capacity increased: starting in July 2020, the Bavarian state (including Munich) provided access to free PCR tests for all citizens, even without symptoms without a limit per person [8]. Antigen rapid tests became available nationwide for institutions like nursing homes or schools towards the end of 2020. By contact tracing more asymptomatic infected individuals could be identified [9–11]. In the third wave, the lock-down from the previous wave still continued with the so-called "emergency brake" starting in mid-April 2021: stronger contact reduction, night-time curfew and closure of many stores [12]. During this wave, the first new virus variant of SARS-CoV-2 was observed [13]: in early March 2021, the Alpha variant (B.1.1.7 variant) was detected in more than 40% of tested positive cases in Germany [14]. From early 2021 on, the testing capacity was further increased nationwide, and antigen test became available for home use [15, 16]. Such low-threshold access to testing supposedly facilitated detecting asymptomatic cases, which entered the official numbers after PCR confirmation. The fourth wave of the pandemic started in Munich with almost all cases classified as Delta (B.1.617.2) variant. Further relaxations were possible in the summer breaks from July 2021: more visitors at outdoor and cultural events, restaurants could stay open longer, mask rules were relaxed, bars could reopen [17, 18]. In October 2021, even clubs were allowed to open again [19].

Decisions on non-pharmaceutical interventions were mostly taken under the guidance of official case reports, which were shown to underestimate the true case numbers especially at the beginning of the pandemic, when testing capacity was still low [20]. In order to gain a better understanding of the true case numbers, we started the prospective Munich COVID-19 cohort (KoCo19) in April 2020 including 5313 participants living in private households. In this population-based cohort study we measured SARS-CoV-2 antibody prevalence at the following times of the pandemic (Fig. 1A):

– May 2020 at the peak of the first wave in Germany,
– December 2020, at the beginning of the second wave,
– March 2021, at the peak of the third wave and at the beginning of the vaccination campaign for the general population,
– August 2021, at the end of the third wave with around 68% of the general population 14 years or older being vaccinated against SARS-CoV-2,
– November 2021, in the middle of the fourth wave and before the spread of the Omicron variant started in Germany.

To the best of our knowledge, KoCo19 is the SARS-CoV-2 cohort with the longest follow-up time in the world. On December 1st, 2020, the KoCo19 cohort joined the ORCHESTRA (Connecting European Cohorts to Increase Common and Effective Response to SARS-CoV-2 Pandemic) project. During the whole pandemic, KoCo19 results were used to advise political decision making.

We here present the evolution of SARS-CoV-2 cumulative sero-positivity in the Munich general population 14 years and older over time. Furthermore, we report on risk factors for SARS-CoV-2 infection over time. The data described here were not published elsewhere.

Methods
Study population and field work
Baseline and follow-up questionnaires
A detailed description of the baseline study can be found in [20, 21]: We randomly sampled the Munich cohort of private households between April 5th and June 12th, 2020. Only household members 14 years and older who gave written informed consent were included in the cohort. For participants younger than 18 years, informed consent was obtained from the parents as well as the participants themselves.

Analyses use information from baseline individual and household questionnaires and from individual follow-up questionnaires. The different questionnaires were already described in detail [20], and included information on: socio-demographics, country of birth, smoking status, chronic conditions, general health, household size, living area per inhabitant, household type, housing type, self-estimated health-related risk taking behaviour, personal contacts, number and intensity of leisure time activities before the pandemic (in February 2020), number and intensity of leisure time activities two weeks prior to the follow-up questionnaire. Starting from Follow-up 2, we also asked about SARS-CoV-2 vaccination including

Le Gleut *et al. BMC Infectious Diseases*   (2023) 23:466

Page 4 of 15

the number of vaccinations, type of vaccine and date of vaccination.

Baseline and follow-ups SARS-CoV-2 antibody study

At recruitment, a serum sample was gathered for 5313 household members 14 years and older. Thereafter, four antibody follow-ups were conducted in December 2020 [20], March 2021, August 2021 and November 2021 (Fig. 1A). Follow-ups were performed by sending out boxes with a self-sampling kit to take a capillary blood sample (dry blood spot; DBS). A detailed description of the DBS analysis procedure can be found in [22]. When self-DBS collection was impossible, participants were invited to give serum and DBS at our study centre.

For the measurements at baseline [23] and Follow-up 1, only the Elecsys® Anti-SARS-CoV-2 anti-N (Roche) (hereafter called Ro-N-Ig) assay was used for antibody detection after infection. From Follow-up 2 on, in addition, also the Elecsys® Anti-SARS-CoV-2 anti-S (Roche) (hereafter called Ro-RBD-Ig) assay was applied. This was necessary to distinguish antibodies due to infection (i.e., anti-S and anti-N present) and antibodies only due to vaccination (i.e., only anti-S present) (Fig. 1B).

For the measurement with full blood sampling, an optimised cut-off of 0.4218 for Ro-N-Ig was applied to indicate sero-positivity [23]. Estimates of sensitivity and specificity of blood Ro-N-Ig compared to reverse-transcription polymerase chain reaction (RT-PCR) were used to adjust the prevalence.

Taking full blood samples as ground truth, sensitivity and specificity of the DBS anti-N method were 99.2% and 98.7%, respectively, applying a cut-off of 0.105 [22]. Based on our internal validation cohort (data not shown here), only samples with Ro-RBD-Ig larger than or equal to 0.115 were considered positive (regarding anti-S) for vaccination and/or infection. Similarly, the DBS anti-S method had sensitivity and specificity of 96.6% and 97.8%, respectively. Since sensitivity and specificity of both tests turned out high, no additional adjustment for sensitivity and specificity was applied. The cut-offs for blood samples, as well as DBS samples, along with their sensitivity and specificity, were determined based on cohorts randomly selected using serology rather than symptom severity. This approach ensured that the assays are suitable for detecting milder community infections [22, 23].

Using the serological values in combination with questionnaire information, we were able to classify participants into the following groups (Fig. 1B):

 – Non-vaccinated, non-infected: negative in both anti-S and anti-N antibodies;

 – Vaccinated, non-infected: positive in anti-S and negative in anti-N antibodies;
 – Non-vaccinated, infected: positive in both anti-S and anti-N antibodies, negative response to the questionnaire item on vaccination;
 – Vaccinated and infected: positive in both anti-S and anti-N antibodies, positive response to questionnaire item on vaccination.

Statistics

All statistical analyses were performed using the softwares R (version 4.1.3, R Development Core Team, 2021) and Python (version ≥ 3.8.5).

After observed sero-conversion, antibody levels were imputed positive in all follow-ups, independently of the actual results of the round or in case of missingness („ever positiveness ", Fig. 2A). We thus disregard potential anit-N waning. Our definition allows us to estimate the cumulative sero-prevalence in the considered population, which in turn we take as a proxy for cumulative infections and compare to the official number of positive cases reported by the authorities, neglecting reinfections. For simplicity, we in the following suppress the word "cumulative" as a specification of the estimated sero-prevalence. In order to estimate the population prevalence, sero-prevalence estimates (adjusted and unadjusted for the sensitivity and specificity of the test) were computed using a weighting scheme. First, sampling weights for each participant at baseline were calculated according to the sampling design of the cohort [21]. These weights were then corrected for the attrition observed at each follow-up, modelling the underlying non-response mechanism [24]. The resulting weights were finally calibrated on the updated Munich structure at each round regarding age, sex, country of birth, presence of children in the household and single member households distributions [25]. For the last three follow-ups (March, August and November 2021), information on the vaccination status of the participants was assessed via questionnaires. The missing values (30% for Follow-up 2, 27% for Follow-up 3 and 8% for Follow-up 4) were imputed via multiple imputation ($m = 100$) crossing for each round the vaccination status with the information on the immune response (Ro-N-Ig and Ro-RBD-Ig results). The probability p of being vaccinated was estimated for each of the four anti-N and anti-S combinations for each of the imputed datasets and each Follow-up 2 to 4, see e.g. the values of one imputed dataset for Follow-up 4 in Table 1. The results for Follow-up 3 are comparable to these ones. At the beginning of the vaccination campaign (Follow-up 2), the probabilities to be vaccinated were lower, especially for anti-S and
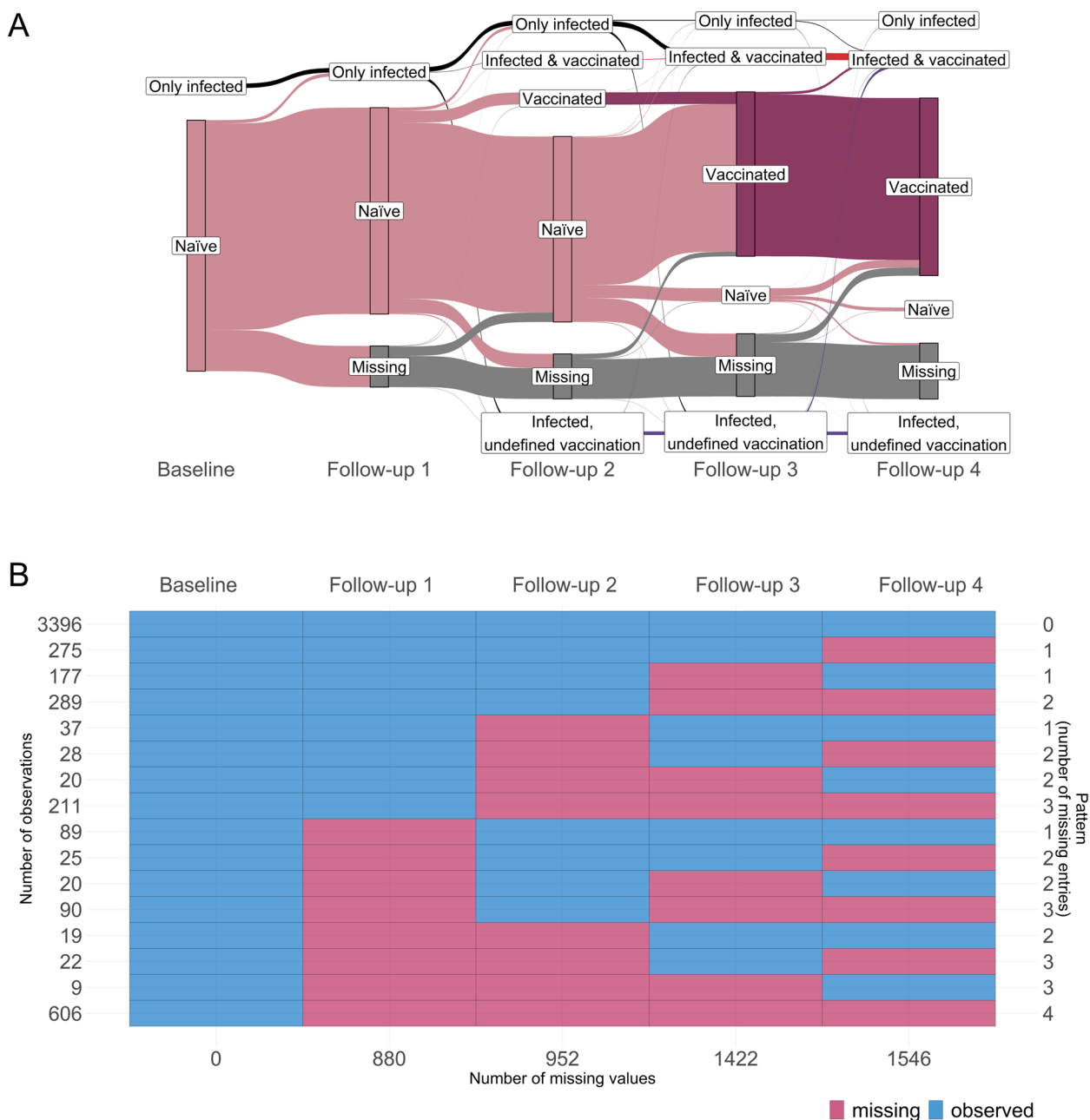
Fig. 2 Cohort description based on the ever-positive principle, i.e. anti-N sero-positivity remains for all rounds after sero-conversion, independently of other blood results or if missing. **A** Change of serological status of participants: only infected (anti-N ever positive and stated to be non-vaccinated in the questionnaire), naïve (anti-N and anti-S always negative), vaccinated (only anti-S ever positive), infected & vaccinated (in previous round only anti-S positive, or stated to be vaccinated in the questionnaire), infected without information on vaccination (infected, undefined vaccination) and non-responders/missing. **B** Observed responder behaviours. Left legend: number of participants. Right legend: number of missing rounds. Bottom legend: number of missing samples per round

anti-N positive ($p = 0.06$) with mostly only infected (and non vaccinated) persons.

The imputation was performed using a Bernoulli distribution with probability p for each participant with missing information.

Considering both Ro-RBD-Ig results and the questionnaire data, in the last two follow-ups 93% and 97%, respectively, of the participants could be assumed vaccinated. In contrast, the city of Munich reported that approximately 68% and 76%, respectively, of the

Le Gleut *et al. BMC Infectious Diseases*   (2023) 23:466

Page 6 of 15

Table 1 Estimated probabilities to be vaccinated used for the imputation of the vaccination status during Follow-up 4

		Anti-N	
		Positive	**Negative**
Anti-S	Positive	$p = 0.94$	$p = 0.99$
	Negative	$p = 0$	$p = 0.19$

Anti-S negative may occur after vaccination in case of a delayed or an absence of antibody response. Moreover, Ro-RBD-Ig (anti-S) with a cut-off at 0.115 does not provide 100% sensitivity and specificity

population older than 14 years have been vaccinated [26]. The calibration of the cohort results is hence of crucial importance. The variance associated with the calibrated sero-prevalence estimates was computed using linearisation [25] and residual [25, 27] techniques. This variance accounts for the uncertainty due to the different stages of the sampling design (selection of the constituencies and of the households), the non-response mechanism [28] and the calibration process. As a sensitivity analysis, unweighted sero-prevalence estimates were also computed together with their uncertainty. The variance was determined by a nonparametric cluster bootstrap procedure that accounts for household clustering [29]. The sero-prevalence estimates were calculated in each of the 5000 bootstrap samples (sampling of households with replacement), and the variance of these 5000 estimates provided the uncertainty of the unweighted estimates. Finally, the variability associated with the multiple imputation procedure was added to the variance of the (weighted and unweighted) sero-prevalence estimates following the approach detailed in Honaker et al. (2011) [30]. In short, the final variance estimate V is a combination of the average of the variance estimates $V_j, j = 1, \ldots, m$ (described above) over the m replications and the variance of the m sero-prevalence estimates $\theta_j, j = 1, \ldots, m$:

$$V = \frac{1}{m}\sum_{j=1}^{m} V_j + S^2\left(1 + \frac{1}{m}\right), with\ S^2 = \frac{1}{m-1}\sum_{j=1}^{m}\left(\theta_j - \overline{\theta}\right)^2$$

The final sero-prevalence estimates were obtained using the means of the m estimates, and 95% confidence intervals were computed assuming a normal distribution.

Breakthrough infections (BTI) are defined as newly infected participants after vaccination. The corresponding SARS-CoV-2-related serological spectrum is hence given by: anti-N negative but anti-S positive in the past and anti-N positive for a given next round (Fig. 1B). Accordingly, newly anti-N positive cases without anti-S antibodies in the previous rounds were defined as infections of naïve subjects (INS). While these estimates could be adjusted for the sensitivity and specificity of the test,

we report in the results Sect. 95% confidence intervals (CI) for the ratio INS/BTI without adjustment. Indeed, the calculation of the variance requires information at the individual level (enabling accounting for the sampling design, the non-response, the calibration and the multiple imputation), while the adjustment of the incidence rates is done directly on the estimates.

Of interest were also risk factors for infection, with the aim to model when, in the course of the pandemic period, the infection (anti-N positiveness) occurred. Right censoring was adopted for anti-N negative participants at the end of the observation period, Follow-up 4. An extended Cox regression model [31, 32] was applied to assess which baseline risk factors increase or decrease the risk of infection. Since positivity of individuals in one household might depend on each other (resulting in a potential high intra-cluster correlation [33]), the Cox regression model follows the count process formulation of Anderson and Gill [31] to adjust for intra-household clustering in the data obtaining robust standard error estimates.

The non-response mechanism (Fig. 2B) over the different rounds of interrogation was studied using a logistic regression. The missingness in the explanatory variables was corrected by multiple imputation with $m = 5$ replications (Table 2). Due to a high number of missing values on the income (Supplemental Figure S1), a sensitivity analysis was performed considering complete cases for all covariates, except for the income where an indicator variable for missingness was used (Supplemental Table S1). The results are similar between the two analyses.

In both the risk factor analysis and the non-response mechanism analysis, for explanatory variables with two categories, a constraint to zero for one category (e.g. females vs. males) was used. For covariates with three and more categories, a sum-to-zero constraint (i.e. compare each category to the average) was applied.

Results

Cohort development

Since anti-S becomes positive after vaccination but also after infection, the definition of being vaccinated for infected persons was obtained using the questionnaires when available (Fig. 1B). When describing the changes of antibody statuses over time, historical information needs to be taken into account. Figure 2A applies the definition of „ever positiveness " (see Supplemental Figure S2 for an alternative serological description) and considers the following major categories: only infected (anti-N ever positive, and vaccination excluded based on other information), naïve (anti-N and anti-S never positive), vaccinated (only anti-S ever positive), and infected & vaccinated (anti-N positive after anti-S positive, or anti-N

Le Gleut *et al. BMC Infectious Diseases*   (2023) 23:466

Page 7 of 15

Table 2 Non-response mechanism at the different follow-ups using multiple imputation

Variable	Categories	Follow-up 2			Follow-up 3			Follow-up 4		
		OR	95% CI	*p*-value	OR	95% CI	*p*-value	OR	95% CI	*p*-value
Sex	Male	0.81	[0.66; 0.98]	*	0.97	[0.82; 1.15]		0.83	[0.69; 0.99]	*
Age *(years)*	14–19	0.82	[0.49; 1.37]		0.59	[0.36; 0.97]	*	0.61	[0.36; 1.05]	
	20–34	0.59	[0.45; 0.76]	***	0.55	[0.43; 0.69]	***	0.62	[0.49; 0.78]	***
	35–49	0.86	[0.67; 1.11]		1.02	[0.81; 1.30]		0.89	[0.70; 1.15]	
	50–64	1.47	[1.15; 1.88]	**	1.41	[1.13; 1.76]	**	1.57	[1.24; 1.98]	***
	65–79	1.87	[1.36; 2.58]	***	2.01	[1.46; 2.75]	***	1.28	[0.95; 1.71]	
	80 +	0.88	[0.57; 1.35]		1.06	[0.69; 1.63]		1.48	[0.96; 2.28]	
Birth country	Not Germany	0.98	[0.76; 1.27]		0.59	[0.47; 0.74]	***	0.63	[0.50; 0.79]	***
Level of education	In school	1.00	[0.58; 1.73]		0.88	[0.52; 1.50]		1.00	[0.57; 1.76]	
	< 12 years	0.94	[0.69; 1.27]		1.10	[0.83; 1.46]		0.93	[0.69; 1.24]	
	≥ 12 years	1.06	[0.78; 1.45]		1.03	[0.77; 1.37]		1.08	[0.78; 1.48]	
Employment status	Employed	1.07	[0.86; 1.32]		1.06	[0.87; 1.30]		0.98	[0.78; 1.22]	
	Self employed	0.89	[0.65; 1.23]		0.85	[0.65; 1.11]		0.90	[0.68; 1.20]	
	Unemployed	0.75	[0.57; 0.99]	*	1.27	[1.00; 1.62]		1.18	[0.90; 1.54]	
	Others	1.40	[0.84; 2.32]		0.87	[0.58; 1.31]		0.96	[0.59; 1.58]	
Risk employment	Yes	0.85	[0.63; 1.14]		1.10	[0.86; 1.41]		1.05	[0.82; 1.34]	
Smoking status	Non smoker	1.00	[0.87; 1.16]		1.17	[1.03; 1.33]	*	0.96	[0.84; 1.09]	
	Past smoker	0.92	[0.78; 1.09]		1.01	[0.87; 1.19]		1.00	[0.87; 1.15]	
	Current smoker	1.08	[0.91; 1.29]		0.84	[0.72; 0.98]	*	1.05	[0.89; 1.23]	
General health	Not good	0.61	[0.42; 0.88]	**	0.84	[0.60; 1.18]		0.59	[0.41; 0.85]	**
	Good	0.92	[0.73; 1.15]		1.08	[0.91; 1.28]		0.90	[0.75; 1.08]	
	Very good	1.28	[1.05; 1.54]	*	1.03	[0.88; 1.21]		1.19	[0.99; 1.44]	
	Excellent	1.39	[1.11; 1.76]	**	1.07	[0.86; 1.33]		1.57	[1.25; 1.97]	***
Respiratory allergies	Yes	0.92	[0.71; 1.19]		1.39	[1.10; 1.74]	**	0.83	[0.67; 1.02]	
Diabetes	Yes	1.37	[0.83; 2.28]		0.78	[0.48; 1.29]		0.81	[0.51; 1.30]	
CVD	Yes	1.10	[0.75; 1.60]		1.16	[0.87; 1.54]		1.15	[0.83; 1.58]	
Obesity	Yes	0.86	[0.50; 1.50]		0.89	[0.60; 1.31]		1.01	[0.67; 1.51]	
Cancer	Yes	0.87	[0.53; 1.43]		0.98	[0.58; 1.67]		1.02	[0.64; 1.63]	
Lung disease	Yes	0.93	[0.59; 1.45]		0.81	[0.58; 1.14]		0.97	[0.69; 1.36]	
Skin allergies	Yes	1.12	[0.81; 1.55]		0.98	[0.76; 1.27]		1.18	[0.90; 1.54]	
Autoimmune disease	Yes	1.28	[0.74; 2.22]		0.97	[0.68; 1.40]		1.34	[0.86; 2.08]	
Household type	Single	1.23	[0.93; 1.62]		1.25	[0.96; 1.62]		0.94	[0.73; 1.21]	
	Couple	1.24	[1.03; 1.49]	*	1.10	[0.94; 1.29]		1.19	[1.01; 1.40]	*
	Family	0.85	[0.69; 1.06]		0.86	[0.70; 1.06]		0.89	[0.73; 1.10]	
	Others	0.77	[0.61; 0.98]	*	0.85	[0.68; 1.06]		1.00	[0.78; 1.29]	
Household income *(Euro)*	≤ 2500	0.84	[0.67; 1.05]		0.81	[0.63; 1.04]		0.94	[0.75; 1.17]	
	2501–4000	1.01	[0.78; 1.30]		0.91	[0.76; 1.10]		0.92	[0.78; 1.08]	
	4001–6000	1.13	[0.95; 1.33]		1.16	[0.92; 1.46]		1.09	[0.92; 1.28]	
	6001 +	1.05	[0.76; 1.44]		1.16	[0.94; 1.44]		1.07	[0.87; 1.32]	
Living area/inhabitant *(sqm/individual)*	≤ 30	1.13	[0.92; 1.38]		0.97	[0.81; 1.17]		0.96	[0.80; 1.16]	
	31–40	1.03	[0.86; 1.23]		0.88	[0.75; 1.03]		1.02	[0.86; 1.21]	
	41–55	0.91	[0.74; 1.10]		1.27	[1.06; 1.51]	*	1.10	[0.91; 1.33]	
	56 +	0.95	[0.74; 1.22]		0.92	[0.74; 1.15]		0.92	[0.75; 1.15]	
Building type *(nb of apartments)*	1–2	1.24	[1.02; 1.51]	*	0.90	[0.76; 1.08]		1.11	[0.92; 1.33]	
	3–4	0.91	[0.70; 1.19]		1.48	[1.14; 1.91]	**	1.03	[0.80; 1.31]	
	5 +	0.88	[0.75; 1.04]		0.75	[0.64; 0.88]	***	0.88	[0.75; 1.03]	
Seropositivity in the previous rounds	Negative	4.52	[3.78; 5.40]	***	5.42	[4.74; 6.19]	***	5.27	[4.63; 6.01]	***
	Positive	2.01	[1.48; 2.72]	***	1.88	[1.54; 2.30]	***	1.90	[1.57; 2.31]	***
	Missing	0.11	[0.09; 0.13]	***	0.10	[0.08; 0.12]	***	0.10	[0.09; 0.12]	***

Variables with 2 categories have contrasts with one category set to 0. For variables with 3 and more categories, constraint sum-to-zero contrasts was applied

OR odds ratio

p-value: *** *p < 0.001*; ** *p < 0.01*; * *p < 0.05*

Le Gleut *et al. BMC Infectious Diseases*   (2023) 23:466

Page 8 of 15

positive with respective questionnaire information). From Follow-up 2 on, participants started moving from the naïve to the vaccinated status, which became the most prominent stage in Follow-ups 3 and 4. The status of non-responders is labelled as missing: 64% (3396/5313) of the participants gave blood in all rounds, 11% (578/5313) / 8% (401/5313) / 6% (332/5313) had exactly one/two/three rounds missing, and 11% (606/5313) dropped out for all four follow-ups after the baseline measurement (Fig. 2B). Some non-responders still answered back in subsequent round(s), thus moving away from stage missing. Overall, the response rate was satisfactory (83% Follow-up 1; 82% Follow-up 2; 73% Follow-up 3; 71% Follow-up 4; Fig. 2B), especially considering the duration of the cohort.

Non-responder analyses

The non-response mechanism for the Follow-up 1 was previously presented [20]. We show the results for the last three follow-ups (Table 2). Females and participants between 50 and 79 years were more likely to take part to the follow-ups, while young participants (age < 35 years old) together with participants with a migration background were less likely to participate. People who reported a bad general health condition tended to drop out of the cohort while those with excellent health continued answering to the survey. Couples were slightly more likely to provide blood samples than other household types. Members of a household with a low or medium-to-low income were less likely to take part in the survey in comparison to households with a medium-to-high or high income, even though the differences were not significant (see Supplemental Table S1 for sensitivity analysis). During Follow-up 2, households in buildings with 1–2 apartments tended to answer more often, while during Follow-up 3, those living in buildings with 3–4 apartments answered more often. Households in buildings with 5 or more apartments answered less often. Participants not taking part in one previous round of interrogation were less likely to take part in the next rounds. Having at least one positive anti-N serological result in the previous rounds lead to a lower response rate in the next follow-ups in comparison to always having negative anti-N results in the past. All other covariates investigated in the non-response mechanism (level of education, employment status, smoking status, etc.) showed no or negligible association to the response behaviour.

SARS-CoV-2 sero-prevalence, underreporting factor and sero-incidence over time

The blue estimate in Fig. 3A shows the calibrated cumulative sero-prevalence (adjusted for sensitivity and specificity) in private households for the Munich population 14 years and older:

- Baseline: 1.6% (1.1 – 2.1%),
- Follow-up 1: 4.1% (3.3%—4.9%), and after adjustment for vaccination status
- Follow-up 2: 7.3% (6.1–8.5%),
- Follow-up 3: 12.4% (10.7—14.1%),
- Follow-up 4: 14.5% (12.7—16.2%).

Without adjustment for vaccination status for the Follow-ups 3 and 4, the sero-prevalence would have been significantly lower: 8.5% (7.2-9.8%) for August 2021 and 10.5% (9.1-11.9%) for November 2021. Indeed, the proportion of vaccinated persons is greater in the cohort in comparison to the general Munich population. Therefore, the calibration on the vaccination status increases the weight of the participants who are not vaccinated. The sero-prevalence being greater in the non-vaccinated population (see below and Fig. 3C), the overall sero-prevalence, including both vaccinated and non-vaccinated, also increases with the calibration.

The official number of positive cases is reported in pink in Fig. 3A for the general population of Munich (including institutions like nursing homes and potential reinfections). Considering that the KoCo19 cohort is limited to private households and that the estimated sero-prevalence does not account for multiple infections, a comparison of this estimate with the official number over time allows us to estimate a lower bound for the underreporting factor (with the false assumption that all cases reported by the authorities occurred in private households and neglecting reinfections). The estimated underreporting factor changed over the rounds:

- Baseline: 3.4 (2.4 – 4.4),
- Follow-up 1: 1.3 (1.0 – 1.6),
- Follow-up 2: 1.8 (1.5 – 2.1),
- Follow-up 3: 2.3 (2.0 – 2.6),
- Follow-up 4: 2.2 (2.0—2.5).

Figure 3B depicts the sero-incidence (adjusted for sensitivity and specificity), i.e. the percentage of new infections between two consecutive rounds:

- Follow-up 1: 2.0% (1.4—2.7%),
- Follow-up 2: 3.1% (2.3—3.9%),
- Follow-up 3: 3.2% (2.5—3.9%),
- Follow-up 4: 2.4% (1.4—3.4%),

with the time interval between Follow-ups 3 and 4 being rather short (three months).
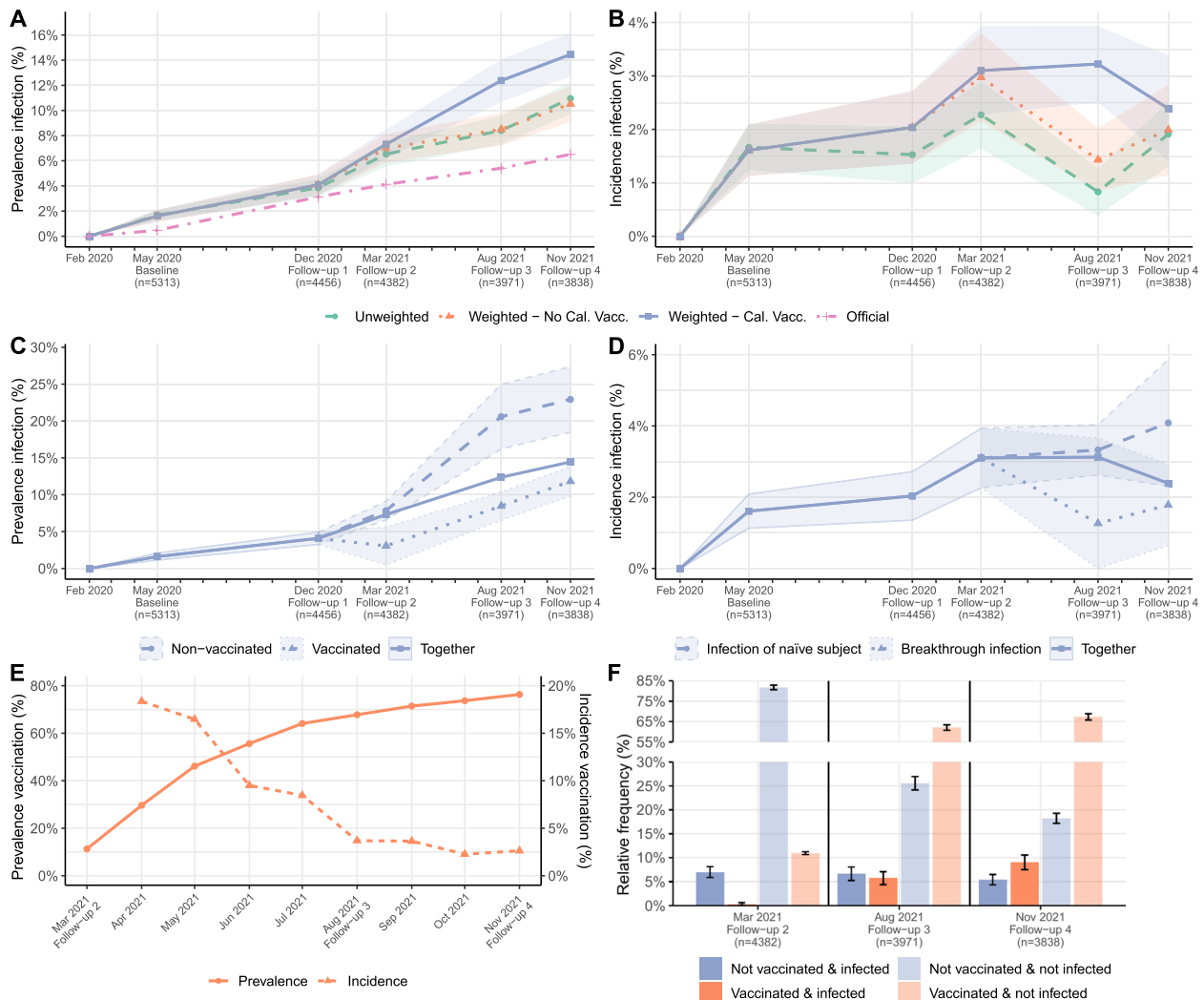
Fig. 3 **A** Weighted and unweighted cumulative anti-N sero-prevalence in private households and official numbers of cases reported by the authorities for the Munich population older than 13 years. **B** Weighted and unweighted anti-N sero-incidence. **C** Anti-N sero-prevalence estimates calibrated on the number of vaccinated people split according to the vaccination status of the same round. **D** Calibrated estimates for the infection of naïve subjects and breakthrough infections. **E** Prevalence and incidence of vaccination in Munich (official numbers). **F** Relative frequencies according to the infection and vaccination status

Breakthrough infections in the Munich population

To better understand the effect of the vaccination campaign (see also next section), the calibrated cumulative sero-prevalence was split between vaccinated versus non-vaccinated people (Fig. 3C):

– Follow-up 2: 3.1% (0.5% - 5.6%) versus 7.8% (6.6 – 9.1%),
– Follow-up 3: 8.5% (6.6 – 10.4%) versus 20.6% (16.2 - 25.0%) and
– Follow-up 4: 11.8% (9.8 - 13.8%) versus 22.9% (18.5 - 27.4%).

The sero-prevalence of the vaccinated group is lower compared to the non-vaccinated group.

Figure 3D compares the adjusted (for sensitivity and specificity) incidence rates for BTI versus INS over the rounds:

– Follow-up 3: 1.3% (0 - 3.7%) versus 3.3% (2.6 - 4%) and
– Follow-up 4: 1.8% (0.6 - 2.9%) versus 4.1% (2.3 - 5.9%).

In August and November 2021, incidence rates of INS were greater than the ones of BTI. Significant

Le Gleut *et al. BMC Infectious Diseases*   (2023) 23:466

Page 10 of 15

differences between unadjusted INS and BTI incidence rates (INS/BTI) could however not be achieved:

- Follow-up 3: ratio of 2.8 (0 - 7.7) and
- Follow-up 4: 2.1 (0.7 - 3.6).

The low sample sizes led to low power and may thus have implied the non-significant findings: In Follow-up 2, the low number of vaccinated persons led to high uncertainty in the estimation of BTI in Follow-up 3; vice versa, in Follow-up 3, the low number of non-vaccinated persons led to high uncertainty in the estimation of INS in Follow-up 4.

The vaccination campaign in the Munich population

The introduction of vaccination quickly changed the SARS-CoV-2-related serological spectrum of the Munich population. The percentage of the Munich population presenting antibodies against the virus (either anti-S after infection and/or vaccination and/or anti-N antibodies after infection) increased fast over time:

- Follow-up 2: 11.2% (9.6 - 12.8%),
- Follow-up 3: 74.2% (72.6 – 75.8%),
- Follow-up 4: 86.8% (85.8 - 87.9%).

Even though the cumulative sero-prevalence and the sero-incidence seemed to be higher among the non-vaccinated population compared to the vaccinated population (Fig. 3C and D), BTI contributed relevantly to the community spread, considering that the size of the population of vaccinated people was much larger than the non-vaccinated one during the last rounds of interrogation (Fig. 3E). Figure 3F illustrates this effect in more detail. The proportion of people vaccinated and infected increased over time, up to Follow-up 4 where this proportion was significantly greater than the one of infected and non-vaccinated people. This figure also shows that the proportion of the population without any antibodies related to SARS-CoV-2 (non-vaccinated and non-infected) was decreasing over time, while the share of people vaccinated and non-infected increased (cf. Fig. 2A).

Risk factors for SARS-CoV-2 sero-prevalence

The results of the risk factor analysis can be found in Fig. 4. The extended Cox regression model suggests that being born outside Germany (hazard ratio (HR) 1.36, 95% confidence interval (CI) 1.01–1.85) and having a job with a high potential of contact to COVID-19 cases (HR 1.31, 95% CI 1.00–1.70) were risk factors for

SARS-CoV-2 sero-positivity. Living area of 30–40 square meters per inhabitant presented a slightly higher risk of infection (HR 1.27, 95% CI 1.01–1.59), while for 40–55 square meters per inhabitant the risk decreased (HR 0.74, 95% CI 0.57–0.97), compared to the average Hazard of all categories of living area. All other socio-demographic (sex, age, level of education, employment status, building type, household income) and health-related variables (smoking status, general health status, different diseases and drug intakes) were not identified as risk factors for infection.

Household and neighbourhood clustering of SARS-CoV-2 cases

SARS-CoV-2 transmission within households was found to be highly significant for baseline [33] and Follow-up 1 [20] analyses and was confirmed until Follow-up 4 (Supplemental Figure S3). While the overall picture obtained in recent rounds showed a lower-than-expected mean variance at 500 m as well, we now could not find sufficient proof of spatial clustering beyond household level, especially if one adjusted *p*-values for multiple testing.

Discussion

We present the development of the SARS-CoV-2 pandemic in the municipality of Munich. To estimate the real number of SARS-CoV-2 infections, the members of the prospective KoCo19 cohort were asked five times to give their blood for study purposes between spring 2020 and fall 2021. SARS-CoV-2 antibodies generated by silent or symptomatic infections and/or vaccination could hence be measured. We could show that the sero-prevalence drastically increased over time, from 1.6% during the baseline to 14.5% in Follow-up 4, with a relevant under-reporting bias. Risk factors for SARS-CoV-2 sero-positivity, such as being born outside of Germany, living area per inhabitant and working in a job with high potential of contact with COVID-19, could be identified together with household clustering.

Sero-prevalence was still low towards the end of the first pandemic wave and increased drastically in every follow-up. Comparison of our results with official numbers reveals an underreporting factor that changes over time. These changes might result from different testing policies as well as different variants of the virus. The estimates present lower bounds of the true under-reporting factor, since our study focused on private households whereas the official number of reported cases included institutions (like nursing homes) as well. Moreover, potential reinfections counted in the official numbers were here neglected. Indeed, our study focuses on the pandemic from its beginning to the Delta variant,
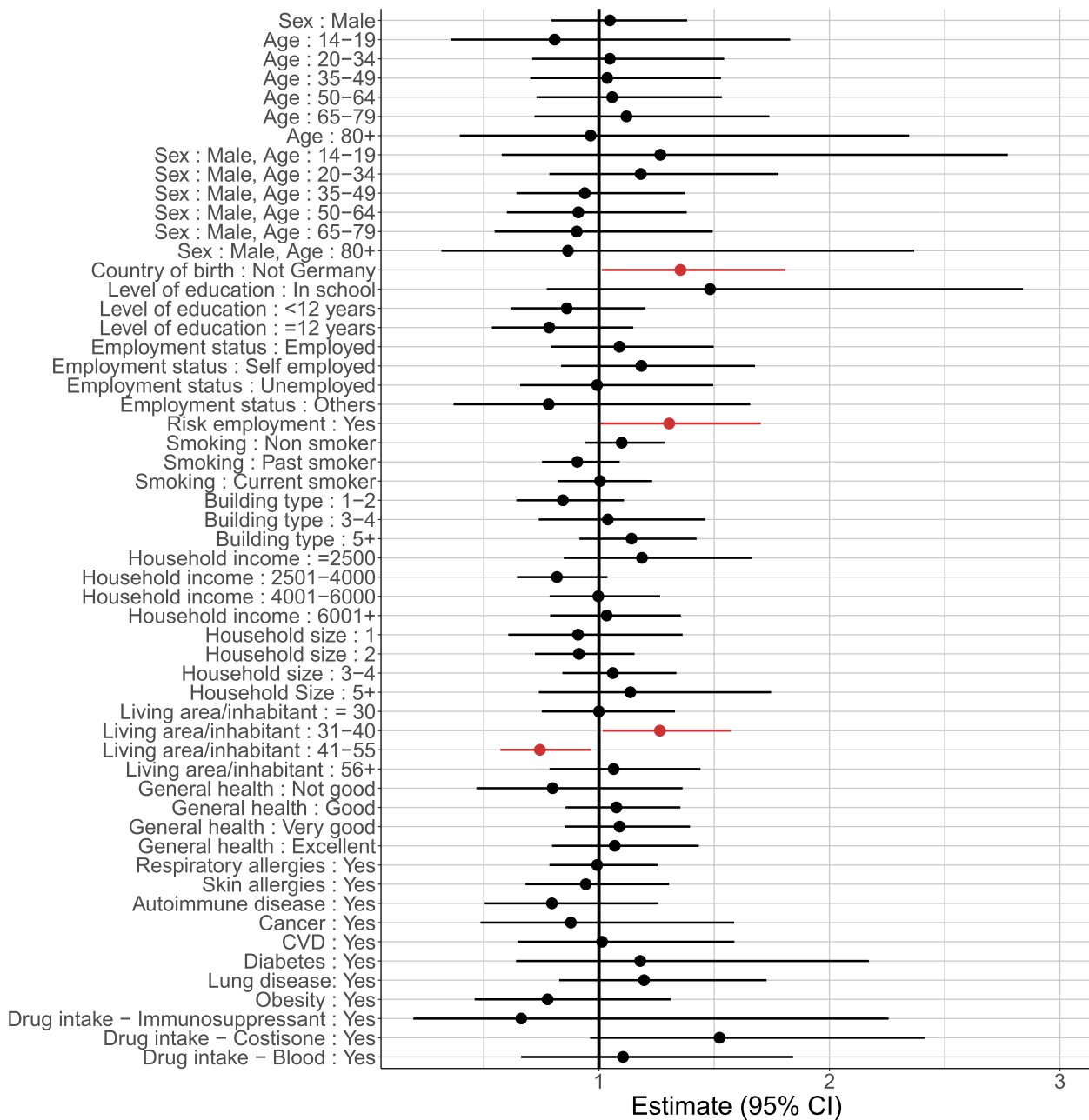
Fig. 4 Association between potential risk factors and SARS-CoV-2 sero-positivity taking into account time between baseline and Follow-up 4; events are thus right-censored. Results are based on multiple imputation. The main individual level risk factors were country of birth outside Germany and being employed in a job more in contact with the epidemic. Living in an apartment with a living area of 30–40 square meters per inhabitant revealed a slightly higher risk, while for 40–55 square meters per inhabitant the hazard ratio decreased

before the spread of the Omicron variant. Therefore, the low number of reinfections did not play a major role during this period [34–36].

In our data it was possible to separate infection of naïve subjects from breakthrough infections in low- and high-incidence time periods. In all follow-ups, our results indicate a contribution of breakthrough infections to the spread of SARS-CoV-2. The findings presented here, based on serology, contribute to current knowledge so far derived from PCR test results. The number of breakthrough infections detected based on PCR tests that were either done routinely, because of symptoms or among case contacts [37, 38] might miss an important number of silent infections,

Le Gleut *et al. BMC Infectious Diseases*   (2023) 23:466

Page 12 of 15

especially as vaccinated individuals tend to have less pronounced symptoms. In our cohort, only a small part was fully vaccinated until March 2021 (Follow-up 2), given the vaccination scheme in Germany at that time. This resulted in a wide confidence interval for breakthrough infections during the next follow-up. During August 2021 (Follow-up 3), almost the complete cohort got vaccinated and therefore, the estimation uncertainty for breakthrough infections during Follow-up 4 decreased. 99.4% of the people stating vaccination in the questionnaire sero-converted in anti-S, indicating a good efficacy of the vaccinations. In concordance with other studies [39, 40], a considerable proportion of breakthrough infections was detected. Our results as well as other studies suggest that vaccination lowers the risk of infection [41]. Moreover, the share of infected persons (sero-prevalence) was shown to be greater in the non-vaccinated population in comparison to the vaccinated one. The sero-incidence of (most likely asymptomatic) infections among vaccinated people in the population was lower than the one in non-vaccinated people; however, the difference was statistically non-significant. BTIs might thus relevantly contribute to the community spread, considering also the fact that the vaccinated population was much larger compared to the non-vaccinated one. This might be even more relevant for highly transmissible variants like Omicron.

With an increasing prevalence of vaccination in the population, silent infections or persons presenting only mild symptoms are common. In this context, population-based sero-prevalence studies are important to estimate the true population prevalence. A couple of German cross-sectional population-based sero-prevalence studies were published especially during the first and second wave of the pandemic [42–44]. To our knowledge, all these studies stopped by mid 2021, leaving our cohort as the only one.

In our first analysis [33], an increased (albeit not statistically significant) risk of infection of having a job with a high potential of contact to COVID-19 cases could be found. With this analysis the risk factor became statistically significant, which is in line with other studies [45–47]. The World Health Organisation reported that among the COVID-19 cases reported worldwide, 14% belong to the group of healthcare workers, whereas in most countries this group represents less than 3% of the general population [48].

Participants with a living area between 31 and 40 square meters per inhabitant showed a significantly increased risk for infection, while the risk of the group with a living area between 41 and 55 square meters per inhabitant significantly decreased. Considering the number of household members, we found that 56%

(76%) of the households with 31 - 40 (41—55) squared meters per inhabitant also have only one or two household members. Knowing that a larger household size implies more possible infectious contacts [49–51] suggests that the risk also depends on the household composition: Less members are associated to lower risk of infection. Household size is included in the model but does not show any significant effect, also not as interaction term, although the risk of infection seems to become higher with more household members (Fig. 4). This might be due to the fact that the variables household size, living area per inhabitant and building type all describe the living situation, with difficulties in separating the risk effects. Nevertheless, no multicollinearity issues were detected for this analysis.

Beside the two aforementioned risks for infection and being born outside Germany, no other socio-demographic or health-related risk factors were identified in our study. These results should rather be seen as exploratory than confirmatory, considering that we made no adjustment for multiple testing.

Major strengths of our study are its population-based approach, the appropriate weighting of results for the general Munich population, the high number of participants, the thorough validation of the assays used, and the use of validated questionnaire items. The overall response to the study was high compared to other population-based epidemiological studies in Germany (64% of the participants gave specimens in all rounds) [52]. While most participants completed the questionnaire online or on paper, we also provided the alternative of telephone interviews, which helped increasing participation. A relevant limitation of our study is the exclusion of children and residents not living in private households. While in general, people with migration background are less likely to participate in population-based studies, the lack of translated questionnaires further limited the number of migrants participating in our study [21]. To increase response, blood samples were collected at participants' homes or via mail with the DBS introduction and not at a centralized testing facility. Although until now a lot of research has been done for the COVID-19 pandemic, definitions like correlate of protection and long COVID symptoms are still not fully understood. Therefore, we aim to continue our longitudinal prospective representative cohort.

Conclusion

Despite the vaccination campaign, SARS-CoV-2 sero-prevalence in the Munich general population increased drastically towards the end of 2021, but was still below 20%. The estimated number of infected persons was nevertheless at least twice as high as the official number

reported by the authorities during the second half of 2021. Workers with a high potential of contact to infected persons experienced an increased risk of infection. Breakthrough infections still contribute to the community spread, thus we conclude that non-pharmaceutical interventions are still relevant, especially in the presence of highly transmissible variants like Omicron.

Abbreviations

anti-N	Anti-Nucleocapsid antibodies
anti-S	Anti-Spike antibodies
BTI	Breakthrough infections
CI	Confidence interval
DBS	Dry blood spot
HR	Hazard ratio
INS	Infections of naïve subjects
KoCo19	Representative COVID-19 Cohort Munich
PCR	Polymerase chain reaction
Ro-N-Ig	Elecsys® Anti-SARS-CoV-2 anti-N (Roche)
Ro-RBD-Ig	Elecsys® Anti-SARS-CoV-2 anti-S (Roche)
RT-PCR	Reverse transcription polymerase chain reaction
SARS-CoV-2	SARS corona virus 2

Supplementary Information

The online version contains supplementary material available at https://doi.org/10.1186/s12879-023-08435-1.

Additional file 1: Figure S1. Missing pattern in the baseline questionnaire. Bottom middle: variable analysed for missing information. Bottom left: bar chart depicting numbers of missing information for that variable. Bottom right: description of intersection pattern between variables (all possible combinations of the variables for which a missing information was given, from left to right e.g. only income information missing, income & living & household type information missing, all variables missing, etc.). Top: bar chart depicting the numbers of participants that did not give information for that intersection pattern.

Additional file 2: Figure S2. Cohort description based on current lab result (in contrast to ever-positivity as in Figure 2). Change of serological status of participants: only infected (anti-N positive and stated to be non-vaccinated in the questionnaire), naïve (anti-N and anti-S negative), vaccinated (only anti-S positive), infected & vaccinated (anti-N positive and in previous round only anti-S positive, or anti-N positive and stated to be vaccinated in the questionnaire), infected without information on vaccination status (infected, undefined vaccination) and non-responders/missing.

Additional file 3: Figure S3. Proximity cluster analysis at Follow-ups 2 to 4. The grey points and curves show the distribution of mean within-cluster variances for 10,000 random permutations of cluster assignments. The horizontal lines show the observed values. Cluster variables are households, buildings, and geospatial clusters of different sizes. Household membership was left invariant when considering buildings and geospatial clusters. p-values indicate the one-sided probability of observing smaller than observed values under random cluster assignments. Results indicate within-household clustering and suggest neighbourhood transmission only in the cluster with 500m.

Additional file 4: Table S1. Non-response mechanism at the different follow-ups using complete cases and indicator of missingness for income.

Authors' contributions

M.H. is the principal investigator of this study and obtained most necessary funds. M.H. and K.R. conceived the study with input from L.O., I.K., and A.W. Sample collection was led by S.W., M.P., C.R., I.N., C.J., and M.H. The laboratory set-up and sample processing were led by R. R.-A., I.P., and A.W. Data acquisition and data management were coordinated by N.C., with contributions of F.R., and S.W. Data was cleaned and prepared by N.C. Statistical analyses and data visualization were performed by N.C. and R.L.G. with contributions from A.B., P.P. and Y.S. C.F. led the statistical analyses. N.C., C.F. and R.L.G. conceptualized the result presentation with input from P.P. and K.R. The manuscript was primarily written by N.C., C.F. and R.L.G., with significant contributions from M.P. All authors have read and agreed to the published version of the manuscript.

Le Gleut *et al. BMC Infectious Diseases*　　(2023) 23:466

Page 14 of 15

Availability of data and materials

Our data are accessible to researchers upon reasonable request to the corresponding author taking data protection laws and privacy of study participants into account. To facilitate reproducibility and reuse, the analysis and figure generation code has been made available on GitHub (https://github.com/koco19/epi3) and will be uploaded to ZENODO for long-term storage.

Declarations

Ethics approval and consent to participate

The study was conducted in accordance with good clinical (GCP) and epidemiological practice (GEP) standards as well as the Declaration of Helsinki in its most recent form (as amended by the 64th WMA General Assembly, Fortaleza, Brazil, in October 2013). The study protocol was approved by the Institutional Review Board of the Medical Faculty at Ludwig Maximilian University Munich, Germany (opinion dated 31 March 2020; number 20–275; opinion date amendment: 10 October 2020), prior to study initiation. Informed consent was obtained from all study participants prior to study inclusion.

Consent for publication

Not applicable.

Competing interests

In addition to the funding disclosed in the funding section, L.O. received non-financial support from Dr. Box Betrobox and grants from the Bavarian State Ministry of Science and the Arts during the conduct of the study. AW and MH report personal fees and non-financial support from Roche Diagnostics, LO reports non-financial support from Roche Diagnostics. AW, MH and LO report non-financial support from Euroimmun, non-financial support from Viramed, non-financial support from Mikrogen. AW, MH, LO report grants, non-financial support and other from German Centre for Infection Research DZIF, grants and non-financial support from Government of Bavaria, non-financial support from BMW, non-financial support from Munich Police, nonfinancial support and other from Accenture. MH and AW report personal fees and nonfinancial support from Dr. Box-Betrobox, non-financial support from Dr. Becker MVZ during the conduct of the study. AW is involved in other different patents and companies not in relation with the serology of SARS-CoV-2. AW reports personal fees and other from Haereaus Sensors, nonfinancial support from Bruker Daltonics, all of which are outside the submitted work, and non-related to SARS-CoV-2. The funders had no role in study design, data collection, data analyses, data interpretation, writing, or submission of this manuscript. All other authors declare no competing interests.

Author details

[1]Institute of Computational Biology, Helmholtz Munich, German Research Centre for Environmental Health, 85764 Neuherberg, Germany. [2]Core Facility Statistical Consulting, Helmholtz Munich, German Research Centre for Environmental Health, 85764 Neuherberg, Germany. [3]Division of Infectious Diseases and Tropical Medicine, University Hospital, LMU Munich, 80802 Munich, Germany. [4]Robert Koch Institute, Nordufer 20, 13353 Berlin, Germany. [5]Institute and Outpatient Clinic for Occupational, Social and Environmental Medicine, University Hospital, LMU Munich, 80336 Munich, Germany. [6]Centre for International Health (CIH), University Hospital, LMU Munich, 80336 Munich, Germany. [7]Comprehensive Pneumology Centre (CPC) Munich, German Centre for Lung Research (DZL), 89337 Munich, Germany. [8]Centre for Mathematics, Technische Universität München, 85748 Garching, Germany. [9]Life and Medical Sciences Institute, University of Bonn, 53115 Bonn, Germany. [10]German Centre for Infection Research (DZIF), Partner Site, Munich, Germany. [11]Fraunhofer Institute for Translational Medicine and Pharmacology ITMP, Immunology, Infection and Pandemic Research, 80799 Munich, Germany. [12]Max Von Pettenkofer Institute, Faculty of Medicine, LMU Munich, 80336 Munich, Germany. [13]Faculty of Business Administration and Economics, Bielefeld University, 33615 Bielefeld, Germany. [14]Institute of Radiation Medicine, Helmholtz Munich, German Research Centre for Environmental Health, 85764 Neuherberg, Germany.

References

1. Huang C, Wang Y, Li X, Ren L, Zhao J, Hu Y, et al. Clinical features of patients infected with 2019 novel coronavirus in Wuhan China. Lancet. 2020;395(10223):497–506.
2. World Health Organization. WHO Director-General's opening remarks at the media briefing on COVID-19 - 11 March 2020. 2020. Cited 2023 May 17. Available from: https://www.who.int/director-general/speeches/detail/who-director-general-s-opening-remarks-at-the-media-briefing-on-covid-19---11-march-2020.
3. Robert Koch-Institut. COVID-19 Datenhub. 2020. Available from: https://npgeo-corona-npgeo-de.hub.arcgis.com/. Cited 2023 Jan 30.
4. Bundesministerium für Justiz. § 28a IfSG - Einzelnorm. Gesetz zur Verhütung und Bekämpfung von Infektionskrankheiten beim Menschen (Infektionsschutzgesetz - IfSG) § 28a Besondere Schutzmaßnahmen zur Verhinderung der Verbreitung der Coronavirus-Krankheit-2019 (COVID-19) bei epidemischer Lage von nationaler Tragweite. Cited 2023 Jan 30. Available from: https://www.gesetze-im-internet.de/ifsg/__28a.html.
5. Robert Koch-Institut. Ergänzung zum Nationalen Pandemieplan – COVID-19 – neuartige Coronaviruserkrankung, Berlin. 2020. Available from: https://www.rki.de/DE/Content/InfAZ/N/Neuartiges_Coronavirus/Ergaenzung_Pandemieplan_Covid.html.
6. Chakraborty S, Mallajosyula V, Tato CM, Tan GS, Wang TT. SARS-CoV-2 vaccines in advanced clinical trials: where do we stand? Adv Drug Deliv Rev. 2021;172:314–38.
7. Fiolet T, Kherabi Y, MacDonald CJ, Ghosn J, Peiffer-Smadja N. Comparing COVID-19 vaccines for their characteristics, efficacy and effectiveness against SARS-CoV-2 and variants of concern: a narrative review. Clin Microbiol Infect. 2022;28(2):202–21.
8. Bayerische Staatsregierung. Bericht aus der Kabinettssitzung – Bayerisches Landesportal. 2020. Cited 2023 May 23. Available from: https://www.bayern.de/bericht-aus-der-kabinettssitzung-2/.
9. Robert-Koch-Institut. Epidemiologisches Bulletin 47/2021. 2021.
10. Kuo SC, Fan B, Zhu H, Wu MH, Lee FJ, Cheng YC, et al. Contribution of testing strategies and contact tracing towards COVID-19 outbreaks control: a mathematical modeling study. Trop Med Infect Dis. 2022;7(11):376.
11. Sah P, Fitzpatrick MC, Zimmer CF, Abdollahi E, Juden-Kelly L, Moghadas SM, et al. Asymptomatic SARS-CoV-2 infection: a systematic review and meta-analysis. Proc Natl Acad Sci U S A. 2021;118(34):e2109229118.
12. Süddeutsche Zeitung. Corona-Notbremse: Was in München ab Mittwoch gilt. Süddeutsche.de. 2021. Cited 2023 Jan 30. Available from: https://www.sueddeutsche.de/muenchen/muenchen-corona-notbremse-mittwoch-1.5263849.
13. Robert-Koch-Institut. RKI - Coronavirus SARS-CoV-2 - Besorgniserregende SARS-CoV-2-Virusvarianten (VOC). 2023. Cited 2023 Jan 30. Available from: https://www.rki.de/DE/Content/InfAZ/N/Neuartiges_Coronavirus/Virusvariante.htm.
14. Robert-Koch-Institut. Bericht zu Virusvarianten von SARS-CoV-2 in Deutschland, insbesondere zur Variant of Concern (VOC) B.1.1.7. 2021.
15. Bundesministerium für Gesundheit. Bundesanzeiger Bundesministerium für Gesundheit Verordnung zum Anspruch auf Testung in Bezug auf einen direkten Erregernachweis des Coronavirus SARS-CoV-2 (Coronavirus-Testverordnung – TestV). Bundesministerium der Justiz und für Verbraucherschutz; 2021.
16. Bundesministerium für Gesundheit. Chronik zum Coronavirus SARS-CoV-2. 2023, Cited 2023 May 23. Available from: https://www.bundesgesundheitsministerium.de/coronavirus/chronik-coronavirus.html.
17. Süddeutsche Zeitung. Corona in Bayern: Newsblog vom 5. bis zum 26. Juli 2021. Süddeutsche.de. 2021. Cited 2023 Feb 1. Available from: https://www.sueddeutsche.de/bayern/corona-bayern-archiv-1.5342370.
18. Kirschner R, Ruppert J, BR24 Redaktion. Corona-Lockerungen: Was jetzt in Bayern gilt Internet. BR24. 2021. Cited 2023 Feb 1. Available from: https://

Le Gleut *et al. BMC Infectious Diseases*   (2023) 23:466

Page 15 of 15

www.br.de/nachrichten/bayern/corona-lockerungen-welche-regeln-jetzt-in-bayern-gelten,SZM7asN.

19. Bayerische Staatsregierung. Bericht aus der Kabinettssitzung vom 04. Oktober 2021 – Bayerisches Landesportal. 2021. Cited 2023 Jan 31. Available from: https://www.bayern.de/bericht-aus-der-kabinettssitzung-vom-04-oktober-2021/.

20. Radon K, Bakuli A, Pütz P, Le Gleut R, GuggenbuehlNoller JM, Olbrich L, et al. From first to second wave: follow-up of the prospective COVID-19 cohort (KoCo19) in Munich (Germany). BMC Infect Dis. 2021;21(1):925.

21. Radon K, Saathoff E, Pritsch M, GuggenbühlNoller JM, Kroidl I, Olbrich L, et al. Protocol of a population-based prospective COVID-19 cohort study Munich, Germany (KoCo19). BMC Public Health. 2020;20(1):1036.

22. Beyerl J, Rubio-Acero R, Castelletti N, Paunovic I, Kroidl I, Khan ZN, et al. A dried blood spot protocol for high throughput analysis of SARS-CoV-2 serology based on the Roche Elecsys anti-N assay. EBioMedicine. 2021;70: 103502.

23. Olbrich L, Castelletti N, Schälte Y, Garí M, Pütz P, Bakuli A, et al. Head-to-head evaluation of seven different seroassays including direct viral neutralisation in a representative cohort for SARS-CoV-2. J Gen Virol. 2021;102(10): 001653.

24. Särndal CE, Swensson B, Wretman J. Model Assisted Survey Sampling. 1st ed. Springer New York, NY; 2003. Cited 2023 Jan 31. XV, 695. (Springer Series in Statistics). Available from: https://link.springer.com/book/97803 87406206.

25. Deville JC, Särndal CE. Calibration Estimators in Survey Sampling. J Am Stat Assoc. 1992;87(418):376–82.

26. Landeshauptstadt München Stadtverwaltung. Corona-Infoportal München. Cited 2023 Jan 31. Available from: https://stadt.muenchen.de/infos/corona-infoportal-muenchen.html.

27. Deville JC. Variance estimation for complex statistics and estimators: linearization and residual techniques. Surv Methodol. 1999;25(2):193–204.

28. Juillard H, Chauvet G. Variance estimation under monotone non-response for a panel survey. Survey Methodology. 2018. Cited 2023 Jan 31. Available from: https://hal.science/hal-01354853.

29. Cameron AC, Gelbach JB, Miller DL. Bootstrap-based improvements for inference with clustered errors. Rev Econ Stat. 2008;90(3):414–27.

30. Honaker J, King G, Blackwell M. Amelia II: a program for missing data. J Stat Softw. 2011;12(45):1–47.

31. Andersen PK, Gill RD. Cox's regression model for counting processes: a large sample study. Ann Stat. 1982;10(4):1100–20.

32. Therneau TM, Grambsch PM. The Cox Model. Modeling Survival Data: Extending the Cox Model. New York, NY: Springer New York; 2000. p. 39–77. https://doi.org/10.1007/978-1-4757-3294-8_3.

33. Pritsch M, Radon K, Bakuli A, Le Gleut R, Olbrich L, GuggenbüehlNoller JM, et al. Prevalence and risk factors of infection in the representative COVID-19 cohort Munich. Int J Environ Res Public Health. 2021;18(7):3572.

34. Michlmayr D, Hansen CH, Gubbels SM, Valentiner-Branth P, Bager P, Obel N, et al. Observed protection against SARS-CoV-2 reinfection following a primary infection: a Danish cohort study among unvaccinated using two years of nationwide PCR-test data. Lancet Region Health Eur. 2022;20. Cited 2023 Feb 2. Available from: https://www.thelancet.com/journals/lanepe/article/PIIS2666-7762(22)00146-6/fulltext.

35. Özüdoğru O, Bahçe YG, Acer Ö. SARS CoV-2 reinfection rate is higher in the Omicron variant than in the Alpha and Delta variants. Ir J Med Sci. 2022. Cited 2023 Feb 2. https://doi.org/10.1007/s11845-022-03060-4.

36. Nielsen KF, Moustsen-Helms IR, Schelde AB, Gram MA, Emborg HD, Nielsen J, et al. Vaccine effectiveness against SARS-CoV-2 reinfection during periods of Alpha, Delta, or Omicron dominance: a Danish nationwide study. PLoS Med. 2022;19(11):e1004037.

37. Lipsitch M, Krammer F, Regev-Yochay G, Lustig Y, Balicer RD. SARS-CoV-2 breakthrough infections in vaccinated individuals: measurement, causes and impact. Nat Rev Immunol. 2022;22(1):57–65.

38. Bates TA, Mc Bride SK, Winders B, Schoen D, Trautmann L, Curlin ME, et al. Antibody Response and Variant Cross-Neutralization After SARS-CoV-2 Breakthrough Infection. JAMA. 2022;327(2):179–8.

39. Angel Y, Spitzer A, Henig O, Saiag E, Sprecher E, Padova H, et al. Association between vaccination with BNT162b2 and incidence of symptomatic and asymptomatic SARS-CoV-2 infections among health care workers. JAMA. 2021;325(24):2457–65.

40. Subramanian SV, Kumar A. Increases in COVID-19 are unrelated to levels of vaccination across 68 countries and 2947 counties in the United States. Eur J Epidemiol. 2021;36(12):1237–40.

41. Dagan N, Barda N, Kepten E, Miron O, Perchik S, Katz MA, et al. BNT162b2 mRNA Covid-19 vaccine in a nationwide mass vaccination setting. N Engl J Med. 2021;384(15):1412–23.

42. Pérez-Olmeda M, Saugar JM, Fernández-García A, Pérez-Gómez B, Pollán M, Avellón A, et al. Evolution of antibodies against SARS-CoV-2 over seven months: experience of the nationwide seroprevalence ENE-COVID study in Spain. J Clin Virol. 2022;149: 105130.

43. Carrat F, de Lamballerie X, Rahib D, Blanché H, Lapidus N, Artaud F, et al. Antibody status and cumulative incidence of SARS-CoV-2 infection among adults in three regions of France following the first lockdown and associated risk factors: a multicohort study. Int J Epidemiol. 2021;50(5):1458–72.

44. Forster F, Kreißl S, Wengenroth L, Vogelberg C, von Mutius E, Schaub B, et al. Third follow-up of the study on Occupational Allergy Risks (SOLAR III) in Germany: design, methods, and initial data analysis. Front Public Health. 2021;9: 591717.

45. Gudbjartsson DF, Norddahl GL, Melsted P, Gunnarsdottir K, Holm H, Eythorsson E, et al. Humoral immune response to SARS-CoV-2 in Iceland. N Engl J Med. 2020;383(18):1724–34.

46. Pollán M, Pérez-Gómez B, Pastor-Barriuso R, Oteo J, Hernán MA, Pérez-Olmeda M, et al. Prevalence of SARS-CoV-2 in Spain (ENE-COVID): a nationwide, population-based seroepidemiological study. The Lancet. 2020;396(10250):535–44.

47. McDade TW, McNally EM, Zelikovich AS, D'Aquila R, Mustanski B, Miller A, et al. High seroprevalence for SARS-CoV-2 among household members of essential workers detected using a dried blood spot assay. PLoS One. 2020;15(8):e0237833.

48. World Health Organization. Keep health workers safe to keep patients safe: WHO. 2020. Cited 2023 Jan 31. Available from: https://www.who.int/news/item/17-09-2020-keep-health-workers-safe-to-keep-patients-safe-who.

49. Cardoso MRA, Cousens SN, de Góes Siqueira LF, Alves FM, D'Angelo LAV. Crowding: risk factor or protective factor for lower respiratory disease in young children? BMC Public Health. 2004;4:19.

50. Martin CA, Jenkins DR, Minhas JS, Gray LJ, Tang J, Williams C, et al. Socio-demographic heterogeneity in the prevalence of COVID-19 during lockdown is associated with ethnicity and household size: results from an observational cohort study. eClinicalMedicine. 2020;25. Cited 2023 Feb 1. Available from: https://www.thelancet.com/journals/eclinm/article/PIIS2589-5370(20)30210-8/fulltext.

51. House T, Keeling MJ. Household structure and infectious disease transmission. Epidemiol Infect. 2009;137(5):654–61.

52. Rach S, Günther K, Hadeler B. Participants who were difficult to recruit at baseline are less likely to complete a follow-up questionnaire – results from the German National Cohort. BMC Med Res Methodol. 2020;20(1):187.

Publisher's Note

Springer Nature remains neutral with regard to jurisdictional claims in published maps and institutional affiliations.

Publication 4:

Integrative modelling of reported case numbers and seroprevalence reveals time-dependent test efficiency and infectious contacts

Lorenzo Contento*, **Noemi Castelletti***, Elba Raimúndez, Ronan Le Gleut, Yannik Schälte, Paul Stapor, Ludwig Christian Hinske, Michael Hoelscher, Andreas Wieser+, Katja Radon+, Christiane Fuchs+, Jan Hasenauer+ and KoCo19 study group

Integrative modelling of reported case numbers and seroprevalence reveals time-dependent test efficiency and infectious contacts

Lorenzo Contento [a,*,1], Noemi Castelletti [b,1], Elba Raimúndez [a,e], Ronan Le Gleut [c,d], Yannik Schälte [c,e], Paul Stapor [c,e], Ludwig Christian Hinske [f], Michael Hoelscher [b,g,h], Andreas Wieser [b,h,2], Katja Radon [h,i,j,2], Christiane Fuchs [c,d,e,k,2], Jan Hasenauer [a,c,e], the KoCo19 study group[3]

[a] Faculty of Mathematics and Natural Sciences, University of Bonn, Bonn, Germany
[b] Division of Infectious Diseases and Tropical Medicine, University Hospital, LMU Munich, Munich, Germany
[c] Institute of Computational Biology, Helmholtz Zentrum München - German Research Center for Environmental Health, Neuherberg, Germany
[d] Core Facility Statistical Consulting, Helmholtz Zentrum München - German Research Center for Environmental Health, Neuherberg, Germany
[e] Center for Mathematics, Technische Universität München, Garching, Germany
[f] Institut für medizinische Informationsverarbeitung, Biometrie und Epidemiologie, Munich, Germany
[g] Center for International Health (CIH), University Hospital, LMU Munich, Munich, Germany
[h] German Center for Infection Research (DZIF), partner site Munich, Germany
[i] Institute and Outpatient Clinic for Occupational, Social and Environmental Medicine, University Hospital, LMU Munich, Munich, Germany
[j] Comprehensive Pneumology Center (CPC) Munich, German Center for Lung Research (DZL), Munich, Germany
[k] Faculty of Business Administration and Economics, Bielefeld University, Bielefeld, Germany

ARTICLE INFO

ABSTRACT

Mathematical models have been widely used during the ongoing SARS-CoV-2 pandemic for data interpretation, forecasting, and policy making. However, most models are based on officially reported case numbers, which depend on test availability and test strategies. The time dependence of these factors renders interpretation difficult and might even result in estimation biases.

Here, we present a computational modelling framework that allows for the integration of reported case numbers with seroprevalence estimates obtained from representative population cohorts. To account for the time dependence of infection and testing rates, we embed flexible splines in an epidemiological model. The parameters of these splines are estimated, along with the other parameters, from the available data using a Bayesian approach.

The application of this approach to the official case numbers reported for Munich (Germany) and the seroprevalence reported by the prospective COVID-19 Cohort Munich (KoCo19) provides first estimates for

---

* Corresponding author.
E-mail address: lorenzo.contento@uni-bonn.de (L. Contento).
[1] Equal contribution first authors.
[2] Equal contribution last authors.

the time dependence of the under-reporting factor. Furthermore, we estimate how the effectiveness of non-pharmaceutical interventions and of the testing strategy evolves over time. Overall, our results show that the integration of temporally highly resolved and representative data is beneficial for accurate epidemiological analyses.

1. Introduction

Social distancing, mask wearing, lockdowns and other non-pharmaceutical interventions (NPIs) are used worldwide to slow the spread of SARS-CoV-2 and to avoid overburdening health care systems. Various studies have analysed how such NPIs influence the contact rate (Latsuzbaia et al., 2020; Jarvis et al., 2020), the infection rate (Courtemanche et al., 2020; Hartl et al., 2020; Li et al., 2020; Lyu and Wehby, 2020; Siedner et al., 2020), the reproduction number (Giordano et al., 2020; Zhao and Chen, 2020; Liu et al., 2021; Brauner et al., 2021; Sypsa et al., 2021) and related quantities. These studies use a broad spectrum of analysis approaches, including statistical methods (e.g., generalized linear models, generalized estimating equations, machine learning) (Streeck et al., 2020; Latsuzbaia et al., 2020; Siedner et al., 2020; Courtemanche et al., 2020), compartmental models based on ordinary differential equations (ODEs) (Barbarossa et al., 2020; Jarvis et al., 2020), and agent-based models (Lorch et al., 2022), and provide important insights. However, a limitation of most studies is that they are exclusively based on official case numbers.

The officially reported case numbers provide in most countries information about the number of positive tests for viral load registered on a specific day. Such tests can either be based on the polymerase chain reaction (PCR) or on antigen detection; for brevity's sake, in the following we will refer to them indiscriminately as diagnostic tests. However, there are several well-known issues with these numbers (Raimúndez et al., 2021). Besides reporting delays, the most important problems are that case numbers depend on the availability of tests and on the test strategy. Clearly, the number of performed tests and the selection criteria have changed over time (e.g., due to the introduction of antigen tests). As an alternative to the officially reported case numbers, the officially reported death numbers, which are generally considered as more reliable (Radon et al., 2021; Pritsch et al., 2021), can be used. However, there the effects of NPIs are smoothed over time and only visible after a substantial delay. Furthermore, the observation can be confounded by the quality of medical care, in particular if the number of beds in intensive-care units becomes a limiting factor. In summary, while case and death numbers provide information on the progression of an epidemic, the interpretation is often difficult.

The ideal data-source for the analysis of NPIs as well as the efficiency of test strategies would be a thorough monitoring of a large representative population cohort. Yet this is rather time- and resource-consuming, and in most cases not realistic. Cross-sectional studies based on diagnostic tests with a high time resolution would provide a comprehensive picture of the spread within populations, but the number of required tests would be very high. For a prevalence of 100 in 100,000 individuals, on average 1000 tests have to be performed to observe a single positive individual. For tight confidence intervals, tens of thousands of diagnostic tests would be necessary per time point. To make things worse, diagnostic tests are only positive for a short period after exposure to the virus.

An alternative to diagnostic tests that allows for the monitoring of epidemics is testing for the presence of antibodies, which assesses seroprevalence. The antibody response is rather stable and can usually be detected even months after the initial infection (Radon et al., 2021; Olbrich et al., 2021; Isho et al., 2020). Accordingly, antibody tests do not only provide a snapshot of the current situation as diagnostic tests do, but inform about previous exposure and hence the past history of the epidemic up to the current point. However, to provide an assessment of NPIs and test strategies with a high temporal resolution, immense resources would be required in this case too.

We believe that the most practical way to monitor at a high temporal resolution the evolution of a pandemic is to combine the frequent but biased official daily case numbers collected by the healthcare authorities with less frequent but more informative seroprevalence measurements from representative population studies. In order to prove that, in this paper we report an analysis of the first COVID-19 wave in Munich during the spring of 2020. The outline of the paper is as follows: (i) we present a compartment model for integrating officially reported case and death numbers, as well as seroprevalence data from the population-based prospective COVID-19 cohort study KoCo19 in Munich (Radon et al., 2020; Pritsch et al., 2021); (ii) we fit the model with and without using seroprevalence data, showing that the additional data drastically reduces uncertainty in the hidden dynamics of the epidemic; (iii) we assess the estimates of the time-dependent effectiveness of NPIs and testing strategies, quantifying their relative contribution to the reduction in the spread of the infection.

2. Results

2.1. Compartmental model for the COVID-19 epidemic

We developed a compartmental model for the dynamics of the COVID-19 epidemic that allows for the integration of the officially reported numbers of positive diagnostic tests and COVID-19 related deaths, hospital bed usage, and seroprevalence in representative cohort studies (Fig. 1). The model describes the state of individuals: susceptible, exposed, infectious, hospitalized, recovered and deceased. Several of these generic states can be further refined (Fig. 1A) by distinguishing infectious individuals with and without symptoms, recovered individuals with and without detectable virus, and hospitalized individuals in ward and intensive care unit (ICU).

Realistic distributions of transition times of individuals between states are achieved by subdividing the illness-related states into multiple sub-states (Fig. 1B). This is often referred to as the Gamma Chain Trick or Linear Chain Trick (Smith, 2011). Many important transition times related to the COVID-19 disease cannot be reasonably modelled by an exponential distribution (single sub-state case) — a fact that is disregarded by many studies. For example, the incubation time has been shown to be reasonably approximated by an Erlang distribution with shape parameter 6 (Lauer et al., 2020), suggesting a split into six sub-states.

The testing process is modelled by splitting illness-related states into two sub-states: infectious individuals that have not been detected, and infectious individuals that have been detected by means of a positive diagnostic test. The rates at which individuals transition from the undetected to the detected branch reflect the efficacy of the testing system set up by the healthcare authorities. As individuals with symptoms are more likely to get tested, we assume that these detection rates depend on the illness phase. In particular, the detection rate for asymptomatic and presymptomatic individuals are especially important since they can be considered a measure of contact tracing effectiveness. Hospitalized individuals are assumed to be immediately detected. The number of reported positive diagnostic tests is then equal to the sum of all fluxes from undetected to detected sub-states.

Since antibodies become detectable only about two weeks after an exposed individual has become infectious (Long et al., 2020), it is not possible to obtain the current number of seropositive individuals from the model state. Instead, we compute the number of individuals who will be seropositive in two weeks' time, which is equal to total population size minus the number of susceptible, exposed (but not yet infectious) and deceased individuals.

A Model of epidemiological process
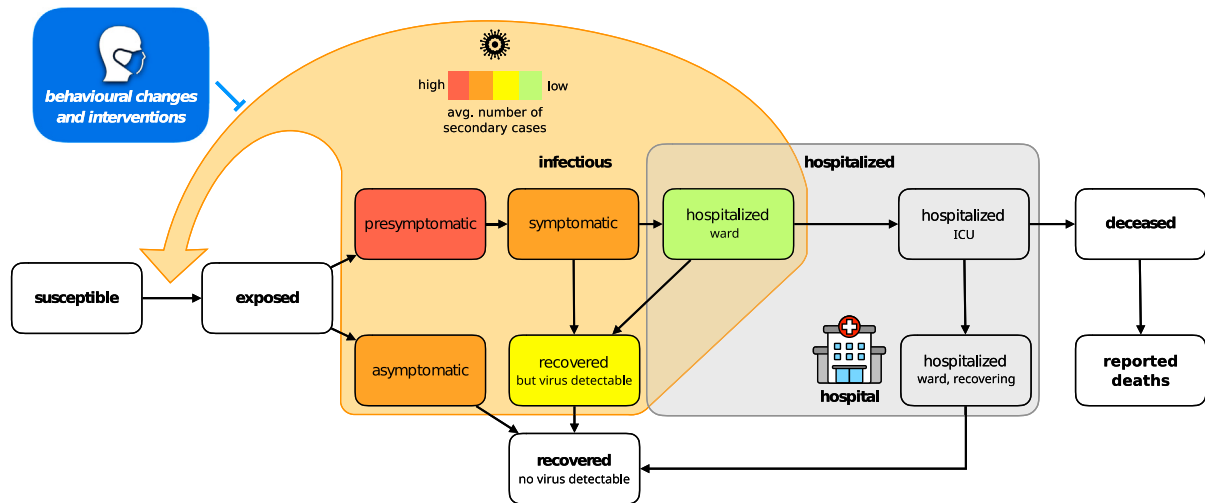
B Model of diagnostic testing process
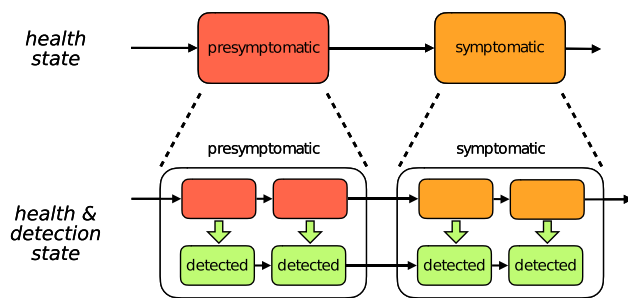
C Model of intervention process
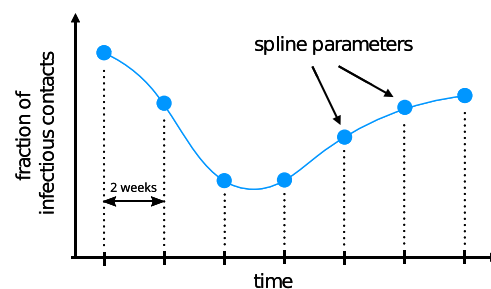
Fig. 1. Structure of the compartment model. (A) High-level structure indicating possible transitions between various illness phases and hospitalization compartments. The delay between death and its reporting to the healthcare authorities is added in order to account for the lower number of deaths observed during weekends. Infectious phases are coloured with different colours encoding our a priori beliefs on the average number of secondary cases generated in a day by an individual in the corresponding compartment. We remark that such a number depends on the degree of infectiousness as well as the total number of inter-personal contacts. For example, on the one hand symptomatic individuals are more infectious than asymptomatic ones, but on the other they are much less likely to encounter other people due to their health condition. It is thus difficult to determine a priori which phase generates more secondary cases and as a first guess they are assigned the same colour in the figure. (B) Detailed structure of the compartment model. Each compartment is split into several sub-states in order to have Erlang-distributed transition times between compartments, and to explicitly model the testing process by tracking individuals reported to the health care authorities on a parallel but separate branch. (C) Time-dependent parameters (here the viral transmission reduction due to NPIs is used as an example) are modelled by splines which can be encoded inside the parameter vector by their values at the grid points.

The rate at which susceptible individuals are infected is proportional to the sum of the number of asymptomatic individuals, presymptomatic individuals, symptomatic individuals, recovered individuals with detectable virus levels, and hospitalized individuals in ward (ICU patients are considered to be not infectious). The elements of this sum must be weighted by the average number of secondary cases generated in a day, which is specific of each compartment. In particular, this number depends both on biological factors, such as the stage to which the illness has progressed, and behavioural factors, which in turn depend strongly on whether the infected individual has been detected or not (detected individuals are quarantined and therefore less likely to spread the disease). The qualitative ordering is indicated by colours in Fig. 1A, but the quantitative contributions are considered to be unknown a priori.

2.2. Statistical framework for inferring testing and intervention effects

The compartment model describes possible transitions between states, but the transition rates are unknown and depend on many factors. Particularly relevant is the influence on the infection and detection rates due to the policies set by the government and the healthcare authorities. We model such effects with three parameters

and, since policies have evolved over time, we assume these parameters to be time-dependent, modelling them using splines (Fig. 1C).

The first two are the detection rates for (i) symptomatic and (ii) asymptomatic/presymptomatic individuals respectively. These rates are influenced by testing capacity, by the effectiveness of contact tracing, and by the criteria to be met in order to be eligible for testing, all of which have undergone considerable changes in the first months of the epidemic. The third is a fractional reduction in the number of infectious contacts compared to the situation at the beginning of the epidemic. Such a reduction is strongly influenced by government restrictions such as business/school closures or lockdowns, but also depends on the compliance of the general population with social distancing and other preventive measures. In all cases time dependency is modelled by cubic splines with an inter-node distance fixed at 2 weeks. Moreover, the evolution of the detection rates has an additional week-periodic component in order to account for the lower case counts during weekends that have been observed in Germany and elsewhere in the world (see *Material and Methods* for more details). A similar week-periodic component is also present in the delay between death and its reporting to the healthcare authorities.

To determine the time-dependent infection and detection rates as well as other unknown parameters, we employ a Bayesian approach to integrate different pieces of information, including seroprevalence

observed in representative cohort studies, reported case numbers, and prior knowledge on process parameters. The publicly available case counts have been modelled with negative binomial distributions, since the variance increases together with the expected value. Since hospital bed counts have a much more limited dynamic range and consequently their variance can be safely considered constant, they are assumed to be normally distributed. Finally, the number of positive antibody tests in a random sample from the population is naturally modelled as the result of a binomial random variable. The priors for the various model parameters were extracted from various published reports (see Supplementary Tables 1 and 2).

2.3. Modelling without representative data provides uncertain estimates

As most studies are only based on officially reported case numbers, we first studied the reliability of such an approach. Therefore, we inferred the model parameters from the reported number of infected, hospitalized and deceased individuals for the city of Munich in Germany. In addition to these commonly used counts, we also employed the publicly available number of reported symptom onsets, which has been rarely used in other modelling efforts but can be easily integrated in our case thanks to our explicit description of the detection process. The number of cases (new infections, deaths and symptom onsets) was extracted from the official report by the Robert Koch Institute (2020), while the hospital usage was obtained from the web-based information system IVENA (2020). The city of Munich was selected as detailed seroprevalence results are available from the KoCo19 study (Radon et al., 2020; Pritsch et al., 2021). The time window used for this study coincides with the first COVID-19 wave in Germany, from the 1st of March to the 7th of June. The first wave is the most interesting phase for assessing the time-dependence of testing efficacy and NPIs, since several NPIs were tried in succession (up to the strictest lockdowns) and the testing capacity quickly ramped up in response to the novel virus.

Inferred parameter estimates capture correctly the case numbers used for fitting (Fig. 2A). Yet, many of the estimated parameters are not well determined, as evinced by the broad credible intervals (Fig. 3A, in blue). To assess the reliability of the predictions, we employed the posterior samples to predict the seroprevalence and compared it with the KoCo19 data, which was not used for fitting (Fig. 2A, bottom-right panel). The prediction given by the most likely parameters encountered during sampling is compatible with the observed seroprevalances. However, as can be seen from Fig. 3B, the total number of cases predicted by the model has very large credible intervals. This shows that officially reported case numbers are, even in combination with prior knowledge, insufficient to predict the actual number of COVID-19 infections during the epidemic with a satisfactory degree of confidence.

2.4. Modelling with representative data reduces uncertainties

In order to quantify the added value provided by prevalence data obtained by extensive serological testing, we extended the previously used dataset with the time-dependent prevalence reported by KoCo19 and performed the same Bayesian parameter estimation procedure. As in the previous analysis, the obtained parameter estimates provide an accurate description of all available data (Fig. 2B) and the uncertainty on the values of the single parameters is quite large (Fig. 3A, in green; for the full posterior distributions see Supplemental Figure 3). The uncertainty on the hidden states of the model (Fig. 3B) is instead greatly reduced, in particular for the total number of cases (not surprisingly, since this quantity is closely linked to the seroprevalence level) and for the number of asymptomatic cases, showing the effectiveness of the seroprevalence data in reducing uncertainty. Fig. 3B also shows how the number of infections predicted by the model is substantially higher than the number of reported cases, highlighting the limitations of the publicly reported case counts.

2.5. Model reveals efficiency of testing strategy

Using the compartment model integrating case reports and representative data, we studied the effectiveness of the testing and NPI strategy. To do that, we computed from the posterior samples the time-dependent detection and number of infectious contacts, along with several secondary properties.

Instead of employing directly the time-dependent detection rates, in order to evaluate the effectiveness of the testing strategy we use a more easily interpretable metric: the probability that an infected individual is reported to the healthcare authorities before the virus is cleared from their system (Fig. 4A). The effectiveness of testing increased gradually as the epidemic progressed. The model estimates that at the beginning of March only 10%–40% (90% CI) of infected individuals were reported, while in April and May the fraction was 25%–50% (90% CI). The largest contribution is the increase in the detection probability for asymptomatic cases, which jumps from 0%–10% (90% CI) to 15%–40% (90% CI).

For the time-dependent reduction in infectious contacts, which models both the effect of government policy and behavioural changes, we observed an opposite effect compared to the detection rate (Fig. 4B). Fixed to be 1 on the first day of March, this factor immediately started to drop quickly. Similarly, the effective reproduction number dropped from above three at the beginning of March to below one after the middle of March (Fig. 5). This coincides with the raising of public awareness (e.g., a speech by the German chancellor) and various interventions.

The effective reproduction number is influenced by both NPIs and by the testing strategy and it is therefore important to deconvolute these two effects. In order to do so, we computed the evolution of the effective reproduction number for three hypothetical scenarios (Fig. 6): (i) neither NPIs are used nor diagnostic testing performed; (ii) only diagnostic testing is performed; (iii) only NPIs are employed (see *Materials & Methods* for more details on the computation). This revealed that diagnostic testing results in a small improvement over what can be achieved with NPIs alone. However, in absence of NPIs such as the lockdown, the testing strategy implemented during the first epidemic wave in Germany would not have been able to lower the reproduction number enough to stop the spreading of the disease.

3. Discussion

Test availability, testing strategy, governmental interventions and various factors have changed over the course of the COVID-19 epidemic in Germany. This renders the interpretations of the reported case numbers difficult, while creating the need to infer time-dependent characteristics (e.g., to assess the impact of strategies). Here, we approached both points by integrating officially reported case numbers with representative seroprevalence observations using integrative modelling and Bayesian parameter estimation framework. Our analysis revealed that the integration of datasets is critical: The amount of available seroprevalance data was too limited to build models just based on them, while case report numbers on their own resulted in very large uncertainties on the hidden states of the model, especially on the number of asymptomatic cases (Fig. 3B). In the last year statistical works integrating case numbers and seroprevalence have been published (Quick et al., 2021), but their number is still rather limited due to the logistical difficulties of wide serological surveys.

In addition to the use of various data sources, a strength of our study is the rigorous application of Bayesian uncertainty quantification. The vast majority of models for the COVID-19 epidemic we have found in the literature were not accompanied by uncertainty quantification. Some exceptions exist, such as a study by Lin et al. (2021), in which uncertainty estimates are given for the observed case number and the parameter values. However, they chose not to estimate most illness related parameters, but to fix them to values taken from the literature.
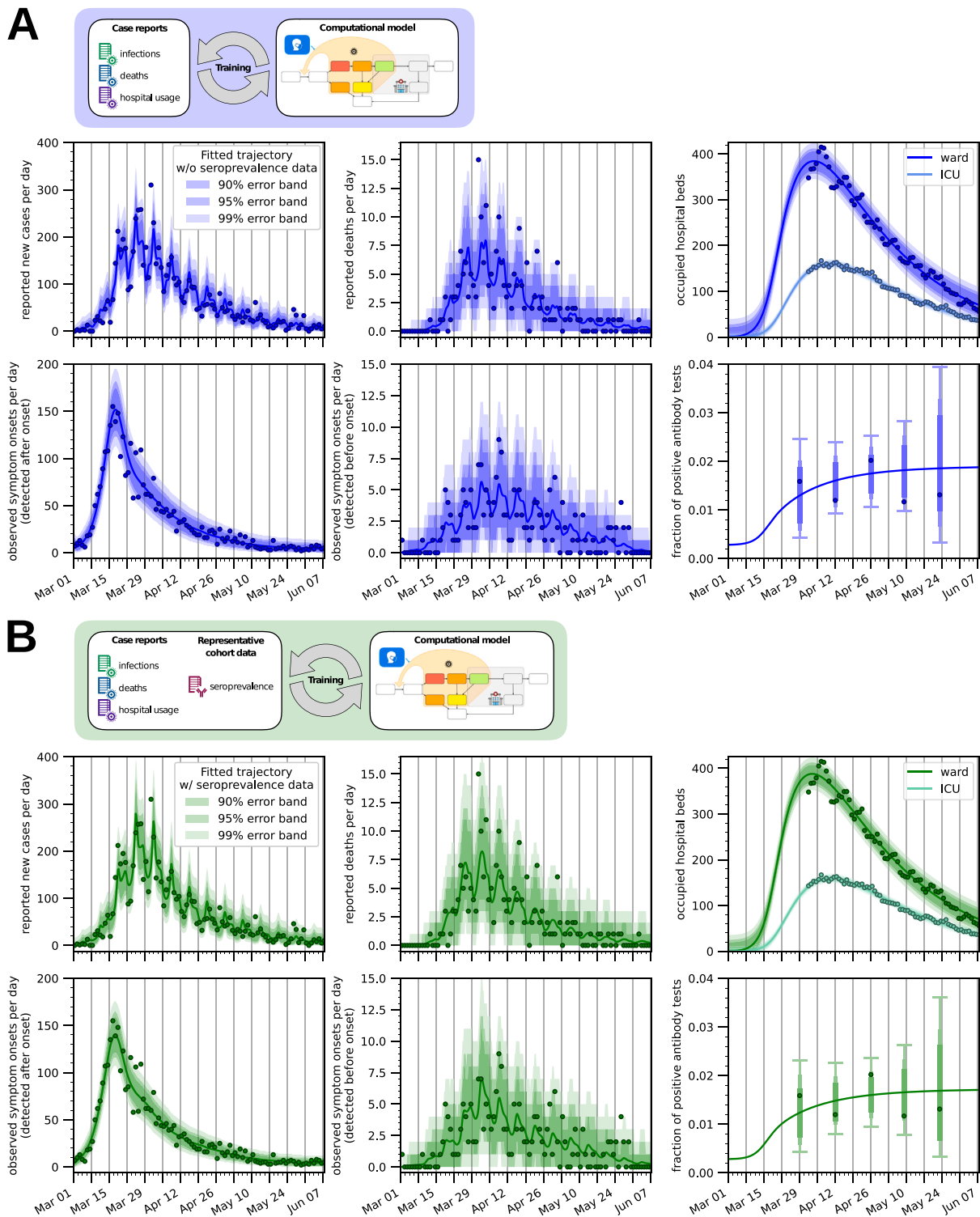
Fig. 2. Model fit for Munich, Germany. Model simulation for the sampled parameter vector with the highest posterior probability compared with the observed data. In (A) only the case numbers reported by the Robert-Koch Institute and hospital usage for Munich are used for fitting, while in (B) seroprevalence data is also employed. The error bands show the range of plausible values for the observation, confirming that the noise models used are appropriate. In the bottom-right panels of (A, B), where the seroprevalence predicted by the model is plotted, the error bars are only shown at the observation times since the variance of each observation is linked to the number of total antibody tests carried out in each sub-batch.

This is problematic for two reasons: Firstly, many parameters are region- and situation-specific and can thus lead to wrong estimates of inferred parameters. Secondly, estimates typically have large uncertainty intervals, as also seen in our study and by Raimúndez et al. (2021). Fixing those to single values may lead to an underestimation of the uncertainty of inferred parameters. This was especially true during

the first wave of the pandemic, when abundant observational data was still not available. For these reasons, we incorporate pre-existing knowledge from the literature only as prior information and estimate all parameters at the same time.

Our integrative modelling framework is able to estimate the effectiveness of the testing strategies employed during the first wave of
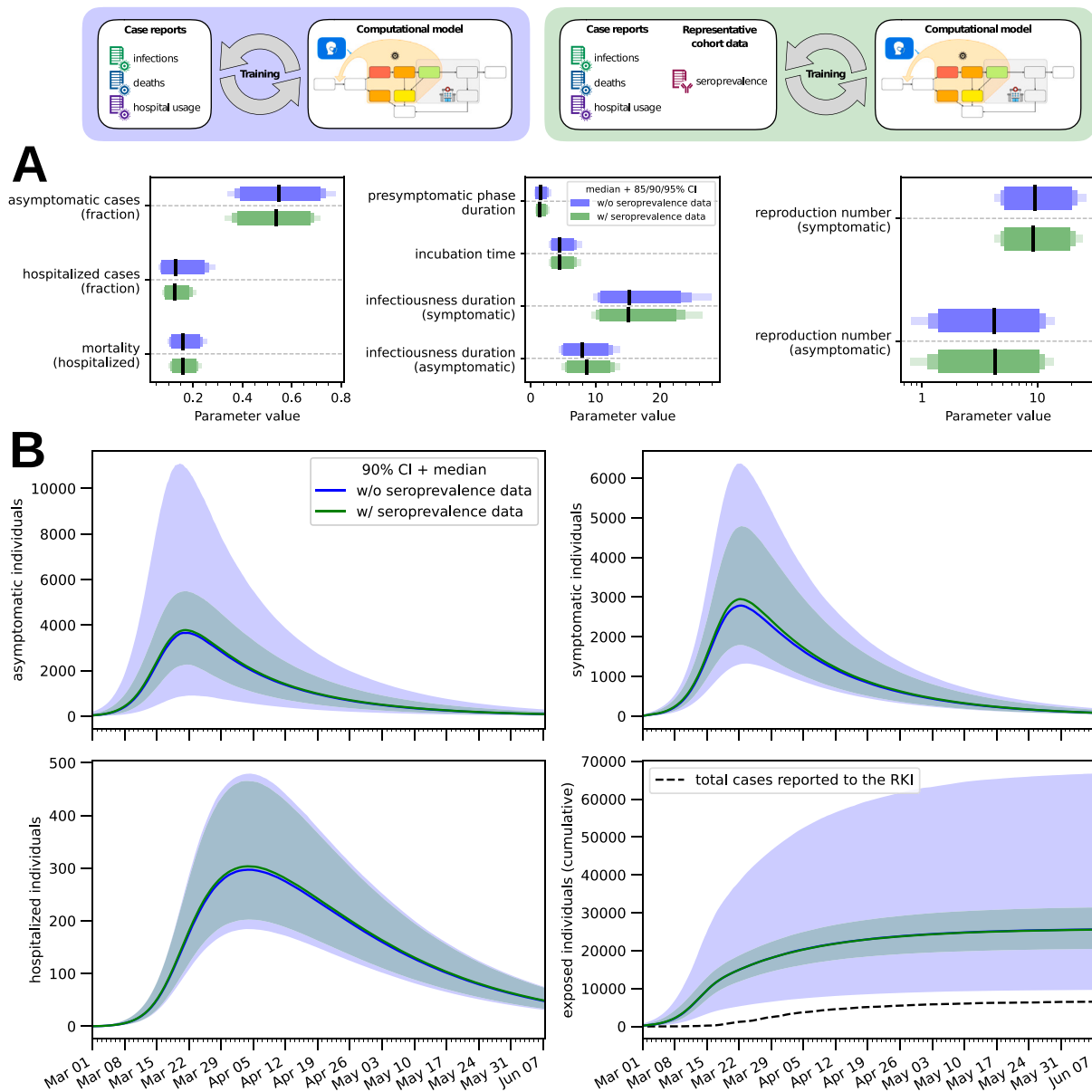
Fig. 3. Uncertainty quantification. (A) 85%/90%/95% credible intervals (bars) and median value (line) for a subset of the model parameters. By reproduction number we mean the basic reproduction number in absence of NPIs and diagnostic testing (see *Materials & Methods* for more details on its computation). (B) The number of individuals in different compartments is plotted as a function of time for both the model fitted with seroprevalence data and the one fitted without. In the bottom-right panel the cumulative number of cases detected by the healthcare authorities is also plotted for reference. The bands correspond to 90% posterior credible intervals, while the solid line denotes the median value. (For interpretation of the references to colour in this figure legend, the reader is referred to the web version of this article.)

the epidemic in Munich (Germany). In particular, it suggests that the fraction of detected asymptomatic SARS-CoV-2 cases quickly saturated. At the beginning of April 20% (90% CI: 10%–30%) of asymptomatic individuals were detected and the numbers changed afterwards only marginally. Indeed, the model predicts even a small drop at the end of May, but the uncertainty is large (due to a low number of observations).

The proposed model relies on a detailed description of the testing process, with the inclusion of symptom onset data and time-dependent detection rates reflecting the varying test capacity of the health care system and the change of the criteria needed for obtaining a test. While still preliminary, we believe such additional modelling to be very important especially in the initial phase of an outbreak. The proposed formulation could be the basis for future studies and expanded by e.g. including age groups and interactions with neighbouring regions.

Our model is rather complex compared to what is commonly found in the literature since we have deliberately striven to model as precisely as possible the viral life cycle and the detection process. In addition

to bringing us closer to the real phenomenon, a more detailed model has the advantage that model states have a more precise interpretation, allowing us to map them to a wider range of data sources, either for fitting or for obtaining prior information. Yet, even the current model does not cover all aspects which might be relevant to the epidemic spread. For example, one could add to the model an explicit compartment for mildly symptomatic individuals, whose mobility is not reduced by their light symptoms but who are more infectious than asymptomatic individuals.

Realistic but complex models have however their limitations. Our detailed model, coupled with our use of weak priors that reflects the lack of information at the beginning of a new pandemic, results in a very large uncertainty on most parameters, some of which are most certainly not identifiable. However, we are not mainly interested in providing tight parameter estimates but rather in assessing the added value brought by seroprevalence datasets. If one looks at the estimates of the evolution of the number of infected individuals (especially
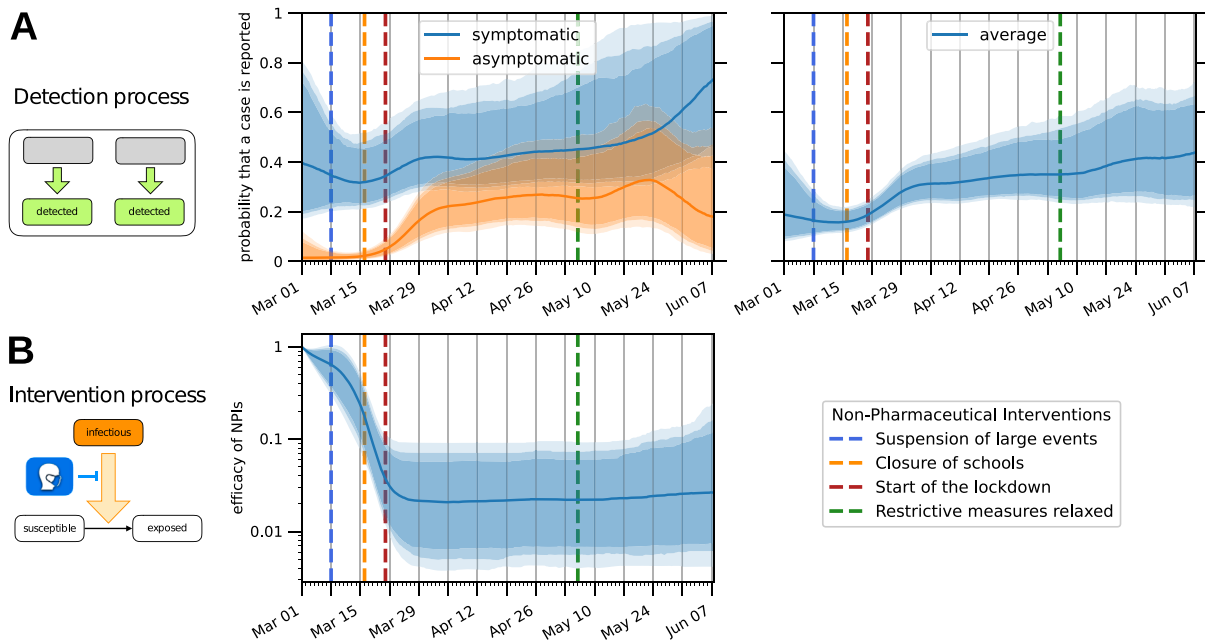
Fig. 4. Estimation of time-dependent parameters. The bands correspond to 85%/90%/95% posterior credible intervals, while the solid line denotes the median value. Dashed lines indicate at which dates specific NPIs were enforced/lifted. (A) Probability that an infected individual is detected and reported to the healthcare authorities before the virus is cleared from their system. The left plot shows such probabilities for symptomatic and asymptomatic infected individuals separately, while the right plot shows their weighted average, i.e. the probability that a generic infected individual is eventually detected. (B) Relative reduction in the number of infectious contacts due to NPIs and behavioural changes.
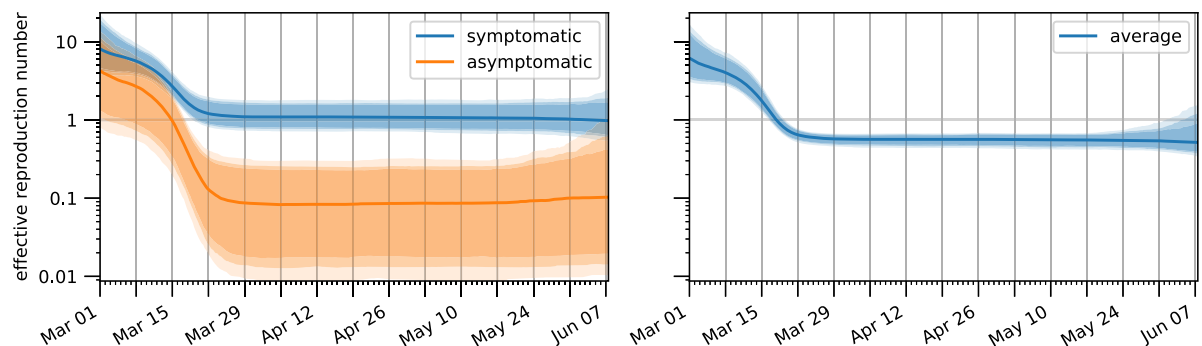
Fig. 5. Temporal evolution of the effective reproduction number. The left plot shows the effective reproduction numbers for symptomatic and asymptomatic infected individuals, while the right plot shows their weighted average, i.e. the reproduction number for a generic infected individual. The bands correspond to 85%/90%/95% posterior credible intervals, while the solid line denotes the median value.
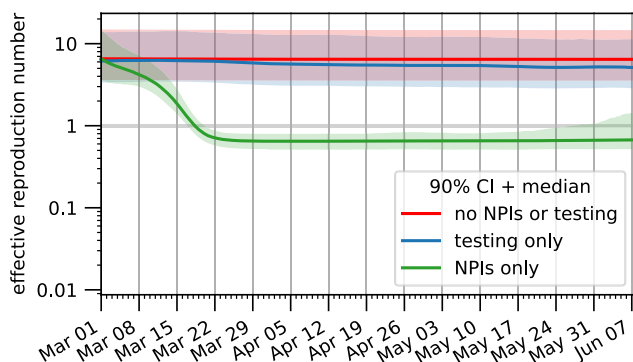
Fig. 6. Relative importance of the detection process and the NPIs on the spread of the epidemic. Estimates for the reproduction number are plotted for three different scenarios: (red) neither diagnostic testing nor NPIs are employed; (blue) only diagnostic testing is performed; (green) only NPIs are applied. The bands correspond to the 90% posterior credible interval, while the solid line denotes the median value. (For interpretation of the references to colour in this figure legend, the reader is referred to the web version of this article.)

asymptomatic ones), the levels of uncertainty are much lower and the improvement due to the integration of seroprevalence data is clear. The real limitation of a complex model lies instead in the computation time it requires. A simpler model with more identifiable parameters and/or stronger priors would be more effective for time-sensitive goals, e.g. in providing online estimation and predictions for an ongoing pandemic.

Overall, the proposed work highlights the importance of seroprevalence data and thereby complements various existing efforts. We expect that it might contribute to a better understanding of the dynamics of epidemics in a dynamic environment, with changing testing capabilities and NPIs.

4. Materials and methods

4.1. Data sources

Case report data We use the official case data for Munich (Germany), which is released on a daily basis by the Robert Koch Institute (2020). We process the data to obtain the total number of new cases and deaths which were communicated to the public health officials for each day.

The delay between diagnosis and recording in the RKI database can be rather long, but since we are only dealing with data from the first pandemic wave this is not a matter of concern in our study.

We can observe in the RKI dataset the so-called "weekend effect": the number of new cases and deaths is significantly lower during the weekend. A similar effect has been observed in other countries and for other diseases as well. However, there is no consensus on the reasons behind such a periodicity. Possible explanations include: reporting delays; decreased diagnostic testing capacity; lower probability of dying during the weekend due to critical therapeutic decisions being made less often during holidays. Our model treats the weekend effect as a kind of reporting delay (see the *Detection process* paragraph for more details). Decreased testing capacity and decreased changes in therapy can also be accounted for by such an approach.

In addition to the case and death counts used in many other studies, for a subset of patients the RKI provides the date at which they first displayed symptoms. To the best of our knowledge such information has not been used in any other modelling effort. By comparing the date of symptom onset to the date of detection we can determine whether the patient was presymptomatic or symptomatic when they were tested. Since our model keeps the progression of detected and undetected individuals separate, these two counts can be fitted simultaneously.

Hospital bed counts In addition to the RKI data, we employed also the number of hospital beds in Munich occupied by COVID-19 patients (IVENA, 2020). Bed counts were aggregated by hospital unit: ward, medium care unit (MCU) and intensive care unit (ICU). Since not all hospitals have a MCU, we further aggregated MCU and ICU bed counts. Due to a non-uniform reporting by the different hospitals (especially in the first days since the reporting system was set up), the data before 25 March 2020 had to be discarded. Some of the smaller hospitals/clinics did not reliably report bed counts even after this date and had to be excluded, leading to a possible, albeit slight, underestimation of the total number of occupied beds.

Another possible problem in the data is that patients may be moved from the surrounding areas to the city, where hospital concentration is higher, resulting in a possible overestimation of the number of occupied beds compared to what can be predicted by a model which does not take into account immigration effects. We thus introduce two under/over-representation factors for the bed counts, one for the occupied beds in ward and the other for the occupied ICU stations (see Supplementary Figure 7 for their posterior distributions). We have to distinguish them since the distribution of patients coming from outside the city may be skewed in favour of severe cases which cannot be treated in smaller hospitals. Evidence for this can be found in the ratio between occupied ICU and ward beds, which differs significantly when comparing the city with the whole of Bavaria (Supplementary Figure 2).

Seroprevalence data We use the serological testing results reported by the "Prospective COVID-19 Cohort Munich" study (KoCo19). KoCo19 is organized by the Ludwig Maximilian University (LMU) Hospital and is currently monitoring nearly 3000 households in the Munich city area (Radon et al., 2020). At regular intervals, blood samples for each household member are gathered and tested for several indicators of the presence of antibodies to SARS-CoV-2 (Olbrich et al., 2021). These tests are then used to impute the lifetime prevalence of COVID-19 in the general population (Pritsch et al., 2021), which due to the potentially large number of asymptomatic cases is impossible to recover from the case counts released by the national health authorities. In this work we employ the results from the first round of testing, spanning the period from April 6th to June 12th, 2020.

4.2. Epidemiological model

Illness phases and states At the coarsest level, individuals can be assigned to compartments corresponding to biologically different phases of the infection. From each of these phases an individual can transition

to a subset of the other phases and a transition probability can be assigned to each of these possible disease progressions. Such a model can be easily visualized in graph form (see Fig. 1A) and converted to a set of ODEs (mostly linear, except for the non-linear infection process). However, as mentioned in the *Results* section, transition times are usually not exponentially distributed and thus each phase is subdivided into distinct model states in order to model Erlang-distributed transition times, in what is usually referred to as the Gamma Chain Trick (Smith, 2011). Additionally, the distribution of the transition times may depend not only on the current illness phase, but also on the future phase (e.g., symptomatic individuals who worsen and are hospitalized transition to the next phase faster than symptomatic individuals who are never hospitalized). When this occurs a different branch for each possible progression must be considered, each with its own transition rates and possibly with a different number of substates for the Gamma Chain Trick.

Detection process As mentioned in the *Results* section, the process by which infected individuals are reported to the healthcare authorities (by means of a positive diagnostic test) is modelled explicitly with additional states that represent detected individuals. The transition rates to the model branch containing detected individuals are denoted by $k_{\text{detect,asym}}$ (for asymptomatic and presymptomatic individuals) and $k_{\text{detect,sym}}$ for symptomatic individuals. Since the efficacy of diagnostic testing strategies has changed during the course of the first wave of the pandemic, these two rates depend on time. We further decompose

$$k_{\text{detect,asym}}(t) = \rho_{\text{detect,asym}}(t)\, k_{\text{detect,sym}}(t),$$

with $\rho_{\text{detect,asym}}(t) \in (0, 1)$, in order to encode our reasonable belief that the detection of asymptomatic individuals is more difficult than the detection of people displaying symptoms. As for the detection rate of symptomatic individuals, we write it as

$$k_{\text{detect,sym}}(t) = \rho_{\text{week,diagnostic}}(t)\, k_{\text{detect,sym,trend}}(t),$$

where $k_{\text{detect,sym,trend}}(t) > 0$ is the long-term variation of the detection rate and $\rho_{\text{week,diagnostic}}(t) > 0$ is a week-periodic term modelling the weekend effect. To reduce non-identifiability we assume that over one week $\rho_{\text{week,diagnostic}}(t)$ averages to one.

Since the weekend effect also influences death counts, a delay is also added between the time a patient dies and the time their death is reported to the healthcare authorities. This can be done by distinguishing deceased but unreported patients from reported deceased individuals, with the rate $k_{\text{detect,death}}(t)$ of the transition between these two states controlling the amount of delay present. We assume that this delay has no long-term trend and is simply given by a week-periodic function. For optimization and interpretability reasons, we decompose this value in the same way as $k_{\text{detect,sym}}$, yielding

$$k_{\text{detect,death}}(t) = \rho_{\text{week,death}}(t)\, k_{\text{detect,death,0}},$$

where $\rho_{\text{week,death}}(t) > 0$ is a week-periodic term which averages to one over one week and $k_{\text{detect,death,0}}$ is consequently the average value of the transition rate.

Reporting of symptom onsets Individuals who are tested while presymptomatic and whose date of symptoms onset is reported to the healthcare authorities are those who leave the presymptomatic phase while being already detected. Individuals who are tested while symptomatic and whose date of symptoms onset is reported are instead only just a fraction of those who leave the presymptomatic phase while not being detected yet. This is due to the fact that, when the detection rate is rather low, some symptomatic individuals may not be detected before the virus is cleared from their system. The fraction of symptomatic individuals who will eventually be detected can be easily computed from the model structure (all differential equations involved are linear) and can be used to correctly scale the number of onsets. We refer to the supplemental material for the full formulas.

In order to account for the incompleteness of the symptom onset data, we introduce two scaling factors: the first ensures that already detected individuals who become symptomatic do not necessarily need to report their symptom onset date; the second allows individuals that were detected after they had developed symptoms to not report their symptom onset date. Though the uncertainty on these scaling factors is large (Supplementary Figure 7), the comparison between the posterior and prior distributions suggests that some useful information can still be extracted. We believe this also helps the model to estimate how many individuals are tested before any symptoms are observed (presumably thanks to contact tracing efforts), which in turn influences the detection rate of asymptomatic individuals.

Infection rate   In a simple SIR model, the equation for the change in the number of susceptible individuals S is given by

$$\frac{\mathrm{d}S}{\mathrm{d}t} = -\frac{\beta I}{N} S,$$

where I is the number of infectious individuals, N is the number of individuals who are alive and β is the (mean) number of infectious contacts an infectious individual has in a time unit, which we will assume to be equal to one day. The total number of infectious contacts occurring in a day is then βI and thus, assuming that such contacts are equally distributed among all alive individuals, each individual will be exposed to the virus an average of $\beta I / N$ times per day. Since only susceptible individuals can get infected, the number of new infections per day will be equal to $\beta I S / N$, as in the above equation. Our model distinguishes several compartments of infectious individuals I_i and we denote by β_i the value of β specific to individuals in compartment I_i. Then, the total number of infectious contacts in a day becomes $\sum_i \beta_i I_i$ and the resulting equation is

$$\frac{\mathrm{d}S}{\mathrm{d}t} = -\frac{\sum_i \beta_i I_i}{N} S.$$

However, there are hidden dependencies between the β_i parameters. In order to make these relationships explicit, we have further decomposed each β_i as $\beta_i = \gamma_i \tilde{\beta}_i$, where $\tilde{\beta}_i$ denotes the number of potentially infectious interactions that an individual from I_i has in a day and γ_i denotes the fraction of such interactions that are actually infectious. The infectiousness factor γ_i only depends on the biology of the disease and therefore on the illness phase. The value $\tilde{\beta}_i$ is instead a measure of the mobility/behaviour of the individuals and can depend on other factors such as the NPIs currently enforced or whether the individual has been detected by the healthcare authorities (and is thus quarantined). While different compartments usually have different values of β_i, they may share either the value for γ_i (e.g., all symptomatic individuals are equally infectious, whether they have been quarantined or not) or the value for $\tilde{\beta}_i$ (e.g., asymptomatic individuals are thought to be less infectious than presymptomatic ones, but their social behaviour is the same since they are both unaware of their illness). This parameter sharing further constrains the model which usually has a beneficial effect on inference. Moreover, while putting priors on β_i would be difficult, the decomposition in biologically interpretable parameters allows us to use additional priors on γ_i and $\tilde{\beta}_i$ to further constrain the model to realistic parameter configurations. For example, it is expected a priori that the infectiousness γ_i of asymptomatic individuals should be lower than the infectiousness for symptomatic and presymptomatic individuals.

The values of $\tilde{\beta}_i$ for asymptomatic and presymptomatic individuals can be considered equal since they are both unaware of their infectiousness and thus their behaviour is the same. However, since individual behaviour and mobility is affected by the NPIs currently enforced by the government, such a value must be time dependent and will be denoted by $\tilde{\beta}_{\mathrm{NPI}}(t)$. On the other hand, symptomatic individuals know they are sick (though not necessarily from COVID-19) and are limited in their mobility by their symptoms. We can safely assume that their number of potentially infectious contacts is time-independent

and denote it by $\tilde{\beta}_{\mathrm{sick}}$. Similarly, individuals detected by diagnostic testing know they are infected and are quarantined, so that we can assign them a constant number of contacts denoted by $\tilde{\beta}_{\mathrm{quarantine}}$ such that $\tilde{\beta}_{\mathrm{quarantine}} < \tilde{\beta}_{\mathrm{sick}}$. Another reasonable assumption is that $\tilde{\beta}_{\mathrm{NPI}}(t) > \tilde{\beta}_{\mathrm{sick}}$. If such an assumption is not included explicitly in the model, uncertainty increases noticeably and $\tilde{\beta}_{\mathrm{NPI}}(t) > \tilde{\beta}_{\mathrm{sick}}$ does not hold for most samples from the posterior. We thus enforce the assumption by further decomposing

$$\tilde{\beta}_{\mathrm{NPI}}(t) = \rho_{\mathrm{NPI}}(t)\, \tilde{\beta}_0 + (1 - \rho_{\mathrm{NPI}}(t))\, \tilde{\beta}_{\mathrm{sick}},$$

where $\tilde{\beta}_0$ is the number of potentially infectious interactions in a pre-pandemic setting and $\rho_{\mathrm{NPI}}(t) > 0$. The choice of $\tilde{\beta}_0$ is somewhat arbitrary, since any change in it can be compensated by an opposite change in the infectiousness level γ_i. Thus, we need to fix it (and not estimate it along with the other parameters) and as its value we choose an estimate of daily social interactions for Germany taken from the pan-European POLYMOD survey (Mossong et al., 2008). The factor $\rho_{\mathrm{NPI}}(t)$ is instead the time-dependent reduction in potentially infectious contacts caused, e.g., by a reduction in mobility or adherence to social distancing norms, which in turn can be influenced by NPIs such as lockdowns. By definition of $\tilde{\beta}_0$, we get that $\rho_{\mathrm{NPI}}(t)$ must be equal to 1 at the beginning of the epidemic.

The relative values for γ_i and β_i have been reported in Supplementary Figures 4 and 5.

Time-dependent parameters   Time-dependent parameters are represented in our model by cubic Hermite splines defined on a grid of uniformly spaced points. The interval length has been set to a relatively large value of two weeks: this may cause some small artifacts in regions where changes occur fast, but a trade-off had to be made in order to keep computation time manageable (splines make up for the majority of model parameters). Each spline is encoded in the parameter vector by its values at grid points only and the spline derivatives are computed by finite differences, i.e., we are using a Catmull–Rom spline (Catmull and Rom, 1974). A standard interpolating cubic spline would have required the same number of parameters and have been smoother (a cubic Hermite spline is only continuous up to the first derivative), but we believe the potential drawbacks were not worth it. First, a standard interpolating cubic spline requires a more difficult and computationally expensive implementation since a linear system must be solved to compute the polynomial coefficients. Second, the value of a standard spline at any given point depends on all the values at the grid points, while for a Hermite spline it depends only on the values at the two nearest grid points, preventing the unrealistic case of having parameter values at later times influence observations at earlier times (even if such influence would probably be quite small).

Our time-dependent parameters are ρ_{NPI}, $k_{\mathrm{detect,sym,trend}}$ and $\rho_{\mathrm{detect,asym}}$ and they must be positive at all times, being transition rates or multiplicative factors. This cannot be enforced with a spline because of possible under-shooting and thus we use splines to describe the logarithm of the parameters of interest instead of the parameter values directly. As regularization, we also add zero-mean normal priors for the derivatives and the curvature of the time-dependent parameter (in its original scale, not in the logarithmic one), encoding our belief that if the data does not strongly suggest otherwise the time-dependent parameters should stay constant in value.

The two week-periodic functions $\rho_{\mathrm{week,diagnostic}}$ and $\rho_{\mathrm{week,death}}$ are (in logarithmic scale) periodic Catmull–Rom splines. In order to approximate the normalization constraint (integral over one week equal to one) imposed to ensure identifiability, by construction we force the mean of their values at the grid points (in this case, the seven days of the week) to be equal to one. As a regularization term to improve smoothness, we use the L2 norm of the derivative.

The estimate for $\tilde{\beta}_{\mathrm{NPI}}/\tilde{\beta}_0$ can be found in Fig. 4B, the estimates for $k_{\mathrm{detect,sym}}$ and $k_{\mathrm{detect,asym}}$ are reported in Supplementary Figure 8 and the estimates for the periodic effects $\rho_{\mathrm{week,diagnostic}}$ and $\rho_{\mathrm{week,death}}$ can be found in Supplementary Figure 9.

4.3. Observation model

Let $\dot{x}(t) = f(x(t), t; \theta)$ be our ODE model of the epidemic, where x is a vector representing the model state and θ is the parameter vector. In most cases the model state is hidden, in the sense that it cannot be directly (or at least not exactly) measured. Let $\{(t_i, y_i)\}_i$ be the data against which the model must be fitted. In order to link this data to the hidden state of the model, random variables $Y_i \sim p_i(y | x(t_i), \theta)$, known as *observable quantities*, must be introduced. Note that these observable quantities cannot be simple deterministic mappings from the state x to the observed values y since (i) measurement noise cannot be avoided; (ii) even if noise were to be eliminated, a practical model is never a perfect representation of reality. The precise distribution of the observables Y_i depends on the particular data source and is often referred to as the *noise model*.

Case counts (infections/deaths/symptom onsets reported to the RKI) The RKI releases the total number of cases reported to the health care authorities on any given day. We compute this from the simulated model trajectory using the midpoint rule, using the instantaneous rate of detection at noon of each day. As the noise in the case counts by the RKI seems to increase as the number of cases increase (Supplementary Figure 1), a simple Gaussian noise model with constant variance is not sufficient and we use a negative binomial distribution instead. The negative binomial distribution is a generalization of the Poisson distribution which is over-dispersed, i.e., for which the *variance-to-mean ratio* (VMR, also known as *index of dispersion*) is greater than one (in the limit case in which the VMR tends to one we recover the Poisson distribution). Due to its higher flexibility the negative binomial distribution is often the preferred choice for count data (Beck and Tolnay, 1995) and has been successfully employed in modelling case numbers for the COVID-19 pandemic (Lin et al., 2021; Chan et al., 2021). We employ it too, parametrizing it by mean (the daily number of cases predicted by the model) and VMR (estimated along with the other parameters, see Supplementary Figure 6 for its posterior distribution). While our data (except for the number of new cases) is not significantly over-dispersed, we have observed the negative binomial noise model to perform much better in practice than constant-variance additive noise or log-normally-distributed multiplicative noise.

Hospitalization data For the hospitalization data too it can be observed that the variance increases with the mean (Supplementary Figure 1). However, since the dynamic range of the bed counts is limited compared to the range spanned by the case counts, such an increase in variance is rather small and we can safely assume it to be approximately constant. We have found it sufficient in this case to use the simpler Gaussian noise model with constant variance instead of the more complex negative binomial distribution. These variances are estimated along with the other parameters and their posterior distributions are reported in Supplementary Figure 6.

As for the time at which bed counts are observed, in this case too we assume it to be noon of each day. In this case the choice is rather arbitrary, since we have no information on when the hospitals count the number of patients and whether the methodology used is the same for all hospitals.

Prevalence estimates The raw data from the serological testing study consists in a test date and test result for each participant. The period corresponding to the first round of testing is split into equal-duration intervals and the antibody test results are aggregated accordingly. Assuming that each of the resulting population subsets is representative of the whole, then the number of positive tests in each interval is a realization of a binomial random variable, with success probability equal to the prevalence (after correcting for the sensitivity and specificity of the test used) and number of trials equal to the total number of tests in that batch.

4.4. Bayesian parameter estimation and priors

Our approach to parameter inference is fully Bayesian: we are interested in sampling probable parameter values according to the posterior distribution

$$p(\theta \mid y) \propto p(y \mid \theta)p(\theta),$$

in which $p(y \mid \theta)$ is the likelihood of the observed data and $p(\theta)$ is a prior distribution on the parameter values. The likelihood can be computed from the probability distributions of the observable quantities as

$$p(y \mid \theta) = \prod_i p_i(y_i | x(t_i), \theta),$$

so that only the prior distribution is left to be defined.

The prior distribution should encode all available information about the parameters not coming directly from the data against which the model is fitted. In our case such information is mainly derived from clinical cases reported in the pre-existing literature. For example, the distribution of the transition times between different illness phases (e.g., incubation time) has been the object of many publications and can be used to obtain a reasonable value for the number of stages in the Gamma Chain Trick expansion. Once the number of stages is set, the same transition time distribution leads to a prior on the transition rates. Often priors can be obtained both for single parameters and for more complex expressions containing several of them. For example, in the case of transition times some overlap may be present: in one source information about the total hospitalization time may be given, in another the distribution of the time spent in the ICU may be presented and in a third the time from symptom onset to death (which in our model must necessarily transit through the ICU compartment) may be described. We have found that adding priors to derived expressions helps to exclude unrealistic values that would not have been excluded by simply putting priors on the basic parameters.

We will now show how we deal with priors on multiple expressions which are not independent. We start from the simple case where we have prior information on two quantities that can be expressed as $g_1(\theta), g_2(\theta) \in \mathbb{R}$. More than one parameter may contribute to both expressions, meaning that, even if the components of the vector $\theta \in \mathbb{R}^n$ are independent, $g_1(\theta)$ and $g_2(\theta)$ may not be independent. The prior information for these two quantities is encoded in two probability distributions $p_1(g_1)$ and $p_2(g_2)$. One could try to construct a prior $p(\theta)$ for the full parameter vector such that the marginal distributions for the expressions $g_1(\theta)$ and $g_2(\theta)$ are exactly $p_1(g_1)$ and $p_2(g_2)$. However, such distribution may not exist (since p_1 and p_2 may be based on different studies and be even slightly incompatible), if it exists it may be not unique and possible solutions can be only obtained by numerical approximation. Instead we define the prior as proportional to the product $p_1(g_1(\theta)) p_2(g_2(\theta))$. The advantage of this choice for the prior is that it has an analytical formula. However, the marginal distributions for the two expressions are not p_1 and p_2. The posterior distribution for $g_1(\theta)$ is not only influenced by the explicit contribution of the term $p_1(g_1(\theta))$ but also by the implicit contribution of $p_2(g_2(\theta))$, since some parameters appear in both expressions. In general, given an arbitrary number of expressions $g_k : \mathbb{R}^n \to \mathbb{R}$ for which we have prior information p_k as a probability distribution, we will use the non-normalized prior distribution

$$p(\theta) \propto \prod_k p_k(g_k(\theta)).$$

Computation of the normalization coefficient is not necessary in order to draw from the posterior distribution using MCMC. The shifting of the marginal for g_k from the explicit contribution p_k may not be a big problem since they are due to the prior taking into account all available evidence.

A summary of literature-derived priors used in our model is reported in Supplementary Tables 1 and 2. We have seen that choosing the appropriate source for prior information is difficult. For example, while

the biology of the virus is constant across all countries (at least during the first wave of the epidemic, before the rise of any variant) other processes such as infection and hospitalization are extremely country specific. For this reason, we have given more weight to reports on German cases over international studies or meta-analyses. A second problem is that there is no standardization in the medical literature regarding what are the quantities of interest that should be described. For example, mean hospitalization times are often reported separately for patients that need ICU care, patients that are ventilated, patients with severe or mild symptoms, or other subsets of patients. In the worst cases the explanations provided are insufficient to exactly determine what was actually measured, making it difficult if not impossible to map the information to the model. For example, hospitalization can be considered to end with death or discharge or both, but not all sources are clear on which definition they use. Additionally, incomplete information is often reported, such as only giving median transition times instead of more accurate statistics, such as interquartile ranges. A third problem is that often prior information obtained from different sources may appear to be somehow contradictory, a problem which is obviously exacerbated by the previous point. We have tried to only include prior information of whose meaning we were quite confident but still some slight incongruities could not be removed. We opted to employ particularly weakened priors in such cases rather than completely throw the information away. A final problem is that unless the reported values are stratified by age group they may not be applicable to different waves of the epidemic in which the affected demographics differ (e.g., fraction of hospitalized individuals). In our case this is not problematic since we have only modelled the first wave of the epidemic using prior information from studies conducted on patients from the same first wave.

4.5. Computational modelling pipeline

We established a reusable computation pipeline to automate the fitting process. The compartment model is encoded in the Systems Biology Markup Language (SBML, Hucka et al., 2003), a widely used standard in the systems biology community. The datasets used for fitting, together with parameter priors and bounds, are stored in the PEtab format (Schmiester et al., 2021), a standard format for the formulation of estimation problems. Both formats are supported by various simulation and analysis tools, which aids accessibility and reusability of model and results.

Using the SBML models and the data in PEtab format, we perform numerical simulation and sensitivity calculation with the C++/Python library AMICI (Fröhlich et al., 2021), and parameter estimation using the Python-based tool pyPESTO (Schälte et al., 2021). This combination of tools offers a broad spectrum of functionalities, including advanced gradient-based nonlinear optimization, profile calculation, sampling and ensemble uncertainty analysis. In the current phase, we are using the optimization and the sampling capabilities to infer the unknown process parameters, including the effects of different interventions.

For sampling from the posterior distribution we use the pyPESTO interface to the state-of-the-art gradient-based No-U-Turn sampler (NUTS, Hoffman and Gelman, 2014) implemented in the library PyMC3 (Salvatier et al., 2016). As parameter estimation with a high number of parameters (75 in our case) is computationally extremely demanding, we employed parallelization on a local high-performance cluster. Yet, as sampling by the NUTS sampler is intrinsically a sequential process, each individual chain can still take weeks before producing a sufficiently high number of samples. In particular, for the results used in the paper we drew 7200 samples (excluding 2100 tuning samples) which took 2 months of wall time with a Intel® Xeon® Gold 6130 CPU @ 2.10 GHz. Even with half the amount of samples, convergence metrics (R-hat and Geweke tests) and visual inspection of the chains were already acceptable. Effective sample size (ESS) for some parameters
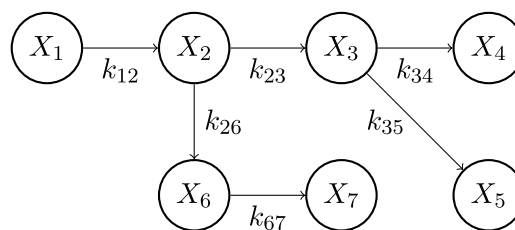

Fig. 7. Computation of the transit probabilities in a toy example. Let p_i be the probability that an individual, starting in X_1, will transit through state X_i. We assume transitions between state X_i and state X_j occur at a rate k_{ij} and that the possible transmissions are given in the graph shown in this figure. Then, $p_1 = 1$, $p_2 = p_1$, $p_3 = p_2 k_{23}/(k_{23}+k_{26})$, $p_4 = p_3 k_{34}/(k_{34}+k_{35})$, $p_5 = p_3 - p_4$, $p_6 = p_2 - p_3$, $p_7 = p_6$.

remains comparatively low, but this is not unexpected for a model with such a large number of parameters.

To facilitate reuse and extension, we openly share the analysis tools with the community.[4]

4.6. Computing the reproduction number

The basic reproduction number R_0 is the average number of secondary cases (new infections) generated in a completely susceptible population by a single primary case. R_0 can be computed as

$$R_0(t) = \sum_i p_i(t)\beta_i(t)\tau_i(t),$$

where p_i is the probability of an exposed individual of transiting through state I_i, β_i is the average number of new cases generated by an infected individual from state I_i in a day and τ_i is the average time an individual in state I_i takes to transition to the next state. Since all equations are linear (except the terms dealing with infection which are not relevant to the calculation of R_0), all of the three quantities can be computed analytically from the reaction rates (see Fig. 7 for the calculation of p_i in a toy example). Moreover, since all three of them depend on time, R_0 depends on time too. Finally, we want to point out that the above formula is not strictly correct, since as an individual progresses through the illness states also time progresses, which would require using different values of t in the different states I_i. However, since the temporal scale at which p_i, β_i and τ_i change (which is dictated by government policies, behavioural shifts and biological evolution of the virus) is rather longer than the time required for the illness to run its course, the proposed formula is a very good approximation of the true reproduction number.

The effective reproduction number R_e is the average number of secondary cases generated by a primary case in a partially susceptible population. It can be easily computed from R_0 as $R_e(t) = R_0(t)S(t)/N$. We can also compute a separate reproduction number $R_{0,\text{sym}}$ (respectively, $R_{0,\text{asym}}$) for symptomatic (respectively, asymptomatic) individuals, defined as the average number of secondary cases generated in a completely susceptible population by a primary case assuming they will (respectively, will not) develop symptoms. The formula to be used is essentially the same, with the only difference being the probabilities p_i have to be conditioned on the individual eventually developing (respectively, never developing) symptoms. It also holds that $R_0(t) = f_{\text{asym}} R_{0,\text{asym}} + (1-f_{\text{asym}}) R_{0,\text{asym}}$, where f_{asym} is the fraction of individuals who will never develop symptoms.

We also compute variants of the reproduction number in the case where NPIs and/or diagnostic testing are removed (see Fig. 6). More precisely, NPIs can be "switched off" by fixing $\rho_{\text{NPI}}(t)$ to be constantly equal to one, while diagnostic testing can be eliminated by setting all detection rates to zero. In order to estimate the base infectiousness of

---

[4] doi:10.5281/zenodo.6983066

the virus (as in the credible intervals of Fig. 3A and in the posterior distributions of Supplemental Figure 3) we use the basic reproduction number in the case where both NPIs and diagnostic testing are absent: having no NPIs in place puts us in a pre-pandemic setting, while removing diagnostic testing removes the additional uncertainty coming from the estimates of the detection rates.

Declaration of competing interest

The authors declare that they have no known competing financial interests or personal relationships that could have appeared to influence the work reported in this paper.

Institutional Review Board Statement

The study protocol was approved by the Institutional Review Board at the Ludwig-Maximilians-University in Munich, Germany (opinion date 31 March 2020, number 20-275, opinion date amendment: 10 October 2020), prior to study initiation.

Appendix A. Supplementary data

Supplementary material related to this article can be found online at https://doi.org/10.1016/j.epidem.2023.100681.

References

Barbarossa, Maria Vittoria, Fuhrmann, Jan, Meinke, Jan H., Krieg, Stefan, Varma, Hridya Vinod, Castelletti, Noemi, Lippert, Thomas, 2020. Modeling the spread of COVID-19 in Germany: Early assessment and possible scenarios. PLOS ONE 15 (9), e0238559. http://dx.doi.org/10.1371/journal.pone.0238559.

Beck, E.M., Tolnay, Stewart E., 1995. Analyzing historical count data. Hist. Methods 28 (3), 125–131. http://dx.doi.org/10.1080/01615440.1995.9956360.

Brauner, Jan M., Mindermann, Sören, Sharma, Mrinank, Johnston, David, Salvatier, John, Gavenčiak, Tomáš, Stephenson, Anna B., Leech, Gavin, Altman, George, Mikulik, Vladimir, Norman, Alexander John, Monrad, Joshua Teperowski, Besiroglu, Tamay, Ge, Hong, Hartwick, Meghan A., Teh, Yee Whye, Chindelevitch, Leonid, Gal, Yarin, Kulveit, Jan, 2021. Inferring the effectiveness of government interventions against COVID-19. Science 371 (6531), http://dx.doi.org/10.1126/science.abd9338.

Catmull, Edwin, Rom, Raphael, 1974. A class of local interpolating splines. In: Barnhill, Robert E., Riesenfeld, Richard F. (Eds.), Computer Aided Geometric Design. Academic Press, pp. 317–326. http://dx.doi.org/10.1016/B978-0-12-079050-0.50020-5.

Chan, Stephen, Chu, Jeffrey, Zhang, Yuanyuan, Nadarajah, Saralees, 2021. Count regression models for COVID-19. Physica A 563, 125460. http://dx.doi.org/10.1016/j.physa.2020.125460.

Courtemanche, Charles, Garuccio, Joseph, Le, Anh, Pinkston, Joshua, Yelowitz, Aaron, 2020. Strong Social Distancing Measures In The United States Reduced The COVID-19 Growth Rate. Health Aff. 39 (7), 1237–1246. http://dx.doi.org/10.1377/hlthaff.2020.00608.

Fröhlich, Fabian, Weindl, Daniel, Schälte, Yannik, Pathirana, Dilan, Paszkowski, Łukasz, Lines, Glenn Terje, Stapor, Paul, Hasenauer, Jan, 2021. AMICI: high-performance sensitivity analysis for large ordinary differential equation models. Bioinformatics http://dx.doi.org/10.1093/bioinformatics/btab227.

Giordano, Giulia, Blanchini, Franco, Bruno, Raffaele, Colaneri, Patrizio, Di Filippo, Alessandro, Di Matteo, Angela, Colaneri, Marta, 2020. Modelling the COVID-19 epidemic and implementation of population-wide interventions in Italy. Nat. Med. 26 (6), 855–860. http://dx.doi.org/10.1038/s41591-020-0883-7.

Hartl, Tobias, Wälde, Klaus, Weber, Enzo, 2020. Measuring the impact of the german public shutdown on the spread of Covid-19. Covid Econom. (1), 25–32.

Hoffman, Matthew D., Gelman, Andrew, 2014. The No-U-turn sampler: Adaptively setting path lengths in Hamiltonian Monte Carlo. J. Mach. Learn. Res. 15 (1), 1593–1623.

Hucka, M., Finney, A., Sauro, H.M., Bolouri, H., Doyle, J.C., Kitano, H., Arkin, A.P., Bornstein, B.J., Bray, D., Cornish-Bowden, A., Cuellar, A.A., Dronov, S., Gilles, E.D., Ginkel, M., Gor, V., Goryanin, I.I., Hedley, W.J., Hodgman, T.C., Hofmeyr, J.-H., Hunter, P.J., Juty, N.S., Kasberger, J.L., Kremling, A., Kummer, U., Le Novère, N., Loew, L.M., Lucio, D., Mendes, P., Minch, E., Mjolsness, E.D., Nakayama, Y., Nelson, M.R., Nielsen, P.F., Sakurada, T., Schaff, J.C., Shapiro, B.E., Shimizu, T.S., Spence, H.D., Stelling, J., Takahashi, K., Tomita, M., Wagner, J., Wang, J., 2003. The systems biology markup language (SBML): a medium for representation and exchange of biochemical network models. Bioinformatics 19 (4), 524–531. http://dx.doi.org/10.1093/bioinformatics/btg015.

Isho, Baweleta, Abe, Kento T., Zuo, Michelle, Jamal, Alainna J., Rathod, Bhavisha, Wang, Jenny H., Li, Zhijie, Chao, Gary, Rojas, Olga L., Bang, Yeo Myong, Pu, Annie, Christie-Holmes, Natasha, Gervais, Christian, Ceccarelli, Derek, Samavarchi-Tehrani, Payman, Guvenc, Furkan, Budylowski, Patrick, Li, Angel, Paterson, Aimee, Yue, Feng Yun, Marin, Lina M., Caldwell, Lauren, Wrana, Jeffrey L., Colwill, Karen, Sicheri, Frank, Mubareka, Samira, Gray-Owen, Scott D., Drews, Steven J., Siqueira, Walter L., Barrios-Rodiles, Miriam, Ostrowski, Mario, Rini, James M., Durocher, Yves, McGeer, Allison J., Gommerman, Jennifer L., Gingras, Anne-Claude, 2020. Persistence of serum and saliva antibody responses to SARS-CoV-2 spike antigens in COVID-19 patients. Sci. Immunol. 5 (52), eabe5511. http://dx.doi.org/10.1126/sciimmunol.abe5511.

IVENA eHealth — interdisziplinärer Versorgungsnachweis, 2020. URL https://www.ivena.de (Accessed 02 September 2021).

Jarvis, Christopher I, Van-Zandvoort, Kevin, Gimma, Amy, Prem, Kiesha, working group, CMMID-COVID-19, Klepac, Petra, Rubin, G James, Edmunds, W John, 2020. Quantifying the impact of physical distance measures on the transmission of COVID-19 in the UK. BMC Med. 18 (124), http://dx.doi.org/10.1186/s12916-020-01597-8.

Latsuzbaia, Ardashel, Herold, Malte, Bertemes, Jean-Paul, Mossong, Joël, 2020. Evolving social contact patterns during the COVID-19 crisis in Luxembourg. PLOS ONE 15 (8), 1–13. http://dx.doi.org/10.1371/journal.pone.0237128.

Lauer, Stephen A., Grantz, Kyra H., Bi, Qifang, Jones, Forrest K., Zheng, Qulu, Meredith, Hannah R., Azman, Andrew S., Reich, Nicholas G., Lessler, Justin, 2020. The incubation period of coronavirus disease 2019 (COVID-19) from publicly reported confirmed cases: Estimation and application. Ann. Intern. Med. 172 (9), 577–582. http://dx.doi.org/10.7326/M20-0504.

Li, Michael Lingzhi, Bouardi, Hamza Tazi, Lami, Omar Skali, Trikalinos, Thomas A., Trichakis, Nikolaos, Bertsimas, Dimitris, 2020. Forecasting COVID-19 and analyzing the effect of government interventions. Operations Research 71 (1), 184–201. http://dx.doi.org/10.1287/opre.2022.2306.

Lin, Yen Ting, Neumann, Jacob, Miller, Ely F., Posner, Richard G., Mallela, Abhishek, Safta, Cosmin, Ray, Jaideep, Thakur, Gautam, Chinthavali, Supriya, Hlavacek, William S., 2021. Daily forecasting of regional epidemics of coronavirus disease with Bayesian uncertainty quantification, United States. Emerg. Infect. Dis. 27 (3), 767–778. http://dx.doi.org/10.3201/eid2703.203364.

Liu, Y, Morgenstern, C, Kelly, J, Lowe, R, CMMID-COVID-19-Working-Group, Jit, M, 2021. The impact of non-pharmaceutical interventions on SARS-CoV-2 transmission across 130 countries and territories. BMC Med. 19, 40. http://dx.doi.org/10.1186/s12916-020-01872-8.

Long, Quan-Xin, Liu, Bai-Zhong, Deng, Hai-Jun, Wu, Gui-Cheng, Deng, Kun, Chen, Yao-Kai, Liao, Pu, Qiu, Jing-Fu, Lin, Yong, Cai, Xue-Fei, Wang, De-Qiang, Hu, Yuan, Ren, Ji-Hua, Tang, Ni, Xu, Yin-Yin, Yu, Li-Hua, Mo, Zhan, Gong, Fang, Zhang, Xiao-Li, Tian, Wen-Guang, Hu, Li, Zhang, Xian-Xiang, Xiang, Jiang-Lin, Du, Hong-Xin, Liu, Hua-Wen, Lang, Chun-Hui, Luo, Xiao-He, Wu, Shao-Bo, Cui, Xiao-Ping, Zhou, Zheng, Zhu, Man-Man, Wang, Jing, Xue, Cheng-Jun, Li, Xiao-Feng, Wang, Li, Li, Zhi-Jie, Wang, Kun, Niu, Chang-Chun, Yang, Qing-Jun, Tang, Xiao-Jun, Zhang, Yong, Liu, Xia-Mao, Li, Jin-Jing, Zhang, De-Chun, Zhang, Fan, Liu, Ping, Yuan, Jun, Li, Qin, Hu, Jie-Li, Chen, Juan, Huang, Ai-Long, 2020. Antibody responses to SARS-CoV-2 in patients with COVID-19. Nat. Med. 26, 845–848. http://dx.doi.org/10.1038/s41591-020-0897-1.

Lorch, Lars, Kremer, Heiner, Trouleau, William, Tsirtsis, Stratis, Szanto, Aron, Schölkopf, Bernhard, Gomez-Rodriguez, Manuel, 2022. Quantifying the effects of contact tracing, testing, and containment measures in the presence of infection hotspots. ACM Trans. Spatial Algorithms Syst. 8 (4), 25. http://dx.doi.org/10.1145/3530774.

Lyu, Wei, Wehby, George L., 2020. Community use of face masks and COVID-19: Evidence from a natural experiment of state mandates in the US. Health Aff. 39 (8), 1419–1425. http://dx.doi.org/10.1377/hlthaff.2020.00818.

Mossong, Joël, Hens, Niel, Jit, Mark, Beutels, Philippe, Auranen, Kari, Mikolajczyk, Rafael, Massari, Marco, Salmaso, Stefania, Tomba, Gianpaolo Scalia, Wallinga, Jacco, Heijne, Janneke, Sadkowska-Todys, Malgorzata, Rosinska, Magdalena, Edmunds, W. John, 2008. Social Contacts and Mixing Patterns Relevant to the Spread of Infectious Diseases. PLOS Med. 5 (3), e74. http://dx.doi.org/10.1371/journal.pmed.0050074.

Olbrich, Laura, Castelletti, Noemi, Schälte, Yannik, Garí, Mercè, Pütz, Peter, Bakuli, Abhishek, Pritsch, Michael, Kroidl, Inge, Saathoff, Elmar, Guggenbuehl Noller, Jessica Michelle, Fingerle, Volker, Le Gleut, Ronan, Gilberg, Leonard, Brand, Isabel, Falk, Philine, Markgraf, Alisa, Deák, Flora, Riess, Friedrich, Diefenbach, Max, Eser, Tabea, Weinauer, Franz, Martin, Silke, Quenzel, Ernst-Markus, Becker, Marc, Durner, Jürgen, Girl, Philipp, Müller, Katharina, Radon, Katja, Fuchs, Christiane, Wölfel, Roman, Hasenauer, Jan, Hoelscher, Michael, Wieser, Andreas, on behalf of the KoCo19 Study Group, 2021. Head-to-head evaluation of seven different seroassays including direct viral neutralisation in a representative cohort for SARS-CoV-2. Journal of General Virology 102 (10), 001653. http://dx.doi.org/10.1099/jgv.0.001653.

Pritsch, Michael, Radon, Katja, Bakuli, Abhishek, Le Gleut, Ronan, Olbrich, Laura, Guggenbüehl Noller, Jessica, Saathoff, Elmar, Castelletti, Noemi, Garí, Mercè, Pütz, Peter, et al., 2021. Prevalence and risk factors of infection in the representative COVID-19 cohort Munich. Int. J. Environ. Res. Public Health 18 (7), 3572. http://dx.doi.org/10.3390/ijerph18073572.

Quick, Corbin, Dey, Rounak, Lin, Xihong, 2021. Regression models for understanding COVID-19 epidemic dynamics with incomplete data. J. Amer. Statist. Assoc. 116 (536), 1561–1577. http://dx.doi.org/10.1080/01621459.2021.2001339.

Radon, Katja, Bakuli, Abhishek, Pütz, Peter, Le Gleut, Ronan, Guggenbuehl Noller, Jessica Michelle, Olbrich, Laura, Saathoff, Elmar, Garí, Mercè, Schälte, Yannik, Frahnow, Turid, Wölfel, Roman, Pritsch, Michael, Rothe, Camilla, Pletschette, Michel, Rubio-Acero, Raquel, Beyerl, Jessica, Metaxa, Dafni, Forster, Felix, Thiel, Verena, Castelletti, Noemi, Rieß, Friedrich, Diefenbach, Maximilian N., Fröschl, Günter, Bruger, Jan, Winter, Simon, Frese, Jonathan, Puchinger, Kerstin, Brand, Isabel, Kroidl, Inge, Wieser, Andreas, Hoelscher, Michael, Hasenauer, Jan, Fuchs, Christiane, on behalf of the KoCo19 study group, 2021. From first to second wave: follow-up of the prospective COVID-19 cohort (KoCo19) in Munich (Germany). BMC Infect. Dis. 21, 925. http://dx.doi.org/10.1186/s12879-021-06589-4.

Radon, Katja, Saathoff, Elmar, Pritsch, Michael, Noller, Jessica Michelle Guggenbühl, Kroidl, Inge, Olbrich, Laura, Thiel, Verena, Diefenbach, Max, Riess, Friedrich, Forster, Felix, Theis, Fabian, Wieser, Andreas, Hoelscher, Michael, Bakuli, Abhishek, Eckstein, Judith, Froeschl, Günter, Geisenberger, Otto, Geldmacher, Christof, Heiber, Arlett, Hoffmann, Larissa, Huber, Kristina, Metaxa, Dafni, Pletschette, Michel, Rothe, Camilla, Schunk, Mirjam, Wallrauch, Claudia, Zimmer, Thorbjörn, Prückner, Stephan, Hasenauer, Jan, Castelletti, Noemi, Zeggini, Eleftheria, Laxy, Michael, Leidl, Reiner, Schwettmann, Lars, 2020. Protocol of a population-based prospective COVID-19 cohort study Munich, Germany (KoCo19). BMC Publ. Health 20, 1036. http://dx.doi.org/10.1186/s12889-020-09164-9.

Raimúndez, Elba, Dudkin, Erika, Vanhoefer, Jakob, Alamoudi, Emad, Merkt, Simon, Fuhrmann, Lara, Bai, Fan, Hasenauer, Jan, 2021. COVID-19 outbreak in Wuhan demonstrates the limitations of publicly available case numbers for epidemiological modeling. Epidemics 34, 100439. http://dx.doi.org/10.1016/j.epidem.2021.100439.

Robert Koch Institute, 2020. COVID-19: Fallzahlen in Deutschland. URL https://npgeo-corona-npgeo-de.hub.arcgis.com/datasets/dd4580c810204019a7b8eb3e0b329dd6_0.

Salvatier, John, Wiecki, Thomas V., Fonnesbeck, Christopher, 2016. Probabilistic programming in Python using PyMC3. PeerJ Comput. Sci. 2016, e55. http://dx.doi.org/10.7717/peerj-cs.55, URL https://github.com/pymc-devs/pymc3.

Schälte, Yannik, Fröhlich, Fabian, Stapor, Paul, Vanhoefer, Jakob, Wang, Dantong, Weindl, Daniel, Jost, Paul Jonas, Lakrisenko, Polina, Raimúndez, Elba, Pathirana, Dilan, Schmiester, Leonard, Sädter, Philipp, Contento, Lorenzo, Dudkin, Erika, Meyer, Kristian, Merkt, Simon, Hasenauer, Jan, 2021. ICB-DCM/pyPESTO: pyPESTO 0.2.5. http://dx.doi.org/10.5281/zenodo.2553546.

Schmiester, Leonard, Schälte, Yannik, Bergmann, Frank T., Camba, Tacio, Dudkin, Erika, Egert, Janine, Fröhlich, Fabian, Fuhrmann, Lara, Hauber, Adrian L., Kemmer, Svenja, Lakrisenko, Polina, Loos, Carolin, Merkt, Simon, Müller, Wolfgang, Pathirana, Dilan, Raimúndez, Elba, Refisch, Lukas, Rosenblatt, Marcus, Stapor, Paul L., Städter, Philipp, Wang, Dantong, Wieland, Franz-Georg, Banga, Julio R., Timmer, Jens, Villaverde, Alejandro F., Sahle, Sven, Kreutz, Clemens, Hasenauer, Jan, Weindl, Daniel, 2021. PEtab—Interoperable specification of parameter estimation problems in systems biology. PLoS Comput. Biol. 17 (1), 1–10. http://dx.doi.org/10.1371/journal.pcbi.1008646.

Siedner, Mark J., Harling, Guy, Reynolds, Zahra, Gilbert, Rebecca F., Haneuse, Sebastien, Venkataramani, Atheendar S., Tsai, Alexander C., 2020. Social distancing to slow the US COVID-19 epidemic: Longitudinal pretest–posttest comparison group study. PLOS Med. 17 (8), 1–12. http://dx.doi.org/10.1371/journal.pmed.1003244.

Smith, Hal, 2011. Distributed delay equations and the linear chain trick. In: An Introduction to Delay Differential Equations with Applications to the Life Sciences. Springer, New York, NY, pp. 119–130. http://dx.doi.org/10.1007/978-1-4419-7646-8_7.

Streeck, Hendrik, Schulte, Bianca, Kümmerer, Beate M, Richter, Enrico, Höller, Tobias, Fuhrmann, Christine, Bartok, Eva, Dolscheid-Pommerich, Ramona, Berger, Moritz, Wessendorf, Lukas, et al., 2020. Infection fatality rate of SARS-CoV2 in a super-spreading event in Germany. Nat. Commun. 11 (1), 1–12.

Sypsa, V, Roussos, S, Paraskevis, D, Lytras, T, Tsiodras, S, Hatzakis, A, 2021. Effects of social distancing measures during the first epidemic wave of severe acute respiratory syndrome infection, Greece. Emerg. Infect. Diseases 27 (2), 452–462. http://dx.doi.org/10.3201/eid2702.203412.

Zhao, S., Chen, H., 2020. Modeling the epidemic dynamics and control of COVID-19 outbreak in China. Quant. Biol. 8, 11–19. http://dx.doi.org/10.1007/s40484-020-0199-0.

Publication 5:

Data suggested hospitalization as pandemic-indicator already at early stages of the COVID-19 pandemic

Stefanie Fuderer*, Christina Kuttler, Michael Hoelscher, Ludwig Christian Hinske and **Noemi Castelletti**

Mathematical Biosciences and Engineering, Dec 2022, IF 2.080

Mathematical Biosciences and Engineering

Research article

Data suggested hospitalization as critical indicator of the severity of the COVID-19 pandemic, even at its early stages

Stefanie Fuderer[1]**, Christina Kuttler**[1]**, Michael Hoelscher**[2,3,4]**, Ludwig Christian Hinske**[5] **and Noemi Castelletti**[2,6,*]

[1] Department of Mathematics, Technical University of Munich, Garching, Germany

[2] Division of Infectious Diseases and Tropical Medicine, Medical Center of the University of Munich, Munich, Germany

[3] German Center for Infection Research (DZIF), partner site Munich, Munich, Germany

[4] Center for International Health (CIH), University Hospital, Munich, Germany

[5] Department of Anesthesiology, University Hospital, Munich, Germany

[6] Institute of Radiation Medicine, Helmholtz Zentrum München, Neuherberg, Germany

* **Correspondence:** Email: noemi.castellitti@med.uni-muenchen.de.

Abstract: COVID-19 has been spreading widely since January 2020, prompting the implementation of non-pharmaceutical interventions and vaccinations to prevent overwhelming the healthcare system. Our study models four waves of the epidemic in Munich over two years using a deterministic, biology-based mathematical model of SEIR type that incorporates both non-pharmaceutical interventions and vaccinations. We analyzed incidence and hospitalization data from Munich hospitals and used a two-step approach to fit the model parameters: first, we modeled incidence without hospitalization, and then we extended the model to include hospitalization compartments using the previous estimates as a starting point. For the first two waves, changes in key parameters, such as contact reduction and increasing vaccinations, were enough to represent the data. For wave three, the introduction of vaccination compartments was essential. In wave four, reducing contacts and increasing vaccinations were critical parameters for controlling infections. The importance of hospitalization data was highlighted, as it should have been included as a crucial parameter from the outset, along with incidence, to avoid miscommunication with the public. The emergence of milder variants like Omicron and a significant proportion of vaccinated people has made this fact even more evident.

Keywords: SARS-CoV-2; modeling; differential equation; hospitalization; prediction; data analysis

1. Introduction

In December 2019, some local health workers in Wuhan city (Hubei region, China) reported cases of pneumonia-like symptoms with an unknown cause. On February 11, 2020, the disease was officially named the coronavirus disease 2019 (COVID-19), and its cause was determined to be the severe acute respiratory syndrome coronavirus 2 (SARS-CoV-2) [1]. Following more than 118,000 confirmed COVID-19 cases in 114 countries and 4,291 deaths, the World Health Organization declared COVID-19 as a pandemic on March 11, 2020 [2]. Since then, there have been outbreaks worldwide with approximately 603 million confirmed cases and over 6.4 million deaths as of September 2022 [3].

The first cases of COVID-19 were detected in Germany's Munich municipality in late January 2020, and, due to the virus' high contagion rate, the number of cases rapidly increased [4]. To prevent the collapse of the healthcare system, the government quickly implemented non-pharmaceutical interventions, such as social distancing, face mask wearing, isolation of infected individuals, nationwide lockdowns and contact tracing, to slow down and control the virus' spread [1, 5]. In addition, vaccines against SARS-CoV-2 were promptly developed, and they have been available in Germany since December 26, 2020 [6]. All vaccines licensed in Germany have been observed to offer a high level of protection against severe cases of the disease [7].

Depending on the severity of symptoms, individuals infected with SARS-CoV-2 can be classified as follows [8]:

- mild,
- moderate (no or mild pneumonia, no or mild upper respiratory infection combined with febrile illness, dry cough and sore throat),
- severe with hospitalization (dyspnea, respiratory rate $\geq$ 30/min, blood oxygen saturation $\leq$ 93% and/or pulmonary infiltrates > 50%) and
- critical with hospitalization (respiratory insufficiency, septic shock due to bacterial superinfections, multiple organ dysfunction or failure, death).

In the first 20 weeks of the outbreak, the Robert Koch Institute (RKI) categorized about 80% of infections as mild or moderate, 18% as severe and the remaining 2% as critical [1, 8]. This resulted in a hospitalization rate of 20%. This value was significantly higher than the hospitalization rate of the flu in 2018–2019 (which was only 1.31%) and demonstrated the potential for a collapse of the healthcare system without intervention [9]. To manage the number of hospitalized cases, the daily number of new cases and the 7-day incidence became critical indicators [10]. However, the relationship between incidence and hospitalization changes depending on the virus variant, making it an unreliable indicator [10]. Due to this variability and the emergence of the Omicron variant, the focus has now shifted to the hospitalization rate [10].

Biology-based mathematical models can be used to contain the pandemic by predicting its spread. Linking such models with data is crucial for making informed decisions about public health, as evidenced by efforts to estimate the number of asymptomatic HIV infections and the impact of SARS and influenza outbreaks [11, 12]. With the ongoing COVID-19 pandemic, many researchers are fitting models to data to analyze the effects of government interventions such as contact restrictions, face mask usage and isolation of infected individuals. For instance, Chumachenko et al. [13] used machine

learning methods to predict COVID-19 incidence in multiple countries, while Ying and O'Clery [14] developed an agent-based model to study the spread of infection in a supermarket. Other researchers used relatively simple deterministic models composed of four or fewer compartments to analyze the spatial spread of COVID-19 [15–17], while Okuonghae and Omame [18] incorporated face mask usage and social distancing into their non-linear models of the SARS-CoV-2 epidemic in Nigeria. Barbarossa et al. [19] extended a deterministic model of SEIR type to simulate the effects of non-pharmaceutical interventions on the COVID-19 outbreak in Germany, and different strategies for mitigating the outbreak were explored.

In this study, we utilized a mathematical model of deterministic differential equations to simulate the spread of COVID-19 in Munich's population from January 2020 for over two years, encompassing four waves of the epidemic. Our approach focused on a biology-based method that mimicked the actual contribution of individuals in various compartments of an extended SEIR model, incorporating non-pharmaceutical interventions and, later, vaccinations. The transmission rates and reproduction number are proportional to the number of infectious contacts, which were reduced by the non-pharmaceutical measures. Our model is unique in that it captured the effects of these measures and quantified them not only between waves, but also within the same wave. Another distinctive aspect of our analysis is the inclusion of the number of patients in the intensive care unit (ICU) and normal hospital ward of Munich's hospitals. We fitted the model's parameters in a two-step process to prevent overfitting and increase stability in the model fitting. First, we fitted a model without hospitalization solely to the incidence data. Second, we extended the model with hospitalization compartments, using the parameters obtained from the first fit as given parameters to support the remaining hospitalization parameters' fit.

The emphasis in previous COVID-19 management strategies has been on tracking the number of cases, rather than focusing on the more critical issue of hospitalization. Our analysis shows that, from the outset of the pandemic, it was possible to simulate hospitalization data as a primary metric alongside case incidence. By doing so, we could have avoided confusion among the public and provided a clearer picture of the pandemic's status. This approach is especially important when dealing with milder variants like Omicron, in conjunction with a significant percentage of vaccinated individuals.

It is widely recognized that the number of infectious contacts is directly proportional to transmission rates and reproduction numbers. As a result, implementing non-pharmaceutical interventions reduces the number of contacts, which is reflected in Eqs (2.1) through (2.6) in the article. This quantification is a crucial aspect of our paper's development.

2. Materials and method

2.1. Prevalence data on daily detected COVID-19 cases

To gain an understanding of the pandemic situation, the daily number of COVID-19 infections can be used as one of multiple indicators. The RKI provides the 7-day incidence, which represents the number of new cases reported in the past 7 days per 100,000 inhabitants, and it is used to guide certain measures like the emergency brake [10]. The RKI platform offers the number of daily detected COVID-19 infections in Munich, starting from the first observed case on January 29, 2021. Figure 1 displays the occurrence of three main waves in Munich until the end of June, with varying (non-)

pharmaceutical interventions and hygiene awareness among the population influencing the pandemic's progression. Consequently, time-dependent model parameters were utilized not just for the three waves, but also for each wave individually (Table 1).

Table 1. Interventions during the first [20], second [21–23], third [24–26] and beginning of the fourth wave of COVID-19 in Munich. For each wave the first day is considered as day 0.

| Intervention	Time interval (date)	Time interval (days)	Contact rate	Transmission probability	Transmission rate
First wave	2020/01/29–2020/06/15	day 0–138			
No interventions	2020/01/29–2020/03/21	day 0–52	c_0	p_0	β_0
Lockdown	2020/03/22–2020/04/19	day 53–81	$0.37c_0$	$0.3p_0$	$0.1 \cdot \beta_0$
Contact interventions	2020/04/20–2020/06/15	day 82–138	$0.5c_0$	$0.3p_0$	$0.15 \cdot \beta_0$
Second wave	2020/06/15–2021/02/15	day 138–383			
Contact interventions	2020/06/15–2020/11/01	day 0–139	$0.6c_0$	$p \cdot p_0$	$0.6 \cdot p\beta_0$
Lockdown light	2020/11/02–2020/12/15	day 140–183	$0.57c_0$	$p \cdot p_0$	$0.57p\beta_0$
Lockdown	2020/12/16–2021/01/18	day 184–217	c_3c_0	$p \cdot p_0$	$c_3p\beta_0$
FFP2 masks	2021/01/19–2020/02/15	day 218–245	c_4c_0	$p_4 \cdot p_0$	$c_4p_4\beta_0$
Third wave	2021/02/15–2021/06/30	day 383–518			
Lockdown	2021/02/15–2021/04/13	day 0–57	$0.35c_0$	$p \cdot p_0$	$0.35p\beta_0$
Emergency brake	2021/04/14–2021/05/10	day 58–84	c_2c_0	$p \cdot p_0$	$c_2p\beta_0$
Relaxations	2021/05/11–2021/06/06	day 85–111	c_3c_0	$p \cdot p_0$	$c_3p\beta_0$
Opening	2021/06/07–2021/06/30	day 112–135	$0.55c_0$	$p \cdot p_0$	$0.55p\beta_0$
Fourth wave	2021/06/30–2021/10/15	day 518–626			$\beta_0^{fourth} = 1.6\beta_0^{third}$
Relaxations	2021/06/30 – 2021/07/31	day 0–31	0.6	$p \cdot p_0$	$0.6p\beta_0^{fourth}$
More relaxations	2021/08/01–2021/09/30	day 32–92	c_2	$p \cdot p_0$	$c_2p\beta_0^{fourth}$
More relaxations	2021/10/01–2021/10/16	day 93–108	c_3	$p \cdot p_0$	$c_3p\beta_0^{fourth}$
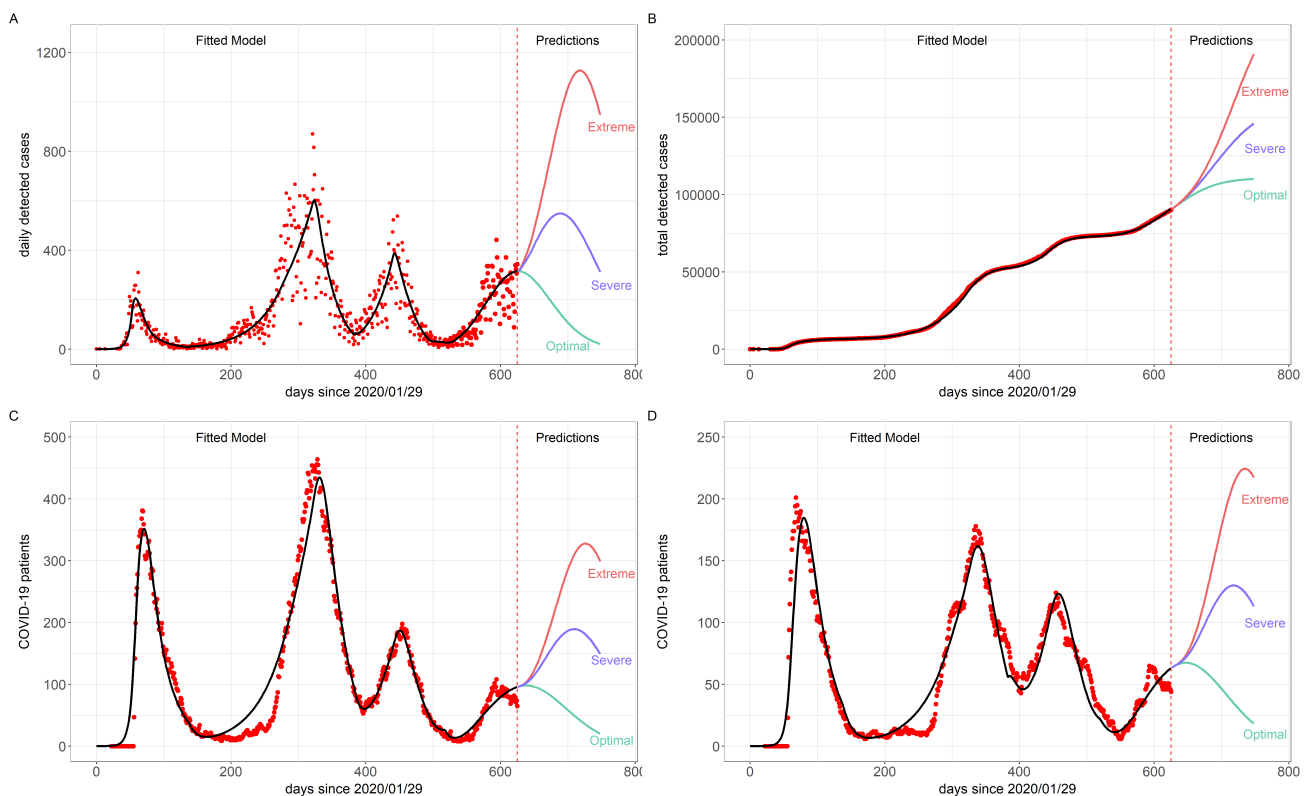
Figure 1. Data description and model results. Detected COVID-19 cases in Munich reported by the RKI [4]: (A) daily and (B) cumulative. Hospitalized COVID-19 cases in Munich for the normal ward (NW) stations (C) and ICUs (D). The solid black lines denote the results of the (A) and (B) preferred model and (C) and (D) hospitalization model. For the first and second waves, no vaccination compartments were needed.

2.1.1. First wave

In Munich, the first wave of COVID-19 occurred from late January to mid-June (refer to Figure 1). Three main interventions were implemented to prevent the spread of the disease:

1) no measures or, at least, no heavy measures were taken;

2) a lockdown was imposed throughout Munich;

3) the lockdown was lifted, but with severe contact reductions still in place (refer to Table 1).

To model the impact of these interventions, the time-dependent contact $c(t)$ and transmission probability $p(t)$ rates were utilized. During the lockdown period, a 63% reduction in contacts compared to normal was assumed, whereas the reduction during the lifting was around 50% [27]. Additionally, it was assumed that the population had greater awareness of hygiene, mask wearing, and social distancing during and after the lockdown, leading to an approximate 70% reduction in the transmission probability during contact [28]. This resulted in the following contact rate $c(t)$ and

transmission probability $p(t)$:

$$c(t) = \begin{cases} c_0 & \text{if } t \le 52 \\ 0.37c_0 & \text{if } 53 \le t \le 81 \\ 0.5c_0 & \text{if } 82 \le t \le 138 \end{cases}, \qquad p(t) = \begin{cases} p_0 & \text{if } t \le 52 \\ 0.3p_0 & \text{if } 53 \le t \le 81 \\ 0.3p_0 & \text{if } 82 \le t \le 138, \end{cases} \qquad (2.1)$$

where c_0 is the normal average contact rate and p_0 is the normal average transmission probability when no interventions are taken. With this it follows that the transmission rate $\beta(t) = c(t) \cdot p(t)$ is also time-dependent

$$\beta(t) = c(t)p(t) \approx \begin{cases} \beta_0 & \text{if } t \le 52, \\ 0.1\beta_0 & \text{if } 53 \le t \le 81, \\ 0.15\beta_0 & \text{if } 82 \le t \le 138, \end{cases} \qquad (2.2)$$

where $\beta_0 = c_0 p_0$ is the normal average transmission rate without interventions.

2.1.2. Second wave

The time frame of the second wave of COVID-19 in Munich was from June 15th, 2020 to February 15th, 2021. Similar to the first wave, the second wave was split into distinct phases aligned with efforts to curb the spread of the disease (refer to Table 1). The initial intervention phase, spanning from June to October, resulted in a contact reduction of roughly 40%, while the subsequent "lockdown light" period saw a contact reduction of about 43% [27].

The contact reduction for the subsequent lockdown was also fitted. During the final intervention period, an FFP2 mask requirement was introduced in addition to the lockdown, which decreased the probability of transmission upon contact. The transmission probability only changed during the last intervention period and was also fitted. Therefore, the transmission rate for asymptomatic infected individuals is given by

$$\beta_a(t) \approx \begin{cases} 0.6p\beta_0 & \text{if } t \le 139, \\ 0.57p\beta_0 & \text{if } 140 \le t \le 183, \\ c_3 p\beta_0 & \text{if } 184 \le t \le 217, \\ c_4 p_4 \beta_0 & \text{if } 218 \le t \le 245, \end{cases} \qquad (2.3)$$

where c_3 and c_4 are the fitted reductions of the transmission rate for the third and fourth intervention periods, respectively. In addition, the fitted reduction in transmission probability is described by p during the first three intervention periods, while p_4 describes the additional reduction of the transmission probability due to wearing the FFP2 masks. During the second wave, the test capacity increased and more infected individuals without symptoms were tested because of contact tracing.

2.1.3. Third wave

Between February 15, 2021 and June 30, 2021, Munich experienced its third wave of COVID-19 infections as shown in Figure 1. During this period, the lockdown measures from the previous wave remained in effect and were strengthened with an "emergency brake" beginning in mid-April. These

new measures included stricter contact reduction, a nighttime curfew and the closure of many stores, as summarized in Table 1 [24]. The contact reduction during the lockdown was assumed to be around 65%, while the contact rate during the "emergency brake" and relaxation period was fitted to the data. For the opening period, the contact rate was assumed to be similar to the beginning of the second wave. Consequently, the transmission rate is given by

$$\beta_a(t) \approx \begin{cases} 0.35 p\beta_0 & \text{if } t \leq 57, \\ c_2 p\beta_0 & \text{if } 58 \leq t \leq 84, \\ c_3 p\beta_0 & \text{if } 85 \leq t \leq 111, \\ 0.55 p\beta_0 & \text{if } 112 \leq t \leq 135. \end{cases} \tag{2.4}$$

New variants of the SARS-CoV-2 virus were detected in the first half of 2021, including the B.1.1.7 variant, also known as Alpha, which became the predominant strain in many countries during this time including Germany [29]. As of early March, the B.1.1.7 variant has accounted for over 40% of positive cases in Germany, with this proportion continuing to rise each week [30]. The B.1.1.7 variant is believed to have increased transmissibility, resulting in a higher transmission rate β_0 [31]. Meanwhile, in Germany, the vaccination campaign started in December 2020, and, by early June 2021, around 40% of Munich's population had received their first dose of the vaccine, while about 20% had received the second dose [32]. To ensure an adequate simulation of the third wave, this vaccination aspect is also taken into account in the model's structure.

2.1.4. Beginning of the fourth wave with further prediction

On June 30, 2021, Munich entered its fourth wave of the pandemic, despite various interventions and progress in vaccination having broken the third wave in spring of 2021. While 50% of Munich's population had received at least one vaccine dose and 36% had been fully vaccinated by the end of June 2021, the number of cases rose again. The Delta variant of SARS-CoV-2, which is approximately 60% more transmissible than the Alpha variant, became increasingly prevalent in Germany during the end of the third wave and the beginning of the fourth wave. By mid-July 2021, the Delta variant accounted for 74% of all cases in Germany [30]. To estimate the transmission rate during the fourth wave, the fitted transmission rate during the third wave for the Alpha variant (β_0) was used as a baseline, as it was the dominant strain at the time:

$$\beta_0^{fourth} = 1.6 \cdot \beta_0^{third}. \tag{2.5}$$

During July 2021, there were additional measures taken to ease COVID-19 restrictions, including increased capacity at outdoor and cultural events, extended hours for restaurants, relaxed mask rules and the reopening of bar interiors, as shown in Table 1 [33–35]. Contact reduction during July 2021 was assumed to be similar to that of the previous summer. For the intervention period from August to September 2021, the contact reduction was estimated. In October 2021, further relaxations were implemented, such as the reopening of clubs in Munich [36]. The contact reduction for October was

also estimated. These measures resulted in an average transmission rate for asymptomatic individuals:

$$\beta_a^{fourth}(t) = \begin{cases} 0.6p\beta_0^{fourth} & \text{if } 0 \leq t \leq 31, \\ c_2 p\beta_0^{fourth} & \text{if } 32 \leq t \leq 93, \\ c_3 p\beta_0^{fourth} & \text{if } 94 \leq t \leq 109. \end{cases} \tag{2.6}$$

According to [33], it has been demonstrated that all vaccines authorized in Germany provide lower protection against the Delta variant, especially in individuals who have only received one dose. As a result, a vaccine ineffectiveness factor σ has been introduced, which depends on the time elapsed since the first dose. The fourth wave was considered to be dominated by the Delta variant approximately one week after it began; σ is hence defined by

$$\sigma(t) = \begin{cases} \sigma_{alpha} & \text{if } 0 \leq t \leq 7, \\ \sigma_{delta} & \text{if } 8 \leq t, \end{cases} \tag{2.7}$$

where $\sigma_{alpha} = 0.25$ is the vaccine inefficacy after the first dose against infection with the Alpha variant and σ_{delta} is the fitted vaccine inefficacy after the first dose against infection with the Delta variant.

The parameters for predicting the number of new COVID-19 cases were fitted by using data from the first few months of the fourth wave, up until October 15, 2021. To make predictions for future periods, various scenarios were considered. These include an optimal scenario, where vaccination rates and contact rates remain constant from October 15, 2021, a severe scenario where vaccination rates decrease while contact rates increase and an extreme scenario where vaccination is completely stopped and contact rates increase rapidly.

2.2. Number of COVID-19 hospitalized patients: IVENA software

The crucial indicators for determining the severity of the pandemic are the number of hospitalized patients and those requiring intensive care (IC), as stated in [10]. Maintaining control over these numbers is essential in making decisions regarding potential interventions.

A web-based software called Interdisciplinary Evidence of Care (IVENA) is utilized to facilitate the exchange of information among emergency departments, ambulance services and clinics. This tool aids in optimizing the allocation of resources and patient management, and it also reports on the number of COVID-19 patients in normal wards and ICUs across Munich hospitals, as cited in [37].

However, in the IVENA dataset, some days in October and November 2021 were missing data on the number of patients in normal wards or ICUs in Munich hospitals. To fill these gaps, alternative data sources were used, as referenced in [32].

2.3. Biology-based deterministic models: Considering different types of infectious individuals

The analysis uses models based on the SEIR theory, which assumes that susceptible individuals (S) can become infected through contact with infected individuals (I) [12]. After infection, individuals move from the susceptible class to the exposed class (E), where they are asymptomatic and not infectious. Infected individuals then move to the infectious class (I) and eventually recover (R) [38]. A more detailed description of the SEIR model is available in the Supplemental Material.
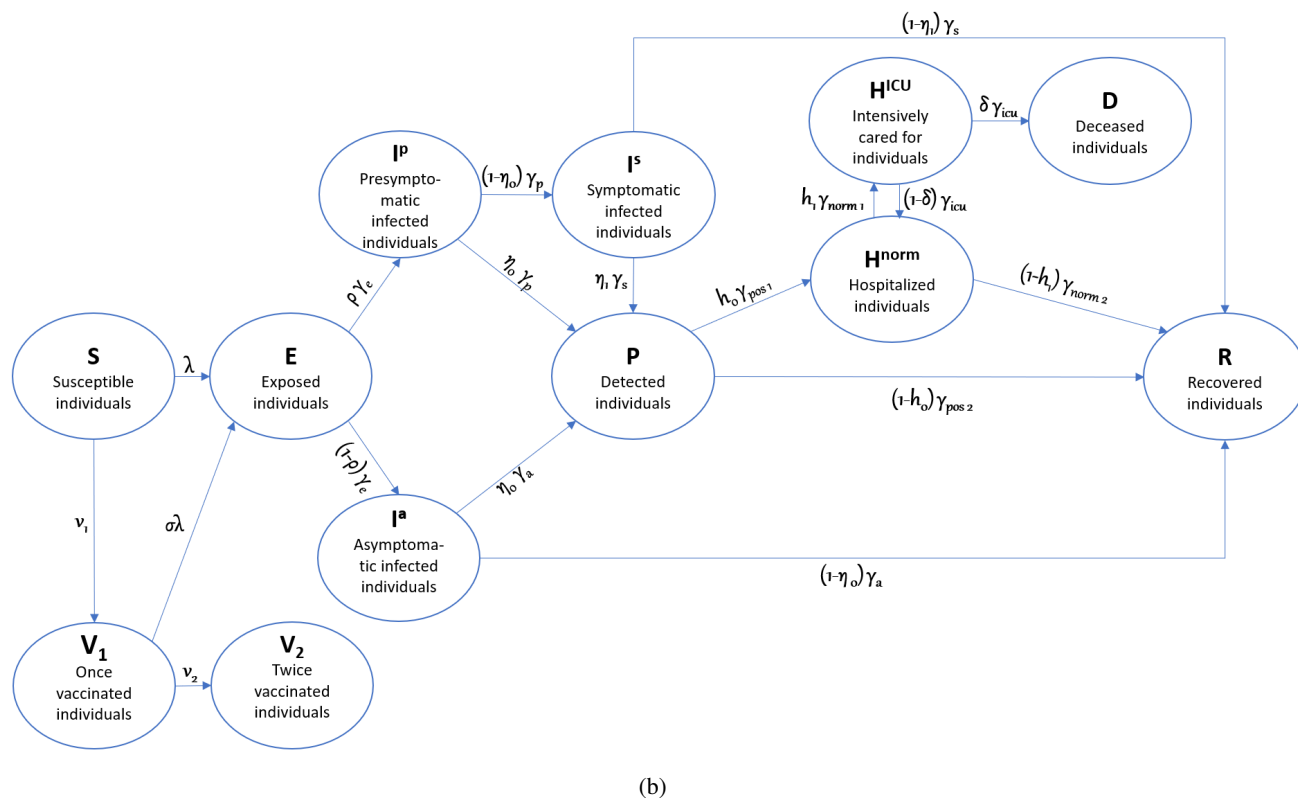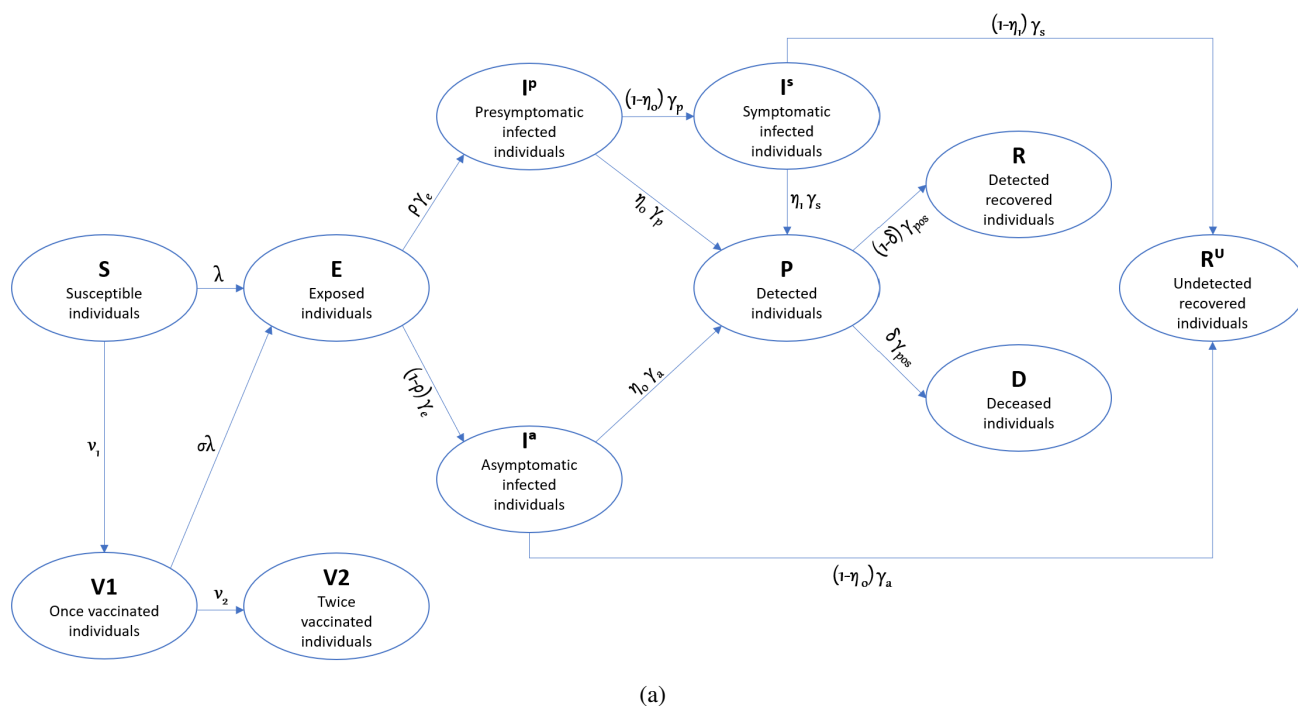
Figure 2. Schematic description of the applied models: (A) the preferred model and (B) the hospitalization model, both with vaccination expansion.

The top of Figure 2 is an extension of the SEIR model, with the infectious class (I) split into asymptomatic infected individuals (I^a), presymptomatic infected individuals (I^p), symptomatic infected individuals (I^s) and detected individuals (P). After infection, individuals move to the exposed class E, where they are asymptomatic and not infectious. Exposed individuals can hence develop symptoms with rate ρ, moving first to the presymptomatic class I^p, then to the symptomatic class I^s and finally to the detected class P with rate η_1. Exposed people staying asymptomatic (probability $1 - \rho$) move directly to the detected class (P) with rate η_0. Individuals in the asymptomatic, presymptomatic, symptomatic and detected classes spend an average time of $\frac{1}{\gamma_a}$, $\frac{1}{\gamma_p}$, $\frac{1}{\gamma_s}$ and $\frac{1}{\gamma_{pos}}$, respectively, before recovering (R from detected and R^u for undetected cases) and becoming immune to reinfection. Individuals who die (D) from COVID-19 are removed from the population. In Germany, it is very likely that a critical infection will be detected. Therefore, we assume that infected individuals who have not been diagnosed with COVID-19 are unlikely to die due to the disease. The case fatality ratio (CFR) of detected infections δ was calculated with the help of the RKI data [4]. The transmission rates for asymptomatic, presymptomatic, symptomatic and detected individuals are β_a, β_p, β_s and β_{pos}, respectively. We assume that asymptomatic and presymptomatic infected individuals do not restrict their contacts to others and therefore have higher transmission rates than symptomatic and detected infective people. Vaccination is assumed to be given only to susceptible individuals (S) at a rate of v_1, who then move to compartment V_1. After the first dose, individuals have approximately 75% protection against infection with SARS-CoV-2, as defined by $(1 - \sigma)$ [39]. After the second dose, individuals move to compartment V_2 at a rate of v_2. Fully vaccinated individuals are assumed to be protected against infection, and the time lag of two weeks after the second dose needed to build up immunity is neglected for simplicity.

The preferred model is presented in Figure 2 (top), and it is described by the following system of differential equations:

$$
\begin{aligned}
\dot{S} &= -\lambda S - v_1 S, \\
\dot{E} &= \lambda S + \sigma \lambda V_1 - \gamma_e E, \\
\dot{V}_1 &= v_1 S - \sigma \lambda V_1 - v_2 V_1, \\
\dot{V}_2 &= v_2 V_1, \\
\dot{I}^a &= (1 - \rho)\gamma_e E - \gamma_a I^a, \\
\dot{I}^p &= \rho \gamma_e E - \gamma_p I^p, \\
\dot{I}^s &= (1 - \eta_0)\gamma_p I^p - \gamma_s I^s, \\
\dot{P} &= \eta_0 \gamma_a I^a + \eta_0 \gamma_p I^p + \eta_1 \gamma_s I^s - \gamma_{pos} P, \\
\dot{R} &= (1 - \delta)\gamma_{pos} P, \\
\dot{D} &= \delta \gamma_{pos} P, \\
\dot{R}^u &= (1 - \eta_1)\gamma_s I^s + (1 - \eta_0)\gamma_a I^a,
\end{aligned}
\tag{2.8}
$$

where $\lambda(t) = \frac{\beta_a I^a + \beta_p I^p + \beta_s I^s + \beta_{pos} P}{N - D}$ is the force of infection and N the total population size. For this model we assume that the transmission rate of asymptomatic infectious individuals β_a is time-dependent (see Chapters 2.1.1–2.1.4). Consequently, it follows that the other transmission rates, β_p, β_s and β_{pos}, are also time-dependent. To model the epidemic already since the first days cases were tested, as initial values for the preferred model, we used $S(0) = N - 2$, $E(0) = V_1(0) = V_2(0) = I^a(0) = I^p(0) = R(0) = D(0) = R^u(0) = 0$ and $I^s(0) = P(0) = 1$. The whole population is susceptible, except for two people: one is a detected individual and the other a symptomatic detected individual. All other compartments are empty. For waves 1 and 2, the initial conditions for the vaccination compartments were $V_1(0) = V_2(0) = 0$ (no vaccination available, so compartments are empty), while for wave 4, $V_1(0) = 25000$ and $V_2(0) = 15000$ (vaccination campaign started fully working). For time intervals without a vaccination campaign, we set the rate $v_1 = 0$, keeping the compartment empty until the start of vaccination. To compare the model results with the RKI data, the newly detected infections $\hat{d}(t)$ at day t need to be defined. At the starting point, the number of daily detected cases corresponds to the number of detected individuals at day 0: $P(0)$. For any further time point $t > 0$, our approach was as follows:

- The population N is constant, including deaths D if included in the model: $N(t) - N(t + 1) = 0$;
- The newly detected cases on day t, $\hat{d}(t)$, correspond only to the individuals who leave compartment S at that day, $S(t)$ and not of interest are all other "internal changes" between different compartments. To calculate this in formula, it is the individuals in S on that day t, $S(t)$, minus the individuals in S the next day, $S(t + 1)$: $S(t) - S(t + 1) = \hat{d}(t)$;
- In an extended SIR-model, the individuals leaving S can go to more compartments than only I. In our specific case, they can go to the compartments of detected individuals (P), to dead individuals (D) and to recovered individuals (R). Therefore, for out model, the total population corresponds to $N = S + P + D + R$, or $S = N - P - D - R$;
- Looking at individuals leaving compartment S, this can be formulated as follows: $\hat{d}(t) = S(t) - S(t + 1) = N(t) - N(t + 1) - P(t) + P(t + 1) - D(t) + D(t + 1) - R(t) + R(t + 1)$;
- Remembering that we assume a constant population $N(t)-N(t+1) = 0$, this leads to $\hat{d}(t) = S(t) - S(t + 1) = P(t + 1) - P(t) + D(t + 1) - D(t) + R(t + 1) - R(t)$.

The formula can be interpreted as follows: the daily detected cases in the RKI data can be located to different compartments in the model. They can be just "detected individuals" by polymerase chain reaction (PCR) or later on by rapid testing. They could be detected after death, which really happened in the first two waves since the laboratories were struggling with test capacities. Or, they could be detected at recovery. The daily detected cases $\hat{d}(t)$ at day t are hence calculated by the following formula:

$$\hat{d}(t) = \begin{cases} P(0) & \text{if } t = 0, \\ [P(t + 1) - P(t)] + [D(t + 1) - D(t)] + [R(t + 1) - R(t)] & \text{if } t > 0. \end{cases}$$

Parameter assumptions are given in Tables 2 and 3.

Table 2. Parameters of the preferred model for wave one and two without hospitalization compartments. Short forms: CFR, mean duration (MD).

Parameter	Description	Value (unit) [Refs.]
First wave		
β_0	Init. transm. rate of asympt. I	$0.66 \frac{1}{d \cdot \text{individual}}$ [fitted]
β_p	Transm. rate of presympt. I	β_a [assumed]
β_s	Transm. rate of symptomatic I	$0.6\beta_a$ [assumed]
β_{pos}	Transm. rate of detected I	$0.1\beta_a$ [assumed]
$\frac{1}{\gamma_e}$	Mean latent period	5.5 d [38, 40]
$\frac{1}{\gamma_a}$	MD of asympt. infection	6 d [assumed]
$\frac{1}{\gamma_p}$	MD of presympt. infection	2 d [38]
$\frac{1}{\gamma_s}$	MD of sympt. infection	7 d [assumed]
$\frac{1}{\gamma_{pos}}$	MD of infection	6 d [fitted]
ρ	Prob. of developing symptoms	0.69 [41]
η_0	Prob. of detection while asympt.	0.07 [assumed]
η_1	Prob. of detection while sympt.	0.56 [fitted]
δ	CFR of detected infections	0.033 [4]
v_1	Vacc. rate first dose	0
v_2	Vacc. rate second dose	0
N	Tot. population size	1,484 million [42]
Second wave (new parameters)		
$p\beta_0$	Init. transm. rate of asympt. I with reduction in transm. prob.	$0.37 \frac{1}{d \cdot \text{individual}}$ [fitted]
c_3	Reduction in contact rate (third intervention period)	0.27 [fitted]
$c_4 p_4$	Reduction in transm. rate (fourth intervention period)	0.24 [fitted]
η_0	Prob. of detection while asympt.	0.15 [assumed]
η_1	Prob. of detection while sympt.	0.85 [assumed]
δ	CFR of detected infections	0.019 [4]

Table 3. Parameters of the preferred model for waves three and four with vaccination compartments. Short forms: CFR.

Parameter	Description	Value (unit) [Refs.]
Third wave (new parameters)		
$p\beta_0$	Init. transm. rate of asympt. I with reduction in transm. prob.	$0.79 \frac{1}{d \cdot \text{individual}}$ [fitted]
c_2	Reduction in contact rate (second intervention period)	0.11 [fitted]
c_3	Reduction in transm. rate (third intervention period)	0.11 [fitted]
η_0	Prob. of detection while asympt.	0.25 [assumed]
η_1	Prob. of detection while sympt.	0.9 [assumed]
δ	CFR of detected infections	0.008 [4]
N	Tot. population size	1,488 million [42]
Third wave with vaccination		
$p\beta_0$	Init. transm. rate of asympt. I with reduction in transm. prob.	$0.82 \frac{1}{d \cdot \text{individual}}$ [fitted]
c_2	Reduction in contact rate	0.15 [fitted]
c_3	Reduction in transm. rate	0.15 [fitted]
v_1	Vacc. rate first dose, $t \leq 75$	$0.0014 \frac{1}{d \cdot \text{individual}}$ [fitted]
	Vacc. rate first dose, $75 \leq t \leq 135$	$0.0243 \frac{1}{d \cdot \text{individual}}$ [fitted]
v_2	Vacc. rate second dose, $t \leq 60$	$0.0325 \frac{1}{d \cdot \text{individual}}$ [fitted]
	Vacc. rate second dose, $60 \leq t \leq 135$	$0.0151 \frac{1}{d \cdot \text{individual}}$ [fitted]
σ	Vacc. inefficacy after first dose	0.25 [39]
Fourth wave with vaccination		
c_2	Reduction in contact rate	0.65 [fitted]
c_3	Reduction in transm. rate	0.66 [fitted]
δ	CFR of detected infections	0.004 [4]
σ_{alpha}	Vacc. inefficacy after first dose against Alpha-variant infection	0.25 [39]
σ_{delta}	Vacc. inefficacy after first dose	0.6 [fitted]
v_1	Vacc. rate first dose, $t \leq 75$	$0.0101 \frac{1}{d \cdot \text{individual}}$ [fitted]
	Vacc. rate first dose, $75 \leq t \leq 108$	$0.0171 \frac{1}{d \cdot \text{individual}}$ [fitted]
v_2	Vacc. rate second dose, $t \leq 50$ against Delta-variant infection	$0.0129 \frac{1}{d \cdot \text{individual}}$ [fitted]
v_2	Vacc. rate second dose, $50 \leq t \leq 108$ against Delta-variant infection	$0.0037 \frac{1}{d \cdot \text{individual}}$ [fitted]

2.4. Model expansion with hospital compartments

In order to simulate the number of COVID-19 patients in both regular hospital wards and ICUs in Munich, the model must be expanded. When a person is diagnosed with the virus and has mild or no symptoms, they stay in compartment P. If a person's symptoms are severe, they are admitted to the regular hospital ward (H^{norm}), with the probability of hospitalization described as h_0. Those in the hospital who develop critical symptoms have a probability of h_1 of being transferred to the ICU (H^{ICU}). Patients in the ICU who do not survive the virus (death rate δ) are moved to the deceased compartment (D). Once a patient's condition stabilizes in the ICU, they are transferred back to the regular ward for continued monitoring, but no longer require IC. Finally, after their infection has resolved, all individuals move to the recovered compartment (R). The hospitalization model's dynamics are displayed at the bottom of Figure 2. Additionally, more information regarding parameter assumptions can be found in Tables 4 and 5. The hospitalization model is then given by the following system of differential equations:

$$
\begin{aligned}
\dot{S} &= -\lambda S - v_1 S, \\
\dot{E} &= \lambda S + \sigma \lambda V_1 - \gamma_e E, \\
\dot{V}_1 &= v_1 S - \sigma \lambda V_1 - v_2 V_1, \\
\dot{V}_2 &= v_2 V_1, \\
\dot{I}^a &= (1 - \rho)\gamma_e E - \gamma_a I^a, \\
\dot{I}^p &= \rho \gamma_e E - \gamma_p I^p, \\
\dot{I}^s &= (1 - \eta_0)\gamma_p I^p - \gamma_s I^s, \\
\dot{P} &= \eta_0 \gamma_a I^a + \eta_0 \gamma_p I^p + \eta_1 \gamma_s I^s - (h_0 \gamma_{pos_1} + (1 - h_0)\gamma_{pos_2})P, \\
\dot{H}^{norm} &= h_0 \gamma_{pos_1} P + (1 - \delta)\gamma_{icu} H^{ICU} - (h_1 \gamma_{norm_1} + (1 - h_1)\gamma_{norm_2})H^{norm}, \\
\dot{H}^{ICU} &= h_1 \gamma_{norm_1} H^{norm} - \gamma_{icu} H^{ICU}, \\
\dot{D} &= \delta \gamma_{icu} H^{ICU}, \\
\dot{R} &= (1 - \eta_0)\gamma_a I^a + (1 - \eta_1)\gamma_s I^s + (1 - h_0)\gamma_{pos_2} P + (1 - h_1)\gamma_{norm_2} H^{norm},
\end{aligned}
\tag{2.9}
$$

where $\lambda(t) = \frac{\beta_a I^a + \beta_p I^p + \beta_s I^s + \beta_{pos} P}{N - D}$ is the force of infection and N is the total population size. $\beta_a(t)$ is time-dependent and defined in Chapters 2.1.1–2.1.4.

Table 4. Parameters of the preferred model with hospitalization for waves one and two. Short forms: CFR, MD, mean time (MT), NW, ICU, IC.

Parameter	Description	Value (unit) [Refs.]
First wave		
$\frac{1}{\gamma_{pos_1}}$	MD from detection to hospitalization	2 d [fitted]
$\frac{1}{\gamma_{pos_2}}$	MD of infection	8 d [fitted]
$\frac{1}{\gamma_{norm_1}}$	MT from hospitalization to ICU	1 d [38]
$\frac{1}{\gamma_{norm_2}}$	MT on NW, no IC	7 d [38]
$\frac{1}{\gamma_{icu}}$	MT on ICU	9 d [8]
h_0	Prob. of hospitalization	0.14 [fitted]
h_1	Prob. of requiring IC	0.07 [fitted]
δ	CFR of detected infections	0.34 [43]
ρ	Prob. of developing symptoms	0.69 [41]
η_0	Prob. of detection while asympt.	0.07 [assumed]
v_1	Vacc. rate first dose	$0 \; \frac{1}{d \cdot \text{individual}}$
v_2	Vacc. rate second dose	$0 \; \frac{1}{d \cdot \text{individual}}$
Second wave		
$\frac{1}{\gamma_{pos_1}}$	MD from detection to hospitalization	2 d [fitted]
$\frac{1}{\gamma_{pos_2}}$	MD of infection	6 [fitted]
h_0	Prob. of hospitalization	0.06 [fitted]
h_1	Prob. of requiring IC	0.04 [fitted]
η_0	Prob. of detection while asympt.	0.15 [assumed]
η_1	Prob. of detection while sympt.	0.85 [assumed]

2.5. Data fitting

In order to accurately represent the data, a two-step method was employed. Initially, a model excluding hospitalization was used to fit the incidence data for all rounds. Subsequently, the model was expanded to incorporate hospitalization compartments, and the parameters from the first fit were utilized as fixed parameters to achieve a proper fit for the remaining hospitalization parameters. This approach prevents overfitting and enhances the stability of the fit, resulting in a final model that accurately fits the hospitalization data. The advantage of this technique is its ability to merge two distinct datasets. The incidence model provides information on pandemic progression, whereas the second step focuses on hospitalization. Since the pandemic's development is identical with or without hospitalization parameters, the parameters obtained in the first fit can be directly integrated into the second model for a better fit.

Table 5. Parameters of the preferred model with hospitalization. Short forms: MD and IC.

Parameter	Description	Value (unit) [Refs.]
Third wave		
$\frac{1}{\gamma_{pos_1}}$	MD from detection to hospitalization	2 d [fitted]
$\frac{1}{\gamma_{pos_2}}$	MD of infection	6 d [fitted]
h_0	Prob. of hospitalization	0.06 [fitted]
h_1	Prob. of requiring IC	0.08 [fitted]
η_0	Prob. of detection while asympt.	0.25 [assumed]
η_1	Prob. of detection while sympt.	0.90 [assumed]
v_1	Vacc. rate first dose, $t \leq 75$	$0.004 \frac{1}{d \cdot \text{individual}}$ [fitted]
	Vacc. rate first dose, $75 \leq t \leq 135$	$0.008 \frac{1}{d \cdot \text{individual}}$ [fitted]
v_2	Vacc. rate second dose, $t \leq 60$	$0.03 \frac{1}{d \cdot \text{individual}}$ [fitted]
	Vacc. rate second dose, $60 \leq t \leq 135$	$0.024 \frac{1}{d \cdot \text{individual}}$ [fitted]
σ	Vacc. inefficacy after first dose	0.25 [39]
Fourth wave		
h_0	Prob. of hospitalization	0.014 [fitted]
h_1	Prob. of requiring IC	0.077 [fitted]
v_1	Vacc. rate first dose, $t \leq 75$	$0.0464 \frac{1}{d \cdot \text{individual}}$ [fitted]
	Vacc. rate first dose, $75 \leq t \leq 108$	$0.04 \frac{1}{d \cdot \text{individual}}$ [fitted]
v_2	Vacc. rate second dose, $t \leq 50$	$0.0085 \frac{1}{d \cdot \text{individual}}$ [fitted]
	Vacc. rate second dose, $50 \leq t \leq 108$	$0.0012 \frac{1}{d \cdot \text{individual}}$ [fitted]

2.6. Positivity and boundedness

To be realistic and meaningful, solutions of our model system should preserve positivity, or, to be more precise non-negativity and boundedness. As is usual in this context, all parameter values are assumed to be non-negative. One can easily see that a solution of (2.9) with non-negative initial values at $t = 0$ for all variables stays non-negative for all $t \geq 0$. For the variables V_2, D and R, this holds in general, as there are only non-negative entries on the corresponding right-hand sides; for all other variables, the derivative is also ≥ 0 if the corresponding variable itself is equal to zero, using that $0 \leq \rho, \eta_0, \eta_1, h_0, h_1 \leq 1$ by definition.

For the boundedness, let us consider the sum of all variables, which corresponds to the total population in the system. Its time derivative satisfies

$$\dot{S} + \dot{E} + \dot{V}_1 + \dot{V}_2 + \dot{I}^a + \dot{I}^p + \dot{I}^s + \dot{P} + \dot{H}^{norm} + \dot{H}^{ICU} + \dot{D} + \dot{R} = 0,$$

as all terms on the right-hand side of (2.9) cancel out. Thus, the total population stays constant, and it is a closed compartmental model. As we have seen already that all variables stay non-negative, it follows directly that all variables are bounded by the sum of the initial values: $S(0) + E(0) + V_1(0) + V_2(0) + I^a(0) + I^p(0) + I^s(0) + P(0) + H^{norm}(0) + H^{ICU}(0) + D(0) + R(0)$.

Please note that this can be shown analogously for the other model variants here.

2.7. Parameter estimation

To obtain the best estimated parameter set $\theta = (p_1, ..., p_k)$ that is dependent on unknown parameters $p_1, ..., p_k$, and to analyze the performance of a model, the model itself has to be validated using real-life data [44]. In this analysis, we first model the prevalence that directly corresponds to the model-output $I(t)$. Following, the fitted parameters are used to support a further fit with the hospitalization data that directly correspond to the model outputs H^{norm} and H^{ICU}.

To find the best estimated parameter set θ, we determine the sum-of-squares error (SSE), i.e., the sum of squares of the vertical distances from the real data points $d(t)$ to the points of the solution curve $I(t)$ of the model [44]:

$$SSE = \sum_t (d(t) - I(t))^2. \tag{2.10}$$

To achieve the optimal performance of the model, the least-squares approach is hence applied, minimizing the SSE [44]:

$$\hat{\theta} = \underset{\theta}{\operatorname{argmin}} \, SSE(\theta). \tag{2.11}$$

The programming language R, version 4.0.5, was used for model fitting. Furthermore, for minimizing, the SSE the *L-BFGS-B* optimization method was used. A definition of the goodness-of-fit method, Akaike information criterion (AIC) and model comparison are presented in detail in the Supplemental Material.

3. Results

3.1. Modeling the number of daily detected and hospitalized COVID-19 cases

The model results for the first wave are presented in Figure 3(A) and (B) and Tables 2 and 4. It can be appreciated that the model adequately simulates the real data. The results obtained for the last day of the first wave will be used as initial values for modeling the second wave, the results of which are presented in Figure 3(C) and (D). Also, for the second wave, it can be seen that the model captures the structure of the data, confirming the fact that neither the virus nor the immune status of the population changed from the first to the second wave. The parameters used for the third wave are summarized in Tables 3 and 5. The results of the last day of the second wave were used as initial values. Results of the third wave can be seen in Figure 3(E) and (F). Although a lockdown was implemented, the number of COVID-19 cases increased again, and the third wave began. As new variants appeared, the model needed to be adapted, and the parameters were changed accordingly. Toward the end of the third wave, there was a discrepancy between the modeled number of daily detected COVID-19 cases and those reported by the RKI, which was solved by adding compartments representing the vaccinated population [32]. The parameters used for this model are presented in Tables 3 and 5, and the results are shown in Figure 4. The accuracy of the model was significantly improved by incorporating the vaccinated population.

Model results of the hospitalizations in Munich are presented in Figure 5 and Tables 4 and 5. It can be noticed that, for all three waves, the structure of the data can be well captured by the model. Due to its importance in the third wave, the model with vaccination compartments was directly applied due to its effectiveness.
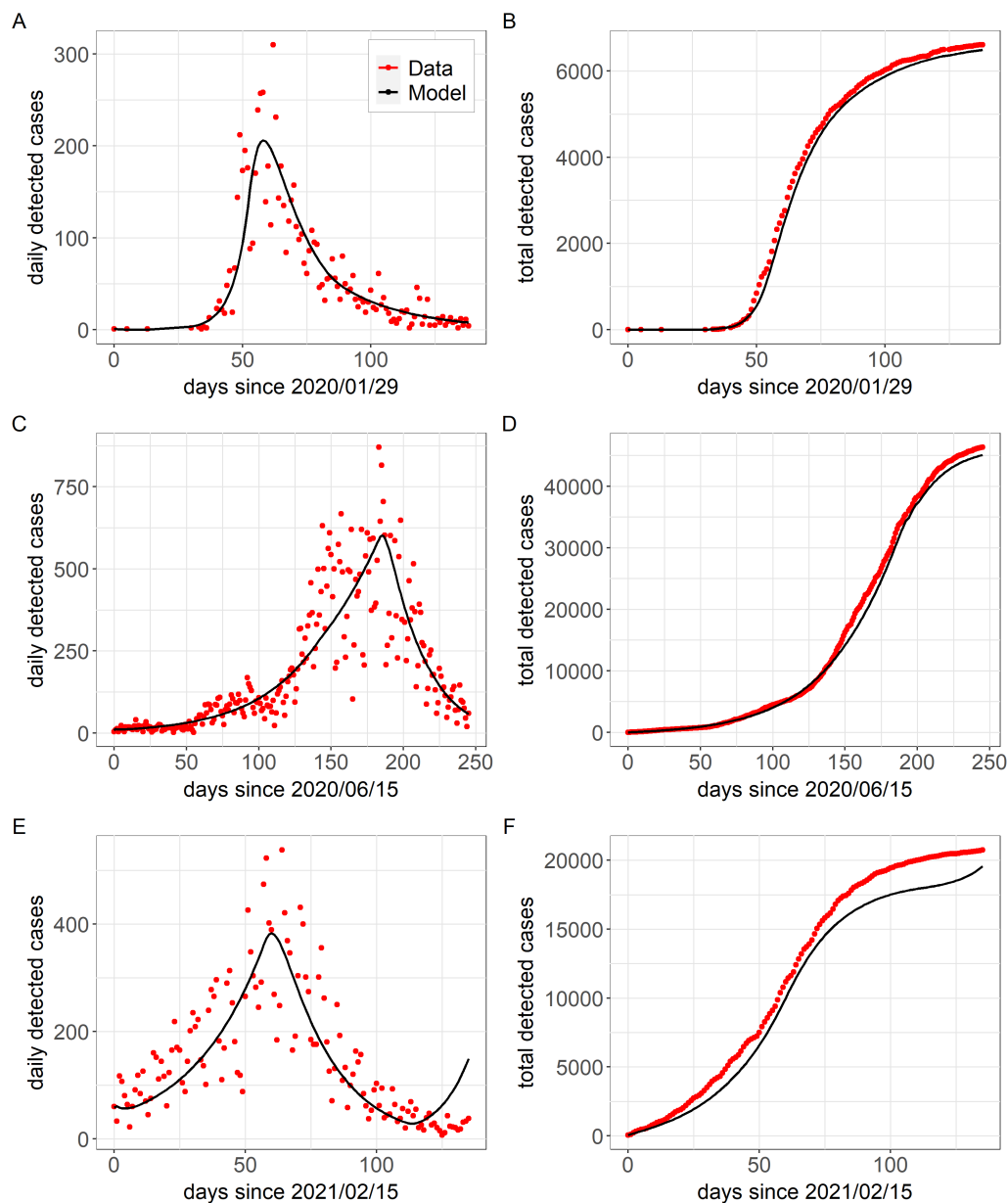
Figure 3. Performance evaluation of the preferred model: Comparison of model output (black) with RKI data (red). (A), (C) and (D): Daily detected COVID-19 cases in Munich in waves one, two and three, respectively. (B), (D) and (E): Total detected COVID-19 cases in Munich in waves one, two and three, respectively. The preferred model captures the structure of the data for the first and second wave very well. For the third wave some discrepancies can be noticed.
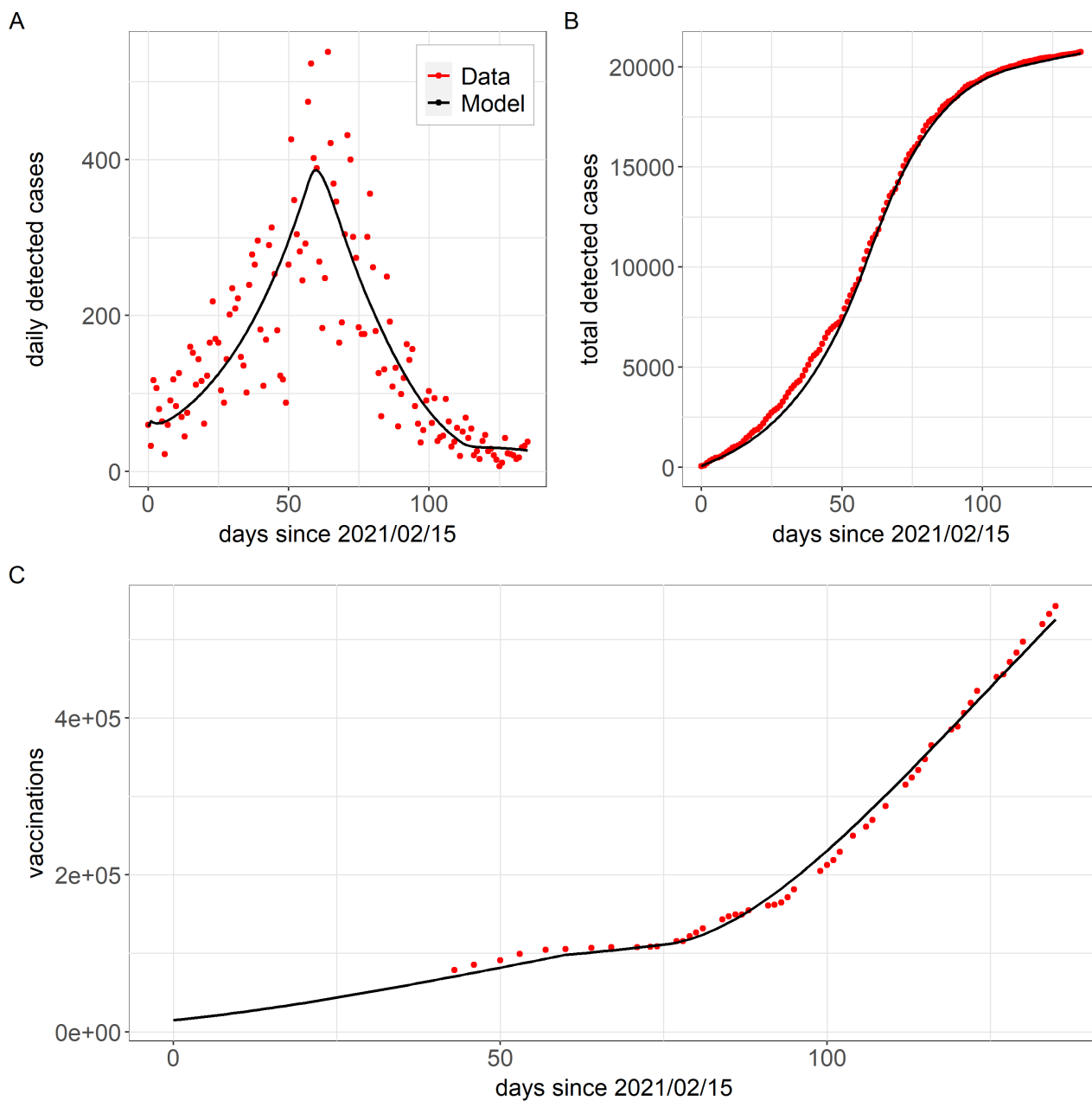
Figure 4. Performance evaluation of the preferred model with vaccination extension for wave three: Comparison of model output (black) with RKI data (red). (A): Daily detected COVID-19 cases in Munich. (B): Total detected COVID-19 cases in Munich. (C): Completely vaccinated individuals in Munich, reported by [32].
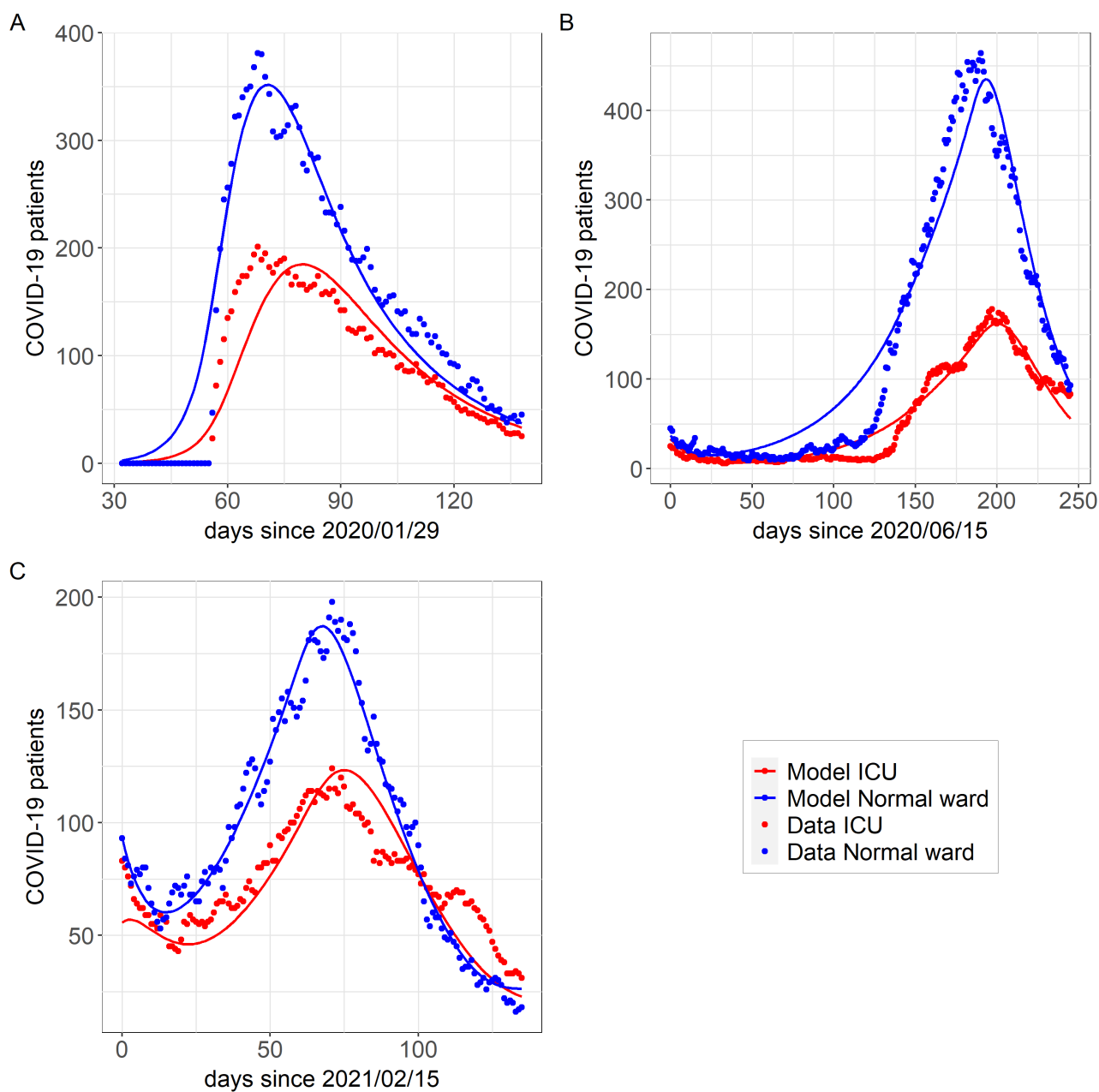
Figure 5. Performance evaluation of the hospitalization model: Comparison of model output (lines) with IVENA data (dots) for (A) the first wave, (B) the second wave and (C) the third wave. The NW station is represented in blue, while the ICU is represented in red. For wave one and two, no vaccination compartments were needed.

3.2. Predictions for the fourth wave

The beginning of the fourth wave was used as the starting point for predictions. From Figure 6, it can be seen that the amount of new COVID-19 cases and, therefore, also the number of hospitalized

patients, dramatically depends on the vaccination campaign. It can be appreciated that the time of the peak shifts with that dependency. The lower the vaccination success, the higher and later the peak.
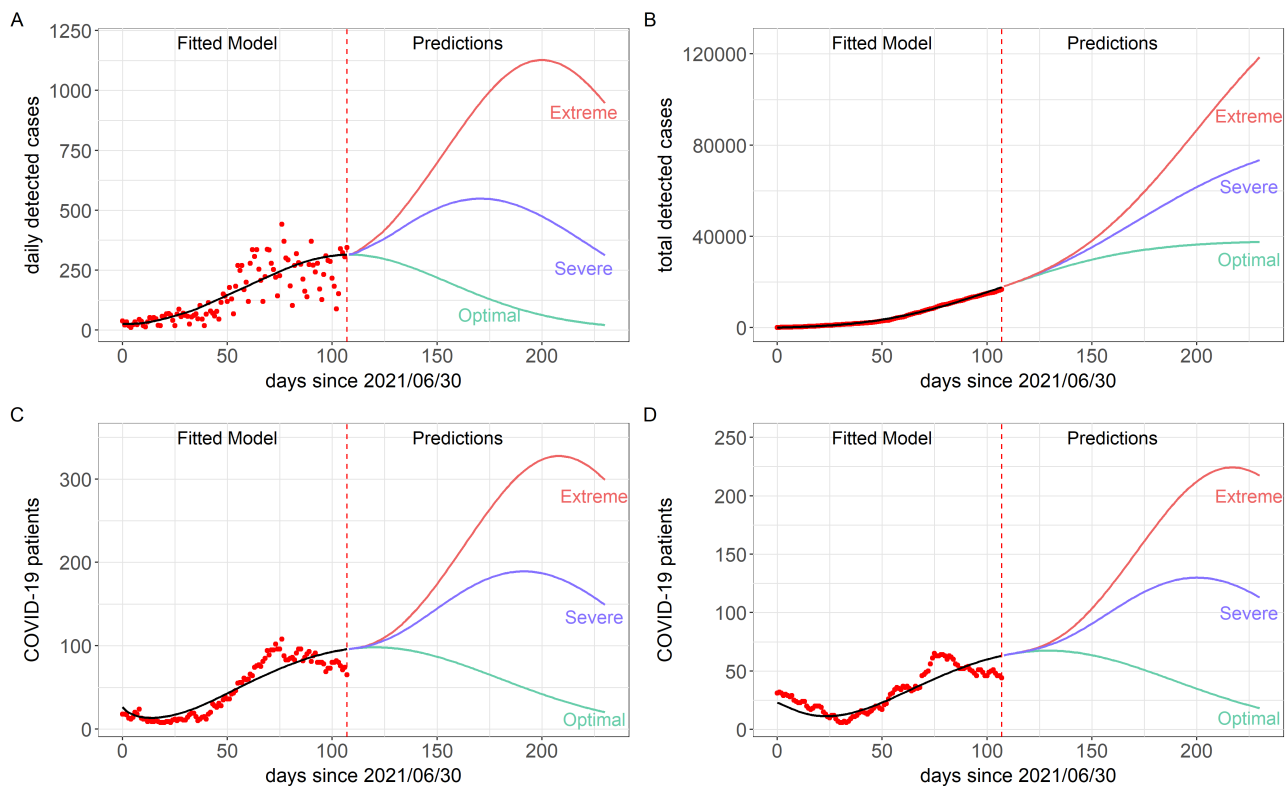
Figure 6. Model predictions for wave four: Optimal scenario (green), severe scenario (blue) and extreme scenario (violet). Model prediction for daily (A) and cumulative (B) detected COVID-19 cases in Munich. Model prediction for hospitalized COVID-19 patients in the ward station (C) and ICU (D).

4. Conclusions

We utilized biology-based mathematical models to simulate the number of new COVID-19 infections and hospitalizations in Munich's ward and ICUs during the first four waves of the pandemic. Our findings suggest that monitoring hospitalized cases may have been crucial at the pandemic's outset.

By comparing various models, we determined that incorporating an exposed class was essential. Neglecting this class would result in an immediate drop in infection numbers, which is not realistic given the latent period of the disease. Our models also included divisions between undetected/detected cases and asymptomatic/symptomatic courses, as these distinctions were necessary. Undetected cases have a higher transmission rate, and a significant proportion of individuals become infected by presymptomatic individuals. We also tried a model with a quarantine state for detected cases, but it did not improve the results (Supplemental Figure A1 bottom,

Supplemental Table A1). While other authors have previously used simpler models [13, 15, 16], our focus was on understanding the biological processes and parameters. Our data cover the first four pandemic's waves, and, therefore, some compartments of our model may not have been necessary for other analyses that concentrate on the reproduction number.

In the first half of 2021, new virus variants of SARS-CoV-2 were observed. When modeling the third wave, the much more contagious Alpha variant resulted in a higher transmission rate, being the cause of the outbreak of the third wave despite a lockdown being in place. In addition, when simulating the third wave, classes representing the vaccinated population had to be included into the model. Without taking into account the progressive immunization of the population at the end of the third wave, the number of cases in the model would increase again, although the data from the RKI show that the number of cases continue to decrease.

Predictions for different scenarios during the fourth wave are summarized in Figure 6. Even though a large proportion of the population is already vaccinated, the number of new COVID-19 cases is predicted to increase with rising contact rates and decreasing willingness to vaccinate. Rapid reopening with a standstill in vaccination could result in an extreme fourth wave with a higher incidence than the previous three. Furthermore, it was assumed that completely vaccinated individuals could no longer become infected with SARS-CoV-2. However, since it has been demonstrated that even completely vaccinated individuals can become infected, especially with the Delta variant, the daily incidence could be even higher than predicted by Model 2.8 [45].

Although the incidence during the fourth wave in the extreme scenario was even greater than during the second wave, we see in Figure 1(B) that the hospitalization rate decreases with an increasing number of fully vaccinated individuals. This confirms that vaccinations help against a severe course of COVID-19. However, the number of patients in normal wards could be higher than predicted since vaccine protection against a severe course wanes after approximately six months.

A discrepancy between IVENA data and model output was observed in Figure 5, where the number of hospitalized patients briefly decreased in the former while continuing to increase in the latter. This may be due to younger individuals being infected, and the lower hospitalization rate among them was not accounted for in the model. Barbarossa et al. [19] applied complex and age-structured SEIR models to incidence data, but they were without hospitalization information. Our models presented here could also be expanded with age structure. Differences in infections would be expected not only between age categories, but also between the pandemic waves.

The ICU occupancy could increase sharply even though the hospitalization rate decreased during the fourth wave due to the increasing immunity of the population. This is because non-vaccinated individuals are hospitalized and a large proportion of inpatients must be admitted to the ICU, which can still lead to an overload of the healthcare system.

In Figure 1(D), the hospitalization rate decreased during the fourth wave due to the increasing immunity of the population, but the number of ICU patients could again increase sharply. This is because non-vaccinated individuals are hospitalized [46] and a large proportion of inpatients must be admitted to the ICU, which can still lead to an overload of the healthcare system.

To summarize, we applied biology-based mathematical models to predict the fourth wave of COVID-19 in Munich. We give a rough idea of the possible courses of the pandemic and not an accurate prediction of a particular outcome. The best, most likely and worst case scenarios are presented to help policymakers make decisions about interventions. During the epidemic,

non-pharmaceutical interventions changed rapidly. Also, the introduction of vaccines and the advent of new variants significantly modified the settings of the pandemic. The models need to be adapted after every change, but since its structure remains similar and the computational time is short, this can be done quickly. The models applied are complex; therefore, the reliability of the parameters was supported by splitting the analysis in two steps: the incidence data supporting the biology-pandemic-dependent parameters, while the hospital data were used to support the hospitalization process. We have to underline that the forecasts presented here completely depend on the previously fitted parameters. The next steps could be to add a sensitivity analysis to show dependencies.

During the first three waves, the incidence and the 7-day incidence were key indicators for interventions, but since a large part of the population in Munich is fully vaccinated, the importance of incidences as an indicative value decreases while that of the hospitalization rate and ICU treatments increases. The incidence must still be monitored in the future since the higher the incidence, the more difficult it will be to track contacts and use interventions to keep infection numbers down. We support the thesis that monitoring the hospitalization should have been introduced at the beginning of the pandemic, together with the 7-day incidence, to clarify its importance and avoid miscommunication with the members of the public.

Acknowledgments

Conflict of interest

The authors declare that there is no conflict of interest.

Code availability

To facilitate reproducibility and reuse, we made the code used to perform the analyses and generate the figures available on GitHub (accessed on November 30, 2022) https://github.com/NoemiCastelletti/Hospitalization_Munich_COVID-19.git.

References

1. B. Ganesh, T. Rajakumar, M. Malathi, N. Manikandan, J. Nagaraj, A. Santhakumar, et al., Epidemiology and pathobiology of SARS-CoV-2 (COVID-19) in comparison with SARS, MERS: An updated overview of current knowledge and future perspectives, *Clin. Epidemiol. Glob. Health*, **10** (2021), 100694. https://doi.org/10.1016/j.cegh.2020.100694

2. World Health Organization, WHO Director-General's Opening Remarks at the Media Briefing on COVID-19-11 March 2020, 2020. Available from: https://www.who.int/director-general/speeches/detail/who-director-general-s-opening-remarks-at-the-media-briefing-on-covid-19---11-march-2020

3. World Health Organization, WHO Coronavirus (COVID-19) Dashboard, 2022. Available from: https://covid19.who.int/

4. Robert Koch-Institute (RKI), Table showing current Covid-19 infections per day as time series, 2021. Available from: https://npgeo-corona-npgeo-de.hub.arcgis.com/datasets/dd4580c810204019a7b8eb3e0b329dd6_0/explore

5. Robert Koch-Institute (RKI), Kontaktpersonen-Nachverfolgung bei SARS-CoV-2-Infektionen, 2021. Available from: https://www.rki.de/DE/Content/InfAZ/N/Neuartiges_Coronavirus/Kontaktperson/Management.html;jsessionid=78E4E999E14B2E6A3E8F02E5957D2C97.internet121?nn=13490888#doc13516162bodyText14

6. Robert Koch-Institute (RKI), Tabelle mit den gemeldeten Impfungen nach Bundesländern und Impfquoten nach Altersgruppen, 2021. Available from: https://www.rki.de/DE/Content/InfAZ/N/Neuartiges_Coronavirus/Daten/Impfquotenmonitoring

7. Robert Koch-Institute (RKI), Kurz und Knapp: Faktenblätter zum Impfen - COVID-19 Impfung, 2021. Available from: https://www.rki.de/DE/Content/Infekt/Impfen/Materialien/Faktenblaetter/Faktenblaetter_inhalt.html

8. J. Schilling, A. Lehfeld, D. Schumacher, M. Diercke, S. Buda, W. Haas, et al., Krankheitsschwere der ersten COVID-19-Welle in Deutschland basierend auf den Meldungen gemäß Infektionsschutzgesetz, *J. Health Monit.*, **5** (2020), 2–20. https://doi.org/10.25646/7169

9. Centers for Disease Control and Prevention (CDC), National Center for Immunization and Respiratory Diseases (NCIRD), Disease Burden of Flu, 2022. Available from: https://www.cdc.gov/flu/about/burden/index.html/

10. Robert Koch-Institute (RKI), Coronavirus SARS-CoV-2: Fallzahlen und Meldungen, 2021. Available from: https://www.rki.de/SharedDocs/FAQ/NCOV2019/FAQ_Liste_Fallzahlen_Meldungen.html

11. R. M. Anderson, The role of mathematical models in the study of HIV transmission and the epidemiology of AIDS, *J. Acquir. Immune Defic. Syndr.*, **1** (1988), 241–256.

12. F. Brauer, C. Castillo-Chavez, *Mathematical Models in Population Biology and Epidemiology*, Springer, New York, 2012.

13. D. Chumachenko, I. Meniailov, K. Bazilevych, T. Chumachenko, S. Yakovlev, Investigation of statistical machine learning models for COVID-19 epidemic process simulation: Random Forest, K-Nearest Neighbors, Gradient Boosting, *Computation*, **10** (2022), 2079–3197. https://doi.org/10.3390/computation10060086

14. F. Ying, N. O'Clery, Modelling COVID-19 transmission in supermarkets using an agent-based model, *PLoS One*, **16** (2021), 0249821. https://doi.org/10.1371/journal.pone.0249821

15. R. Nistal, M. de la Sen, J. Gabirondo, S. Alonso-Quesada, A. J. Garrido, I. Garrido, A Study on COVID-19 incidence in Europe through two SEIR epidemic models which consider mixed contagions from asymptomatic and symptomatic individuals, *Appl. Sci.*, **11** (2021), 2076–3417. https://doi.org/10.3390/app11146266

16. R. Nistal, M. de la Sen, J. Gabirondo, S. Alonso-Quesada, A. J. Garrido, I. Garrido, A Modelization of the Propagation of COVID-19 in regions of Spain and Italy with evaluation of the transmission rates related to the intervention measures, *Biology*, **10** (2021), 121. https://doi.org/10.3390/biology10020121

17. J. Ozaki, Y. Shida, H. Takayasu, M. Takayasu, Direct modelling from GPS data reveals daily-activity-dependency of effective reproduction number in COVID-19 pandemic, *Sci Rep.*, **12**, (2022), 17888. https://doi.org/10.1038/s41598-022-22420-9

18. D. Okuonghae, A. Omame, Analysis of a mathematical model for COVID-19 population dynamics in Lagos, Nigeria, *Chaos, Solitons Fractals*, **139** (2020), 110032. https://doi.org/10.1016/j.chaos.2020.110032

19. M. V. Barbarossa, J. Fuhrmann, J. H. Meinke, S. Krieg, H. V. Varma, N. Castelletti, et al., Modeling the spread of COVID-19 in Germany: Early assessment and possible scenarios, *PLoS ONE*, **15**, (2020). https://doi.org/10.1371/journal.pone.0238559

20. Süddeutsche Zeitung, Coronavirus-Pandemie in Bayern: Rückblick April 2020, *Süddeutsche Zeitung*, 2020. Available from: https://www.sueddeutsche.de/bayern/coronavirus-bayern-rueckblick-april-1.4873340

21. Norddeutscher Rundfunk, Corona-Chronologie: November 2020, 2020. Available from: https://www.ndr.de/nachrichten/info/Corona-Chronologie-November-2020,coronachronologie128.html

22. Norddeutscher Rundfunk, Corona-Chronologie: Dezember 2020. Available from: https://www.ndr.de/nachrichten/info/Corona-Chronologie-Dezember-2020,coronachronologie130.html

23. Norddeutscher Rundfunk, Corona-Chronologie: Januar 2021, 2021. Available from: https://www.ndr.de/nachrichten/info/Corona-Chronologie-Januar-2021,coronachronologie134.html

24. Süddeutsche Zeitung, Was in München ab heute gilt, 2021. Available from: https://www.sueddeutsche.de/muenchen/muenchen-corona-notbremse-mittwoch-1.5263849

25. Süddeutsche Zeitung,Diese Corona-Regeln gelten nun in München, 2021. Available from: https://www.sueddeutsche.de/muenchen/muenchen-corona-lockerungen-gastronomie-ausgangssperre-1.5288681

26. Bayerische Staatsregierung, Pressemitteilungen: Bericht aus der Kabinettssitzung vom 4. Juni 2021, 2021. Available from: https://www.bayern.de/bericht-aus-der-kabinettssitzung-vom-4-juni-2021/

27. Deutsche Akademie der Naturforscher Leopoldina, Ad-hoc-Stellungnahmen zur Coronavirus-Pandemie: Zusammenfassung der Stellungnahmen zur Coronavirus-Pandemie, 2020.

28. H. Panknin, S. Schröder, Konsequente Schutzmaßnahmen gegen Ansteckung, *Procare*, **25**, (2020), 20–22. https://doi.org/10.1007/s00735-020-1261-x

29. Robert Koch-Institute (RKI), Übersicht zu besorgniserregenden SARS-CoV-2-Virusvarianten (VOC), 2021. Available from: https://www.rki.de/DE/Content/InfAZ/N/Neuartiges_Coronavirus/Virusvariante.html

30. Robert Koch-Institute (RKI), Berichte zu Virusvarianten von SARS-CoV-2 in Deutschland, 2021. Available from: https://www.rki.de/DE/Content/InfAZ/N/Neuartiges_Coronavirus/DESH/Berichte-VOC-tab.html

31. Robert Koch-Institute (RKI), SARS-CoV-2: Virologische Basisdaten sowie Virusvarianten, 2021. Available from: https://www.rki.de/DE/Content/InfAZ/N/Neuartiges_Coronavirus/Virologische_Basisdaten.html;jsessionid=A1752CE0733B8B43969A64CD80B9B253.internet082?nn=13490888

32. Landeshauptstadt München-Das offizielle Stadtportal, Coronavirus-Fälle in München: Aktuelle Zahlen, 2021. Available from: https://www.muenchen.de/rathaus/Stadtinfos/Coronavirus-Fallzahlen.html

33. E. Callaway, Delta coronavirus variant: scientists brace for impact, *Nature*, (2021), 17–18. https://doi.org/10.1038/d41586-021-01696-3

34. BR24, Corona-Regeln: Was aktuell in Bayern gilt, 2021. Available from: https://www.br.de/nachrichten/bayern/corona-regeln-in-bayern-was-gilt,Sbtbuu0

35. Süddeutsche Zeitung, Corona in Bayern: Newsblog vom 5. bis zum 26. Juli 2021, 2021. Available from: https://www.sueddeutsche.de/bayern/corona-bayern-archiv-1.5342370

36. Süddeutsche Zeitung, Corona-Regeln Bayern: Welche Regeln aktuell in Bayern gelten, 2021. Available from: https://www.sueddeutsche.de/bayern/bayern-corona-regeln-2g-3g-maskenpflicht-1.4878824

37. C. Walter, F. Fischer, Interdisciplinary Supply Proof (IVENA): Improving Emergency Care through E-Health?, *NOTARZT*, **33**, (2017), 50.

38. Robert Koch-Institute (RKI), Epidemiologischer Steckbrief zu SARS-CoV-2 und COVID-19, 2021. Available from: https://www.rki.de/DE/Content/InfAZ/N/Neuartiges_Coronavirus/Steckbrief.html;jsessionid=1E68F40DA18BE45CC49EE51EA8FA8CC8.internet051?nn=2386228

39. S. Amit, G. Regev-Yochay, A. Afek, Y. Kreiss, E. Leshem, Early rate reductions of SARS-CoV-2 infection and COVID-19 in BNT162b2 vaccine recipients, *Lancet*, **397**, (2021), 875–877. https://doi.org/10.1016/s0140-6736(21)00448-7

40. H. Xin, Y. Li, P. Wu, Z. Li, E. H. Y. Lau, Y. Qin, et al., Estimating the latent period of coronavirus disease 2019 (COVID-19), *Clin. Infect. Dis.*, **74** (2022), 1678–1681. https://doi.org/10.1093/cid/ciab746

41. D. Buitrago-Garcia, D. Egli-Gany, M. J. Counotte, S. Hossmann, H. Imeri, A. M. Ipekci, et al., Occurrence and transmission potential of asymptomatic and presymptomatic SARS-CoV-2 infections: A living systematic review and meta-analysis, *PLoS Med.*, **17**, (2020). https://doi.org/10.1371/journal.pmed.1003346

42. Bayerisches Landesamt für Statistik, Die Datenbank des Bayerischen Landesamtes für Statistik, 2023. Available from: https://www.statistikdaten.bayern.de/genesis/online;jsessionid%3D6CB3363574391F9435FD661D9125B699?sequenz%3DtabelleErgebnis%26selectionname%3D12411-001

43. N. Potere, E. Valeriani, M. Candeloro, M. Tana, E. Porreca, A. Abbate, et al., Acute complications and mortality in hospitalized patients with coronavirus disease 2019: A systematic review and meta-analysis, *Crit. Care*, **24** (2020), 1–12. https://doi.org/10.1186/s13054-020-03022-1

44. M. Martcheva, *An Introduction to Mathematical Epidemiology*, Springer, New York, 2015.

45. Y. Goldberg, M. Mandel, Y. M. Bar-On, O. Bodenheimer, L. S. Freedman, E. Haas, et al., Waning immunity of the BNT162b2 vaccine: A nationwide study from Israel, *New Engl. J. Med.*, (2021). https://doi.org/10.1056/nejmoa2114228

46. BR24, Covid-19 in den Kliniken: Die Welle der Ungeimpften, 2021. Available from: https://www.br.de/nachrichten/bayern/covid-19-in-den-kliniken-die-welle-der-ungeimpften,SjYWL3B

47. K. P. Burnham, D. R. Anderson, *Model Selection and Multimodel Inference*, Springer, New York, 2002.

48. M. L. Gavrilova, O. Gervasi, V. Kumar, C. J. K. Tan, D. Taniar, A. Laganà, et al., Computational science and its applications-ICCSA 2006: international conference, Glasgow, in *ICCSA: International Conference on Computational Science and Its Applications*, **3982** (2006).

Supplementary

Model selection

Model selection is the task of choosing the best model out of a set of candidate models with the smallest possible number of parameters, which still represents the data adequately [47]. A model with too few parameters can lead to underfitting, not capturing the true relationship in the data. In contrast, a model with too many parameters can lead to overfitting, capturing the noise in the underlying data [47]. Assume a set of data $D : (x_i, y_i)$ is generated by a true function $y = f(x) + \epsilon$, where ϵ is the noise of the data (normally distributed with mean $E[\epsilon] = 0$ and variance $Var[\epsilon] = \sigma^2$). The unknown function $\hat{f}(x)$ can be fitted to the data minimizing the SSE, and the formula for the expected error has the form [48]

$$E[(y^* - \hat{f}(x^*))^2] = \sigma^2 + Bias^2(\hat{f}(x^*)) + Variance(\hat{f}(x^*)). \tag{A.1}$$

From (A.1) we can see that the expected error between the data points and the model depends on the noise, the bias and the variance. The noise is difficult to reduce because, in practice, it is often unknown. Bias and variance depend instead on the complexity of the model. If model complexity (i.e., the number of parameters) increases, the bias decreases, whereas the variance increases. On the other hand, if model complexity decreases, the bias increases while the variance decreases [48]. The goal is to minimize the expected error between the model and the data, which is equivalent to minimizing the bias and the variance of the model. It follows that both a too simple model and a too complex model are not optimal, as the data will either be underfitted or overfitted.

In this analysis, model selection was performed by applying the AIC, which measures the relative goodness of fit of a mathematical model [44]. For a given model, the AIC is computed as

$$AIC = n[\ln(\frac{SSE}{n})] + 2(k + 1), \tag{A.2}$$

where n is the number of available data points in the dataset, k is the number of unknown parameters to be fitted, and SSE is the least-squares error [44].

We calculate the AIC for each candidate model. The best model is the one with the smallest AIC. From (A.2), we can see that the AIC is directly proportional to the number of fitted parameters, penalizing too complex models and, hence, preventing overfitting [44]. In addition, the AIC rewards models with a good fit, i.e., models with a small SSE, which prevents underfitting.

Table A1. Comparison of model attempts

Model	SSE	No. Parameters	AIC
Model 1	659041.0	1	937.6512
Model 2	231249.3	1	825.5912
Preferred model	108642.9	3	748.7602
Model 3	114436.7	3	754.3195

Defining the preferred model

Now, the question is, which models can capture the data best while also not being unnecessarily complicated? For this purpose, the AIC values of the four different models are compared in Table A1. We can see that the preferred model has the smallest AIC value. Therefore, the preferred model is the most appropriate among all four candidate models for simulating the first wave of COVID-19 in Munich. By comparing the AIC from Model 1 and Model 2, it follows that the inclusion of an exposed class is essential, as the AIC decreases significantly. Additionally, a significant improvement in AIC follows from the differentiation between undetected and detected cases, as well as between individuals with asymptomatic and symptomatic course. This suggests that undetected infectious individuals and individuals without any symptoms also play an important role in the dynamics of the pandemic. For instance, according to the RKI, a relevant proportion of people become infected via presymptomatic individuals [38]. The inclusion of a quarantine compartment does not improve the AIC, at least under the current conditions, which suggests that Model 3 is unnecessarily complicated. Since the preferred model can best simulate the first wave of the COVID-19 pandemic in Munich, it is also the model used for the analysis of the other pandemic waves.

Model Attempts

Model 1: SIR Model

First, we attempted to model the first wave of COVID-19 by using the basic SIR model (Figure A1(A)) [12]. It was assumed that the susceptible individuals (S) have not yet had the disease but can become infected through contact with an infected individual (I). Furthermore, for this model, only detected cases are considered to make it possible to compare model output and the RKI data. Approximately 10 days after symptom onset, the contagiousness of the infected person decreases

significantly [38]. After recovery of infected individuals (R), they become immune to reinfection. Further details on parameter assumptions are given in Table A2. Model 1 is then given by the following system of differential equations:

$$\dot{S} = -\lambda S,$$
$$\dot{I} = \lambda S - \alpha I,$$
$$\dot{R} = \alpha I,$$

where $\lambda(t) = \beta(t)\frac{I(t)}{N}$ is the force of infection and $N \approx 1.484$ million is the total population size of Munich [42]. Furthermore, $\beta(t)$ is the time-dependent transmission rate. Since the RKI reported one COVID-19 case on the first day of the first wave, we used $S(0) = N - 1$, $I(0) = 1$ and $R(0) = 0$ as initial values for the three compartments.
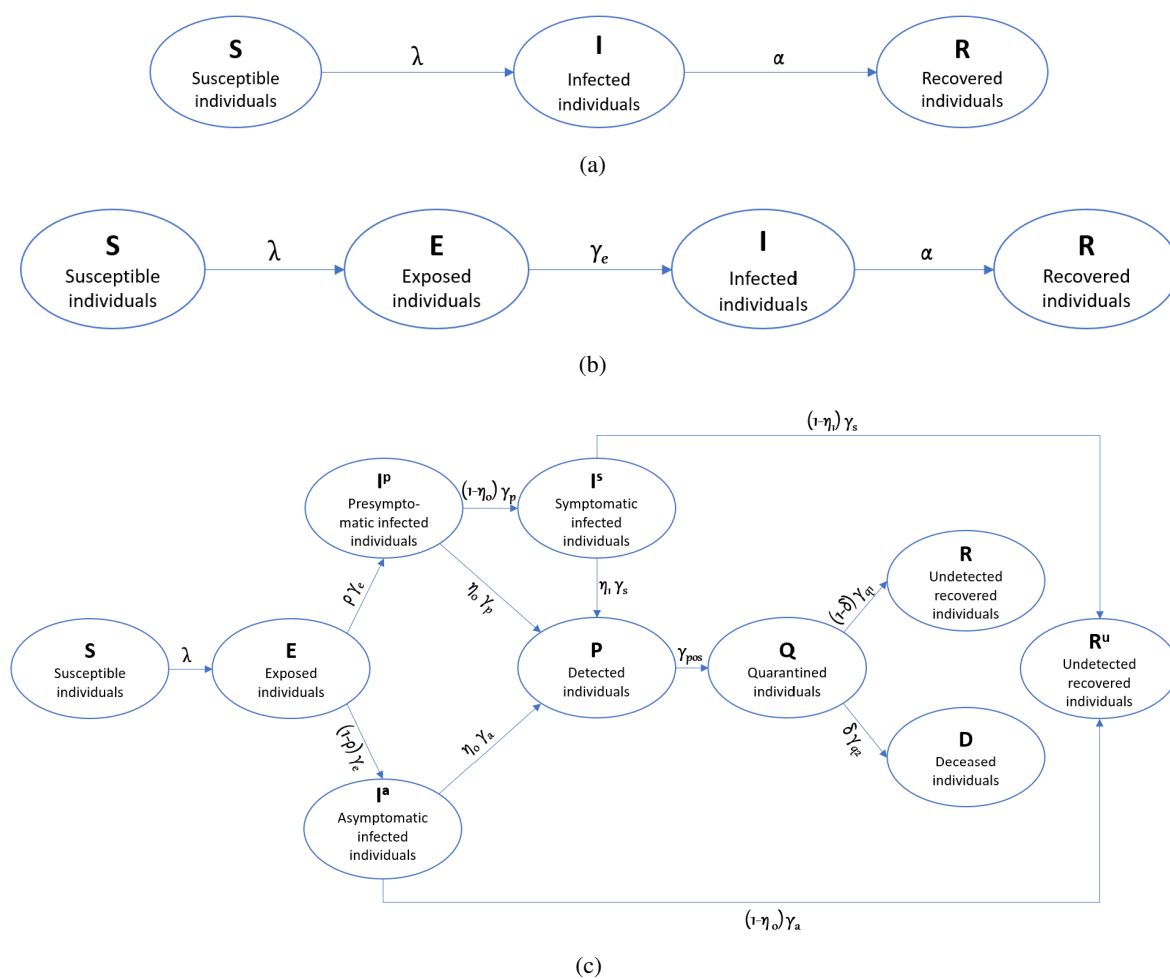
Figure A1. Scheme of the model attempts: (A) Model 1, (B) Model 2 and (C) Model 3.
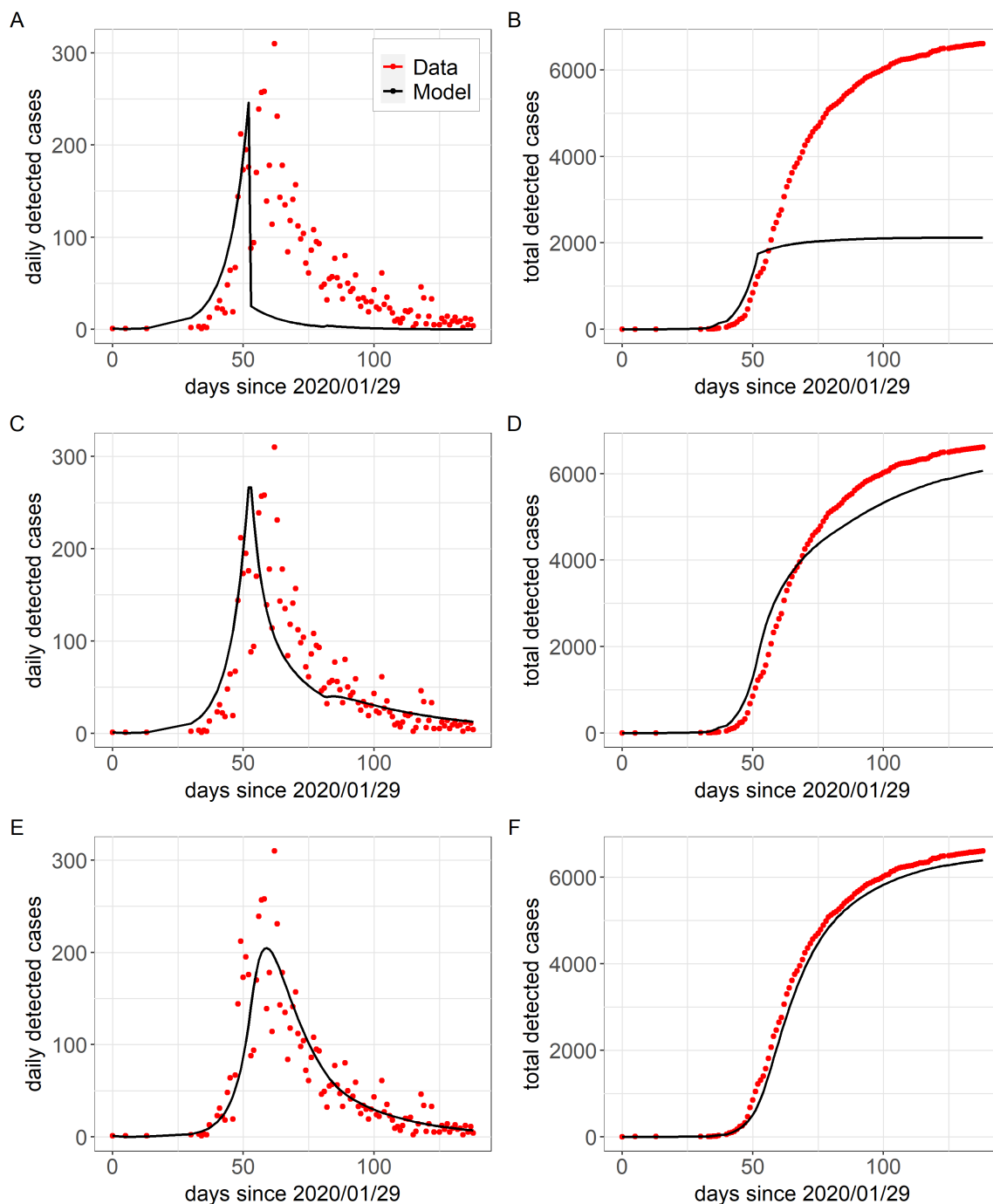
Figure A2. Performance evaluation of the model attempts. Comparison of model output (black) with RKI data (red). (A), (C) and (D): Daily detected COVID-19 cases in Munich in wave one for Models 1, 2 and 3, respectively. (B), (D) and (E): Total detected COVID-19 cases in Munich in wave one for Models 1, 2 and 3, respectively. The basic SIR Model 1 cannot capture the structure of the data. The SEIR Model 2 shows a clear improvement compared to the SIR model. The more complex Model 3 can capture the structure of the data very well, with, however, a worse AIC than the preferred model.

To compare Model 1 with the RKI data, we calculate the newly detected infections $\hat{d}(t)$ at day t from the output of Model 1 as follows:

$$\hat{d}(t) = \begin{cases} I(0) & \text{if } t = 0 \\ S(t) - S(t+1) & \text{if } t > 0. \end{cases}$$

In Figure A2(A) and (b), it can be seen that the simple SIR model cannot capture the spread of COVID-19 in Munich during the first wave. One reason for this is the exclusion of an exposed class. When the lockdown starts after 52 days and the transmission rate decreases, we can see that the number of infected individuals immediately drop off. However, this is not realistic because, at this point in time, there are a lot of individuals who are already infected with COVID-19 but neither have symptoms nor are they infectious. These individuals are called exposed individuals. After infection with the disease, the virus needs some time to develop in the human body. The time during which an individual is infected but not yet infectious is called the latent period [44]. So, at the start of the lockdown, there are still a lot of individuals moving to the infected class although there are no or less new infections. So, for the next model, we will include an exposed (latent) class.

Model 2: Including an Exposed Class

In addition to the three compartments of the previous model, an exposed class (E) is now included in Model 2 (Figure A1 middle). After infection, individuals move from the susceptible to the exposed class, where they have neither symptoms nor are they infectious. After a latent period of approximately 5.5 days, the infected individuals become infectious and develop symptoms and therefore move to class I [38]. Details on parameter assumptions are given in Table A2.
Model 2 is then given by the following system of differential equations:

$$\begin{aligned} \dot{S} &= -\lambda S, \\ \dot{E} &= \lambda S - \gamma_e E, \\ \dot{I} &= \gamma_e E - \alpha I, \\ \dot{R} &= \alpha I, \end{aligned}$$

where, again, $\lambda(t) = \beta(t)\frac{I(t)}{N}$ is the force of infection and $\beta(t)$ the time-dependent transmission rate. As initial values for the four compartments, $S(0) = N - 1$, $E(0) = 0$, $I(0) = 1$ and $R(0) = 0$ were used.

The newly infected individuals $\hat{d}(t)$ at day t are calculated from the output of the SEIR model as follows:

$$\hat{d}(t) = \begin{cases} I(0) & \text{if } t = 0, \\ [I(t+1) - I(t)] + [R(t+1) - R(t)] & \text{if } t > 0. \end{cases}$$

After minimizing the SSE between the daily detected COVID-19 cases $d(t)$ reported by the RKI and $\hat{d}(t)$ from the model output, the results of the fitted model can be seen in Figure A2(c)–(d). Compared to Model 1, a significant improvement in the performance of Model 2 can be recognized.

Table A2. Parameters of Models 1, 2 and 3 for the first wave

Parameter	Description	Value (unit) [Refs.]
Model 1		
β_0	Initial transmission rate	0.24 $\frac{1}{d \cdot \text{individual}}$ [fitted]
$\frac{1}{\alpha}$	Mean duration of infection	10 d [38]
Model 2		
(added parameters)		
β_0	Initial transmission rate	0.45 $\frac{1}{d \cdot \text{individual}}$ [fitted]
$\frac{1}{\gamma_e}$	Mean duration of latent phase	5.5 d [38]
Model 3		
(added parameters)		
β_0	Initial transmission rate	0.67 $\frac{1}{d \cdot \text{individual}}$ [fitted]
η_0	Prob. of detection while asympt.	0.62 [fitted]
$\frac{1}{\gamma_{pos}}$	Mean duration to go to quarantine	1 d [assumed]
$\frac{1}{\gamma_{q_1}}$	Mean duration of quarantine	14 d [5]
$\frac{1}{\gamma_{q_2}}$	Mean duration from start of quarantine until death	2 d [fitted]

Model 3: Including Quarantine

We extended the model presented in the main manuscript (called the preferred model in the following) and have included a compartment representing the quarantined individuals (Q) (Figure A1 bottom). All people with a detected SARS-CoV-2 infection go directly into quarantine, where they are supposed to have no contact with other people. Therefore, we assume that individuals who are in compartment Q can no longer infect anyone. During quarantine, individuals can die because of the disease and then move to the deceased compartment D, or they leave quarantine after approximately 14 days and go to the recovered compartment R [5].

Model 3 is then given by the following system of differential equations:

$$\dot{S} = -\lambda S,$$
$$\dot{E} = \lambda S - \gamma_e E,$$
$$\dot{I}^a = (1 - \rho)\gamma_e E - \gamma_a I_a,$$
$$\dot{I}^p = \rho\gamma_e E - \gamma_p I_p,$$
$$\dot{I}^s = (1 - \eta_0)\gamma_p I_p - \gamma_s I_s,$$
$$\dot{P} = \eta_0\gamma_a I_a + \eta_0\gamma_p I_p + \eta_1\gamma_s I_s - \gamma_{pos}P,$$
$$\dot{Q} = \gamma_{pos}P - (1 - \delta)\gamma_{q_1}Q - \delta\gamma_{q_2}Q,$$
$$\dot{R} = (1 - \delta)\gamma_{q_1}Q,$$
$$\dot{D} = \delta\gamma_{q_2}Q,$$
$$\dot{R}^u = (1 - \eta_1)\gamma_s I_s + (1 - \eta_0)\gamma_a I_a,$$

where the force of infection $\lambda(t)$ is time-dependent and defined like before in the model presented in the main manuscript. In addition to the initial values from the main model, we used $Q(0) = 0$. The

parameters can be found in Table A2.

It follows that the number of daily detected infections in Model 3 is described by the class P, i.e., $\hat{d}(t) = P(t)$. After minimizing the SSE between the daily detected COVID-19 cases $d(t)$ reported by the RKI and $\hat{d}(t)$, the results of the fitted model can be seen in Figure A2(e)–(f). The performance of Model 3 seems very similar to that of the preferred model, however, without any improvement in the goodness of fit (Table A1).

Model analysis

As part of a standard analysis for such epidemiological models, one may be interested in the reproduction number R. To establish a unique disease-free equilibrium, we modify the model in such a way that we take into account the (slow) population dynamics. For that, we assume that all newborns (constant rate Λ) go into the susceptible compartment, and we have a natural per capita death rate μ for all compartments. The compartment D is left out for that purpose. The model version for this analysis reads as

$$
\begin{aligned}
\dot{S} &= \Lambda - \lambda(t)S - v_1 S - \mu S, \\
\dot{E} &= \lambda(t)S + \sigma\lambda V_1 - \gamma_e E - \mu E, \\
\dot{V}_1 &= v_1 S - \sigma\lambda V_1 - v_2 V_1 - \mu V_1, \\
\dot{V}_2 &= v_2 V_1 - \mu V_2, \\
\dot{I}^a &= (1 - \rho)\gamma_e E - \gamma_a I^a - \mu I^a, \\
\dot{I}^p &= \rho\gamma_e E - \gamma_p I^p - \mu I^p, \\
\dot{I}^s &= (1 - \eta_0)\gamma_p I^p - \gamma_s I^s - \mu I^s, \\
\dot{P} &= \eta_0\gamma_a I^a + \eta_0\gamma_p I^p + \eta_1\gamma_s I^s - (h_0\gamma_{pos_1} + (1 - h_0)\gamma_{pos_2})P - \mu P, \\
\dot{H}^{norm} &= h_0\gamma_{pos_1} P + (1 - \delta)\gamma_{icu} H^{ICU} - (h_1\gamma_{norm_1} + (1 - h_1)\gamma_{norm_2})H^{norm} - \mu H^{norm}, \\
\dot{H}^{ICU} &= h_1\gamma_{norm_1} H^{norm} - \gamma_{icu} H^{ICU} - \mu H^{ICU}, \\
\dot{R} &= (1 - \eta_0)\gamma_a I^a + (1 - \eta_1)\gamma_s I^s + (1 - h_0)\gamma_{pos_2} P + (1 - h_1)\gamma_{norm_2} H^{norm} - \mu R,
\end{aligned}
\tag{A.3}
$$

still with $\lambda(t) = \frac{\beta_a I^a + \beta_p I^p + \beta_s I^s + \beta_{pos} P}{N - D}$ and N the total population size. In this model version, as well as in the versions in the main part, the non-negativity of solutions is kept when starting with non-negative initial values. This can be easily seen because all negative terms on the right-hand side are proportional to the respective variable. Furthermore, by having a compartmental model including a constant birth term and death terms in all compartments, the solutions stay bounded. Here, we use a constant $\beta_a(t)$. Setting the right-hand sides of (A.3) equal to zero, we can easily solve it for the disease-free equilibrium, which reads as

$$
(\hat{S}, 0, \hat{V}_1, \hat{V}_2, 0, 0, 0, 0, 0, 0, 0) = (\Lambda/(v_1 + \mu), 0, \frac{v_1}{(v_2 + \mu)(v_1 + \mu)}\Lambda, \frac{v_2 v_1}{\mu(v_2 + \mu)(v_1 + \mu)}\Lambda, 0, 0, 0, 0, 0, 0, 0).
$$

The total population in this equilibrium situation is $N = \Lambda \cdot \frac{(v_2 + \mu)\mu + v_1\mu}{(v_1 + \mu)(v_2 + \mu)\mu}$.

Please note that, for the disease-free equilibrium, it does not matter that $\lambda(t)$ is not constant, as this term becomes equal to zero; also, it is an autonomous equation, which means that, even if we calculate an endemic equilibrium, it would work.

We follow the van den Driessche and Watmough approach for calculating the reproduction number as formulated in [44]. For that, we need to sort the compartments into infected ones, $X = (E, I^a, I^p, I^s, P)$, and the non-infected ones, $Y = (S, V_1, V_2, R)$ (the hospital compartments are left out for this purpose, as they do not have any further influence). Next, we split the right-hand side terms of X into new infections in the compartment and remaining terms, i.e.,

$$X' = F(X, Y) - V(x, Y) = \begin{pmatrix} \lambda(t)S + \sigma\lambda V_1 \\ (1 + \rho)\gamma_e E \\ \rho\gamma_e E \\ (1 - \eta_0)\gamma_p I_p \\ \eta_0\gamma_a I_a + \eta_0\gamma_p I_p + \eta_1\gamma_s I_s \end{pmatrix} - \begin{pmatrix} \gamma_e E \\ \gamma_a I_a \\ \gamma_p I_p \\ \gamma_s I_s \\ (h_0\gamma_{pos1} + (1 - h_0)\gamma_{pos2})P \end{pmatrix};$$

F and V have to satisfy some general conditions, as $F_i(0, Y) = 0$ and $V_i(0, Y) = 0$ for $i = 1, \ldots, 5$, $F_i(X, Y) \geq 0$ for all $X, Y \geq 0$, $V_i(X, Y) \leq 0$ for $X_i = 0, i = 1, \ldots, 5$, and $\sum_{i=1}^5 V_i(X, Y) \geq 0$ for all $X, Y \geq 0$, which is easy to see in this case. Next, we need two matrices (using the notation $Y_0 = (\hat{S}, \hat{V}_1, \hat{V}_2, 0)$):

$$\mathcal{F} = \left[\frac{\partial F_i(0, Y_0)}{\partial X_j} \right] = \begin{pmatrix} 0 & \frac{\beta_a\hat{S}}{N} + \frac{\sigma\beta_a\hat{V}_1}{N} & \frac{\beta_p\hat{S}}{N} + \frac{\sigma\beta_p\hat{V}_1}{N} & \frac{\beta_s\hat{S}}{N} + \frac{\sigma\beta_s\hat{V}_1}{N} & \frac{\beta_{pos}\hat{S}}{N} + \frac{\sigma\beta_{pos}\hat{V}_1}{N} \\ (1 - \rho)\gamma_e & 0 & 0 & 0 & 0 \\ \rho\gamma_e & 0 & 0 & 0 & 0 \\ 0 & 0 & (1 - \eta_0)\gamma_p & 0 & 0 \\ 0 & \eta_0\gamma_a & \eta_0\gamma_p & \eta_1\gamma_s & 0 \end{pmatrix}$$

and

$$\mathcal{V} = \left[\frac{\partial V_i(0, Y_0)}{\partial X_j} \right] = \begin{pmatrix} \gamma_e & 0 & 0 & 0 & 0 \\ 0 & \gamma_a & 0 & 0 & 0 \\ 0 & 0 & \gamma_p & 0 & 0 \\ 0 & 0 & 0 & \gamma_s & 0 \\ 0 & 0 & 0 & 0 & \underbrace{(h_0\gamma_{pos1} + (1 - h_0)\gamma_{pos2})}_{=:h^*} \end{pmatrix}.$$

The latter one, being a diagonal matrix, can be easily inverted, which we need in the following step. For easier writing and to make the structure of the matrix more visible, we introduce the short notations $B_1 := \frac{\beta_a\hat{S}}{N\gamma_1} + \frac{\sigma\beta_a\hat{V}_1}{N\gamma_1}$, $B_2 := \frac{\beta_p\hat{S}}{N\gamma_p} + \frac{\sigma\beta_p\hat{V}_1}{N\gamma_p}$, $B_3 := \frac{\beta_s\hat{S}}{N\gamma_s} + \frac{\sigma\beta_s\hat{V}_1}{N\gamma_s}$ and $B_4 := \frac{\beta_{pos}\hat{S}}{Nh^*} + \frac{\sigma\beta_{pos}\hat{V}_1}{Nh^*}$. Then, we find that

$$K = \mathcal{F}\mathcal{V}^{-1} = \begin{pmatrix} 0 & B_1 & B_2 & B_3 & B_4 \\ (1 - \rho) & 0 & 0 & 0 & 0 \\ \rho & 0 & 0 & 0 & 0 \\ 0 & 0 & (1 - \eta_0) & 0 & 0 \\ 0 & \eta_0 & \eta_0 & \eta_1 & 0 \end{pmatrix}.$$

The corresponding characteristic polynomial has the form

$$0 = \lambda \cdot \{-\lambda^4 + (\rho - 1)[-B_1\lambda^2 - \eta_0 B_4\lambda^2] + \rho[B_2\lambda^2 + B_4\eta_0\lambda + B_4(1 - \eta_0)\eta_1]\}$$

(λ denotes here the eigenvalues, not to mix up with the $\lambda(t)$ from the model formulation).

The square root of the spectral radius of this matrix would yield us the reproduction number. Unfortunately, only one eigenvalue can be read out easily, and that is the 0. For the others, we maintain the roots of a polynomial of grade four, but this formula is not convenient, and is thus not useful in the general form. But, using concrete parameter values, one could apply these in matrix K and calculate the eigenvalues, and, consequently, numerically calculate the spectral radius. Please recall that $\beta_a(t)$ may vary, e.g., due to restrictions, and also influence the reproduction number.

The calculation and consideration of the endemic equilibrium is left out here, as the long-time behavior might not be so relevant for this purpose, as too many other properties and environmental conditions change with time.

Publication 6:

The interplay of viral loads, clinical presentation, and serological responses in SARS-CoV-2 – Results from a prospective cohort of outpatient COVID-19 cases

Kerstin Puchinger*, **Noemi Castelletti***, Raquel Rubio-Acero, Christof Geldmacher, Tabea M. Eser, Flora Deák, Ivana Paunovic, Abhishek Bakuli, Elmar Saathoff, Alexander von Meyer, Alisa Markgraf, Philline Falk, Jakob Reich, Friedrich Riess, Philipp Girl, Katharina Müller, Katja Radon, Jessica Michelle Guggenbuehl Noller, Roman Wölfel, Michael Hoelscher, Inge Kroidl+, Andreas Wieser+, Laura Olbrich+, KoCo19 study team

Since January 2020 Elsevier has created a COVID-19 resource centre with free information in English and Mandarin on the novel coronavirus COVID-19. The COVID-19 resource centre is hosted on Elsevier Connect, the company's public news and information website.

The interplay of viral loads, clinical presentation, and serological responses in SARS-CoV-2 – Results from a prospective cohort of outpatient COVID-19 cases

Kerstin Puchinger [a,1], Noemi Castelletti [a,b,1,*], Raquel Rubio-Acero [a], Christof Geldmacher [a,c], Tabea M. Eser [a,c], Flora Deák [a,c], Ivana Paunovic [a], Abhishek Bakuli [a], Elmar Saathoff [a,c], Alexander von Meyer [d], Alisa Markgraf [a], Philine Falk [a], Jakob Reich [a], Friedrich Riess [a,c], Philipp Girl [c,e], Katharina Müller [c,e], Katja Radon [g], Jessica Michelle Guggenbuehl Noller [a], Roman Wölfel [c,e], Michael Hoelscher [a,c], Inge Kroidl [a,c,2], Andreas Wieser [a,c,2], Laura Olbrich [a,c,f,2], on behalf on theKoCo19 study group

[a] Division of Infectious Diseases and Tropical Medicine, University Hospital, LMU Munich, 80802, Munich, Germany
[b] Institute of Radiation Medicine, Helmholtz Zentrum München, 85764, Neuherberg, Germany
[c] German Center for Infection Research (DZIF), Partner Site Munich, Germany
[d] Institute for Laboratory Medicine, Medical Microbiology and Technical Hygienics, Munich Municipal Hospital Group, 81675, Munich, Germany
[e] Bundeswehr Institute of Microbiology, 80937, Munich, Germany
[f] Oxford Vaccine Group, Department of Paediatrics, And the NIHR Oxford Biomedical Research Centre, University of Oxford, OX1 2JD, Oxford, UK
[g] Center for International Health, Institute and Outpatient Clinic for Occupational, Social and Environmental Medicine, University Hospital Munich (LMU), Ziemssenstr. 1, 80336, Munich, Germany

ARTICLE INFO

ABSTRACT

Risk factors for disease progression and severity of SARS-CoV-2 infections require an understanding of acute and long-term virological and immunological dynamics. Fifty-one RT-PCR positive COVID-19 outpatients were recruited between May and December 2020 in Munich, Germany, and followed up at multiple defined timepoints for up to one year. RT-PCR and viral culture were performed and seroresponses measured. Participants were classified applying the WHO clinical progression scale. Short symptom to test time (median 5.0 days; p = 0.0016) and high viral loads (VL; median maximum VL: $3 \cdot 10^8$ copies/mL; p = 0.0015) were indicative for viral culture positivity. Participants with WHO grade 3 at baseline had significantly higher VLs compared to those with WHO 1 and 2 (p = 0.01). VLs dropped fast within 1 week of symptom onset. Maximum VLs were positively correlated with the magnitude of Ro-N-Ig seroresponse (p = 0.022). Our results describe the dynamics of VLs and antibodies to SARS-CoV-2 in mild to moderate cases that can support public health measures during the ongoing global pandemic.

1. Introduction

At the end of 2019, cases of pneumonia of unknown origin were registered in Wuhan, China, and a novel coronavirus was subsequently identified as the causative agent (Sun et al., 2020; Zhou et al., 2020; Carvalho et al., 2021). On January 27th, 2020, the first SARS-CoV-2 (Severe Acute Respiratory Syndrome Coronavirus 2) infection was confirmed in Germany at the Division of Infectious Diseases and Tropical Medicine in Munich (Rothe et al., 2020). Shortly after, on January 30th, the WHO declared the outbreak as a public health emergency of

---

international concern.

The current reference standard to diagnose acute SARS-CoV-2 infection is reverse transcriptase-polymerase chain reaction (RT-PCR), from nasopharyngeal swabs or other respiratory samples (van Kampen et al., 2021). Active, replicating SARS-CoV-2 virus can also be detected by viral culture in Biosafety Level 3 laboratories and correlates with infectivity. In patients with positive viral culture results, viral loads (VLs) tend to be significantly higher than in patients with negative culture results. In addition, patients with high VLs are described to have more active virus replication and thus being more infectious than those with low VLs (van Kampen et al., 2021; Jefferson et al., 2020; Wölfel et al., 2020).

Dynamics of viral shedding as well as their association with demographic and clinical characteristics during the acute phase of SARS-CoV-2 infection have been described. These indicate that VL decrease gradually after symptom onset and serological responses mostly develop within the first two weeks after infection (Bullard et al., 2020; Sui et al., 2021; Mahallawi et al., 2021; Wellinghausen et al., 2020; Wang et al., 2020a). Studies also suggest that in some cases, RT-PCR positivity can persist more than 30 days from symptom onset, which is described as prolonged viral shedding (Wang et al., 2020b; Jin et al., 2020). The probability of positive culture decreases 10–14 days after symptom onset jointly with declining VLs (Bullard et al., 2020; Kim et al., 2021). Most published studies were conducted in inpatient settings, and data on the interplay of viral, clinical, and serological characteristics in an outpatient cohort are limited.

In the here-presented study, we aimed to assess acute phase VL and shedding dynamics, clinical information, and the SARS-CoV-2-specific antibody response within a long-term prospective cohort in Munich, Germany. We investigated a group of 51 individuals with acute SARS-CoV-2 infection who underwent an in-depth analysis during multiple early time points and for up to week 52 after symptom onset.

2. Materials and methods

2.1. Study design, setting and population

Individuals with a documented positive SARS-CoV-2 RT-PCR result were recruited in a prospective longitudinal cohort (n = 51) from May to December 2020, under the umbrella of the KoCo19 studies (Pritsch et al., 2021; Radon et al., 2021; Olbrich et al., 2021). Participants were consented and recruited as fast as possible upon RT-PCR confirmation of SARS-CoV-2 infection and followed during weekly visits up to week 4. Additional visits were performed at week 8, 26, and 52. Nasopharyngeal swabs were collected for RT-PCR analyses and viral culture. Semi-quantitative and quantitative antibody responses against nucleocapsid as well as spike/RBD were determined at all timepoints respectively. During time of recruitment, only the SARS-CoV-2 Wuhan strain (lineage A) was circulating in Germany, hence no further viral sequencing was performed within the study.

Questionnaires on clinical and demographic information were collected as previously published (Pritsch et al., 2021; Radon et al., 2021). Symptom to Test Time (STT) was defined as the number of days from the onset of symptoms to documented positive SARS-CoV-2 RT-PCR to reflect the onset of disease more accurately. The clinical presentation of the participants was classified using the WHO clinical progression scale (WHO clinical scale), a scoring system for disease severity during SARS-CoV-2 infection including the following codes: (0) uninfected, (1) asymptomatic cases, (2) mild symptomatic, (3) moderate symptomatic cases who needed assistance, but hospitalization was not necessary, (4) hospitalised but no oxygen therapy, (5) hospitalised and oxygen by mask or nasal prongs, (6) hospitalised and oxygen by NIV or high flow, (7) intubation and mechanical ventilation, (8) mechanical ventilation or vasopressors, (9) mechanical ventilation and vasopressors, dialysis or ECMO, (10) dead (Marshall et al., 2020). The participants of the study were all outpatients, therefore all patients fell within WHO category 1–3.

The study was approved by the Ethics Committee of the Faculty of Medicine at LMU Munich (20–371). Informed consent was obtained prior to any study procedure.

2.2. Viral testing methods

Per protocol, two respiratory swabs per sampling time point were obtained per patient, one of which was incubated for viral culture at the Bundeswehr Institute of Microbiology as described elsewhere (Wölfel et al., 2020). Quantitative RT-PCR was performed following RNA extraction using the TANBead Maelstrom™ 9600 (Taiwan Advanced Nanotech) Instrument with the OptiPure Viral Auto Plate (TANBead, Taiwan) kit. Quantification and detection of SARS-CoV-2 RNA was done using the Allplex 209-nCoV assay on a SeeGene Starlet IVD (SeeGene, Germany) automated platform. VL were then calculated back based on the SARS-CoV-2 standard dilution series of INSTAND (Germany) standards, taking Cycle threshold (CT) values of the two amplified targets into consideration. Viral cultures were attempted mostly for samples with a VL above the RKI (Robert-Koch-Institute) defined threshold of $1 \cdot 10^6$ RNA copies/ml, as chance for culture positivity is minimal in samples below this threshold (Robert-Koch-Institut, 2021a). However, for some samples a viral culture was not possible due to limited lab-capacities. For some samples below the threshold the viral culture was attempted to verify negativity.

2.3. Serologic testing methods/laboratory assays

Serological assays were performed as previously published (Pritsch et al., 2021; Radon et al., 2021). Commercially available assays were conducted following the manufacturer's instructions. For all sample time-points, the following assays were performed: Euroimmun Anti-SARS-CoV-2-ELISA anti-S1 IgG (hereafter called EI-S1-IgG; Euroimmun, Lübeck, Germany), Roche anti-N and Elecsys Anti-SARS-CoV-2 S anti-S1 (hereafter called Ro-N-Ig and Ro-RBD-Ig-quant, respectively; Roche, Mannheim, Germany). Elecsys Anti-SARS-CoV-2 is an immunoassay for the *in vitro* qualitative detection of antibodies using a double-antigen sandwich format. In this format, the capture as well as detection is performed by using respectively labelled antigens. Thus, the assay is antibody subclass agnostic by design. In addition, the SARS-CoV-2 surrogate virus neutralisation test (GS-cPass; GenScript®, Piscataway, New Jersey, USA) was performed. We chose serological assays based on the following criteria: availability in large quantities, enabled for at least semi-automated workup, acceptable pricing, licenced for the use in Europe, and well-described performance (Olbrich et al., 2021).

3. Data analysis

Prior to analysis, data was cleaned and locked. Statistical analysis and visualisation were performed using the software R, version 4.0.5 (https://cloud.r-project.org/). For operational replicates, the first measurement of EI-S1-IgG was used. In the case of Ro-N-Ig and GS-cPass the latest measurement was included, while for Ro-RBD-Ig-quant the most diluted was selected. We report Pearson's correlation coefficient *R* for association among continuous variables. For multiple group comparisons, Kruskal-Wallis tests, followed by post-hoc Dunn tests using the Benjamini Yekutieli adjustment for pairwise comparisons were applied (Yoav and Daniel, 2001).

4. Results

We recruited a total of 51 participants and analysed virological, serological, and clinical data. Table 1 provides an overview of the main demographic and clinical cohort characteristics. 57% (29/51) of the cohort were female with a median age of 32 years (IQR 27–47), while

Table 1

Overview: Cohort characteristics. Response rate of question-naires: 86% (44/51).

Total number of participants	51
Median age in years (IQR)	32 (26–49)
Age distribution in years (%)	
<18	7 (13.7)
18-29	10 (19.6)
30-39	16 (31.4)
40-50	7 (13.7)
>50	11 (21.6)
WHO Grading	
WHO 1 (%)	6 (11.8)
WHO 2 (%)	20 (39.2)
WHO 3 (%)	25 (49.0)
Most common symptoms	
Headache (%)	27 (61.4)
Cough (%)	21 (47.7)
Fatigue (%)	21 (47.7)
Loss of Smell (%)	18 (40.9)
Loss of Taste (%)	18 (40.9)

IQR = Inter Quartile Range; WHO Grading = Grading by WHO Clinical Progression Scale.

43% (22/51) were male with median age of 35 years (IQR 26–51).

4.1. Viral dynamics

Out of 51 participants with an initially documented positive RT-PCR, 82% (42/51) tested RT-PCR positive after recruitment during at least one subsequent visit. Overall, a total of 78 (43%, 78/182) positive samples from different time-points were available for VL assessment. The highest measured VL was $1 \cdot 10^{11}$ copies per mL. Fig. 1 presents the VL dynamics, demonstrating that in our cohort, peak SARS-CoV-2 RNA levels declined rapidly in all but one patient in the first two weeks after symptom onset. One participant was classified as false-positive, as all follow-up RT-PCR tests remained negative and no seroresponse was detected. Five days after symptom onset, 71% (36/51) of the participants were RT-PCR positive and after 10 days, 59% (30/51) were still above the detection limit (~10 copies per mL). The mean VL decreased three orders of magnitude between the first and the second week and four orders of magnitude between the first and third week after symptom onset. After three weeks of STT, 22% (11/51) of the participants were tested positive in the RT-PCR while only 6% (3/38) tested positive after 45 days of STT. All participants tested negative in the RT-PCR after day 61, except one who was still tested positive on day 252. During the whole period, this specific participant had varying positive as well as negative RT-PCRs; and viral sequencing revealed the same strain for the whole follow-up period.

Viral culture was attempted mostly on samples with a VL > 10^6 RNA

copies and could be obtained for 33 samples of 27 patients. Overall, 52% (17/33) of viral culture attempts were successful. 76% (13/17) of these were from samples collected within the first week after symptom onset. Samples with positive and negative viral culture results presented significantly different STT distributions (Fig. 2A, p = 0.0016, STT available for 32 samples). Positive viral cultures were obtained with a median time of 5.0 days after symptom onset. In contrast, swabs resulting in negative cultures were taken at 13.0 days median time after symptom onset. No culture was successful beyond day 22 after symptom onset. Positive samples had significantly higher maximum VLs compared to negative and not attempted cultures (Fig. 2B; KW p = 0.0002; Dunn's post-test: positive-negative p = 0.0084, positive-not attempted p = 0.0003, negative-not attempted P = 0.98; median maximum VL with positive viral culture: $9 \cdot 10^8$ copies/mL; one sample per patient and for three patients the VL was unavailable).

4.2. Demographic and clinical data in correlation with VLs

Data on symptoms at baseline (week 1 of study participation) was available for 86% (44/51) of the participants. Out of 23 different symptoms reported (Supplemental Fig. 1), headache was the most frequent (61.4%, 27/44, range of symptom duration 1–11 days), followed by cough (47.7%, 21/44, 3–11 days), fatigue (47.7%, 21/44, 2–12 days), loss of taste (40.9%, 18/44, 3–120 days), and loss of smell (40.9%, 18/44, 3–120 days) (see also Table 1). Following the WHO scale for disease severity (Table 1), most participants were classified as WHO 2 (20/51, 39%) or 3 (25/51, 49%), with mild or moderate symptoms not requiring hospitalization (Characterisation, 2020). To assess the association between individual participants' characteristics and the course of disease, we correlated VLs with sex (p = 0.27) and age (R = 0.24, p = 0.101), none of which were statistically significant (Fig. 3A and B). Multiple linear regression model showed no significant correlation also in the interaction term between sex and age (F-statistics p = 0.4658; p = 0.266; p = 0.121; p = 0.230, respectively).

Participants graded as WHO 3 had significantly higher VLs compared to those graded as WHO 1/2 (median VLs: 7.45 and 3.78, respectively), demonstrating strong evidence of a significant association between VLs and disease severity (p = 0.01, Fig. 4).

4.3. Serological analysis

Alongside clinical and virological information, the seroresponse at all sample time points for all participants was examined. As participants were included up to four days after their first RT-PCR result, a number of participants were reactive in one or more of the assays at time of study recruitment: 26% for Ro-N-Ig (13/51), 35% for Ro-RBD-Ig-quant (18/51), 18% for El-S1-IgG (9/51), and 59% (30/51) using GS-CPass.

Fig. 5 visualises the association of VL and antibody responses as
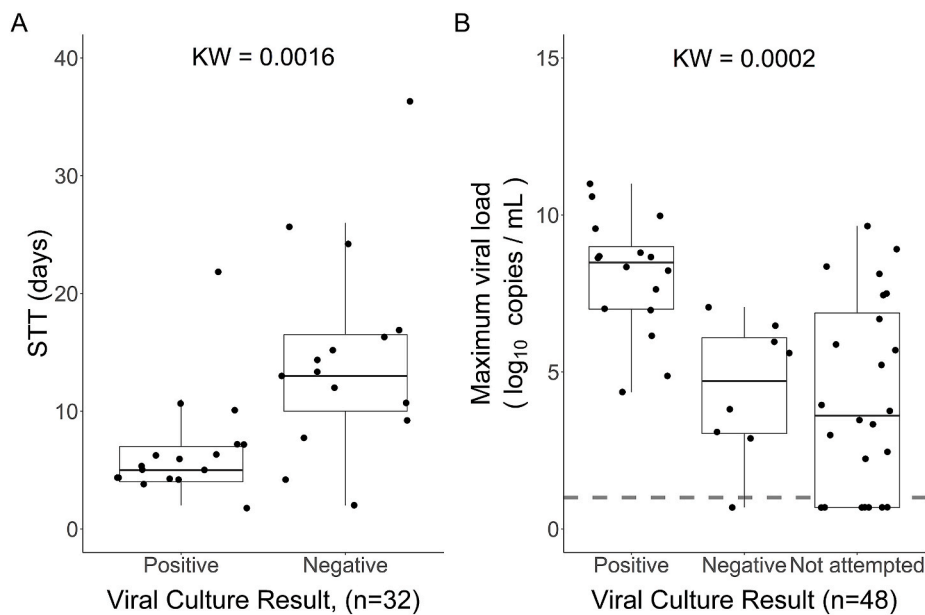

Fig. 1. Viral load (log₁₀ copies per millilitre) over time. Each colour presents one participant, each dot is one sample. The thick black line shows the LOESS estimation (locally estimated scatterplot smoothing or local regression), modelling the VL drop over Symptom to Test Time (STT) in days. The grey region represents the 95% confidence band of the LOESS. In the first week since symptom onset, the median VL was $7.3 \cdot 10^7$ copies per mL and decreased subsequently. (For interpretation of the references to colour in this figure legend, the reader is referred to the Web version of this article.)

Fig. 2. Viral culture result analysis. A: Viral Culture Result and Symptom to Test Time (STT) in days (Kruskal Wallis test = 0.0016, N = 32) for all samples where the viral culture was attempted. Each black dot represents one measurement (n = 32) of 27 patients. A positive viral culture result was characterised by a short STT, and the culture result tended to be negative when STT was high; B: SARS-CoV-2 maximum viral load of each participant and positivity of viral culture (Kruskal-Wallis test = 0.0002). Each black dot represents one patient (n = 48, for three patients no viral load was measured). The grey dashed line represents the detection limit of the VL. Viral culture results were positive when the maximum VLs were high and negative when maximum VLs were low. Positive viral culture results revealed to have significantly different maximum VL distributions compared to negative and not attempted viral cultures (Dunn's post-test = 0.0084 and 0.0003, respectively), while the distributions of negative results and not attempted viral cultures were not significantly different (Dunn's post-test = 0.98).
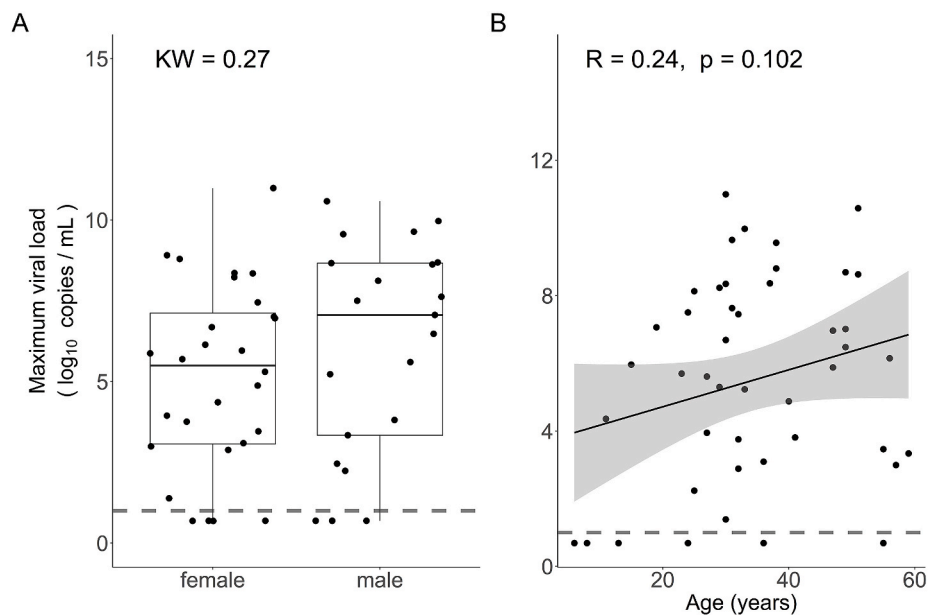
Fig. 3. SARS-CoV-2 maximum viral load and baseline characteristic analysis. Each black dot represents one participant and the grey dashed line represents the detection limit of the VL. Maximum VL and A: Sex (Kruskal-Wallis test = 0.27), without significant difference between females and males. B: Age in years (rho = 0.22, P = 0.14). No significant correlation between age and VLs were detected. The grey area is the 95% confidence band on the linear model (black solid line).

detected in the different assays. The highest antibody titre obtained for each participant correlated positively with VLs (p = 0.022) for Ro-N-Ig. Inhibition in GS-cPass showed a trend towards positive association with VL, without reaching statistical significance (p = 0.15). The other assays did not indicate any associations with maximum VLs (Ro-RBD-Ig-quant p = 0.55; El-S1-IgG p = 0.97). Correlation of seroresponse and disease severity were also assessed, however, as shown in Supplemental Fig. 2, no significant association was observed.

5. Discussion

In this study, we performed in-depth analyses of association between viral, clinical, and serological data over a long-term follow-up in a prospective cohort of SARS-CoV-2 RT-PCR positive individuals. To our

knowledge, this is one of the few studies elucidating the interplay of those factors over an extensive time period in an outpatient setting.

VL decreased fast after the first week of symptoms, suggesting lower infectivity one to two weeks after symptom onset, as described in previous studies (Sui et al., 2021; He et al., 2020). While RT-PCR remains the gold standard for detection of SARS-CoV-2 due to the high sensitivity and specificity, it does not necessarily inform on infectivity as it also detects non-viable virus (Bullard et al., 2020). Understanding how long an individual remains infectious is of major public health interest, informing infection prevention and quarantine durations (Bullard et al., 2020). Detection of culturable virus can be understood as a proxy for infectivity. Consistent with the published literature, probability of a positive viral culture was significantly higher in participants with high VL and short STT in our cohort. No viral culture was successful beyond
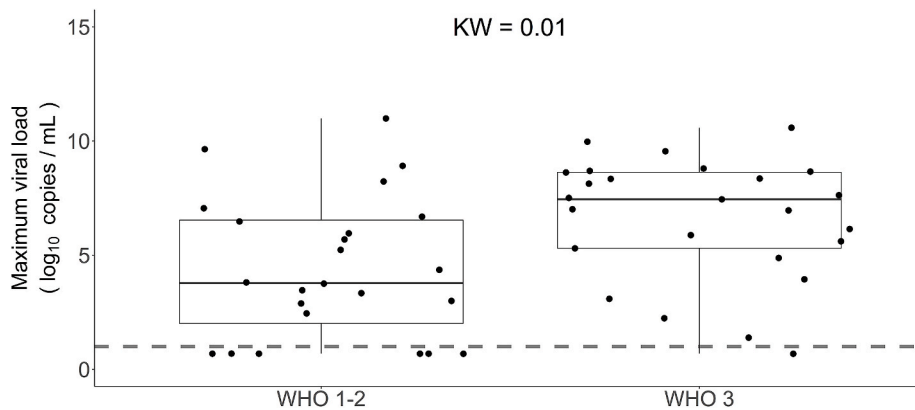
Fig. 4. Viral load and WHO Grading. Maximum VL and WHO Scale 1–2 and 3; WHO 1–2 includes asymptomatic and mildly ill participants (left boxplot) and WHO 3 represents moderate cases without the need of hospitalization (right boxplot). Each black dot represents one participant. The grey dashed line represents the detection limit of the VL. Participants graded as WHO 1 and 2 showed lower VLs than those graded as WHO 3 (Kruskal Wallis test = 0.01).
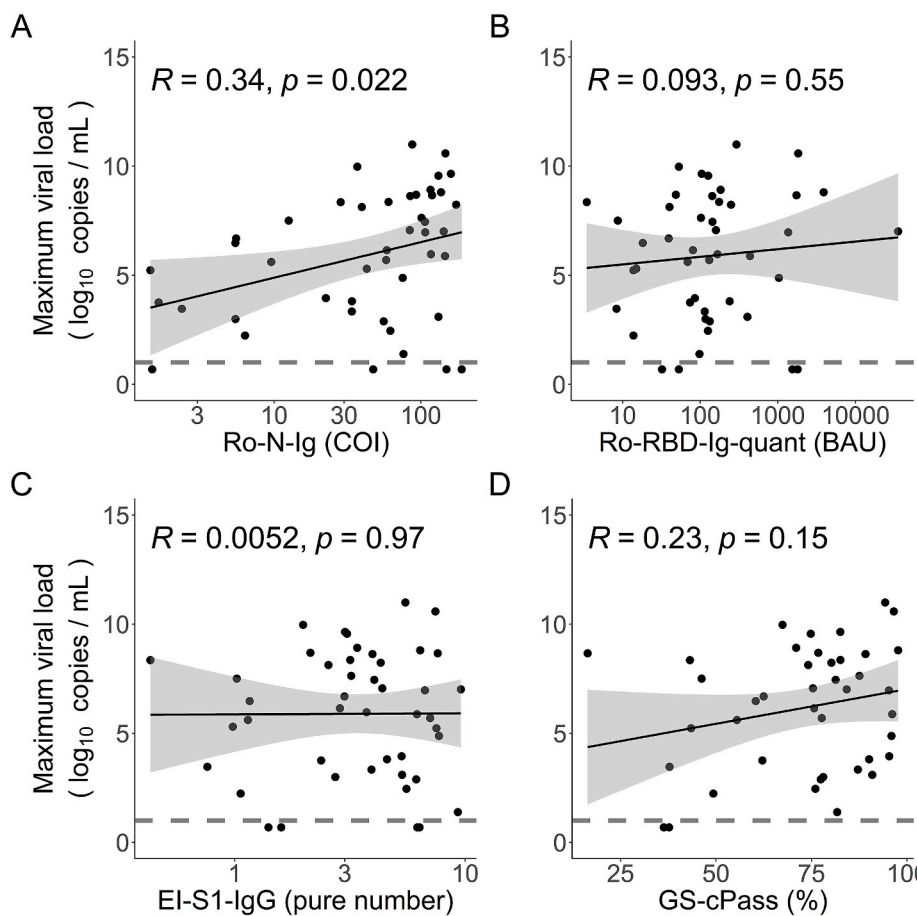
Fig. 5. Maximum viral loads and antibody response. The grey area shows the 95% confidence band of the linear model (black solid line) and the grey dash line represents the detection limit of the VL. Each black dot represents one participant. Correlation of maximum VL with A: Ro-N-Ig (R = 0.34, p = 0.0022): Showing significant positive correlation between maximum VL and highest measured Ro-N-Ig value; B: Ro-RBD-Ig-quant (R = 0.093, p = 0.55): Showing no significant correlation between maximum VL and highest measured Ro-RBD-Ig-quant value; C: El-S1-IgG (R = 0.0052, p = 0.97): Showing no positive correlation between maximum VL and highest measured El-S1-IgG value; D: GS-cPass (R = 0.23, p = 0.15): Showing a trend of positive correlation between maximum VL and highest measured GS-cPass value, although not significant.

week 3 since symptom onset which is in line with published literature (Bullard et al., 2020; Kim et al., 2021).

The adaptive immune response of patients infected with SARS-CoV-2, especially antibody responses and their long-term dynamics, is a topic of great relevance, as antibody levels correlate with protection from (re) infection and are used diagnostically to define previous SARS-CoV-2 exposure. Beside factors such as sex, age, or extent of lung infiltration, VL seems likely to have impact on the time to seropositivity and antibody titers (Masia et al., 2021a). For example, in one study which measured the antibodies IgG, IgA, and IgM, non-seroconverters tended to have lower median VLs than seroconverters (Masia et al., 2021b). The

four serological tests chosen here had different target structures: Elecsys Ro-N-Ig and Ro-RBD-Ig-quant detect nucleocapsid or a shortened spike, respectively, and all binding immunoglobulin isotypes, while El-S1-IgG targets specifically IgG binding to spike S1. In contrast, GS-cPass is a neutralisation surrogate test and assesses the ability to block the interaction between ACE2 and the RBD of spike, regardless of antibody subclass. In our study, higher VLs correlated significantly with the highest signal detected in the Ro-N-Ig assay, however, this was not the case for the other tests evaluated. This might be due to the abundance of the nucleocapsid antigen in the early phases of viral replication, while the appearance of the anti-S response leads to quick viral control. Here,

the functional neutralisation seems to be more relevant than the titre. This is in line with GS-cPass as functional assay showing a trend to correlation with VL as well. Significance might be reached with better statistical power (larger sample size). Our cohort also includes only outpatients with mild disease severity.

The clinical presentation of SARS-CoV-2 has been described extensively, and it is assumed that infection mostly causes symptoms of common cold such as cough and fever, while severe cases of pneumonia occur in 1% of cases (Robert-Koch-Institut, 2021b; Menni et al., 2020). In this cohort, most participants were asymptomatic- or oligosymptomatic, reporting cough, loss of taste, and loss of smell as the predominant symptoms. This is in accordance with the reports by the Robert Koch Institute (RKI) (Robert-Koch-Institut, 2021b) where most clinical manifestations resolve in the first two weeks after symptom onset. In other studies, loss of smell and loss of taste persisted for up to 4 months and patients with anosmia are likely to recover within 12 months (Robert-Koch-Institut, 2021b; Renaud et al., 2021). This was also observed in two participants in this study.

In our cohort, there was a non-significant trend of higher VLs in male compared to female participants, a finding also described in other studies (Mahallawi et al., 2021; He et al., 2020). Age is reportedly another demographic factor potentially impacting VL, with higher VLs found in older patients and respectively lower VLs in younger individuals (Masia et al., 2021b; Westblade et al., 2020; Pradhan and Olsson, 2020). In our cohort, younger participants tended to have lower VLs, although this observation was not significant. This could be explained by the composition of the cohort, as the median age in years was 32 and only 6% (3/51) of the participants were above 60 years of age. There are ambiguous descriptions regarding an association between VL and severity of disease in published studies. Some studies report a strong association between higher SARS-CoV-2 VL and increasing disease severity (Wang et al., 2020a; Fajnzylber et al., 2020), while others do not find this association (He et al., 2020; Jacot et al., 2020). This might be explained by the time point chosen for VL-assessment, Munker et al. described no difference at admission but saw a significantly higher VL in severely ill patients two weeks following admission (Munker et al., 2021). In our analyses, we used the highest measured VL for each participant and observed a significant correlation with disease severity classified by WHO grading. Munker et al. demonstrated that the site of sampling may influence the magnitude of VLs and disease severity. In their study, samples collected from the lower respiratory tract, especially in severe cases, exhibited higher VL (Munker et al., 2021). However, we focused on upper respiratory samples and bronchial tract samples were not analysed in this study.

Our study has important limitations: Firstly, we have a relatively small sample size of 51 individuals in our cohort. Secondly, due to the study design, participants were recruited at different time points after infection, likely missing the acute phase with highest VLs in some. Thirdly, we did no radiological analysis and have no information about VLs in the lungs.

This study demonstrates that positive viral culture results have high VLs and low STT suggesting increased infectivity in that time range, an essential information for the containment of the SARS-CoV-2 pandemic. Furthermore, lower peak VLs suggest a lower magnitude of seropositivity mainly for anti-N. This data is consistent with published literature and confirms the guidelines for isolation, testing strategies and contact tracing. While the analyses presented here contribute to a deeper understanding of viral, serological, and clinical features of SARS-CoV-2-infection during the acute phase and the first year following infection, further studies with larger cohorts are needed.

CRediT authorship contribution statement

Kerstin Puchinger: Formal analysis, Conceptualization, Writing – original draft, Resources. **Noemi Castelletti:** Data curation, Visualization, Formal analysis, Software, Writing – original draft, Validation, Conceptualization. **Raquel Rubio-Acero:** Resources. **Christof Geldmacher:** Writing – review & editing, Conceptualization. **Tabea M. Eser:** Resources. **Flora Deák:** Resources. **Ivana Paunovic:** Resources. **Abhishek Bakuli:** Software. **Elmar Saathoff:** Resources. **Alexander von Meyer:** Resources. **Alisa Markgraf:** Resources. **Philine Falk:** Resources. **Jakob Reich:** Resources. **Friedrich Riess:** Resources. **Philipp Girl:** Resources. **Katharina Müller:** Resources. **Katja Radon:** Resources. **Jessica Michelle Guggenbuehl Noller:** Resources. **Roman Wölfel:** Resources. **Michael Hoelscher:** Investigation, Funding acquisition. **Inge Kroidl:** Conceptualization, Supervision, Project administration, Methodology, Data curation, Funding acquisition, Writing – review & editing, Investigation. **Andreas Wieser:** Conceptualization, Methodology, Writing – review & editing, Investigation, Funding acquisition. **Laura Olbrich:** Conceptualization, Supervision, Project administration, Methodology, Data curation, Funding acquisition, Writing – review & editing, Investigation.

Declaration of competing interest

The authors declare the following financial interests/personal relationships which may be considered as potential competing interests:

AW and MH (on the behalf of the institute) report personal fees and non-financial support from Roche Diagnostics, LO reports non-financial support from Roche Diagnostics. AW, MH and LO report non-financial support from Euroimmun, non-financial support from Viramed, non-financial support from Mikrogen. AW, MH, LO report grants, non-financial support and other from German Center for Infection Research (DZIF), grants and non-financial support from Government of Bavaria, non-financial support from BMW, non-financial support from Munich Police, non-financial support and other from Accenture. MH and AW report non-financial support from Dr. Becker MVZ during the conduct of the study. In addition, MH and AW have a patent on a sample system for sputum diagnostics of SARS-CoV-2 pending.

Data availability

Data will be made available on request.

Ute Eberle, Judith Eckstein, Jonathan Frese, Felix Forster, Turid Frahnow, Günter Fröschl, Otto Geisenberger, Kristina Gillig, Arlett Heiber, Christian Hinske, Janna Hoefflin, Tim Hofberger, Michael Höfinger, Larissa Hofmann, Sacha Horn, Kristina Huber, Christian Janke, Ursula Kappl, Charlotte Kiani, Arne Kroidl, Michael Laxy, Reiner Leidl, Felix Lindner, Rebecca Mayrhofer, Anna-Maria Mekota, Hannah Müller, Dafni Metaxa, Leonie Pattard, Michel Pletschette, Stephan Prückner, Konstantin Pusl, Elba Raimúndez, Camila Rothe, Nicole Schäfer, Paul Schandelmaier, Lara Schneider, Sophie Schultz, Mirjam Schunk, Lars Schwettmann, Heidi Seibold, Peter Sothmann, Paul Stapor, Fabian Theis, Verena Thiel, Sophie Thiesbrummel, Niklas Thur, Julia Waibel, Claudia Wallrauch, Simon Winter, Julia Wolff, Pia Wullinger, Houda Yaqine, Sabine Zange, Eleftheria Zeggini, Thomas Zimmermann, Anna Zielke, Mohamed Ibraheem Mohamed Ahmed, Marc Becker, Paulina Diepers, Yannik Schälte, Mercè Garí, Peter Pütz, Michael Pritsch, Volker Fingerle, Ronan Le Gleut, Leonard Gilberg, Isabel Brand, Max Diefenbach, Tabea Eser, Franz Weinauer, Silke Martin, Ernst-Markus Quenzel, Jürgen Durner, Philipp Girl, Katharina Müller, Katja Radon, Christiane Fuchs, Jan Hasenauer.

Appendix A. Supplementary data

Supplementary data to this article can be found online at https://doi.org/10.1016/j.virol.2022.02.002.

References

Bullard, J., et al., 2020. Predicting infectious severe acute respiratory Syndrome coronavirus 2 from diagnostic samples. Clin. Infect. Dis. 71 (10), 2663–2666.

Carvalho, T., Krammer, F., Iwasaki, A., 2021. The first 12 months of COVID-19: a timeline of immunological insights. Nat. Rev. Immunol. 21 (4), 245–256.

Characterisation, W.H.O.W.G.o.t.C. and C.-i. Management of, A minimal common outcome measure set for COVID-19 clinical research. Lancet Infect. Dis. 20 (8), 2020, e192–e197.

Fajnzylber, J., et al., 2020. SARS-CoV-2 viral load is associated with increased disease severity and mortality. Nat. Commun. 11 (1), 5493.

He, X., et al., 2020. Temporal dynamics in viral shedding and transmissibility of COVID-19. Nat. Med. 26 (5), 672–675.

Jacot, D., et al., 2020. Viral load of SARS-CoV-2 across patients and compared to other respiratory viruses. Microb. Infect. 22 (10), 617–621.

Jefferson, T., et al., 2020. Viral Cultures for COVID-19 Infectious Potential Assessment – a Systematic Review. Clinical Infectious Diseases.

Jin, C.C., et al., 2020. Correlation between viral RNA shedding and serum antibodies in individuals with coronavirus disease 2019. Clin. Microbiol. Infect. : Off. Publ. Eur. Soc. Clin. Microbiol. Infect. Dis. 26 (9), 1280–1282.

Kim, M.-C., et al., 2021. Duration of Culturable SARS-CoV-2 in Hospitalized Patients with Covid-19, vol. 384, pp. 671–673, 7.

Mahallawi, W.H., et al., 2021. Association of viral load in SARS-CoV-2 patients with age and gender. Front. Med. 8, 608215.

Marshall, J.C., et al., 2020. A minimal common outcome measure set for COVID-19 clinical research. Lancet Infect. Dis. 20 (8), e192–e197.

Masia, M., et al., 2021a. SARS-CoV-2 seroconversion and viral clearance in patients hospitalized with COVID-19: viral load predicts antibody response. Open Forum Infect. Dis. 8 (2), ofab005.

Masia, M., et al., 2021b. SARS-CoV-2 seroconversion and viral clearance in patients hospitalized with COVID-19: viral load predicts antibody response. Open Forum Infect. Dis. 8 (2), ofab005.

Menni, C., et al., 2020. Real-time tracking of self-reported symptoms to predict potential COVID-19. Nat. Med. 26 (7), 1037–1040.

Munker, D., et al., 2021. Dynamics of SARS-CoV-2 shedding in the respiratory tract depends on the severity of disease in COVID-19 patients. Eur. Respir. J. 58 (1).

Olbrich, L., et al., 2021. Head-to-head Evaluation of Seven Different Seroassays Including Direct Viral Neutralisation in a Representative Cohort for SARS-CoV-2, vol. 102, 10.

Pradhan, A., Olsson, P.E., 2020. Sex differences in severity and mortality from COVID-19: are males more vulnerable? Biol. Sex Differ. 11 (1), 53.

Pritsch, M., et al., 2021. Prevalence and risk factors of infection in the representative COVID-19 cohort Munich. Int. J. Environ. Res. Publ. Health 18 (7).

Radon, K., et al., 2021. From First to Second Wave: Follow-Up of the Prospective Covid-19 Cohort (KoCo19) in Munich (Germany). https://doi.org/10.1101/2021.04.27.21256133.

Renaud, M., et al., 2021. Clinical outcomes for patients with anosmia 1 Year after COVID-19 diagnosis. JAMA Netw. Open 4 (6), e2115352.

Robert-Koch-Institut, 2021a. COVID-19-Diagnostik [cited 2021 14.10.2021]; Available from: www.rki.de/covid-19-diagnostik.

Robert-Koch-Institut, 2021b. Epidemiologischer Steckbrief zu SARS-CoV-2 und COVID-19 [cited 2021 03.12.201]; Available from: https://www.rki.de/DE/Content/InfAZ/N/Neuartiges_Coronavirus/Steckbrief.html.

Rothe, C., et al., 2020. Transmission of 2019-nCoV infection from an asymptomatic contact in Germany. N. Engl. J. Med. 382 (10), 970–971.

Sui, Z., et al., 2021. Viral dynamics and antibody responses in people with asymptomatic SARS-CoV-2 infection. Signal Transduct. Targeted Ther. 6 (1), 181.

Sun, J., et al., 2020. COVID-19: epidemiology, evolution, and cross-disciplinary perspectives. Trends Mol. Med. 26 (5), 483–495.

van Kampen, J.J.A., et al., 2021. Duration and key determinants of infectious virus shedding in hospitalized patients with coronavirus disease-2019 (COVID-19). Nat. Commun. 12 (1), 267.

Wang, Y., et al., 2020a. Kinetics of viral load and antibody response in relation to COVID-19 severity. J. Clin. Invest. 130 (10), 5235–5244.

Wang, X., et al., 2020b. Long-term existence of SARS-CoV-2 in COVID-19 patients: host immunity, viral virulence, and transmissibility. Virol. Sin. 35 (6), 793–802.

Wellinghausen, N., et al., 2020. SARS-CoV-2-IgG response is different in COVID-19 outpatients and asymptomatic contact persons. J. Clin. Virol. : Off. Publ. Pan Am. Soc. Clin. Virol. 130, 104542-104542.

Westblade, L.F., et al., 2020. SARS-CoV-2 viral load predicts mortality in patients with and without cancer who are hospitalized with COVID-19. Cancer Cell 38 (5), 661–671.e2.

Wölfel, R., et al., 2020. Virological assessment of hospitalized patients with COVID-2019. Nature 581 (7809), 465–469.

Yoav, B., Daniel, Y., 2001. The control of the false discovery rate in multiple testing under dependency. Ann. Stat. 29 (4), 1165–1188.

Zhou, P., et al., 2020. A pneumonia outbreak associated with a new coronavirus of probable bat origin. Nature 579 (7798), 270–273.

Publication 7:

Head-to-head evaluation of seven different seroassays including direct viral neutralisation in a representative cohort for SARS-CoV-2

Laura Olbrich*, **Noemi Castelletti***, Yannik Schälte*, Mercè Garí*, Peter Pütz, Abhishek Bakuli, Michael Pritsch, Inge Kroidl, Elmar Saathoff, Jessica Michelle Guggenbuehl Noller, Volker Fingerle, Ronan Le Gleut, Leonard Gilberg, Isabel Brand, Philine Falk, Alisa Markgraf, Flora Deák, Friedrich Riess, Max Diefenbach, Tabea Eser, Franz Weinauer, Silke Martin, Ernst-Markus Quenzel, Marc Becker, Jürgen Durner, Philipp Girl, Katharina Müller, Katja Radon, Christiane Fuchs, Roman Wölfel+, Jan Hasenauer+, Michael Hoelscher+, Andreas Wieser+, On Behalf Of The KoCo-Study Group

Head-to-head evaluation of seven different seroassays including direct viral neutralisation in a representative cohort for SARS-CoV-2

Laura Olbrich[1,2]†, Noemi Castelletti[1,3]†, Yannik Schälte[4,5]†, Mercè Garí[4]†, Peter Pütz[4,6], Abhishek Bakuli[1], Michael Pritsch[1], Inge Kroidl[1,2], Elmar Saathoff[1,2], Jessica Michelle Guggenbuehl Noller[1], Volker Fingerle[2,7], Ronan Le Gleut[4,8], Leonard Gilberg[1], Isabel Brand[1], Philine Falk[1], Alisa Markgraf[1], Flora Deák[1], Friedrich Riess[1], Max Diefenbach[1], Tabea Eser[1], Franz Weinauer[9], Silke Martin[9], Ernst-Markus Quenzel[9], Marc Becker[10,11], Jürgen Durner[10,11], Philipp Girl[2,12], Katharina Müller[2,12], Katja Radon[13,14,15], Christiane Fuchs[4,5,6,8], Roman Wölfel[2,12]†, Jan Hasenauer[4,5,16]†, Michael Hoelscher[1,2,14]†, and Andreas Wieser[1,2,*,†] on behalf of the KoCo19-Study Group

Abstract

A number of seroassays are available for SARS-CoV-2 testing; yet, head-to-head evaluations of different testing principles are limited, especially using raw values rather than categorical data. In addition, identifying correlates of protection is of utmost importance, and comparisons of available testing systems with functional assays, such as direct viral neutralisation, are needed. We analysed 6658 samples consisting of true-positives (n=193), true-negatives (n=1091), and specimens of unknown status (n=5374). For primary testing, we used Euroimmun-Anti-SARS-CoV-2-ELISA-IgA/IgG and Roche-Elecsys-Anti-SARS-CoV-2. Subsequently virus-neutralisation, GeneScriptcPass, VIRAMED-SARS-CoV-2-ViraChip, and Mikrogen-*recom*Line-SARS-CoV-2-IgG were applied for confirmatory testing. Statistical modelling generated optimised assay cut-off thresholds. Sensitivity of Euroimmun-anti-S1-IgA was 64.8%, specificity 93.3% (manufacturer's cut-off); for Euroimmun-anti-S1-IgG, sensitivity was 77.2/79.8% (manufacturer's/optimised cut-offs), specificity 98.0/97.8%; Roche-anti-N sensitivity was 85.5/88.6%, specificity 99.8/99.7%. In true-positives, mean and median Euroimmun-anti-S1-IgA and -IgG titres decreased 30/90 days after RT-PCR-positivity, Roche-anti-N titres decreased significantly later. Virus-neutralisation was 80.6% sensitive, 100.0% specific (≥1:5 dilution). Neutralisation surrogate tests (GeneScriptcPass, Mikrogen-*recom*Line-RBD) were >94.9% sensitive and >98.1% specific. Optimised cut-offs improved test performances of several tests. Confirmatory testing with virus-neutralisation might be complemented with GeneScriptcPass™ or *recom*Line-RBD for certain applications. Head-to-head comparisons given here aim to contribute to the refinement of testing strategies for individual and public health use.

INTRODUCTION

In December 2019, a cluster of atypical pneumonia of unknown origin was described in the region of Wuhan, Hubei province, China. Subsequently, a previously unknown coronavirus was identified as the causative agent: SARS-CoV-2 (Severe Acute Respiratory Syndrome Coronavirus 2) [1]. As the virus spread rapidly across the globe, the Corona Virus Disease 2019 (COVID-19) was declared a pandemic on 12 March 2020.

Direct detection of viral nucleic acids or the virus itself in bodily fluids is considered the reference standard for diagnosis of acute infection. It is primarily performed using nasopharyngeal swabs or other respiratory samples [2]. Additionally, serodiagnostics are valuable to identify past infections, asymptomatic or symptomatic, and to elucidate transmission dynamics within populations. Both are highly relevant to inform evidence-based political decision making [3, 4].

Several serological test systems have been introduced since the beginning of the SARS-CoV-2 pandemic [5]. Most target one of two specific viral structures: parts of the trimeric CoV spike (S1-2) complex, or the nucleocapsid (N) protein [6]. While the receptor binding domain (RBD) of S1 binds to the angiotensin-converting enzyme 2 (ACE2) as a receptor, the N-protein is involved in viral assembly and replication [7]. Head-to-head comparisons evaluating qualitative assay performances have been described, yet mostly with limited additional workup and sample characterisation [8–11]. Some authors have proposed adapted cut-off thresholds to increase assay performance, depending on application and local epidemiology [4, 12].

Here, we present a head-to-head cross-comparison of seven independent tests. We screened with Euroimmun Anti-S1-SARS-CoV-2-ELISA-IgA and -IgG and Elecsys Anti-SARS-CoV-2 Roche N pan–Ig and confirmed with direct viral neutralisation, GeneScriptcPass, Mikrogen-*recom*Line-RBD IgG line immunoassay, and VIRAMED-SARS-CoV-2-ViraChip microarray. The tests were conducted on a total of 6658 samples from (i.) RT-PCR positive individuals (true-positives), (ii.) blood donors from the pre-COVID-19 era (true-negatives), and (iii.) subjects with unknown disease status from a representative population cohort in Munich (KoCo19; unknown serostatus) [13]. We were able to generate reliable performance estimates for both primary and confirmatory tests by using true-positive and true-negative individuals and hereby generate optimised cut-offs.

METHODS

Study design and participants

Samples are derived from the representative COVID-19 Cohort Munich (KoCo19), a prospective sero-incidence study initiated in Munich, Germany, in April 2020 [13, 14]. For this study, we tested 6658 samples, including a set of SARS-CoV-2 RT-PCR positives ('true-positives', *n*=193), individuals from historical cohorts, blood donors without any indication

Impact statement

We present an evaluation of seven serological SARS-CoV-2 tests used as screening or confirmation tests in a large, well-defined cohort including true-positive and true-negative individuals, as well as subjects with unknown SARS-CoV-2 status. A total of 6658 individual samples were derived from the Representative COVID-19 Cohort Munich (KoCo19), a prospective seroincidence study initiated in Munich, Germany, in a low-prevalence setting of a large German city, not considered a specific 'hot-spot' at time of sampling. This comprehensive collection allowed us to correlate the different tests to identify concordance as well as discordance for the individual samples. This also enabled the evaluation of confirmatory test systems, like direct virus-neutralisation or the recently FDA-approved GeneScriptcPassTM, compared to different serological tests, including receptor binding domain (RBD)-based assays. In addition, we assessed their overall performances in KoCo19, and adjusted cut-offs; furthermore, we analysed the seroconversion rate in patients with a history of positive RT-PCR.

of SARS-CoV-2 infection ('true-negatives', *n*=1091), and specimen of unknown status (*n*=5374); details on the cohort characteristics, including collection time points, can be found in the appendix (p.1; Table S1, available in the online version of this article).

The study was approved by the Ethics Committee of the Faculty of Medicine at LMU Munich (20–275 V), the protocol is available online (www.koco19.de) [13]. Informed consent was obtained prior to any study investigations where applicable. The study is registered in the German Clinical Trials Register (DRKS00021698; https://www.drks.de/drks_web/navigate.do?navigationId=trial.HTML&TRIAL_ID= DRKS00021698).

Laboratory assays

All described analyses were performed using EDTA-plasma samples (appendix pp.1 for further details on assays performed, and Table S3 for details on platforms and units applied).

Euroimmun Anti-SARS-CoV-2-ELISA anti-S1 IgA/IgG (called EI-S1-IgG, EI-S1-IgA; Euroimmun, Lübeck, Germany) test kits were used according to the manufacturer's instructions. Measurement values were obtained using the quotient of the optical density measurement provided by the manufacturer's software. We evaluated Elecsys Anti-SARS-CoV-2 Roche anti-N pan-Ig (hereafter called Ro-N-Ig; Roche, Mannheim, Germany) in accordance with the manufacturer's guidelines. Values reported are the Cut-Off-Index (COI) of the individual samples. Operative replicates of the same samples were performed to assess reliability of primary assay performance.

For confirmatory testing, we conducted micro-virus neutralisation assays (NT) as described previously [15], with the exception that confluent cells were incubated instead of adding cells following neutralisation reaction (appendix pp.1). We classified samples with a titre <1:5 as 'NT-negative' and samples with a titre ≥1:5 as 'NT-positive'. The dilution steps indicated are <5, 5, 10, 20, 40 and >80.

SARS-CoV-2 surrogate virus neutralisation test (GS-cPass; GenScript, Piscataway, New Jersey, USA) was used to measure binding inhibition, according to the manufacturer's instructions. The inhibition was calculated in percentages, ranging from −30 to 100.

For SARS-CoV-2 ViraChip microarray (VIRAMED Biotech AG, Planegg, Germany; hereafter named VC-N-IgA/IgM/IgG; VC-S1-IgA/IgM/IgG; VC-S2-IgA/IgM/IgG) execution followed the manufacturer's instructions. We obtained measurement values by the automated ELISA-processor in arbitrary units.

We conducted the *recom*Line SARS-CoV-2 IgG line immunoassay (MG-S1, MG-N, MG-RBD; Mikrogen, Neuried, Germany) as outlined by the manufacturer. Values below the cut-off of 1 were categorised as 'negative' without quantitative information.

Statistical analysis

Prior to analysis, we cleaned and locked the data. For the analyses and visualisation, we used the software R, version 4.0.2. Only one sample per subject was included in the statistical analyses; in the case of individuals with multiple blood samples, we only considered the sample with the most complete dataset. For multiple measurements with complete datasets, we only included the first measurement; for operational replicates we used the latest one. We subsequently carried out sensitivity and specificity analyses for true-negative and true-positive samples over all the tests performed.

We report square roots R of coefficients of determination for association among continuous variables. For paired sample comparisons, we applied Wilcoxon-sign-rank tests, whereas for multiple group comparisons we applied Kruskal-Wallis tests, followed by post-hoc Dunn tests using the Benjamini-Yekutieli adjustment for pairwise comparisons [16].

Using true-positives and true-negatives, we determined optimised cut-off thresholds and their confidence intervals by a nonparametric bootstrap. In a similar way, we trained random forest and support vector machine classifiers. We calculated estimates for sensitivities, specificities, and overall prediction accuracies for all considered cut-off values and classifiers. This calculation was done on out-of-sample observations to avoid overfitting and thus overoptimistic performance measures. Details on the algorithms are outlined in the appendix (pp.3).

Data and code sharing

Data are accessible subject to data protection regulations upon reasonable request to the corresponding author. To facilitate reproducibility and reuse, the code used to perform the analyses and generate the figures was made available on GitHub (https://github.com/koco19/lab_epi) and has been uploaded to ZENODO (is https://doi.org/10.5281/zenodo.4699432) for long-term storage.

RESULTS

We assessed SARS-CoV-2 antibodies in a total of 6658 independent samples using Euroimmun Anti-SARS-CoV-2-ELISA anti-S1 IgA (henceforth called EI-S1-IgA; *n*=6657), Euroimmun Anti-SARS-CoV-2-ELISA anti-S1 IgG (EI-S1-IgG; *n*=6658), and Elecsys Anti-SARS-CoV-2 Roche anti-N pan-Ig (Ro-N-Ig; *n*=6636) (details on cohort and sample characteristics are outlined in Fig. S1, Table S1). Sensitivity and specificity estimates of both primary and confirmatory tests of manufacturer and optimised cut-offs are shown in Tables 1 and S2 features an overview of all tests performed.

Performance of primary tests

Sensitivity and specificity of EI-S1-IgA were 64.8 and 93.3% when applying the manufacturer's cut-off. Optimising the cut-off through statistical learning (see Methods) did not improve EI-S1-IgA performance (sensitivity 64.8%, specificity 92.6%). For EI-S1-IgG, the sensitivity of 77.2 % (manufacturer's cut-off) was increased to 79.8% (optimised cut-off), while the specificity remained similar at 98.0/97.8 % (manufacturer's/optimised cut-off; Table 1). The distribution of results for the EI-assays is depicted in Fig. 1. Raw values for EI-S1-IgA show a slightly asymmetric but unimodal distribution for the overall population, while EI-S1-IgG raw values present with a second clearly distinct positive population. EI-S1-IgA classified 65% of the true-positives correctly as positive and 7% of the true-negatives incorrectly as positive, while EI-S1-IgG classified 80% of the true-positives correctly and 2% of the true-negatives incorrectly. A total of 61% of the true-positives were identified correctly by both tests unanimously.

The sensitivity of Ro-N-Ig with the manufacturer's cut-off was 85.5%, and was increased to 88.6% by applying an optimised cut-off, similarly to EI-S1-IgG. Specificity was similar with both cut-offs at 99.8/99.7 % (manufacturer's/optimised cut-off; Table 1). Ro-N-Ig raw values (Cut-off index, COI) demonstrate a narrow distribution with the bulk of values in the range COI 0.1 and below, whereas a clearly separated second population above COI 10 was observed. For EI-S1-IgG and Ro-N-Ig, the cut-offs separate the subpopulations more reliably than for EI-S1-IgA (Fig. 1).

For evaluation of primary test concordance, we excluded EI-S1-IgA due to inferior performance in sensitivity and specificity. The concordance between EI-S1-IgG and Ro-N-Ig was 98.5% (6538/6636). From the whole sample set, 4.0% (264/6636) were unanimously classified as positive while 94.5% (6274/6636) were classified as negative, of these 88.1% (5846/6635) tested negative in all three tests (being 93.2% (5846/6274) of those negative in Ro-N-Ig+EI-S1-IgG). The remaining 1.5% of samples (98/6636) were classified

Table 1. Manufacturer's and optimised cut-offs, sensitivity, specificity and accuracy

Evaluation of diagnostic accuracy of primary tests was conducted with samples from true-positives (*n*=193) and true-negatives (*n*=1073); subsequently, optimised cut-offs were applied to the KoCo19-cohort samples (see Methods).

Sample composition True pos. / true neg.	Test	Manuf.'s cut-off	Optimised cut-off [CI]	Sensitivity [%] (Manuf.'s / Optim. cut-off)	Specificity [%] (Manuf.'s / Optim. cut-off)	Overall accuracy [%] (Manuf.'s / Optim. cut-off)
193/1073	EI-S1-IgA	1.100	1.085 [0.855; 1.705]	64.77/64.77	93.29/92.64	88.94/88.39
193/1073	EI-S1-IgG	1.100	1.015 [0.850; 1.395]	77.20/79.79	98.04/97.76	94.87/95.02
193/1073	Ro-N-Ig	1.000	0.422 [0.295; 0.527]	85.49/88.60	99.81/99.72	97.63/98.03
107/106	NT	–	5.0*	- / 73.83	- / 100.00	- / 86.85
108/106	GS-cPass	20.000	20.538 [13.768; 24.241]	96.30/96.30	100.00/99.06	98.13/97.66
108/111	VC-N-IgG	100.000	18.500 [13.500; 23.000]	39.81/93.52	99.10/91.89	69.86/92.69
108/111	VC-S1-IgG	100.000	10.000 [10.000; 10.000]	65.74/95.37	100.00/100.00	83.11/97.72
108/111	VC-S2-IgG	100.000	10.000 [10.000; 10.000]	17.59/63.89	100.00/99.10	59.36/81.74
78/106	MG-N	1.000	1.000 [1.000; 1.600]	94.87/94.87	98.11/98.11	96.74/96.74
78/106	MG-RBD	1.000	1.000 [1.000; 1.000]	94.87/94.87	100.00/100.00	97.83/97.83
78/106	MG-S1	1.000	1.000 [1.000; 1.000]	96.15/96.15	100.00/100.00	98.37/98.37
193/1073	Random Forest	–	–	88.60†	99.81†	98.10†
193/1073	Support Vector Machine	–	–	84.46†	99.91†	97.47†

*For NT, dilutions starting at 1:5 were used; see Methods.
†The random forest and the support vector machine combine all three primary tests, the accuracy measures thus do not relate to specific cut-offs.

discordantly. Of these, 56.1% (55/98) were rated as positive by EI-S1-IgG and as negative by Ro-N-Ig (Fig. 2a), while the remaining 43.9% (43/98) were rated as negative by EI-S1-IgG and as positive by Ro-N-Ig.

We investigated seropositivity following positive RT-PCR using one measurement per subject (Fig. 3). EI-S1-IgA titres were found to decline >30 days (*P*=0.01), with only 65% being positive at the last interval, while EI-S1-IgG remained stable over the time period (*P*=0.85). In contrast, antibody levels measured with Ro-N-Ig increased over time (*P*<0.001).

Performance of confirmatory tests

We subjected a sample subset (*n*=362; composition see Fig. S1) to confirmatory testing; the overall confirmatory test performance is presented in Fig. 4 and Table 1. The sensitivity of direct neutralisation titres (NT; 1:5 dilution) was 80.6%,
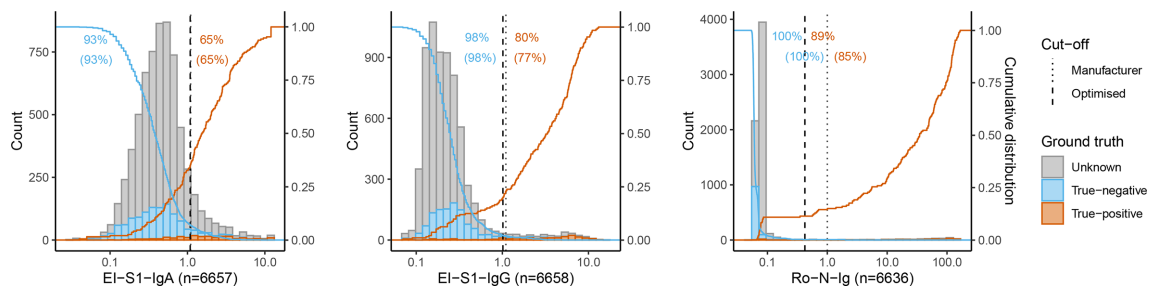
Fig. 1. Performance of primary tests. Results of primary tests for true-negatives (*blue*), true-positives (*orange*), and individuals with unknown SARS-CoV-2 status (*grey*). Absolute number of subjects (count/*y-axis*) and distribution of raw values (*x-axis*) measured for EI-S1-IgA (*left*), EI-S1-IgG (*centre*), and Ro-N-Ig (*right*). Dotted lines mark the manufacturer's cut-off value (between indeterminate and positive for EI, and between negative and positive in Ro). Dashed lines mark the optimised cut-off value as determined in this study (overlapping with the dotted line for EI-S1-IgA). Orange and blue solid lines represent the percentage of test results for true-positives and true-negatives above (*blue*) or below (*orange*) the value on the x-axes, respectively. Orange and blue numbers give the percentages of true-positives and true-negatives that were correctly detected by the test (within brackets: manufacturers' cut-offs; without brackets: optimised cut-offs).
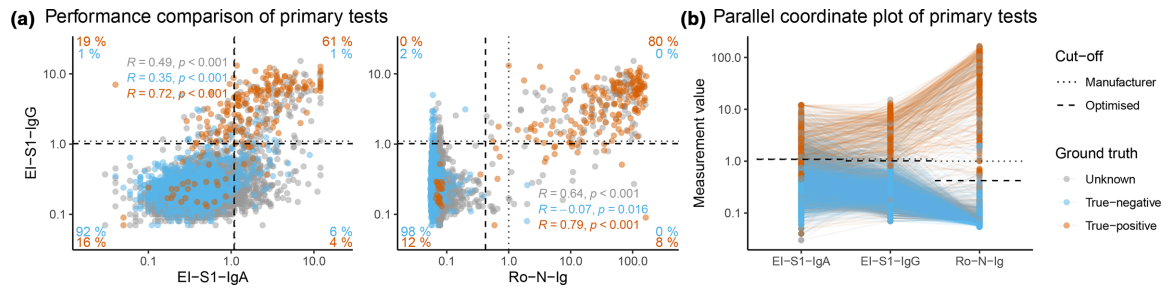
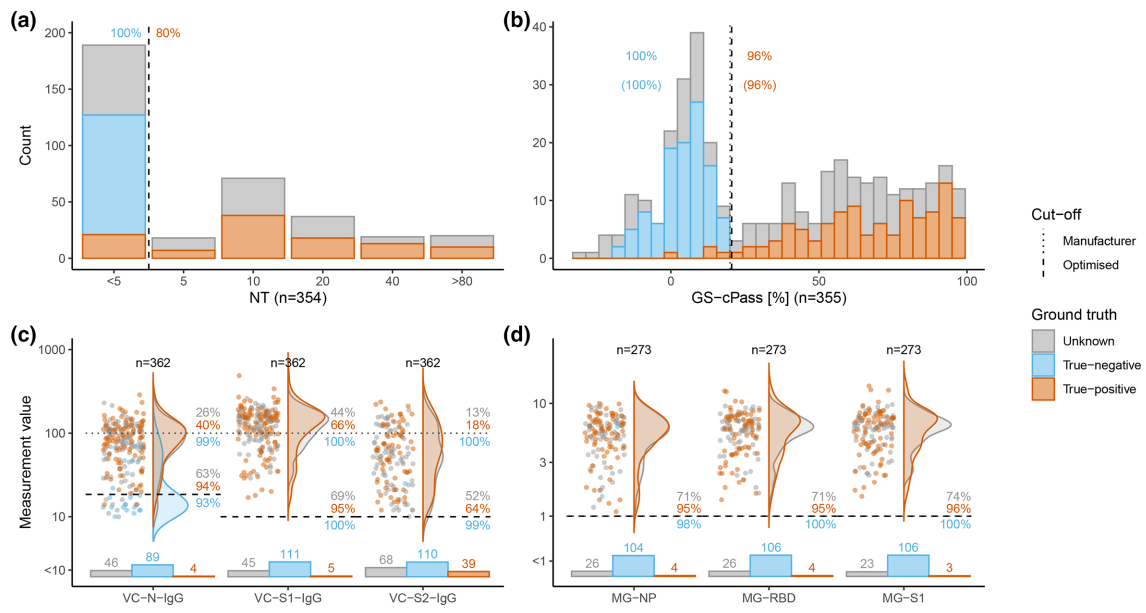**Fig. 2.** Comparison of primary tests. Results of primary tests compared to ground truth for true-negatives (*blue*), true-positives (*orange*), and individuals with unknown SARS-CoV-2 status (*grey*). The dotted lines represent the manufacturer's cut-offs, the dashed lines the optimised cut-offs defined within this study. (a) Pairwise scatter plots for EI-S1-IgA vs. EI-S1-IgG (left; *n*=6657), and Ro-N-Ig vs. EI-S1-IgG (right; *n*=6636). Percentages in orange indicate fractions of true-positives in the respective quadrant with respect to all true-positives; blue for true-negatives. Percentages were calculated using the optimised cut-off. (b) Parallel coordinate plot of the same three tests.

96.3% for GS-cPass, and 94.9 % for MG-RBD. All three tests had a specificity close to 100 % (Fig. 4). Adjustments of the cut-off in these three systems did not improve the performance (shown in parentheses in the Figures). NT-titres in our cohort were low – mostly 1:5 – and only few subjects had high NT of 1 : 80 or above (Fig. 4a).

For the VC-array, sensitivities of both VC-S1-IgG and VC-N-IgG were improved markedly by optimising cut-offs, with gains of >30% (VC-N-IgG 39.8/93.5%; VC-S1-IgG 65.7/95.4%; see Table 1, Fig. 4c). Performance of VC-S2-IgA and VC-S2-IgM are presented for reference in Fig. S5.

The categorical endpoints of NT and the continuous results of GS-cPass were positively related ($R2$=0.74), agreement with the ground truth was frequent (80%). However, more than

17% of true-positive samples were negative in NT (*n*=21, Fig. 5a). Correlation between NT and MG-RBD was similar to GS-cPass (*n*=272, Fig. 5b). However, separation between the negative and positive population was better in MG-RBD than with GS-cPass, especially in those true-positives with low direct neutralisation capacity (NT <5). Association between GS-cPass and MG-RBD was good (*n*=272, Fig. 5c), discordant results were observed in 8% of true-positives. The distribution presented as increasingly narrower in higher titre ranges.

Associations of confirmatory and primary tests

To examine pre-test probability of assays following positive initial testing, the measurement values of all primary and confirmatory tests were correlated (Figs 6, S7–9). Overall,
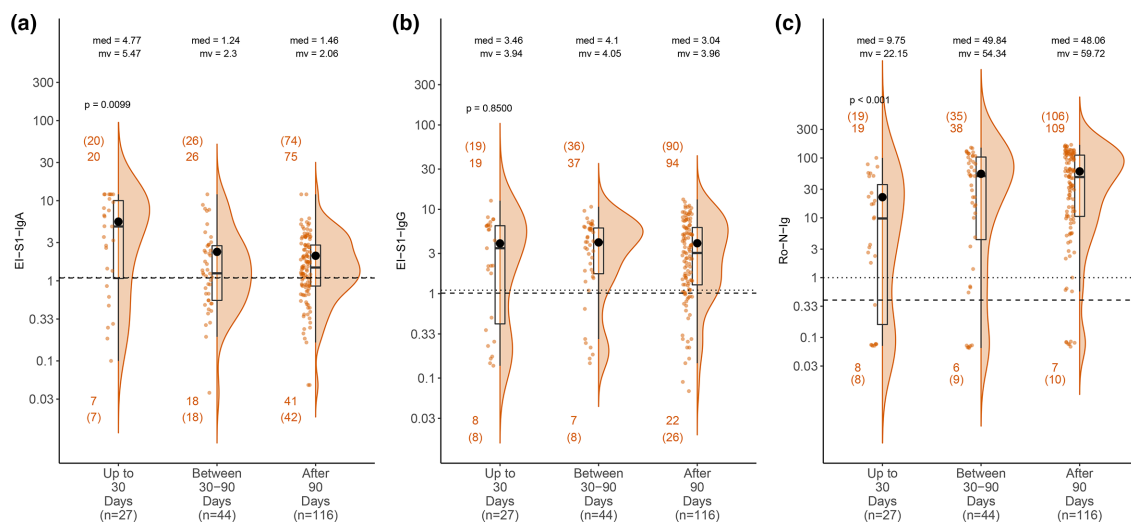
Fig. 3. Time dependence in primary tests for RT-PCR true-positives. Titre values of 187 true-positives with available data on time between RT-PCR and blood sampling for (a) EI-S1-IgA, (b) EI-S1-IgG, and (c) Ro-N-Ig. The read-outs were categorised according to the time after positive RT-PCR (<30 days, 30–90 days and >90 days). Plots show the individual read-out (orange dots), a density estimate (orange area), the 25-,50- and 75-percentiles (black boxes), and the means (black dots). Counts *n* (*n* refer to the number of observations above/below manufacturer's (optimised) cut-off for each of the temporal groups). Pairwise differences are considered only after adjusting for multiple testing and can be found in Table S4. Mean values (mv) and median values (med) are given for each group.

Fig. 4. Confirmatory tests. Results of confirmatory tests compared to ground truth for true-negatives (*blue*), true-positives (*orange*), and individuals with unknown SARS-CoV-2 status (*grey*). Black dotted and dashed lines represent the manufacturers and the optimised cut-offs, respectively. Orange/blue numbers indicate percentages of true-positives/-negatives correctly detected by the test using the respective cut-offs (identical in a, b, d). Distribution of results of NT (a) and GS-cPass (b). Distribution of IgG results of the VC-array (c) and the MG-line blot (d). Bar charts below violin plots represent information on the categorical part of the values below linear range. Grey numbers give the percentages of positive samples with unknown SARS-CoV-2 as determined by the manufacturers and optimised cut-offs. Percentages were calculated over the total number of samples of unknown SARS-CoV-2 status with available test results.

we observed high correlations, particularly for GS-cPass and MG-RBD with EI-S1-IgG, and MG-N with Ro-N-Ig (Fig. 6).

The categorical concordance for GS-cPass, MG-RBD, and MG-N with both Ro-N-Ig and EI-S1-IgG was similar (94 % or above), while the concordance of NT with both primary tests was lower (80%; Fig. 6). Concordances were improved by applying the optimised cut-offs, especially for VC-S1-IgG and VC-S2-IgG (Fig. S7).

DISCUSSION

We performed head-to-head comparisons of seven seroassays for SARS-CoV-2 and derived optimised cut-offs for several tests in a well-defined cohort with a total of 6658 samples [13, 14]. Although several reports have emerged that investigate the seroresponse to SARS-CoV-2 [4, 7, 17–25], only few feature direct head-to-head comparisons of many different assays in one set of samples [9, 11, 12, 26]. Studies have
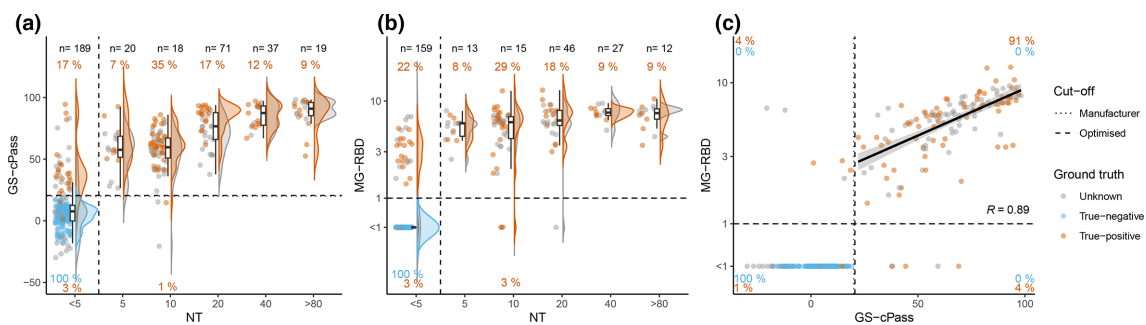
Fig. 5. Comparison of confirmatory tests. Comparison of confirmatory tests for true-negatives (*blue*), true-positives (*orange*), and individuals with unknown SARS-CoV-2 status (*grey*). At the top, in black, total number of cases (n) for each NT category. (a) Association between the categorical endpoint of NT and the continuous results of GS-cPass (*n*=354). (b) Association between the categorical endpoint of NT and the continuous results of MG-RBD (*n*=272). (c) Association between GS-cPass and MG-RBD (*n*=272). The solid black line represents a linear regression for the positive measurements.
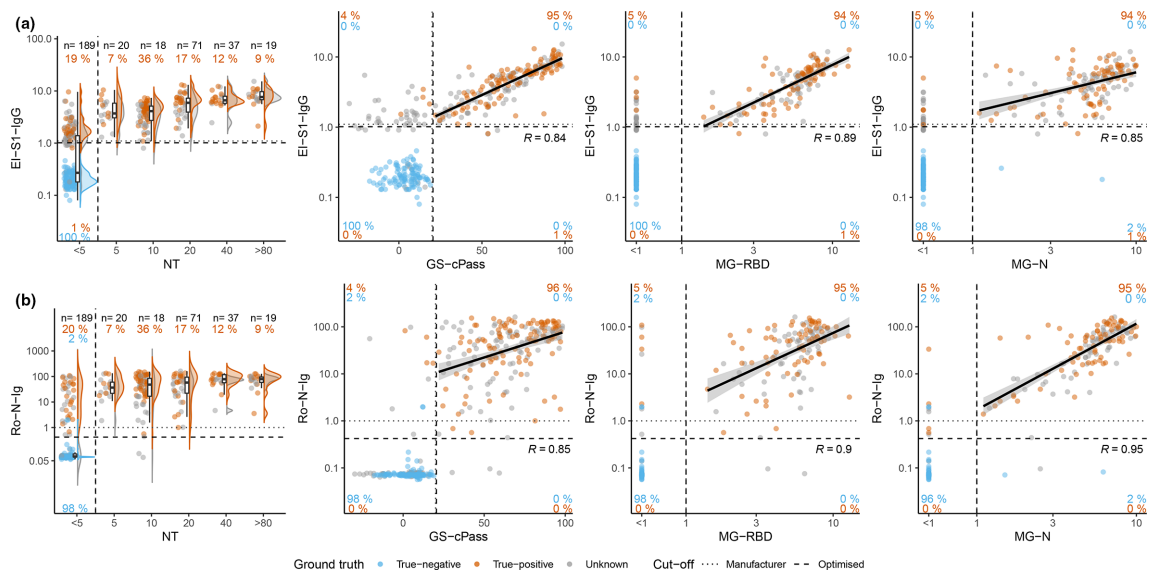
Fig. 6. Comparison of primary tests (EI-S1-IgG, Ro-N-Ig) with confirmatory tests (NT, GS-cPass MG-RBD, MG-N). Comparison of EI-S1-IgG and Ro-N-Ig with confirmatory tests for true-negatives (*blue*), true-positives (*orange*), and individuals with unknown SARS-CoV-2 status (*grey*) using the optimised cut-offs. The solid black line represents a linear regression for the positive measurements. (a) From left to right, association of EI-S1-IgG with the confirmatory test NT (*n=354*), GS-cPass (*n=361*), MG-RBD (*n=272*) and MG-N (*n=355*). We observed a population in the upper left quadrant, clearly negative in the confirmatory tests GS-cPass, MG-RBD and MG-N. (b) From left to right, association of Ro-N-Ig with the confirmatory test NT (*n=362*), GS-cPass (*n=273*), MG-RBD (*n=354*), and MG-N *n=354*).

often used widely different patient populations, hampering direct comparisons of testing systems. In contrast, our study provides data generated from a representative cohort of the inhabitants of Munich, and not selected patient cohorts [13], allowing a more generalisable interpretation of results presented. When choosing the primary tests, we considered four main characteristics (i) availability in large quantities, (ii) enabled for at least semi-automated workup, (iii) acceptable pricing and iv) licenced for the use in europe. These criteria excluded tests such as VC-Array as they were too expensive (>20 EUR/test). GS-cPass was excluded, as at the time of the study it was not licensed for use yet, although this has changed by now, however still lacking automation. The EI-S1-IgG and IgA as well as Ro-N-Ig tests fulfilled all criteria and were thus applied.

Several studies have shown a relationship between disease severity and both antibody kinetics [6, 18, 20, 27, 28] and neutralisation capacity [17, 29–31]. Our data is derived from a population- and not primarily a patient based approach, thus the interpretation of the data is mainly for epidemiological use. Here, our data suggest that Ro-N-Ig performs more reliably than EI-S1-IgA and EI-S1-IgG, especially in low prevalence settings due to the lack of specificity in EI-S1-IgA and -IgG, similarly to previously published reports [4]. We would not recommend using serology to diagnose acute infections, as RT-PCR is positive during the acute phase of the infection and serology will become positive only later. Nevertheless, singling out subjects who require only one booster vaccination to save vaccination doses, or to identify possible re-infections might be important questions in direct patient care currently,

besides epidemiological questions such as the assessment of possible herd immunity levels in the population.

In addition to the previously mentioned primary screening tests, we assessed confirmatory test performances using a subset of true-positive and true-negative samples, comparing assays targeting the highly-specific receptor binding domain (NT, GS-cPass, MG-RBD), which are considered direct or surrogate markers for viral neutralisation [32]. Our true-positive sample set was mainly derived from subjects with few to no symptoms, with often a rather low neutralising activity, allowing an in-depth cross-comparison of direct viral neutralisation (NT) with surrogate neutralisation markers (GS-cPass, MG-RBD) in oligo- or asymptomatic individuals. While NT is a direct representation of viral neutralisation, GS-cPass assesses the antibody-mediated inhibition of ACE2-interaction with SARS-CoV-2-S1-RBD and is therefore a cell-free surrogate neutralisation marker [33]. The cell-culture free tests performed particularly well with sensitivities of 96.3% for GS-cPass and 94.9% for MG-RBD, using the manufacturers' thresholds. In contrast, NT performed sub-optimally with a sensitivity of 80.6%. A compelling explanation would be a rapid decline in neutralising capacity, which has been reported previously and is in line with our observations [30, 34]. As NT requires a complex BSL-3-laboratory infrastructure, it currently represents a critical bottleneck, while the surrogate tests can be performed under BSL2 conditions. Furthermore, NT might miss a substantial part of cases especially with lower titres, thus GS-cPass or MG-RBD might be considered in these cases as they offer similar specificity.

To investigate the potential yield from combining primary tests, we applied machine learning techniques (random forest and support vector machine, see Methods). However, these hardly improved the performance beyond what was achieved by Ro-N-Ig alone (Table 1). Similarly to previously published studies, we could not demonstrate an added value of performing more than one confirmatory test [4]. By extending our true positive cohort using combinations of two or more positive confirmatory tests, we repeated the analysis, using the raw value of the primary tests as a decision criterion. Some performance improvement could be achieved by combining EI-S1-IgG with GS-cPass or MG-RBD in the materials with raw values between 0.8 and 2.55 (22% of the samples). In these cases, overall accuracy improved from 93–98% and 99%, respectively. For further details on these combinations, see supplemental material (Table S5, Figs S10 and S11).

Situation-specific cut-off optimization has been proposed as a tool to improve seroassay performances for SARS-CoV-2 [4, 12]. We therefore derived optimised cut-offs based on the true-positive and true-negative cohorts; hereby, we were able to improve sensitivity in EI-S1-IgG and Ro-N-Ig, while specificity remained similar. Meyer *et al.* proposed optimised thresholds for EI-S1-IgG, and suggested evaluating the manufacturer's cut-off before routine testing, highlighting the dilemma of securing both rule-in and rule-out properties to mitigate the risk of incorrect classification in a situation with highly-dynamic pre-test probabilities [4]. Whether these optimised cut-offs are generalisable remains uncertain: A seroprevalence study in Geneva compared both recommended and optimised cut-offs and did not observe any qualitative changes [25]. In our study, optimised cut-offs were similarly derived for confirmatory tests. Here, we could improve the sensitivity markedly for the VC-array with gains of >50% points for VC-N-IgG (39.8–94.4%) and close to 30% points for VC-S1-IgG (65.8–95.4%).

Even though some changes in performance estimates seem minimal, they might translate into a higher number of correctly classified diagnoses when testing is performed on a large scale. This is especially pertinent in low-prevalence settings, as particularly a high specificity is crucial to achieve a high positive predictive value. It may also be preferable to have a more sensitive cut-off for a primary test and confirm the positives with a highly-specific secondary test system [14].

In a systematic review by Huang *et al.* in 2020, the median detection time across different antibodies against SARS-CoV-2 was 11 days, similar to SARS-CoV-1 [6]. We therefore additionally assessed the seropositivity stratified with the date of the first positive RT-PCR test. In our cohort of mostly oligosymptomatic true-positive subjects, 11.4% (22/193) were not detected in the primary serological tests, with a third of those being <30 days after positive RT-PCR. Overall, in our dataset of samples >30 days after positive RT-PCR, a modest 8.1% (13/160) remained negative. Late or lacking seroconversion has been described previously, mostly in oligo- or asymptomatic subjects [31, 35], and authors have speculated

about vastly varying proportions of subjects unable to mount an antibody response detectable by commonly used assays [20, 21, 36, 37].

Different studies have reported a rapid decline of antibody titres over time [20, 30, 34]. In our cohort, antibody levels measured with EI-S1-IgA declined early on, most pronouncedly within the first 30 days, resulting in 40% of the subjects being below the positive cut-off >30 days after RT-PCR positivity. In contrast, antibody levels detected with EI-S1-IgG remained stable and detectable over longer periods. Moreover, titres measured with Ro-N-Ig increased, with more than 80% of true-positive subjects being rated as positive >90 days. Studies published so far show ambiguous results, partly suggesting that overall, antibody responses to S might be more stable than responses to N [38]; our results suggest that the observed differences are more attributed to the testing approach than the antigen itself.

Our study has several limitations. The sample set is derived from a representative cohort in Munich, Germany. Despite being an ethnically diverse city, the results presented here might not be representative of other geographical regions. Additionally, it was not feasible to perform all confirmatory tests on all samples; a subset, namely those with positive results in at least one primary test as well as a known negative/positive cohort, were tested using these systems. Finally, we did not have information on underlying health conditions of all subjects, e.g. conditions known to affect the quantity of polyclonal antibodies.

In conclusion, our study provides a cross-comparison of seven different widely used serological assays for SARS-CoV-2 and proposes new cut-offs for several tests. This study can be used as a resource to enable the refinement of testing strategies for individual and public-health use. Our approach presented here used a well-defined sample set with true-positive as well as true-negative specimens. Subsequently, we extrapolated the established findings to samples derived from a population-based seroprevalence cohort and were therefore able to generate a robust head-to-head comparison for diagnostic performance estimates of several serological tests for SARS-CoV-2.

Author contributions

M.H., is the principal investigator and obtained funds. A.W., M.H., J.H., and R.W., designed the study and experimental setup with input from C.F., K.R., M.B., and J.D. The clinical work and study design of KoCo19 was led by L.O., M.P., and I.K., with support by J.M.G.N., L.G., P.F., and A.M. BSL-3 work and viral RT-PCRs measurements were planned, conducted and evaluated by M.K., J.D., P.G., K.M., and R.W. Serological testing was designed and conducted with A.W., V.F., P.G., K.M., M.B., P.G., K.M., R.W., F.D., and T.E., while S.M., E.M.Q., and F.W., contributed participants' samples. Data was cleaned and prepared by N.C., M.N.D., and S.W. Statistical analysis was performed by N.C., Y.S., M.G., and P.P., with support by A.B., E.S., R.L.G., M.D., C.F., and J.H. The manuscript was primarily written by L.O., N.C., and A.W., with contributions from Y.S., M.G., C.F., J.H., and M.H., and input from I.K., P.P., and M.P. All authors revised and approved the final version of this manuscript.

Ethical statement

The study was approved by the Ethics Committee of the Faculty of Medicine at LMU Munich (20–275 V) and the protocol is available online (www.koco19.de) [13]. Informed consent was obtained prior to any study investigations where applicable. The study is registered in the German Clinical Trials Register (DRKS00021698; https://www.drks.de/drks_web/navigate.do?navigationId=trial.HTML and TRIAL_ID=DRKS00021698).

References

1. Huang C, Wang Y, Li X, Ren L, Zhao J, *et al*. Clinical features of patients infected with 2019 novel coronavirus in Wuhan, China. *The Lancet* 2020;395:497–506.

2. Amanat F, Stadlbauer D, Strohmeier S, Nguyen THO, Chromikova V, *et al*. A serological assay to detect SARS-CoV-2 seroconversion in humans. *Nat Med* 2020;26:1033–1036.

3. Chen X, Pan Z, Yue S, Yu F, Zhang J, *et al*. Disease severity dictates SARS-CoV-2-specific neutralising antibody responses in COVID-19. *Signal Transduct Target Ther* 2020;5:180.

4. Meyer B, Torriani G, Yerly S, Mazza L, Calame A, *et al*. Validation of a commercially available SARS-CoV-2 serological immunoassay. *Clin Microbiol Infect* 2020;26:1386–1394.

5. (FIND) FfIND. SARS-CoV-2 diagnostic pipeline. 2020. https://www.finddx.org/covid-19/pipeline/

6. Huang AT, Garcia-Carreras B, Hitchings MDT, Yang B, Katzelnick LC, *et al*. A systematic review of antibody mediated immunity to coronaviruses: kinetics, correlates of protection, and association with severity. *Nat Commun* 2020;11:4704.

7. Cheng MP, Yansouni CP, Basta NE, Desjardins M, Kanjilal S, *et al*. Serodiagnostics for severe acute respiratory syndrome-related coronavirus 2: a narrative review. *Ann Intern Med* 2020;173:450–460.

8. Jääskeläinen AJ, Kuivanen S, Kekäläinen E, Ahava MJ, Loginov R, *et al*. Performance of six SARS-CoV-2 immunoassays in comparison with microneutralisation. *J Clin Virol* 2020;129:104512.

9. Kohmer N, Westhaus S, Rühl C, Ciesek S, Rabenau HF. Brief clinical evaluation of six high-throughput SARS-CoV-2 IgG antibody assays. *J Clin Virol* 2020;129:104480.

10. Weidner L, Gänsdorfer S, Unterweger S, Weseslindtner L, Drexler C, *et al*. Quantification of SARS-CoV-2 antibodies with eight commercially available immunoassays. *J Clin Virol* 2020;129:104540.

11. National SARS-CoV-2 Serology Assay Evaluation Group. Performance characteristics of five immunoassays for SARS-CoV-2: a head-to-head benchmark comparison. *Lancet Infect Dis* 2020;20:1390–1400.

12. Plebani M, Padoan A, Negrini D, Carpinteri B, Sciacovelli L. Diagnostic performances and thresholds: the key to harmonization in serological SARS-CoV-2 assays? *medRxiv* 2020.

13. Radon K, Saathoff E, Pritsch M, Guggenbühl Noller JM, Kroidl I, *et al*. Protocol of a population-based prospective COVID-19 cohort study Munich, Germany (KoCo19). *BMC Public Health* 2020;20:1036.

14. **Pritsch M**, **Radon K**, **Bakuli A**, **Le Gleut R**, **Olbrich L**, *et al*. Prevalence and risk factors of infection in the representative COVID-19 cohort Munich. *Int J Environ Res Public Health* 2021;18:3572.

15. **Haselmann V**, **Özçürümez MK**, **Klawonn F**, **Ast V**, **Gerhards C**, *et al*. Results of the first pilot external quality assessment (EQA) scheme for anti-SARS-CoV2-antibody testing. *Clin Chem Lab Med* 2020;58:2121–2130.

16. **Benjamini Y**, **Yekutieli D**. The control of the false discovery rate in multiple testing under dependency. *Ann Stat* 2001:1165–1188.

17. **Chew KL**, **Tan SS**, **Saw S**, **Pajarillaga A**, **Zaine S**, *et al*. Clinical evaluation of serological IgG antibody response on the Abbott Architect for established SARS-CoV-2 infection. *Clinical microbiology and infection: the official publication of the European Society of Clinical Microbiology and Infectious Diseases* 2020;26.

18. **Eyre DW**, **Lumley SF**, **O'Donnell D**, **Stoesser NE**, **Matthews PC**, *et al*. Stringent thresholds for SARS-CoV-2 IgG assays result in underdetection of cases reporting loss of taste/smell. *medRxiv* 2020.

19. **Gudbjartsson DF**, **Helgason A**, **Jonsson H**, **Magnusson OT**, **Melsted P**, *et al*. Spread of SARS-CoV-2 in the Icelandic population. *N Engl J Med* 2020;382:2302–2315.

20. **Long QX**, **Liu BZ**, **Deng HJ**, **GC W**, **Deng K**, *et al*. Antibody responses to SARS-CoV-2 in patients with COVID-19. *Nat Med* 2020;26:845–848.

21. **Long Q-X**, **Tang X-J**, **Shi Q-L**, **Li Q**, **Deng H-J**, *et al*. Clinical and immunological assessment of asymptomatic SARS-CoV-2 infections. *Nat Med* 2020;26:1200–1204.

22. **Pollán M**, **Pérez-Gómez B**, **Pastor-Barriuso R**, **Oteo J**, **Hernán MA**, *et al*. Prevalence of SARS-CoV-2 in Spain (ENE-COVID): a nationwide, population-based seroepidemiological study. *The Lancet* 2020.

23. **Shakiba M**, **Hashemi Nazari SS**, **Mehrabian F**, **Rezvani SM**, **Ghasempour Z**, *et al*. Seroprevalence of COVID-19 virus infection in Guilan province, Iran. *medRxiv* 2020.

24. **Streeck H**, **Schulte B**, **Kuemmerer B**, **Richter E**, **Hoeller T**, *et al*. Infection fatality rate of SARS-CoV-2 infection in a German community with a super-spreading event. *medRxiv* 2020.

25. **Stringhini S**, **Wisniak A**, **Piumatti G**, **Azman AS**, **Lauer SA**, *et al*. Seroprevalence of anti-SARS-CoV-2 IgG antibodies in Geneva, Switzerland (SEROCoV-POP): a population-based study. *Lancet* 2020;396:313–319.

26. **Mahajan S**, **Redlich CA**, **Wisnewski AV**, **Fazen LE**, **Rao LV**, *et al*. Performance of abbott architect, ortho vitros, and euroimmun assays in detecting prior SARS-CoV-2 infection. *medRxiv* 2020.

27. **Seow J**, **Graham C**, **Merrick B**, **Acors S**, **Pickering S**, *et al*. Longitudinal observation and decline of neutralising antibody responses in the three months following SARS-CoV-2 infection in humans. *Nat Microbiol* 2020;5:1598–1607.

28. **Seow J**, **Graham C**, **Merrick B**, **Acors S**, **Steel KJA**, *et al*. Longitudinal evaluation and decline of antibody responses in SARS-CoV-2 infection. *medRxiv* 2020.

29. **Long Q-X**, **Tang X-J**, **Shi Q-L**, **Li Q**, **Deng H-J**, *et al*. Clinical and immunological assessment of asymptomatic SARS-CoV-2 infections. *Nat Med* 2020:1–5.

30. **Seow J**, **Graham C**, **Merrick B**, **Acors S**, **Pickering S**, *et al*. Longitudinal observation and decline of neutralising antibody responses in the three months following SARS-CoV-2 infection in humans. *Nat Microbiol* 2020;5:1598–1607.

31. **Staines HM**, **Kirwan DE**, **Clark DJ**, **Adams ER**, **Augustin Y**, *et al*. Dynamics of IgG seroconversion and pathophysiology of COVID-19 infections. *medRxiv* 2020.

32. **Chi X**, **Liu X**, **Wang C**, **Zhang X**, **Li X**, *et al*. Humanized single domain antibodies neutralise SARS-CoV-2 by targeting the spike receptor binding domain. *Nat Commun* 2020;11:4528.

33. **Tan CW**, **Chia WN**, **Qin X**, **Liu P**, **Chen MIC**, *et al*. A SARS-CoV-2 surrogate virus neutralisation test based on antibody-mediated blockage of ACE2–spike protein–protein interaction. *Nat Biotechnol* 2020;38:1073–1078.

34. **Marot S**, **Malet I**, **Leducq V**, **Zafilaza K**, **Sterlin D**, *et al*. Rapid decline of neutralising antibodies against SARS-CoV-2 among infected healthcare workers. *Nat Commun* 2021;12:844.

35. **Tuaillon E**, **Bolloré K**, **Pisoni A**, **Debiesse S**, **Renault C**, *et al*. Detection of SARS-CoV-2 antibodies using commercial assays and seroconversion patterns in hospitalized patients. *J Infect* 2020;81:e39–e45.

36. **Gallais F**, **Velay A**, **Wendling M-J**, **Nazon C**, **Partisani M**, *et al*. Intrafamilial exposure to SARS-CoV-2 induces cellular immune response without seroconversion. *medRxiv* 2020.

37. **Okba NM**, **Müller MA**, **Li W**, **Wang C**, **GeurtsvanKessel CH**, *et al*. Severe acute respiratory syndrome coronavirus 2– specific antibody responses in coronavirus disease patients. *Emerging Infect Dis* 2020;26:1478–1488.

38. **Ripperger TJ**, **Uhrlaub JL**, **Watanabe M**, **Wong R**, **Castaneda Y**, *et al*. Orthogonal SARS-CoV-2 serological assays enable surveillance of low-prevalence communities and reveal durable humoral immunity. *Immunity* 2020;53:e4.

Publication 8:

In Search of the SARS-CoV-2 Protection Correlate: Head-to-Head Comparison of Two Quantitative S1 Assays in Pre-characterized Oligo-/Asymptomatic Patients

Raquel Rubio-Acero*, **Noemi Castelletti***, Volker Fingerle, Laura Olbrich, Abhishek Bakuli, Roman Wölfel, Philipp Girl, Katharina Müller, Simon Jochum, Matthias Strobl, Michael Hoelscher, Andreas Wieser+, KoCo19 study team

In Search of the SARS-CoV-2 Protection Correlate: Head-to-Head Comparison of Two Quantitative S1 Assays in Pre-characterized Oligo-/Asymptomatic Patients

Raquel Rubio-Acero · Noemi Castelletti · Volker Fingerle · Laura Olbrich · Abhishek Bakuli ·

Roman Wölfel · Philipp Girl · Katharina Müller · Simon Jochum · Matthias Strobl ·

Michael Hoelscher · Andreas Wieser on behalf of the KoCo19 study team

ABSTRACT

Background: Quantitative serological assays detecting response to SARS-CoV-2 are needed to quantify immunity. This study analyzed the performance and correlation of two quantitative anti-S1 assays in oligo-/asymptomatic individuals from a population-based cohort.
Methods: In total, 362 plasma samples (108 with reverse transcription-polymerase chain

reaction [RT-PCR]-positive pharyngeal swabs, 111 negative controls, and 143 with positive serology without confirmation by RT-PCR) were tested with quantitative assays (Euroimmun Anti-SARS-CoV-2 QuantiVac enzyme-linked immunosorbent assay [EI-S1-IgG-quant]) and Roche Elecsys® Anti-SARS-CoV-2 S [Ro-RBD-Ig-quant]), which were compared with each other and confirmatory tests, including wild-type virus micro-neutralization (NT) and Gen-Script®cPass™. Square roots R of coefficients of determination were calculated for continuous variables and non-parametric tests were used for paired comparisons.
Results: Quantitative anti-S1 serology correlated well with each other (true positives, 96%; true negatives, 97%). Antibody titers decreased over time (< 30 to > 240 days after initial positive RT-PCR). Agreement with GenScript-cPass

Raquel Rubio-Acero and Noemi Castelletti contributed equally/share first authorship.

The members of the KoCo19 study team are listed in the Acknowledgements.

R. Rubio-Acero · N. Castelletti · L. Olbrich ·
A. Bakuli · M. Hoelscher · A. Wieser (✉)
Division of Infectious Diseases and Tropical
Medicine, University Hospital, Ludwig-Maximilians-
Universität (LMU) Munich, Leopoldstr. 5, 80802
Munich, Germany
e-mail: Wieser@mvp.lmu.de

N. Castelletti
Institute of Radiation Medicine, Helmholtz Zentrum
München, 85764 Neuherberg, Germany

V. Fingerle · L. Olbrich · R. Wölfel · P. Girl ·
K. Müller · M. Hoelscher · A. Wieser
German Center for Infection Research (DZIF),
Partner Site, Munich, Germany

V. Fingerle
Bavarian Health and Food Safety Authority (LGL),
Oberschleissheim, Germany

M. Hoelscher
Center for International Health (CIH), University
Hospital, LMU Munich, 80336 Munich, Germany

R. Wölfel · P. Girl · K. Müller
Bundeswehr Institute of Microbiology, 80937
Munich, Germany

S. Jochum · M. Strobl
Roche Diagnostics GmbH, 82377 Penzberg,
Germany

was 96%/99% for true positives and true negatives, respectively, for Ro-RBD-Ig-quant and 93%/97% for EI-S1-IgG-quant. Ro-RBD-Ig-quant allowed distinct separation between positives and negatives, and less non-specific reactivity versus EI-S1-IgG-quant. Raw values (95% CI) $\geq$ 28.7 U/mL (22.6–36.4) for Ro-RBD-Ig-quant and $\geq$ 49.8 U/mL (43.4–57.1) for EI-S1-IgG-quant predicted NT > 1:5 in 95% of cases. *Conclusions*: Our findings suggest both quantitative anti-S1 assays (EI-S1-IgG-quant and Ro-RBD-Ig-quant) may replace direct neutralization assays in quantitative measurement of immune protection against SARS-CoV-2 in certain circumstances. However, although the mean antibody titers for both assays tended to decrease over time, a higher proportion of Ro-RBD-Ig-quant values remained positive after 240 days.

Keywords: COVID-19; Direct virus neutralization assay S1; Quantitative serology; SARS-CoV-2

Key Summary points

Quantitative serological assays detecting response to SARS-CoV-2 infection are urgently needed to quantify immunity.

This manuscript presents the results of direct comparison of two independent quantitative anti-S1 assays (Euroimmun Anti-SARS-CoV-2 QuantiVac ELISA [IgG] and Roche Elecsys® Anti-SARS-CoV-2 S) in oligo-/asymptomatic individuals from a previously characterized population-based cohort.

Both assays showed similar performance and a high level of agreement with direct virus neutralization and surrogate neutralization tests, arguing for their utility in quantifying immune protection against SARS-CoV-2.

In certain circumstances and following rigorous validation, these quantitative assays may replace direct neutralization assays (the current gold standard) which are unsuitable for large-scale studies and diagnostic routine testing.

DIGITAL FEATURES

This article is published with digital features, including a summary slide, to facilitate understanding of the article. To view digital features for this article go to https://doi.org/10.6084/m9.figshare.14697141.

INTRODUCTION

Severe acute respiratory syndrome coronavirus 2 (SARS-CoV-2), the causative agent of coronavirus disease 2019 (COVID-19), emerged in Wuhan, China, in December 2019, and within months caused millions of infections and deaths across the globe [1]. Despite multiple interventions, including social distancing, wearing of protective equipment in public, and introducing enhanced disinfection procedures, the number of infected individuals worldwide continued to rise beyond the end of 2020 [2].

The gold standard for diagnosis of acute COVID-19 is molecular detection of the viral ribonucleic acid (RNA) by reverse transcription-polymerase chain reaction (RT-PCR) [3]. In addition, antibody testing can be used to detect humoral immune responses after the infection. Immunoassays detecting anti-SARS-CoV-2 antibodies can be especially valuable to confirm the extent of population exposure and to quantify vaccine responses [4, 5].

Seroconversion typically starts 5–7 days after SARS-CoV-2 infection [4]. All antibody types (immunoglobulin [Ig] A, IgG, and IgM) can be detected within the same time frame around week 2–4, and the IgG response persists the longest [4, 6]. The most important targets of humoral response are the nucleocapsid protein (N), involved in viral RNA replication and viral assembly, and parts of the trimeric spike

complex, in particular the receptor-binding domain (RBD) of S1 which interacts with the angiotensin-converting enzyme 2 (ACE2) receptor on human cells [7, 8]. Antibodies that bind to RBD in a way that prevents its attachment to the host cell have a convincing functional likelihood to neutralize the virus and are viewed as the key indicator of immune protection [9–11]. In line with these observations, the spike protein became the leading antigen target in vaccine development [12].

Accumulating data suggest that high titers of IgG in convalescent plasma correlate with the presence of neutralizing antibodies, which may correlate with protection against infection [8, 13–15]. However, the long-term persistence of neutralizing antibodies and the degree of protection they confer, as well as the degree and clinical significance of seroconversion in asymptomatic individuals, remain largely unknown.

A number of immunoassays from different manufacturers are currently available and have been compared directly in several head-to-head studies [16–19]. Since most are qualitative in nature, the emergence of quantitative assays is needed for a precise evaluation of immune response to viral antigens. Importantly, a reliable quantitative assay can be used to quantify protection in different settings (e.g., mild disease or vaccination). Such evaluation will require robust data on quantitative assay performance and its correlation with available neutralization tests.

Here, we present the results of a direct comparison of two novel quantitative anti-S1/RBD antibody tests applied to a subset of samples derived from a prospective population-based cohort study of COVID-19 incidence/prevalence in Munich, Germany. The ongoing KoCo19 study investigates the prevalence of SARS-CoV-2 infections among a randomly selected cohort, analyzes transmission within households and risk factors, and compares the performance of various immunoassays in testing asymptomatic and oligosymptomatic individuals [20]. The primary results were reported elsewhere including the estimated seroprevalance in Munich [21] and a comparison of seven qualitative seroassays to identify effective testing strategies [22]. This manuscript reports the analysis of the performance and correlation of quantitative Euroimmun Anti-SARS-CoV-2 QuantiVac enzyme-linked immunosorbent assay (ELISA) IgG assay that recognizes S1 (hereafter called EI-S1-IgG-quant) and quantitative Elecsys® Anti-SARS-CoV-2 S pan-Ig assay that recognizes S1 RBD (hereafter called Ro-RBD-Ig-quant) in a subset of samples derived from the KoCo19 cohort. Both assays were compared with previously described qualitative primary assays, namely Euroimmun Anti-SARS-CoV-2 ELISA IgG (hereafter called EI-S1-IgG) [23, 24] and Elecsys Anti-SARS-CoV-2 Roche anti-N pan-Ig (hereafter called Ro-N-Ig) [25]. The primary tests were also assessed alongside assays that confirm infection, including direct virus neutralization test (NT) with SARS-CoV-2 wild-type virus (SARS-CoV-2 strain MUC-IMB-01 isolated in January 2020), GenScript®cPass™ (hereafter called GS-cPass) and Mikrogen-recomLine-N/RBD IgG line (hereafter called MG-N and MG-RBD) immunoassays.

METHODS

Study Design and Participants

Samples were derived from the population-based prospective COVID-19 cohort KoCo19 from Munich, Germany [20]. Out of the total 6658 samples analyzed previously [22], 362 (due to having NT arrays and all other confirmatory tests) were included in this analysis. These included samples from (i) asymptomatic or oligosymptomatic individuals who had at least one RT-PCR-positive SARS-CoV-2 test on a pharyngeal swab (true positive samples), (ii) those who did not have an RT-PCR-positive test, but experienced seroconversion in at least one of the primary tests used ("other seropositive" samples), and (iii) negative controls—partially blood donors collected before the surge of SARS-CoV-2/COVID-19, and negative samples obtained during the pandemic (true negative samples). All samples were collected during the same time period (between April and June 2020), except for true negative samples from blood donors (October 2019 and March 2020,

i.e., before and after the seasonal common cold period). Samples were defined as "other seropositive" if one of the serological tests yielded a positive result, suggesting a likely but unconfirmed SARS-CoV-2 infection. To ensure a dataset with exclusively independent variables, only one serum sample per participant was used for analyses.

The study was approved by the Ethics Commission of the Faculty of Medicine at Ludwig-Maximilians-Universität Munich (reference numbers 20–275-V, 20–371-V, and 20–262-V) and the protocol is available online (www. koco19.de) [20]. This study was conducted in accordance with the principles of the Declaration of Helsinki and Good Clinical Practice Guidelines. Informed written consent was obtained from all study participants.

Laboratory Assays

Blood samples were obtained as previously described [20]. Briefly, blood was collected in ethylenediaminetetraacetic acid-coated tubes, refrigerated and maintained at 4 °C from the moment of extraction until centrifugation to separate the cell pellet from the plasma. Plasma samples were analyzed and stored at − 80 °C in temperature-controlled biobank freezers; freeze–thaw cycles were minimized to avoid sample degradation.

The presence of antibodies was analyzed using appropriate assay kits according to the manufacturers' instructions.

An overview of all assays, their cutoff values, and readouts are shown in Supplementary Table 1. The World Health Organization (WHO) reference sera (National Institute for Biological Standards and Control [NIBSC] code 20/268) were measured on the individual assays in replicates ($n = 3$) to standardize the results [26].

Primary Assays
EI-S1-IgG-quant and EI-S1-IgG results were measured on a Euroanalyzer-1 robot (Euroimmun, Lübeck, Germany). For the qualitative assay EI-S1-IgG, presented values show quotients of the optical density measurements given by the manufacturer's software. For the

quantitative assay EI-S1-IgG-quant, values are shown in units per milliliter (U/mL). Two cutoffs were applied as recommended by the manufacturer: 25.6 U/mL to separate negative values from indeterminate values, and 35.2 U/mL to separate indeterminate values from positive values (Supplementary Table 1). Values between 1 and 120 U/mL represent linear range, samples with values below 1 U/mL were assigned a categorical value of 0, whereas samples with values above 120 U/mL were diluted 1:4 with sample buffer (Euroimmun, Lübeck, Germany) and measured again.

Ro-RBD-Ig-quant and Ro-N-Ig results were measured on cobas e411 and/or e801 modules (Roche, Mannheim, Germany). For the qualitative assay Ro-N-Ig, values correspond to the sample cutoff index. For the quantitative assay Ro-RBD-Ig, values are shown in U/mL. Manufacturer cutoff was applied to separate negative and positive values. Values between 0.4 and 250 U/mL represent linear range. Samples with values below 0.4 U/mL were assigned a categorical value of 0, whereas samples with values above 250 U/mL were diluted 1:10 with sample diluent buffer (Roche, Mannheim, Germany).

Assays Confirming Infection
Confirmatory testing was performed using micro-virus NT assays as described previously [27], with the exception that confluent cells were incubated instead of adding cells following neutralization reaction, and the serum dilutions started with 1:5 instead of 1:10. Samples with a titer < 1:5 were classified as NT-negative, and samples with a titer ≥ 1:5 as NT-positive.

Binding inhibition was measured using the SARS-CoV-2 surrogate virus neutralization test (GS-cPass; GenScript®, Piscataway, New Jersey, USA) according to the manufacturer's instructions. Photometric measurements were performed using the Tecan Sunrise (Tecan, Männedorf, Switzerland). Binding inhibition was calculated in percentages (range from − 30% to 100%; cutoff was 20% as recommended by the manufacturer).

The recomLine SARS-CoV-2 IgG line immunoassay (MG-N and MG-RBD; Mikrogen, Neuried, Germany) based on nitrocellulose strips with recombinant SARS-CoV-2 antigens N

and RBD was measured using the fully automated *recom*Line strip processor CarL (Mikrogen, Neuried, Germany) according to the manufacturer's instructions. Raw values were presented in arbitrary units, and manufacturer's cutoffs were applied.

Statistical Analysis

Only one sample per participant was included in the statistical analyses; in case of individuals with multiple blood samples, the sample with the most comprehensive dataset was included. For multiple measurements with complete datasets, only the first measurement was considered; for operational replicates the latest measurement was included. Assay comparison was performed as described previously [22]. Statistical analysis and visualization was performed using software R, version 4.0.2 (https://cloud.r-project.org/).

Square roots R of coefficients of determination (R^2) were calculated for continuous variables. Paired sample comparisons were performed using Wilcoxon-sign-rank tests; multiple group comparisons were performed using Kruskal–Wallis tests, followed by post hoc Dunn tests and the Benjamini–Yekutieli adjustment for pairwise comparisons [28].

RESULTS

A total of 362 samples from the KoCo19 cohort were included in the analysis: 108 samples from individuals who had viral RNA detected in pharyngeal swabs (true positives), 143 "other seropositive" samples, and 111 negative controls [20].

Performance of Anti-S1 Tests

The diagnostic accuracy measurements of all primary and confirmatory tests are presented in Table 1.

The raw value distributions of Ro-RBD-Ig-quant on $n = 357$ evaluable samples and EI-S1-IgG-quant on $n = 354$ evaluable samples are presented in Fig. 1. Both assays showed a

bimodal distribution. Ro-RBD-Ig-quant assay showed a better signal spread with a clear separation of true negative and true positive samples, and did not produce discordant results. Ro-RBD-Ig-quant detected 100% of the positive and 100% of the negative samples, whereas EI-S1-IgG-quant detected 96% of the positive and 97% of the negative samples. Thirteen samples produced discordant results in EI-S1-IgG-quant and were categorized as indeterminate as they did not meet criteria for the positive or negative categories (Table 1).

Titer values of true positive samples with available data on time between RT-PCR and blood sampling for Ro-RBD-Ig-quant ($n = 232$) and EI-S1-IgG-quant ($n = 228$) are shown in Fig. 2. Values were widespread in the cohort with < 30 days between RT-PCR and antibody test for both assays. The mean titer values tended to decrease over time, with statistically significant differences between value distribution in the cohort with < 30 days vs cohort with > 240 days for both assays ($p < 0.0001$). After 240 days, the majority (80%) of Ro-RBD-Ig-quant values remained in the positive range whereas almost half of EI-S1-IgG-quant values no longer met the positivity threshold. Pairwise comparison between time-dependent groups after adjustment for multiple comparison are shown in Table 2.

Concordance Between Quantitative and Semi-quantitative Anti-S1 Tests

To allow for comparison of scale, results of individual assays with the WHO reference panel (NIBSC 20/168) are presented in Table 3.

Pairwise comparison of primary tests is shown in Supplementary Fig. 1; agreement of 95–98% was observed for all comparisons. When categorical values were excluded, Ro-RBD-Ig-quant showed a high numerical correlation with EI-S1-IgG ($R = 0.72$, $p < 0.0001$; Supplementary Fig. 1A), while the numerical correlation with Ro-N-Ig was lower ($R = 0.34$; $p < 0.0001$; Supplementary Fig. 1B). EI-S1-IgG-quant showed a high numerical correlation with EI-S1-IgG ($R = 0.55$, $p < 0.0001$; Supplementary Fig. 1C) while with Ro-N-Ig the

Table 1 Performance of primary tests and confirmatory tests

Test	N	n (true positive)	n (true negative)	Positive result (% of true positive)	Negative result (% of true negative)
EI-S1-IgG-quant	354	103	111	208 (96)	133 (97)
					Indeterminate: 13 (1)[a]
Ro-RBD-Ig-quant	357	107	111	202 (100)	155 (100)
EI-S1-IgG	362	108	111	232 (98)	130 (98)
Ro-N-Ig	361	108	111	201 (98)	160 (98)
NT	354	107	106	165 (80)	189 (100)
GS-cPass	360	108	111	198 (96)	162 (99)
MG-N	273	78	106	139 (95)	134 (98)
MG-RBD	273	78	106	137 (95)	136 (100)

RBD receptor-binding domain

[a] Thirteen samples (1%) produced discordant results and were categorized as indeterminate
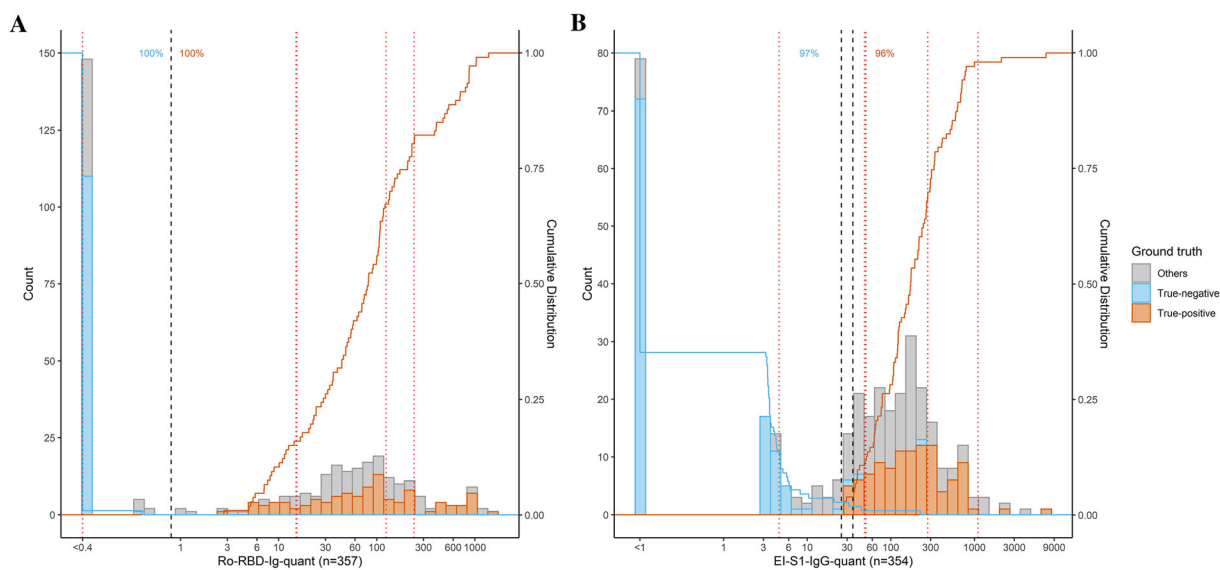

Fig. 1 Performance of primary tests Ro-RBD-Ig-quant (**a**) and EI-S1-IgG-quant (**b**). Black dashed lines represent manufacturers' cutoff values and red dotted lines represent WHO standards (from the left to the right: 20/142, 20/144, and 20/140 for **a** (20/140 and 20/144 for **b**) with almost identical values, 20/148, 20/150). Histograms show counts of individual samples, whereas solid blue and orange lines show cumulative distribution of true positive and true negative samples. Orange and blue numbers give the percentage of true positive and true negative samples, which were correctly detected by the tests

correlation was lower ($R = 0.20$, $p < 0.001$; Supplementary Fig. 1D). A high level of categorical agreement was observed between Ro-RBD-Ig-quant and EI-S1-IgG-quant with a
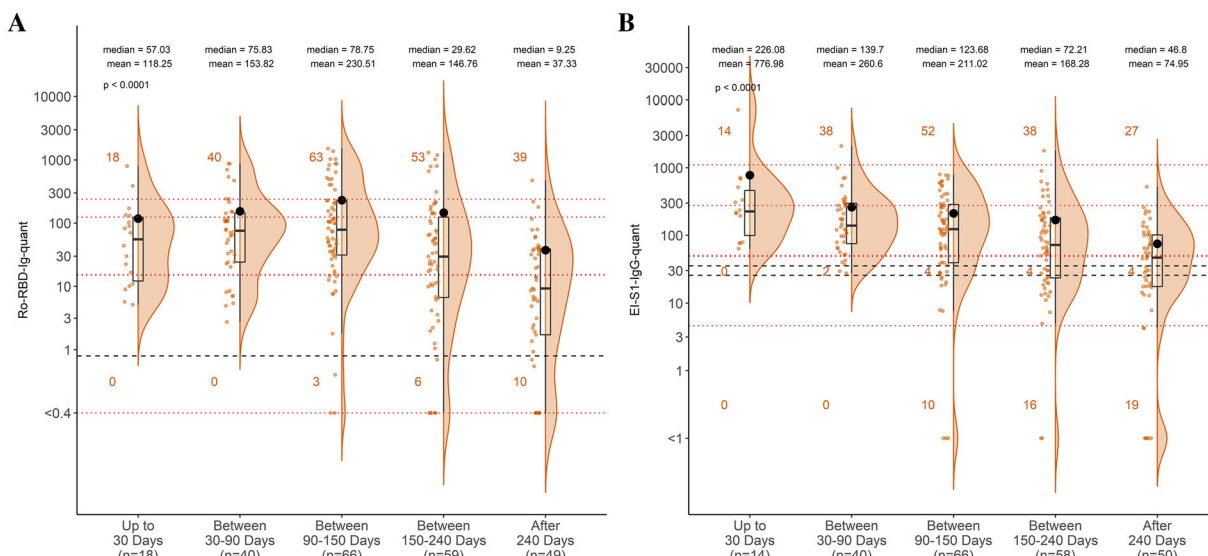
Fig. 2 Time-dependent values of positive samples in primary tests Ro-RBD-Ig-quant (**a**) and EI-S1-IgG-quant (**b**). Black dashed lines represent manufacturers' cutoff values and red dotted lines represent the WHO standards (from the bottom to the top: 20/142, 20/144, and 20/140 for **a** (20/140 and 20/144 for **b**) with almost identical values, 20/148, 20/150). Assay results were categorized according to the time after the positive RT-PCR test (< 30 days, 30–90 days, 90–150 days, 150–240 days, and > 240 days). Plots show the individual read-out (orange dots), a density estimate (orange area), the 25th, 50th, and 75th percentiles (black box), and the mean (black dot); mean and median numbers are included for each group

Table 2 Pairwise comparison between the time-dependent groups after adjusting for multiple comparison

Group comparison	Adjusted *p* value	
	Ro-RBD-Ig-quant	**EI-S1-IgG-quant**
Up to 30 days–between 30 and 90 days	1.000	0.71
Up to 30 days–between 90 and 150 days	1.000	0.28
Up to 30 days–between 150 and 240 days	1.000	< 0.05*
Up to 30 days–after 240 days	< 0.05*	< 0.001*
Between 30 and 90 days–between 90 and 150 days	1.000	1.000
Between 30 and 90 days–between 150 and 240 days	0.169	0.06
Between 30 and 90 days–after 240 days	< 0.001*	< 0.001*
Between 90 and 150 days–between 150 and 240 days	< 0.05*	0.16
Between 90 and 150 days–after 240 days	< 0.0001*	< 0.01*
Between 150 and 240 days–after 240 days	< 0.05*	0.30

NISBC National Institute for Biological Standards and Contro, *SD* standard deviation

*Indicates the different levels of significance as shown by the *p* values

Table 3 Results from individual assays with the WHO reference panel for anti-SARS-CoV-2 immunoglobulin (NIBSC code 20/268)

Reference level (NISBC code)	Mean titer value ($n = 3$),[a] (SD)			
	EI-S1-IgG-quant	Ro-RBD-Ig-quant	EI-S1-IgG	Ro-N-Ig
Negative (20/142)	4.62 (0.27)	< 1 (–)	0.21 (0.007)	0.14 (0.005)
Low (20/140)	48.61 (2.36)	15.32 (0.39)	1.37 (0.06)	4.68 (0.17)
Low anti-S, high anti-N (20/144)	50.35 (1.43)	14.98 (0.32)	1.3 (0.09)	75.05 (2.52)
Mid (20/148)	276.62 (10.45)	124.47 (2.49)	4.33 (0.12)	101.89 (1.00)
High (20/150)	1103.25 (4.95)	239.87 (2.75)	6.56 (0.13)	118.29 (3.16)

[a] Tests were repeated × 3 and mean titer calculated

high correlation (96% of positive samples and 97% of negative samples; $R = 0.50$, $p < 0.0001$; Supplementary Fig. 1E). Notably, Ro-RBD-Ig-quant gave a clearer separation of positive and negative values than EI-S1-IgG-quant; EI-S1-IgG-quant showed many values at the intermediate range and some non-specific reactivity among the negative samples (3%).

Concordance with Tests Confirming Infection

Ro-RBD-Ig-quant values showed significant increases between NT dilution categories ($p < 0.001$), with mean values increasing from 39.64 in the NT dilution category < 1:5 to 486.24 in the NT dilution category > 1:80 (Fig. 3a). Notably, NT at dilution 1:5 still contained approximately 20% of true positive samples. Ro-RBD-Ig-quant also showed a high categorical agreement and correlation with GS-cPass (96%/99%, $R = 0.54$, $p < 0.0001$; Fig. 3b).

EI-S1-IgG-quant values also showed significant increases between NT dilution categories, with mean values of EI-S1-IgG-quant increasing from 44.33 (NT dilution < 1:5) to 956.6 (NT dilution > 1:80; Fig. 3c). NT at dilution 1:5 still contained approximately 16% of true positive samples. EI-S1-IgG-quant showed a high level of correlation with GS-cPass (93%/97%, $R = 0.41$, $p < 0.0001$; Fig. 3d), although some unspecific reactivity in the negative samples was detected for EI-S1-IgG (3%).

The predictive value (95% accordance of the positive predictive value) of the two quantitative tests at different thresholds was investigated through the alignment of their results with NT dilution categories ≥ 1:5 and ≥ 1:10, and GS-cPass categories ≥ 20% and ≥ 30%. The lowest Ro-RBD-Ig-quant and EI-S1-IgG-quant values [with 95% CI] for which GS-cPass is ≥ 20% (6.99 and 27.49, respectively) or ≥ 30% (11.60 and 40.62) and NT is ≥ 1:5 (28.67 and 49.78) or ≥ 1:10 (51.41 and 104.06) are presented in Table 4 and Supplementary Fig. 2. These values refer to the intersection of the linear fit with the selected values for GS-cPass and NT of Fig. 3.

Ro-S1-Ig-quant showed a high level of correlation with line blot assay MG-RBD and a lower numerical correlation with MG-N ($R = 0.44$, $p < 0.0001$ and $R = 0.32$, $p < 0.001$, respectively; Supplementary Fig. 3A, B). EI-S1-IgG-quant showed a high level of correlation with MG-RBD ($R = 0.46$, $p < 0.0001$; Supplementary Fig. 3C), but the agreement with MG-N was not statistically significant ($R = 0.15$, $p = 0.089$; Supplementary Fig. 3D).

DISCUSSION

Since the surge of the COVID-19 pandemic, the number of serological assays continues to increase, and the comparative assessment of their analytical performance is essential to inform strategies in diagnostic, epidemiological,
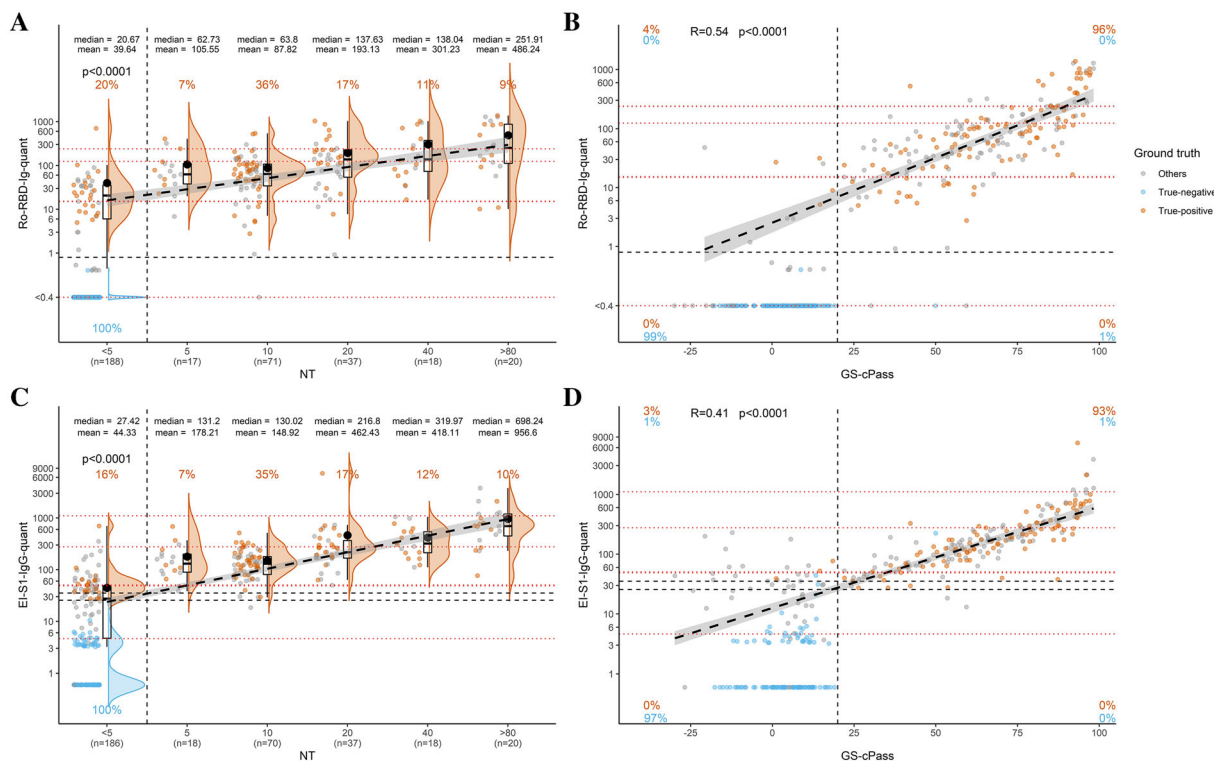
Fig. 3 Pairwise comparison of primary tests with confirmatory tests. Bivariate comparisons shown as violin and scatter plots for quantitative Ro-RBD-Ig-quant vs NT at indicated dilutions (**a**) and vs GS-cPass (**b**) and for quantitative EI-S1-IgG-quant vs NT at indicated dilutions (**c**) and vs GS-cPass (**d**). Black dashed lines represent manufacturers' cutoff values and red dotted lines represent the WHO standards (from the bottom to the top: 20/142, 20/144, and 20/140 for **a** (20/140 and 20/144 for **c**) with almost identical values, 20/148, 20/150). Orange and blue numbers give the percentage of true positive and true negative samples, which were correctly detected by the tests. Bold dashed lines are linear fit and gray areas surrounding them represent 95% CI; for the interested region, the polynomial fit was within the 95% CI of the linear fit. Square root R of coefficients of determination is given for association among continuous variables. Pairwise comparison between NT dilution categories (for **a** and **c**) after adjustment for multiple comparison are shown in Table S2

and vaccination studies. In this study, we performed a head-to-head direct comparison of two independent quantitative assays directed against S1 and compared their performance with two qualitative primary assays and several assays that confirm infection, including direct virus neutralization. Samples from oligo-/asymptomatic patients from a population-based cohort were utilized to help understand the true impact of COVID-19, given mild/asymptomatic cases are predominant in the population and data regarding immunity protection that develops in such patients are limited but of critical importance for policy makers worldwide.

The quantitative tests Ro-RBD-Ig-quant and EI-S1-IgG-quant showed a high level of correlation when used in a population cohort containing samples from mostly oligo- or asymptomatic individuals; both assays showed categorical agreement with Ro-N-Ig, micro-virus neutralization assay, GS-cPass and *recom*Line. This suggests both tests can detect correlates of neutralization, which is understood to mediate humoral protection following SARS-CoV-2 infection. While the mean titers for both assays tended to decrease after their peak (ca. 1 month or ca. 3 months after infection for EI-S1-IgG-quant and Ro-RBD-Ig-quant, respectively) to > 240 days after positive RT-PCR, a higher

Table 4 Predictive value of quantitative tests

NT/NT-surrogate	Quantitative serology (95% CI)	
	Ro-S1-Ig-quant	EI-S1-IgG-quant
GS-cPass ≥ 20	≥ 6.99 (5.30–9.21)	≥ 27.49[a] (23.94–31.57)
GS-cPass ≥ 30	≥ 11.60 (9.22–14.60)	≥ 40.62 (36.00–45.83)
NT ≥ 1:5	≥ 28.67 (22.61–36.35)	≥ 49.78 (43.42–57.06)
NT ≥ 1:10	≥ 51.41 (42.42–62.32)	≥ 104.06 (91.34–118.54)

Presented as lowest values (with 95% accordance of the positive predictive value [95% CI]) of the quantitative tests for which NT is ≥ 1:5 and ≥ 1:10 and GS-cPass is ≥ 20% and ≥ 30%

CI confidence interval, *NT* neutralization

[a] This value is below the positivity threshold

proportion of Ro-RBD-Ig-quant values remained positive after 240 days.

Finally, both quantitative assays showed a good level of concordance with each other, with Ro-RBD-Ig-quant performing slightly better in terms of clearer separation of positive and negative samples and less non-specific reactivity.

Currently, the most reliable method of detecting antibody response indicative of protection is direct virus neutralization; however, this test requires intact virus and has to be performed under biosafety level 3 conditions, making it infeasible for large-scale studies and diagnostic routine testing [17]. There are also numerous different protocols for direct viral neutralization with poor overall comparability. Commercial high-throughput tests use parts of viral proteins instead and combine these with other components of chemiluminescence detection or ELISA [3, 6]. Although all viral proteins are likely to elicit some degree of immune response, most efforts concentrated on measuring antibodies directed against N and S1/RBD so far [5]. Some studies suggest that S1 may be the optimal antigen for SARS-CoV-2 serological tests, as it is more sensitive than RBD and more specific than S trimer [29]; however, this assumption could not be confirmed in this study.

Quantitative anti-S1 assays will be a valuable tool for measuring antibody responses to SARS-CoV-2. Importantly, quantitative assays will allow us to precisely enumerate and compare antibody titers in individuals who had severe disease, mild disease, asymptomatic individuals, and those who achieved immunity after vaccination. The assays may also be applied to screen for plasma samples that contain specific high-affinity neutralizing antibodies and help identify potential donors of plasma for convalescent plasma therapy [30]. Once established and rigorously validated, these assays may replace the current gold standard of direct neutralization, which requires handling at biosafety level 3 and has severe limitations in signal resolution at the lower end of the range.

In this study, both EI-S1-IgG-quant and Ro-RBD-Ig-quant showed a high level of correlation with direct virus micro-neutralization and surrogate neutralization test, GS-cPass. For example, raw values above 28.67 U/mL for Ro-RBD-Ig-quant and above 49.78 U/mL for EI-S1-IgG-quant, respectively, predicted virus neutralization > 1:5 in 95% of cases. We may hypothesize that when the value of the quantitative tests is above the predictive value (e.g., 95%), there is little benefit in performing NT and that this could act as a surrogate marker for neutralizing titers, e.g., after mass vaccinations or post-infection.

CONCLUSIONS

To the best of our knowledge, we present for the first time a comparison with quantitative tests which can be reproduced by others to assess

neutralization as a bridge to serologically mediated immunoprotection. Our results suggest that both quantitative assays may be useful in future studies aimed to assess immunization efficiency, determine the degree of herd immunity, and estimate how long the response persists over time.

ACKNOWLEDGEMENTS

data preparation and data cleaning, and together with Abhishek Bakuli, performed statistical analysis and figure generation. Laura Olbrich and Andreas Wieser provided samples and selected the patients from the KoCo19 study. Simon Jochum, Matthias Strobl, Noemi Castelletti, Raquel Rubio Acero, and Andreas Wieser prepared the manuscript. All authors have read and approved the final version of the manuscript.

REFERENCES

1. Al-Rohaimi AH, Al OF. Novel SARS-CoV-2 outbreak and COVID19 disease; a systemic review on the global pandemic. Genes Dis. 2020;7(4):491–501.

2. European Centre for Disease Prevention and Control. COVID-19 country overviews. Week. 2020;51: 2020.

3. Yan Y, Chang L, Wang L. Laboratory testing of SARS-CoV, MERS-CoV, and SARS-CoV-2 (2019-nCoV): current status, challenges, and countermeasures. Rev Med Virol. 2020;30(3):e2106.

4. Carrillo J, Izquierdo-Useros N, Avila-Nieto C, Pradenas E, Clotet B, Blanco J. Humoral immune responses and neutralizing antibodies against SARS-CoV-2; implications in pathogenesis and protective immunity. Biochem Biophys Res Commun. 2020;538:187–91.

5. Petherick A. Developing antibody tests for SARS-CoV-2. Lancet. 2020;395(10230):1101–2.

6. Sethuraman N, Jeremiah SS, Ryo A. Interpreting diagnostic tests for SARS-CoV-2. JAMA. 2020;323(22):2249–51.

7. Cheng MP, Yansouni CP, Basta NE, et al. Serodiagnostics for severe acute respiratory syndrome-related Coronavirus 2: a narrative review. Ann Intern Med. 2020;173(6):450–60.

8. Huang AT, Garcia-Carreras B, Hitchings MDT, et al. A systematic review of antibody mediated immunity to coronaviruses: kinetics, correlates of protection, and association with severity. Nat Commun. 2020;11(1):4704.

9. Piccoli L, Park YJ, Tortorici MA, et al. Mapping neutralizing and immunodominant sites on the SARS-CoV-2 spike receptor-binding domain by structure-guided high-resolution serology. Cell. 2020;183(4):1024–42 (e21).

10. Shi R, Shan C, Duan X, et al. A human neutralizing antibody targets the receptor-binding site of SARS-CoV-2. Nature. 2020;584(7819):120–4.

11. Wang S, Peng Y, Wang R, et al. Characterization of neutralizing antibody with prophylactic and therapeutic efficacy against SARS-CoV-2 in rhesus monkeys. Nat Commun. 2020;11(1):5752.

12. Krammer F. SARS-CoV-2 vaccines in development. Nature. 2020;586(7830):516–27.

13. Brouwer PJM, Caniels TG, van der Straten K, et al. Potent neutralizing antibodies from COVID-19 patients define multiple targets of vulnerability. Science. 2020;369(6504):643–50.

14. Rogers TF, Zhao F, Huang D, et al. Isolation of potent SARS-CoV-2 neutralizing antibodies and protection from disease in a small animal model. Science. 2020;369(6506):956–63.

15. To KK-W, Tsang OT-Y, Leung W-S, et al. Temporal profiles of viral load in posterior oropharyngeal saliva samples and serum antibody responses during infection by SARS-CoV-2: an observational cohort study. Lancet Infect Dis. 2020;20(5):565–74.

16. Jaaskelainen AJ, Kuivanen S, Kekalainen E, et al. Performance of six SARS-CoV-2 immunoassays in comparison with microneutralisation. J Clin Virol. 2020;129:104512.

17. Kohmer N, Westhaus S, Ruhl C, Ciesek S, Rabenau HF. Brief clinical evaluation of six high-throughput SARS-CoV-2 IgG antibody assays. J Clin Virol. 2020;129:104480.

18. Weidner L, Gansdorfer S, Unterweger S, et al. Quantification of SARS-CoV-2 antibodies with eight commercially available immunoassays. J Clin Virol. 2020;129:104540.

19. National S-C-SAEG. Performance characteristics of five immunoassays for SARS-CoV-2: a head-to-head benchmark comparison. Lancet Infect Dis. 2020;20(12):1390–400.

20. Radon K, Saathoff E, Pritsch M, et al. Protocol of a population-based prospective COVID-19 cohort study Munich, Germany (KoCo19). BMC Public Health. 2020;20(1):1036.

21. Pritsch M, Radon K, Bakuli A, et al. Prevalence and risk factors of infection in the representative COVID-19 cohort Munich. Int J Environ Res Public Health. 2021;18(7):3572.

22. Olbrich L, Castelletti N, Schälte Y, et al. A serology strategy for epidemiological studies based on the comparison of the performance of seven different test systems: the representative COVID-19 cohort Munich. medRxiv. 2020. https://doi.org/10.1101/2021.01.13.21249735.

23. EUROIMMUN anti-SARS-CoV-2 ELISA IgG, Package Insert. 2020.

24. Beavis KG, Matushek SM, Abeleda APF, et al. Evaluation of the EUROIMMUN Anti-SARS-CoV-2 ELISA Assay for detection of IgA and IgG antibodies. J Clin Virol. 2020;129:104468.

25. Muench P, Jochum S, Wenderoth V, et al. Development and Validation of the elecsys anti-SARS-CoV-2 immunoassay as a highly specific tool for determining past exposure to SARS-CoV-2. J Clin Microbiol. 2020;58(10). https://doi.org/10.1128/JCM.01694-20.

26. World Health Organization Expert Committee on Biological Standardization. WHO/BS.2020.2403 Establishment of the WHO International Standard and Reference Panel for anti-SARS-CoV-2 antibody, 9–10 December 2020. https://www.who.int/publications/m/item/WHO-BS-2020.2403. Accessed 16 Feb 2021.

27. Haselmann V, Ozcurumez MK, Klawonn F, et al. Results of the first pilot external quality assessment (EQA) scheme for anti-SARS-CoV2-antibody testing. Clin Chem Lab Med. 2020;58(12):2121–30.

28. Yekutieli D, Benjamini Y. The control of the false discovery rate in multiple testing under dependency. Ann Stat. 2001;29(4):1165–88.

29. Tian Y, Lian C, Chen Y, et al. Sensitivity and specificity of SARS-CoV-2 S1 subunit in COVID-19 serology assays. Cell Discov. 2020;6:75.

30. Ouyang J, Isnard S, Lin J, et al. Convalescent plasma: the relay baton in the race for coronavirus disease 2019 treatment. Front Immunol. 2020;11:570063.

Publication 9:

Deterministic approaches for head lice infestations and treatments

Noemi Castelletti, Maria Vittoria Barbarossa

Infectious Disease Modelling, Jun 2020, IF 2.318
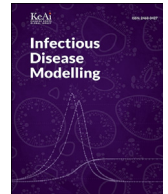
Deterministic approaches for head lice infestations and treatments

Noemi Castelletti [a], Maria Vittoria Barbarossa [b, *, 1]

[a] Institute of Radiation Medicine, Helmholtz Zentrum München, Ingolstädter Landstraße 1, D-85764, Neuherberg, Germany
[b] Institute of Applied Mathematics, Heidelberg University, Im Neuenheimer Feld 205, D-69120 Heidelberg, Germany

A B S T R A C T

Pediculus humanus capitis are human ectoparasites which cause infestations, mostly in children, worldwide. Understanding the life cycle of head lice is an important step in knowing how to treat lice infestations, as the parasite behavior depends considerably on its age and gender. In this work we propose a mathematical model for head lice population dynamics in hosts who could be or not quarantined and treated. Considering a lice population structured by age and gender we formulate the model as a system of hyperbolic PDEs, which can be reduced to compartmental systems of delay or ordinary differential equations. Besides studying fundamental properties of the model, such as existence, uniqueness and nonnegativity of solutions, we show the existence of (in certain cases multiple) equilibria at which the infestation persists on the host's head. Aiming to assess the performance of treatments against head lice infestations, by mean of computer experiments and numerical simulations we investigate four possible treatment strategies. Our main results can be summarized as follows: (i) early detection is crucial for quick and efficient eradication of lice infestations; (ii) dimeticone-based products applied every 4 days effectively remove lice in at most three applications even in case of severe infestations and (iii) minimization of the reinfection risk, e.g. by mean of synchronized treatments in families/classrooms is recommended.

1. Introduction

Pediculus humanus capitis, commonly known as head lice, are obligate exclusively human ectoparasites, source of annoying infestations worldwide (Cummings, Finlay, & MacDonald, 2018; Feldmeier, 2014). The main head lice transmission route being close head-to-head contact (Meister & Ochsendorf, 2016; Speare, Thomas, & Cahill, 2002), pediculus capitis epidemics occur mostly in schools and kindergartens, independently on the country of origin, ethnic groups and socio-economic status of the host (Feldmeier, 2012).

Wingless and up to 4 mm long head lice live on the human scalp, feeding 4—8 times a day by sucking blood from the host and injecting saliva simultaneously (Cummings et al., 2018; Takano-Lee, Yoon, Edman, Mullens, & Clark, 2003). The life cycle

of the louse is structured into five stages. After mating, breeding females can lay up to 6 eggs per day for 30 days (Cummings et al., 2018), close to the scalp, where temperature and humidity are optimal for their growth. Lice eggs (also called nits) hatch 6–11 days after ovoposition into nymphs that molt twice over the next 8–10 days to become adult lice. In contrast to nymphs after the first and second molt, first stage nymphs are not motile (Takano-Lee et al., 2003). Differentiation into female or male louse occurs after the third molt, when the insect becomes adult and sexually active. During mating both female and male louse might die (Rasmussen, Burgess, Rozsa, & Søholt Larsen, 2019). Adult insects live about 30 days (Takano-Lee et al., 2003), but can survive for only 1–2 days away from the human host (Burkhart, 2003).

Pediculosis-induced itching occurs when the host develops an allergic reaction to the lice saliva, usually four to six weeks from the beginning of the infestation. Diagnosis of head lice infestations is based on the detection of adults, nymphs and/or viable eggs on the host hair and scalp. Well-established treatment options for head lice infestations include therapeutic wet combing, topical application of a pediculicide, and oral treatments (Feldmeier, 2012), the last not being considered in our study. Wet combing is a non-chemical treatment, optimal for detection of head lice infestations (Gallardo, Toloza, Vassena, Picollo, & Mougabure-Cueto, 2013), but very time consuming when performed for taking advantage of its therapeutic effects (Feldmeier, 2012). Most pediculicides, such as those based on malathion, pyrethrins and its synthetic derivates, can kill nymphs and adult lice, but are in general non-ovocidal. Extensive use of these compounds has led to the development of resistant head lice populations (Cummings et al., 2018; Feldmeier, 2012). In contrast, dimeticone-based pediculicides showed moderate to high efficacy against live lice and eggs and the development of resistance to such products is less likely (Feldmeier, 2012).

Whereas mathematical models for the dynamics and control of vector-borne diseases, such as mosquitoes or ticks, are well established (see e.g. Ch.4 in (Martcheva (2015)) for an introductory overview), to the best of our knowledge only two groups have previously proposed mathematical approaches for understanding the spread of pediculosis. An epidemic model for transmission among hosts based on a stochastic SIS approach was suggested by Stone, Wilkinson-Herbots, and Isham (2008). This model describes only the macroscopic level (host interactions) and it does not consider the biology of the lice life cycle. Laguna and Risau-Gusman (2011) proposed a discrete model based on Leslie-Lefkovitch matrices and studied growth and interactions of colonies of head lice. This model was used in computer simulations to estimate the efficacy of different control strategies on the growth of the lice colony. In a further recent work (Toloza et al., 2018) the mathematical model was combined with data collected from schools in order to estimate the most likely events that can give rise to infestations.

We propose here a mechanistic mathematical model for understanding the biology of the life cycle of head lice and assessing the efficiency of different treatments to eradicate lice infestations. Our first and more general approach is based on structured populations which are continuous in time and age, hence hyperbolic partial differential equations (PDEs). In contrast to the model by Laguna and Risau-Gusman (2011) we explicitly include the dynamics of the male lice and propose a mating function for pair formation. In Sect. 2 we show under which conditions our PDE model can be reduced to systems of delay differential equations or ordinary differential equations. The latter are first analyzed (Sect. 3) and then used for computer experiments and numerical simulations (Sect. 4) to investigate the efficacy of four possible treatments against head lice.

2. Modeling head lice life cycle and transmission

In this section we propose mathematical models for head lice infestations based on the biology of the lice life cycle. We first consider a lice population in an isolated environment, such as the head of an infected quarantine host. In a second step we extend the models to include lice transmission between hosts.

2.1. Populations structured by age

One possibility for modeling the lice life cycle is to use continuous age structures (Cushing, 1998). We shall adapt and extend here the approach proposed by Hoppensteadt (1975) for a population structured by age with distinction of the two sexes.

Let $w(t, a)$ denote the density of single female lice of age $a \geq 0$ at time $t \geq 0$, that is, females which are not breeding and are available for mating. Respectively, we denote by $w^B(t, a)$ the density of breeding females, and by $m(t, a)$ the density of single male lice. We assume that the death rates are age-dependent functions. Birth rates are not relevant for the moment and shall be introduced later. Let $\mu_w(a)$ and $\mu_m(a)$ denote the death rate of female and male lice, respectively. In contrast to the model proposed in Laguna and Risau-Gunsman (2011), in which it is assumed that males are readily available and that with only one fertilization female lice are able to lay eggs until they die, we explicitly introduce the mating component and the possibility of multiple fertilization. Models for pair formation in structured populations, were previously proposed by several authors, including Hadeler (1989, 1993) and Castillo-Chavez, Busenberg, and Gerow (1991). Let $p(t, x, y)$ be the lice pairs which, at time $t \geq 0$, are formed by females of age $x \geq 0$ and males of age $y \geq 0$. We describe pair formation by mean of a function $\varphi(w, m)(t, x, y) := \tilde{\rho}(x, y)\pi(w(t, x), m(t, y))$, where $\tilde{\rho}(x, y)$ is the age-dependent mating rate and $\pi(w, m)$ represents the mating behavior. We assume that the following properties hold:

(i) $\tilde{\rho}(x, y) \geq 0$ for all $x \geq 0$, $y \geq 0$,
(ii) $\pi(w, m) \geq 0$ and continuously differentiable in both variables.

As pair formation is not possible when only females or only males are present we require that

(iii) $\pi(0,m) = 0$, $\pi(w,0) = 0$, for all $m \geq 0$, $w \geq 0$
(iv) $\partial_w \pi(w,m)|_{(w,0)} = 0 = \partial_m \pi(w,m)|_{(0,m)}$.

Among the functions which satisfy the above assumptions (i)-(iv), possible choices for $\pi(w, m)$ are given by the incidence law,

$$\pi(w(t,x), m(t,y)) = \frac{w(t,x)m(t,y)}{\displaystyle\int_0^\infty w(t,u)\,du + \int_0^\infty m(t,u)\,du},$$

as suggested in Li (2004) for mating of mosquitoes, or by the mass action law

$$\pi(w(t,x), m(t,y)) = w(t,x)m(t,y),$$

often used for modeling contacts in epidemiological models (Martcheva, 2015). In this paper we shall use the latter mating function. During a mating process both female and male louse might die. In particular it has been reported that if one of the two insects dies during the mating process, the other one dies as well (Rasmussen et al., 2019). To capture this phenomenon we introduce the probability $\xi \in [0, 1]$ that a pair does not survive the mating process. Respectively, with probability $1 - \xi$ both insects survive. We assume that pairs split at some constant rate $\sigma > 0$, independent of the age of the insects. That is, for a pair formed by a female of age x and a male of age y, let the pair splitting rate be $\sigma(x,y) \equiv \sigma \geq 0$. In time, single female lice age, might die due to natural death, and can mate with males. It is still discussed whether a female which had a fertile mating will be breeding for its whole life (Maunder, 1993), as it has been observed for the pubic louse (Bourgess, Maunder, & Myint, 1983), or it needs a new mating for a new ovoposition (Boutellis, Abi-Rached, & Raoult, 2014; Mehlhorn, 2012). To keep the model as general as possible, we introduce the return rate, ϑ_α, of breeding females to the nonbreeding compartment. This parameter is defined as the product $\vartheta_\alpha := \alpha\vartheta$, where $1/\alpha > 0$ corresponds to the average length of the breeding period and $\vartheta \in [0, 1]$ is the probability that after the breeding period a female lice returns to the nonbreeding compartment. From balance laws and classical approaches for age-structured populations (Webb, 2008) we obtain the equation

$$\partial_t w(t, a) = -\underbrace{\partial_a w(t, a)}_{\text{aging}} - \underbrace{\mu_w(a)w(t, a)}_{\text{death}} - \underbrace{\int_0^\infty \phi(w, m)(t, a, y)\,dy}_{\text{pair formation}} + \underbrace{\vartheta_\alpha w^B(t, a).}_{\substack{\text{females which are} \\ \text{no longer breeding}}} \tag{1}$$

Analogously, the dynamics of the male population is given by

$$\partial_t m(t, a) = -\underbrace{\partial_a m(t, a)}_{\text{aging}} - \underbrace{\mu_m(a)m(t, a)}_{\text{death}} - \underbrace{\int_0^\infty \phi(w, m)(t, x, a)\,dx}_{\text{pair formation}} + \underbrace{\sigma(1 - \xi)\int_0^\infty p(t, x, a)\,dx}_{\text{pairs split}}. \tag{2}$$

The equation for pairs is given by

$$\partial_t p(t, x, y) = -\partial_x p(t, x, y) - \partial_y p(t, x, y) - \underbrace{(1 - \xi)\sigma p(t, x, y)}_{\text{pairs split}} - \underbrace{\xi\sigma p(t, x, y)}_{\text{pairs die}} + \underbrace{\phi(w, m)(t, x, y)}_{\text{pair formation}}. \tag{3}$$

After pair splitting the female moves to the breeding stage which culminates with an ovoposition. The dynamics of breeding females is given by

$$\partial_t w^B(t, a) = -\partial_a w^B(t, a) - \mu_{w^B}(a)w^B(t, a) - \vartheta_\alpha w^B(t, a) + \int_0^\infty (1 - \xi)\sigma p(t, a, y)\,dy. \tag{4}$$

New individuals are born by females in the breeding stage (in contrast, in (Hadeler (1993)) they were born by pairs). Let $b(t, a)$ be the fertility rate of a breeding female of age a at time t. With a certain probability $r \in [0, 1]$ the egg will evolve into a male, respectively, with probability $1 - r$ into a female. It is biological plausible to assume that there is no breeding female of age zero, nor pair in which one of the two insects is of age zero. Hence for all $t \geq 0$ we have the boundary conditions:

$$w(t,0) = (1-r)\int_0^\infty b(t,a)w^B(t,a)\,da,$$

$$m(t,0) = r\int_0^\infty b(t,a)w^B(t,a)\,da,$$

$$w^B(t,0) = 0, \text{ and } p(t,0,y) = 0 = p(t,x,0) \quad \text{for all } x,\, y \geq 0.$$

(5)

Nonnegative initial age distributions complete the model (1)–(5).

2.2. Transmission

Parasite transmission is dependent on the life cycle of the louse (Meister & Ochsendorf, 2016), in particular adult lice can move from host to host, while eggs or early stage nymphs are not motile (Rasmussen et al., 2019). We define the *transferring rates* $\alpha_w(t,a)$ and $\beta_w(t,a)$ of female lice moving onto the host's head, respectively away from the host's head. Analogously, let $\alpha_m(t,a)$ and $\beta_m(t,a)$ be the transferring rates for males. Following (Rasmussen et al., 2019), we assume that neither breeding females nor pairs move from host to host. Then equations (1) and (2) change into

$$\partial_t w(t,a) = -\partial_a w(t,a) - \mu_w(a)w(t,a) - \int_0^\infty \phi(w,m)(t,a,y)\,dy + \vartheta_\alpha w^B(t,a) - \beta_w(t,a)w(t,a) + \alpha_w(t,a),$$

(6)

respectively,

$$\partial_t m(t,a) = -\partial_a m(t,a) - \mu_m(a)m(t,a) - \int_0^\infty \phi(w,m)(t,x,a)\,dx + \sigma(1-\xi)\int_0^\infty p(t,x,a)\,dx - \beta_m(t,a)m(t,a) + \alpha_m(t,a).$$

(7)

Note that in equations (6) and (7) we chose age- and time-dependent transferring rates: dependence on age is for considering different transmission rates at different life stages of the louse, whereas dependence on time allows to model situations such as quarantine or interactions with other hosts (see Sec. 4).

2.3. From the age structure to delay equations

In spite of their elegance, continuous age-structured models such as (1)–(5) are hardly comparable to collected data, which are commonly of discrete nature, counting lice in a certain age group or life stage (Takano-Lee et al., 2003). To provide a qualitative description of the head lice life cycle, such that it could be compared to experimental data, one might use compartmental models formulated as systems of ordinary differential equations (ODEs) or delay differential equations (DDEs). In the following we apply methods from Barbarossa, Hadeler, and Kuttler (2014) and Bocharov and Hadeler (2000) and show how to obtain a system of DDEs from the above PDE model (1)–(5). Let us suppose that we want to make use of mathematical models to understand lice reproduction or to fine-tune specific treatments which target adult lice only (or eggs only). Then we can simplify the continuous age structure in model (1)–(5) and consider two classes of insects, namely, head lice in the juvenile phase (eggs and nymphs, $a \leq \tau$) and adult lice ($a > \tau$). During the juvenile phase of length τ days, lice are either in the egg stage or in one of the nymphs stages, and do not mate nor move. The biology suggests that $\tau \in [13-16]$ days (cf. Sec. 1 and Table 1). Let us define for all $t \geq 0$ the following model variables:

$$J(t) = \int_0^\tau (m(t,a) + w(t,a))\,da, \quad \text{the total number of juveniles,}$$

$$W(t) = \int_\tau^\infty w(t,a)\,da, \quad \text{the total number of nonbreeding adult females,}$$

$$M(t) = \int_\tau^\infty m(t,a)\,da, \quad \text{the total number of adult males,}$$

$$P(t) = \int_0^\infty \int_0^\infty p(t,x,y)\,dx\,dy, \quad \text{the total number of pairs,}$$

$$W^B(t) = \int_\tau^\infty w^B(t,a)\,da, \quad \text{the total number of adult breeding females.}$$

We characterize these populations in terms of fertility, death, motility and mating rates. We assume that single females and male lice die at the same rate, hence:

Table 1
Model parameters, description and values used for numerical simulations.

Rate	Description	Value (Unit)	Reference
b_1	laid eggs per adult female	3 [1/day]	(Lebwohl, Clark, & Levitt, 2007; Takano-Lee et al., 2003)
μ_0	eggs death rate	0.35 [1/day]	(Takano-Lee et al., 2003)
μ_N	nymphs death rate	0.195 [1/day]	(Takano-Lee et al., 2003)
μ_1	adult lice death rate	1/30 [1/day]	(Lebwohl et al., 2007; Takano-Lee et al., 2003)
μ_B	breeding females death rate	1/25 [1/day]	(Lebwohl et al., 2007; Takano-Lee et al., 2003)
$1/\eta$	egg stage duration	7 [days]	(Takano-Lee et al., 2003)
$1/\omega$	nymph stage duration	9 [days]	(Takano-Lee et al., 2003)
r	prob. for egg to turn into male louse	0.367	(Perotti et al., 2004)
ρ	mating rate	0.9	(Lebwohl et al., 2007; Takano-Lee et al., 2003)
ϑ	prob. for W^B to return to W	100%	(Boutellis et al., 2014; Mehlhorn, 2012)
$1/\alpha$	duration of breeding stage	3 [days]	(Takano-Lee et al., 2003)
ξ	death prob. during mating	5%	assumed
β_W	transferring rate females (outgoing)	0.35 [1/day]	assumed
β_M	transferring rate males (outgoing)	0.35 [1/day]	assumed
α_W	transferring rate females (incoming)	1 [1/day]	assumed
α_M	transferring rate males (incoming)	1 [1/day]	assumed

$$\mu_w(a) \equiv \mu_m(a) = \begin{cases} \mu_0 & a \le \tau, \\ \mu_1 & a > \tau, \end{cases} \quad \text{with} \quad \mu_1 \ge \mu_0 > 0.$$

Pair formation occurs only among adult lice, thus for the age-dependent mating rate $\tilde{\rho}(x,y)$ we set

$$\tilde{\rho}(x,y) = \begin{cases} 0 & \text{if} \quad x \le \tau \quad \text{or} \quad y \le \tau, \\ \rho & \text{if} \quad x > \tau \quad \text{and} \quad y > \tau. \end{cases}$$

As a result, $p(t,x,y) = 0$ for $x \le \tau$ or $y \le \tau$. It follows that there is no breeding female of age $x \le \tau$, that is,

$$p(t,x,y) = 0, \quad \text{for } x \le \tau \text{ or } y \le \tau, \\ w^B(t,a) = 0, \quad a \le \tau. \tag{8}$$

For simplicity, let us assume that the fertility rate of breeding females,

$$b(t,a) = \begin{cases} 0 & \text{if} \quad a \le \tau, \\ b_1 \ge 0 & \text{if} \quad a > \tau, \end{cases}$$

and the death rate, $\mu_{w^B}(a) = \mu_B > 0$, are constant values for all $t \ge 0$, $a > \tau$. It is biologically meaningful to assume that there is no "infinitely old" female, that is, $w(t,a) \to 0$ for $a \to \infty$. Similarly,

$$m(t,a) \to 0, \quad w^B(t,a) \to 0 \quad \text{for} \quad a \to \infty, \\ p(t,x,y) \to 0, \quad \text{for} \quad x \to \infty \quad \text{or} \quad y \to \infty.$$

As in Sect. 2.2, we use transmission coefficients to observe head-lice moving from one head to another. Under the assumption that juvenile lice do not move, we set

$$\beta_w(t,a) = \begin{cases} 0 & a \le \tau, \\ \beta_W(t) \ge 0 & a > \tau, \end{cases} \qquad \alpha_w(t,a) = \begin{cases} 0 & a \le \tau, \\ \alpha_W(t) \ge 0 & a > \tau, \end{cases}.$$

Analogously, we set $\beta_m(t,a) = \beta_M(t) \ge 0$, respectively $\alpha_m(t,a) = \alpha_M(t) \ge 0$, for $a > \tau$ and zero otherwise. Under the above assumptions, differential equations for variables J, M, W and W^B can be rigorously obtained (cf. Barbarossa, Hadeler, & Kuttler, 2014; Bocharov & Hadeler, 2000) from system (1)–(5). We show in the following how to obtain the equation for the juveniles.

$$\dot{J}(t) = \partial_t \int_0^\tau (w(t,a) + m(t,a)) \, da$$

$$= -\int_0^\tau (\partial_a w(t,a) + \partial_a m(t,a)) \, da \; - \int_0^\tau (\mu_w(a)w(t,a) + \mu_m(a)m(t,a)) \, da \; - \int_0^\tau \beta_m(t,a)m(t,a) \, da$$

$$+ \int_0^\tau \alpha_m(t,a) \, da - \int_0^\tau \beta_w(t,a)w(t,a) \, da + \int_0^\tau \alpha_w(t,a) \, da$$

$$= -w(t,\tau) - m(t,\tau) + w(t,0) + m(t,0) - \mu_0 J(t)$$

$$\underset{(5)}{=} -w(t,\tau) - m(t,\tau) + \int_0^\infty b(t,a)w^B(t,a) \, da - \mu_0 J(t)$$

$$= -w(t,\tau) - m(t,\tau) + \int_\tau^\infty b(t,a)w^B(t,a) \, da - \mu_0 J(t)$$

$$= -w(t,\tau) - m(t,\tau) + b_1 W^B(t) - \mu_0 J(t).$$

In the last expression we still find the addends $w(t,\tau)$, $m(t,\tau)$, related to the PDE approach. These shall be formulated in terms of the new variables J, M, W, W^B. Applying the method of characteristics, for $t > \tau$ we find

$$w(t,\tau) = w(t-\tau,0)e^{-\mu_0\tau} = (1-r)b_1 W^B(t-\tau)e^{-\mu_0\tau},$$
$$m(t,\tau) = m(t-\tau,0)e^{-\mu_0\tau} = rb_1 W^B(t-\tau)e^{-\mu_0\tau}.$$

Hence, the equation for the juveniles is given by

$$\dot{J}(t) = b_1 W^B(t) - b_1 W^B(t-\tau)e^{-\mu_0\tau} - \mu_0 J(t). \tag{9}$$

Similarly, one can obtain the equations for adult females, adult males and breeding females. For the total number of pairs it is useful to recall condition (8).

Then we have

$$\dot{P}(t) = \partial_t \int_0^\infty \int_0^\infty p(t,x,y) \, dx \, dy$$

$$= -\int_\tau^\infty \int_\tau^\infty \partial_x p(t,x,y) \, dx \, dy - \int_\tau^\infty \int_\tau^\infty \partial_y p(t,x,y) \, dx \, dx - \int_\tau^\infty \int_\tau^\infty \sigma p(t,x,y) \, dx \, dy + \int_\tau^\infty \int_\tau^\infty \phi(w,m)(t,x,y) \, dx \, dy$$

$$= -\sigma P(t) + \rho W(t)M(t).$$

Mating is rather fast compared to other processes, such as death or reproduction, in the life cycle of head lice (Rasmussen et al., 2019). Hence, we can assume the pairs dynamics to occur on a fast time scale, hence that it holds $\varepsilon\dot{P} = -\sigma P + \rho WM$, for $\varepsilon > 0$ small. Considering the limit $\varepsilon \to 0$ we obtain the quasi-steady state approximation, $P = \rho WM/\sigma$, and substitute this in the equations for M and W^B. Thus the DDE model is reduced to a system of four equations:

$$\begin{aligned}
\dot{J}(t) &= b_1 W^B(t) - b_1 W^B(t-\tau)e^{-\mu_0\tau} - \mu_0 J(t) \\
\dot{W}(t) &= (1-r)b_1 W^B(t-\tau)e^{-\mu_0\tau} - (\mu_1 + \rho M(t) - \beta_W(t))W(t) + \vartheta_\alpha W^B(t) + \alpha_W(t) \\
\dot{M}(t) &= rb_1 W^B(t-\tau)e^{-\mu_0\tau} - (\mu_1 + \xi W(t) - \beta_M(t))M(t) + \alpha_M(t) \\
\dot{W}^B(t) &= -(\vartheta_\alpha + \mu_B)W^B(t) + (1-\xi)\rho W(t)M(t).
\end{aligned} \tag{10}$$

A similar model was proposed in the master thesis of the first author (Castelletti, 2015). It can be observed that whereas in the equations for W and M the delay appears in form of a positive feedback term, in the juvenile population we find a negative feedback due to maturation ($-b_1 W^B(t-\tau)e^{-\mu_0\tau}$). In the unfortunate case $J(0) = 0$, $W^B(0) = 0$ and $W^B(t) > 0$ for $t < 0$ this would lead to a negative solution for J. For guaranteeing nonnegativity of solutions proper initial data can be chosen, as we explain below.

A general expression for the number of juvenile lice at time $t \geq 0$ is given by

$$J(t) = \int_0^t b_1 W^B(v)e^{-\mu_0(t-v)}\Pi(t-v) \, dv, \tag{11}$$

meaning that juveniles at time t are those eggs deposited in the interval of time $[0,t]$, which did not die nor exited the juvenile compartment. The probability $\Pi(a)$ relates to the maturation rate and transition to the adult compartment of juveniles of age

a. Dependent on the choice of the probability distribution one can obtain various types of differential equations (Yuan & Bélair, 2014). For example, if we choose the uniform distribution

$$\Pi(a) = \begin{cases} 1, & \text{for } a \in [0, \tau] \\ 0, & \text{otherwise}, \end{cases}$$

then substitution in (11) yields

$$J(t) = \int_0^\tau b_1 W^B(t-v) e^{-\mu_0 v} \, dv = \int_{t-\tau}^t b_1 W^B(w) e^{-\mu_0(t-w)} \, dw. \tag{12}$$

Differentiating (12) with respect to the time *t* we obtain equation (9). Equation (12) could be used for defining biologically meaningful initial data for the DDE model (10) and guaranteeing nonnegativity of solutions. Alternatively, starting from the PDE approach, one could obtain a nonautonomous ODE system on $[0, \tau]$ whose right-hand side depends on the initial age distribution of the underlying PDE model (cf. Bocharov & Hadeler, 2000; Mohr, Barbarossa, & Kuttler, 2014).

2.4. When treatments target specific life stages

Treatments of head lice infestations are based on products (cf. Sec. 1) which target specific life stages of the lice. In particulars certain treatments are effective only against nymphs and adult lice, whereas others target also eggs. To model treatments we shall use time dependent functions. Further we shall include compartments for all lice stages of interest, in particular we shall refine the juvenile class in (11) and consider eggs and nymphs separately.

We go back to the integral equation (11). Choosing for Π an exponential distribution,

$$\Pi(a) = e^{-\eta a},$$

and substituting in (11), we obtain

$$J(t) = \int_0^t b_1 W^B(t-v) e^{-\mu_0(t-v)} e^{-\eta(t-v)} \, dv.$$

Differentiation with respect to the time *t* yields the ordinary differential equation

$$\dot{J}(t) = b_1 W^B(t) - (\mu_0 + \eta) J(t).$$

The maturation term $\eta J(t)$ indicates that $1/\eta$ is the average duration of the juvenile stage. Assuming as above that transitions between one life stage and the next follow an exponential distribution, one can introduce a new compartment for each life stage to observe. The result is a system of ODEs with linear transitions between compartments (MacDonald, 1978), namely

$$
\begin{aligned}
\dot{U}(t) &= b_1 W^B(t) - (\mu_0 + \eta) U(t) - T_U(t) U(t) \\
\dot{N}(t) &= \eta U(t) - (\omega + \mu_N + T(t)) N(t) \\
\dot{W}(t) &= (1-r)\omega N(t) - (\mu_1 + \rho M(t) + T(t) + \beta_W(t)) W(t) + \vartheta_\alpha W^B(t) + \alpha_W(t) \\
\dot{M}(t) &= r\omega N(t) - (\mu_1 + \xi W(t) + \beta_M(t) + T(t)) M(t) + \alpha_M(t) \\
\dot{W}^B(t) &= (1-\xi)\rho M(t) W(t) - (\mu_B + \vartheta_\alpha + T(t)) W^B(t),
\end{aligned}
\tag{13}
$$

with sub-populations for eggs (U), nymphs (N), single adult females (W), males (M) and breeding females (W^B). Maturation from eggs to nymphs, and from nymphs to adult, occurs at rate $\eta > 0$ and $\omega > 0$, respectively. A schematic representation of the mathematical model (13) is presented in Fig. 1. The terms $T_U(t)$ and $T(t)$ describe the effect of treatments against eggs and nymphs/adult lice, such as shampoos or combs. For the numerical tests shown in Sect. 4 we will choose these functions to be equal to zero in absence of treatment and nonzero at the time of the treatment.

2.5. Limit cases

We conclude this section with few considerations on the limit cases, $\vartheta = 0, 1$ and $\xi = 0, 1$. When $\xi = 0$, no louse dies during the mating process. This assumption simplifies the equations for $M(t)$ and $W^B(t)$, as all females which mate will be able to lay eggs. In contrast, the case $\xi = 1$ is not of biological interest. If all insects which mate die, the whole population will soon die out.
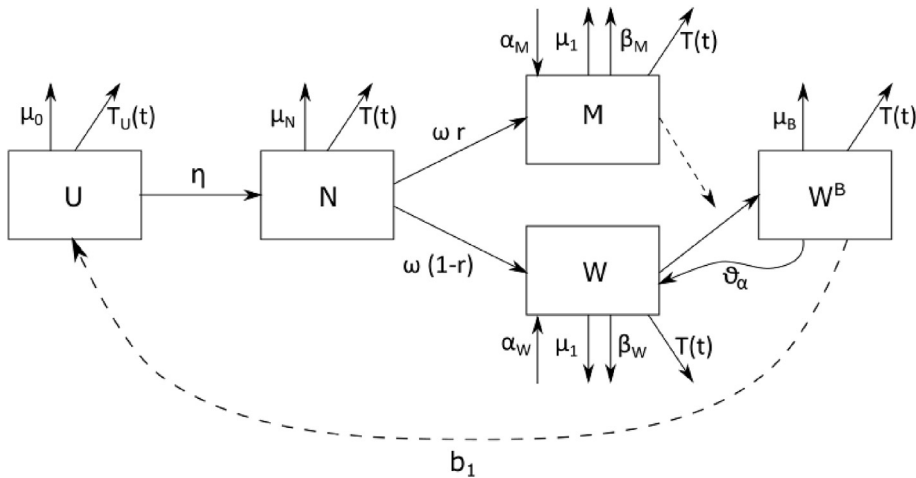
Fig. 1. A schematic representation of the five compartment model (13), with sub-populations for eggs (U), nymphs (N), females (W), males (M) and breeding females (W^B). The model includes reproduction (b_1), maturation from one compartment into the next one (η, ω), death (μ_j), migration (α_j, β_j) and time-dependent treatments ($T_U(t)$, $T(t)$).

Setting $\vartheta = 0$, hence $\vartheta_\alpha = 0$, one assumes that after the first mating a female will lay eggs for its whole lifetime, as it was assumed in Laguna and Risau-Gusman (2011). On the other hand, $\vartheta = 1$, that is, $\vartheta_\alpha = \alpha$, means that females are breeding for a time $1/\alpha$, then need to mate again for a new ovoposition.

3. Analytical results

In this section we present analytical results on the autonomous version of model (13), with $T(t) \equiv 0 \equiv T_U(t)$, for all $t \geq 0$. In the first step we consider isolated hosts, hence no lice transmission ($\alpha_j(t) \equiv 0 \equiv \beta_j(t), j = W, M$), and study existence and stability of biologically relevant equilibria.

Theorem 1. *Consider system* (13) *with* $\alpha_j(t) \equiv 0 \equiv \beta_j(t)$, $j = W, M$, $T(t) \equiv 0 \equiv T_U(t)$ *for all* $t \geq 0$, *and let nonnegative initial values be given. Then the autonomous system admits a unique nonnegative solution.*

Proof. Existence and uniqueness of the solution are guaranteed by the theorem of Picard–Lindelöf and the proof is trivial, given the smoothness of the right-hand side. For the nonnegativity of solutions we consider the right-hand side at the boundaries of the positive cone. Let us assume that for some $\bar{t} > 0$ the solution $U(\bar{t}) = 0$, while all others components are nonnegative, then we have $\dot{U}(\bar{t}) = b_1 W^B(\bar{t}) \geq 0$. Hence the component U does not drop below zero. Similarly, one can show nonnegativity for all other model components.

Theorem 2. *Consider system* (13) *with* $\alpha_j(t) \equiv 0 \equiv \beta_j(t)$, $j = W, M$, *and* $T(t) \equiv 0 \equiv T_U(t)$ *for all* $t \geq 0$. *There is only one lice-free-equilibrium (LFE)* $P_0 = (0, 0, 0, 0, 0)$, *and there is no other equilibrium of the system in which at least one component is equal to zero. The lice-free-equilibrium is locally asymptotically stable.*

Proof. We omit the trivial computation to show that the LFE is unique and that there is no further equilibrium with one or more components equal to zero. Shortly, if any component of the equilibrium is zero, then recursively all other components turn out to be zero.

For the proof of local asymptotic stability we linearize about P_0 and obtain the linear system $\dot{Z}(t) = J(P_0)Z(t)$, with the Jacobian matrix

$$J(P_0) = \begin{pmatrix} -\mu_0 - \eta & 0 & 0 & 0 & b_1 \\ \eta & -\omega - \mu_N & 0 & 0 & 0 \\ 0 & (1-r)\omega & -\mu_1 & 0 & \vartheta_\alpha \\ 0 & r\omega & 0 & -\mu_1 & 0 \\ 0 & 0 & 0 & 0 & -\mu_B - \vartheta_\alpha \end{pmatrix}$$

Local stability of P_0 is determined by the real parts of the roots λ of the characteristic polynomial, $\det(J(P_0 - \lambda I)) = 0$. As by assumption all parameters in (13) are nonnegative, and in particular all death rates are strictly positive, it can be quickly shown that $\lambda_j < 0$, $j = 1, \ldots, 5$. Thus, the LFE is a locally asymptotically stable node. ∎

Assume from here on that $\xi > 0, \rho > 0$. For the proof of existence and uniqueness of a nontrivial equilibrium it is convenient to define the nonnegative constants

$$\mathscr{R}_0^W := \frac{(1-\xi)r\omega\eta b_1\rho}{\xi(\mu_0+\eta)(\omega+\mu_N)(\mu_B+\vartheta_\alpha)},$$

$$\mathscr{R}_0^M := \frac{(1-\xi)[(1-r)\omega\eta b_1 + \vartheta_\alpha(\mu_0+\eta)(\omega+\mu_N)]}{(\mu_0+\eta)(\omega+\mu_N)(\mu_B+\vartheta_\alpha)}.$$

These can be interpreted as "basic reproduction numbers" of adult male ($\mathscr{R}_0^M$) and female ($\mathscr{R}_0^W$) lice, respectively.

Theorem 3. *Consider system* (13) *with* $\alpha_j(t)\equiv 0\equiv\beta_j(t), j = W,M,$ *and* $T(t)\equiv 0\equiv T_U(t)$ *for all* $t \geq 0$. *If* $\mathscr{R}_0^M > 1$ *and* $\mathscr{R}_0^W > 1$ *then there is a unique positive equilibrium point of system* (13), $P_1 = (U_1^*, N_1^*, W_1^*, M_1^*, W_1^{B*})$, *which is unstable. The coordinates of* P_1 *are given by*

$$W_1^* = \frac{\mu_1}{\xi\left(\mathscr{R}_0^W - 1\right)}, \qquad M_1^* = \frac{\mu_1}{\rho\left(\mathscr{R}_0^M - 1\right)},$$

$$W_1^{B*} = \frac{\mu_1^2(1-\xi)}{\left(\mathscr{R}_0^M - 1\right)\left(\mathscr{R}_0^W - 1\right)(\mu_B+\vartheta_\alpha)}, \tag{14}$$

$$U_1^* = \frac{b_1}{\mu_0+\eta}W_1^{B*}, \qquad N_1^* = \frac{\eta}{\omega+\mu_N}U_1^*.$$

Proof. The equilibrium conditions are obtained by setting the right-hand side of system (13) equal to zero,

$$0 = b_1 W^{B*} - (\mu_0+\eta)U^* \tag{15}$$

$$0 = \eta U^* - (\omega+\mu_N)N^* \tag{16}$$

$$0 = (1-r)\omega N^* - (\mu_1+\rho M^*)W^* + \vartheta_\alpha W^{B*} \tag{17}$$

$$0 = r\omega N^* - (\mu_1+\xi W^*)M^* \tag{18}$$

$$0 = (1-\xi)\rho M^* W^* - (\mu_B+\vartheta_\alpha)W^{B*}. \tag{19}$$

From the first and second equation (15) and (16) we calculate, respectively, U^* and N^* as (linear) functions of W^{B*},

$$U^* = \frac{b_1}{\mu_0+\eta}W^{B*}, \qquad N^* = \frac{\eta}{\omega+\mu_N}U^* = \frac{\eta}{\omega+\mu_N}\frac{b_1}{\mu_0+\eta}W^{B*}. \tag{20}$$

With the last relation we obtain an expression for W^{B*} as a function of M^* and W^*,

$$W^{B*} = \frac{(1-\xi)\rho}{\mu_B+\vartheta_\alpha}M^* W^*. \tag{21}$$

Now we substitute (20), (21) into equation (17) and find a linear equation in M^* which (assuming $W^* \neq 0$) yields

$$M^* = \frac{\mu_1}{\frac{(1-\xi)(1-r)\omega\eta b_1\rho}{(\mu_0+\eta)(\omega+\mu_N)(\mu_B+\vartheta_\alpha)} + \vartheta_\alpha\frac{(1-\xi)\rho}{\mu_B+\vartheta_\alpha} - \rho} = \frac{\mu_1}{\rho\left(\mathscr{R}_0^M - 1\right)}.$$

This value is nonnegative if $\mathscr{R}_0^M > 1$. Similarly, assuming $M^* \neq 0$, from (18) we find

$$W^* = \frac{\mu_1}{\frac{(1-\xi)r\omega\eta b_1\rho}{(\mu_0+\eta)(\omega+\mu_N)(\mu_B+\vartheta_\alpha)} - \xi} = \frac{\mu_1}{\xi\left(\mathscr{R}_0^W - 1\right)},$$

hence $W^* > 0$ if $\mathscr{R}_0^W > 1$. If either W^* or M^* are zero, we are in the case of Theorem 2 and we find the lice-free equilibrium P_0. For the proof of linearized stability we introduce a slightly more compact notation and define the constants

$$\kappa_1 = 1 - \xi \in [0,1], \ \kappa_2 = \vartheta_\alpha + \mu_B > 0, \ \kappa_3 = \mu_0 + \eta > 0,$$
$$\kappa_4 = (1-r)\omega > 0, \ \kappa_5 = r\omega > 0, \ \kappa_6 = \omega + \mu_N > 0, \ \kappa_7 = \eta b_1 > 0. \tag{22}$$

We consider the linearized system about P_1, governed by the Jacobian matrix

$$J(P_1) = \begin{pmatrix} -k_3 & 0 & 0 & 0 & b_1 \\ \eta & -k_6 & 0 & 0 & 0 \\ 0 & k_4 & -\mu_1 - \rho M^* & -\rho M^* & \vartheta_\alpha \\ 0 & k_5 & -\xi M^* & -\mu_1 - \xi W^* & 0 \\ 0 & 0 & k_1\rho M^* & k_1\rho W^* & -k_2 \end{pmatrix}$$

Long computation leads to the characteristic polynomial of P_1,

$$f(\lambda) = -f_a(\lambda) + f_b(\lambda)$$
$$= \underbrace{-(\kappa_3 + \lambda)(\kappa_6 + \lambda)(\mu_1 + \lambda)\left(\lambda^2 + \lambda\phi_1 + \phi_0\right)}_{f_a(\lambda)} + \underbrace{\chi_0 + \chi_1\lambda}_{f_b(\lambda)}, \tag{23}$$

where

$$\varphi_1 = \kappa_2 + \mu_1 + \xi W^* + \rho M^* > 0,$$

$$\varphi_0 = (\vartheta_\alpha\xi + \mu_B)\rho M^* + \kappa_2(\mu_1 + \xi W^*) > 0,$$

$$\chi_1 = \kappa_1\kappa_7\rho(\kappa_4 M^* + \kappa_5 W^*) > 0,$$

$$\chi_0 = \mu_1\chi_1 > 0.$$

The local asymptotic stability of P_1 is determined by the zeros of $f(\lambda)$ in Martcheva (2015), or equivalently by the intersections of the fifth order curve $f_a(\lambda)$ with the line $f_b(\lambda) = \chi_0 + \chi_1\lambda$. The latter has positive slope and positive intercept with the y-axis. The quadratic factor in $f_a(\lambda)$ can be written as the product $(\lambda - A_1)(\lambda - A_2)$, with $A_{1,2} = (-\varphi_1 \pm \sqrt{\varphi_1^2 - 4\varphi_0})/2$. Observe that $A_{1,2}$ are either both real and negative (because $\varphi_0, \varphi_1 > 0$), or complex conjugated with negative real part. Hence $f_a(\lambda)$ is a fifth order polynomial with zeros laying all on the left half of the complex plane. Further, it has positive intercept with the y-axis, $f_a(0) = \kappa_3\kappa_6\mu_1\varphi_0 > 0$. Moreover, it holds that $f_b(0) > f_a(0) > 0$. Indeed

$$f_b(0) - f_a(0) = \mu_1(\kappa_1\kappa_7\rho(\kappa_4 M^* + \kappa_5 W^*) - \kappa_3\kappa_6\phi_0)$$

$$= \mu_1\left(\rho M^*\underbrace{(\rho\kappa_1\kappa_4\kappa_7 - \kappa_3\kappa_6\rho(\kappa_2 - \vartheta_\alpha\kappa_1))}_{=(\mathscr{R}_0^M - 1)\kappa_3\kappa_6\kappa_2} + W^*\underbrace{(\rho\kappa_1\kappa_5\kappa_7 - \xi\kappa_2\kappa_3\kappa_6)}_{=\xi(\mathscr{R}_0^W - 1)\kappa_2\kappa_3\kappa_6} - \mu_1\kappa_2\kappa_3\kappa_6\right)$$

$$= \mu_1^2\kappa_2\kappa_3\kappa_6 > 0.$$

It follows that the characteristic polynomial (23) has at least one root with positive real part, hence the coexistence equilibrium P_1 is unstable. ∎

Let us assume the infected host is not quarantined, that is, $\alpha_j(t), \ \beta_j(t), j = M, W$ are not identically zero for $t \geq 0$. For simplicity of calculation, we consider the special case of constant transferring rates, $\alpha_j(t) = \alpha_j > 0$ and $\beta_j(t) = \beta_j > 0, j = M, W$. As in the proof of Theorem 3, in what follows we denote by X^* the steady state of the variable X. Let M_1^* be the male component of P_1, as indicated in (14). Further we define

$$\phi_a := \xi\left(\mathscr{R}_0^W - 1\right)\left(M_1^* + \frac{\beta_W}{\rho\left(\mathscr{R}_0^M - 1\right)}\right),$$

$$\phi_b := \alpha_M - \frac{\alpha_W\xi\left(\mathscr{R}_0^W - 1\right) + (\mu_1 + \beta_M)\left(\beta_W + M_1^*\rho\left(\mathscr{R}_0^M - 1\right)\right)}{\rho\left(\mathscr{R}_0^M - 1\right)},$$

$$\phi_c := \alpha_W \frac{\mu_1 + \beta_M}{\rho\left(\mathscr{R}_0^M - 1\right)},$$

$$\Delta_\phi := \phi_b^2 - 4\phi_a\phi_c.$$

$$(24)$$

The proof of the following Lemma is immediate.

Lemma 1. *Let $\alpha_j(t) = \alpha_j > 0$ and $\beta_j(t) = \beta_j > 0$, $t \geq 0$, $j = M, W$ and $T(t) \equiv 0 \equiv T_U(t)$ for all $t \geq 0$ in system* (13). *If $\mathscr{R}_0^M > 1$, $\mathscr{R}_0^W > 1$ then both quantities φ_a and φ_c in* (24) *are positive.*

Theorem 4. *Let the assumptions of [Lemma 1](#) be satisfied. Assume that φ_b, Δ_φ, in* (24) *satisfy $\varphi_b < 0$, $\Delta_\varphi > 0$, and that $\widehat{\mathscr{R}}_0^W :=$ $\frac{\beta_W}{\alpha_W}\frac{\sqrt{\Delta_\varphi}-\varphi_b}{2\varphi_a} > 1$. Then system* (13) *has two positive equilibria, $P_j = (U_j^*, N_j^*, W_j^*, M_j^*, W_j^{B*})$, $j = 2, 3$, where $W_{2,3}^* = (-\varphi_b \pm \sqrt{\Delta_\varphi})/2\varphi_a$ and*

$$M_j^* = M_1^* + \frac{\beta_W}{\rho\left(\mathscr{R}_0^M - 1\right)} - \frac{\alpha_W}{\rho\left(\mathscr{R}_0^M - 1\right)W_j^*}, \quad j = 2, 3$$

$$W_j^{B*} = \frac{\rho(1-\xi)}{\vartheta_\alpha + \mu_B}M_j^*W_j^*, \quad U_j^* = \frac{b_1}{\mu_0 + \eta}W_j^{B*}, \quad N_j^* = \frac{\eta}{\omega + \mu_N}U_j^*, \quad j = 2, 3.$$

Proof. Also in this proof we use the compact notation [(22)](#). We first show that when the transferring rates are nonzero, the LFE is not an equilibrium. Let us assume $N^* \geq 0$. The steady state conditions yield

$$M^* = 0 \Leftrightarrow \underbrace{\kappa_5 N^*}_{\geq 0} = \underbrace{-\alpha_M}_{<0},$$

which is a contradiction. On the other hand, if $W_B^* = 0 = N^*$ then from the W-equation we find $\alpha_W = 0$ which contradicts the assumption on the positive transferring rates. Hence, $M^* > 0$, $W^* > 0$, implying all other components are also nonzero.

Now we compute the nontrivial equilibrium, analogously to P_1 in [Theorem 3](#). The relations [(15)](#), [(16)](#) and [(19)](#) hold true also in the case of a non-quarantined host. We consider the algebraic equation given by $\dot{W} = 0$. Assuming $W^* \neq 0$, we obtain an expression for M^* as a function of W^*,

$$M^* = \frac{(\mu_1 + \beta_W)W^* - \alpha_W}{\underbrace{\rho W^*\left(\frac{\kappa_1\kappa_4\kappa_7}{\kappa_2\kappa_3\kappa_6} + \frac{\kappa_1}{\kappa_2}\vartheta_\alpha - 1\right)}_{=\rho(\mathscr{R}_0^M - 1)W^*}} = M_1^* + \frac{\beta_W}{\rho\left(\mathscr{R}_0^M - 1\right)} - \frac{\alpha_W}{\rho\left(\mathscr{R}_0^M - 1\right)W^*}. \quad (25)$$

Observe that M_1^* is nonnegative if $\mathscr{R}_0^M > 1$. Hence $\widehat{\mathscr{R}}_0^W > 1$ provides a sufficient condition for $M^* > 0$. From the algebraic equation $\dot{M} = 0$ we calculate

$$\underbrace{M^*}_{equ. (25)}\left(\underbrace{\left(\frac{\kappa_1\kappa_5\kappa_7}{\kappa_2\kappa_3\kappa_6}\rho - \xi\right)}_{=\xi(\mathscr{R}_0^W - 1)}W^* - (\mu_1 + \beta_B)\right) + \alpha_M = 0,$$

equivalently, a quadratic expression in W^*,

$$\varphi_a W^{*2} + \varphi_b W^* + \varphi_c = 0,$$

with φ_a, φ_b and φ_c defined as in (24). Lemma 1 implies that the parabola opens up and has positive intercept with the y-axis. If $\varphi_b > 0$, then the vertex of the parabola lies on the left half of the plane and the zeros $W^*_{2,3}$ are not of biological interest. In contrast, if $\varphi_b < 0$ the vertex of the parabola lies on the right half plane. The condition $\Delta_\varphi > 0$ guarantees the existence of two positive real roots $W^*_{2,3}$. ∎

4. How to treat infestations: four possible strategies

Untreated infestations lead to large lice colonies and possibly to secondary bacterial infections (Cummings et al., 2018). Fig. 2a shows the evolution in time of a lice colony which develops from a small group of adults if untreated for about 6 weeks. For the numerical simulations in Fig. 2a and for all other figures in this section we use, if otherwise not explicitly mentioned, parameter values as indicated in Table 1 and the initial conditions $U(0) = 0, N(0) = 0, W(0) = 4, M(0) = 4, W^B(0) = 0$. Such initial values mirror the fact that an initial infestation usually involves less than 10 live lice (Cummings et al., 2018) and it is due to adult lice, which are able to move from host to host (cf. Sec. 1).

In the following we present and compare four different strategies for treatment of head lice infestation, aiming to fast and effective lice eradication. We shall denote a treatment as effective, if the infected host is "lice-free" for two weeks (14 days) after the last treatment application. Similar to Laguna and Risau-Gusman (2011), we introduce a critical detection threshold and define a host "lice-free" when the egg/live lice population has dropped below this threshold. In all plots in Figs. 2—5 and Fig. 7, the solid black curve represents eggs (U), whereas the dashed black curve represents live lice (that is, the sum of nymphs and adults). Red and blue dotted lines indicate the detection threshold (assumed here to correspond to 2 eggs/live lice) and applications of treatments, respectively. We assume that lice are discovered about three weeks after initial infestation and that treatments start immediately after detection (day 21). We start considering lice on an isolated host, who cannot be reinfected while or after being treated. That is, for all $t > 0$ we set $\alpha_j(t) \equiv 0 \equiv \beta_j(t), j = W, M$.

Strategy nr. 1: Classical topical treatments, non-ovocidal. Shampoos and lotions based on insecticides such as malathion, pyrethis and its derivatives (e.g. permethrin) kill mature nymphs and adult lice but are mostly non-ovocidal (Speare, Canyon, Cahill, & Thomas, 2007). It is recommended to apply two-three treatments with shampoos one week apart, the third one being necessary in severe cases (Speare et al., 2007). Hence, in our first attempt we shall simulate three applications of a topical non-ovocidal treatment at days 21, 28 and 35. Assuming that the treatment is perfectly working and eliminates no eggs but 100% of live lice, then the strategy is effective, that is, three treatments are sufficient to get rid of the infestation (Fig. 2b). The timing of application of insecticide-based shampoo relies on the biology of the lice life-cycle. Being non-ovocidal, shampoos do not harm eggs, which will hatch and evolve into new adults, if the gap between the applications is too short. See for example in Fig. 2c simulations for a shampoo applied three days in a row following detection. Analogously, when treatments are repeated once a month, the adult lice population has time to fully regenerate and the infestation persists after three treatments (Fig. 2d). If the treatment is perfectly working against nymphs and adult lice, then gaps between the applications can be extended to two weeks, and three applications allow to eradicate the infestation (Fig. 2e).

Extensive use of topical treatments has led to selection and development of resistant head lice populations (Yoon et al., 2003; Feldmeier, 2012) so that no shampoo nor lotion truly kills 100% of live lice. In an experimental study, Yoon et al. (2003) showed that 13—87% lice were resistant to permethrin. Simulations in Fig. 2f indicate that in case of 40% resistant lice, the recommended "three times in two weeks" strategy is not sufficient to eradicate the infestation. Feldmeier (2012) suggested to treat resistant lice with dimeticones (see Strategy 4).

Strategy nr. 2: Conditioner and Combing method. Less expensive than topical treatments and non-chemical, wet combing is an optimal method for detection of head lice infestations (Feldmeier, 2012). Health care institutions recommend that the hair is divided into small sections and each section is combed completely, repeating the combing procedure every one-two days until no lice are detected for 10 consecutive days (Department of Health, 2019). It is difficult to assess and quantify the efficacy of wet combing from previous scientific studies (Feldmeier, 2014) as this depends on a number of factors, including the nature of the comb (Gallardo et al., 2013; Speare et al., 2002). Therefore, for numerical simulations we consider here three scenarios: (i) low effectiveness (combing removes 20% of live lice/eggs), (ii) moderate effectiveness (combing removes 50% of live lice/eggs), and (iii) high effectiveness (combing removes 80% of live lice/eggs). As recommended in Department of Health (2019) we apply combing every second day until no lice/eggs are detected (meaning that both populations dropped below the detection threshold) and observe how the lice population evolves in the following two weeks. Simulations in Fig. 3 show that the duration of the treatment importantly depends on the effectiveness of the combing procedure, varying from 25 applications (Fig. 3a) when combs remove only 20% lice/eggs, to 2 applications (Fig. 3e) when combs remove 80% lice/eggs. The duration of the treatment can be reduced, in particular when the treatment eliminates only 20% of live lice/eggs, by combing the hair every day instead of every second day (Fig. 3(b,d,f)). Notice that interrupting the treatment here is not necessarily implying that the treatment strategy was effective. Indeed, in all cases considered in Fig. 3 the host is lice free for a few days, but the lice population grows above the detection threshold within 14 days from the last treatment, with borderline values in some cases (Fig. 3d).

Fig. 2. Evolution in time of a lice colony which develops from a small group of adults. (a) Lice colony untreated for 40 days. (b−f) Strategy nr.1. Starting from day 21 (first treatment) since the beginning of the infection, two further applications with a fully working topical treatment (killing 100% of nymphs/adults) are repeated (b) after 7 days (day 28 and 35), (c) after 1 day (day 22 and 23), (d) after 30 days (day 51 and 81), and (e) after 14 days from each previous treatment (day 35 and 49). (f) Topical treatments applied as in (b) assuming 40% resistance in nymphs and adult lice.
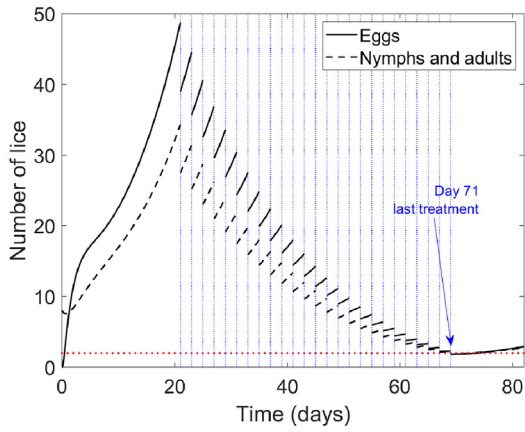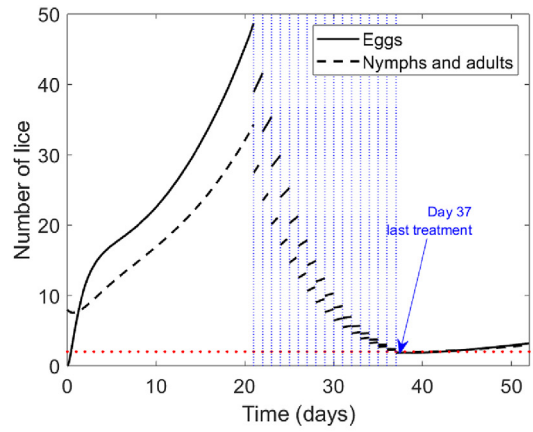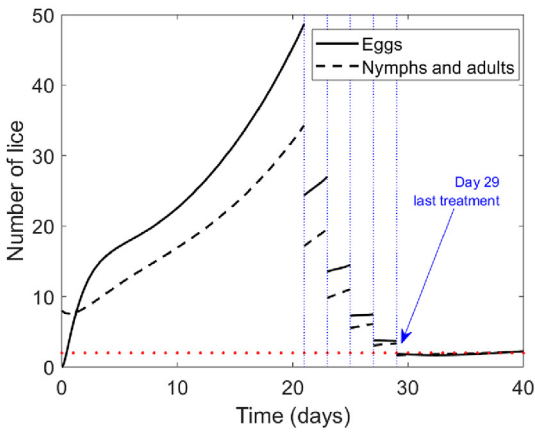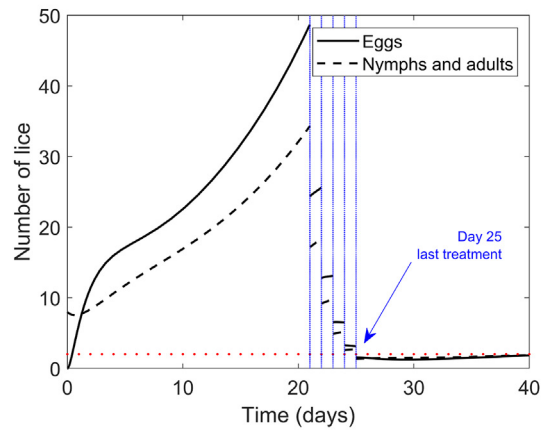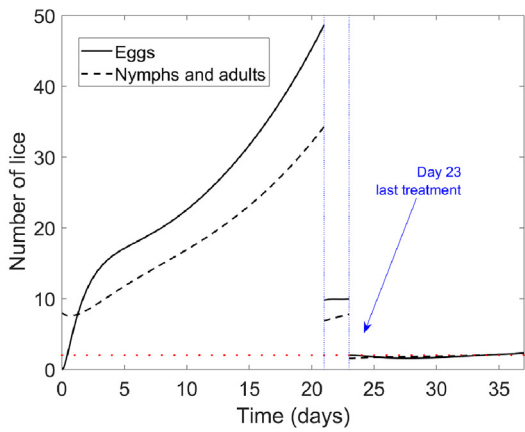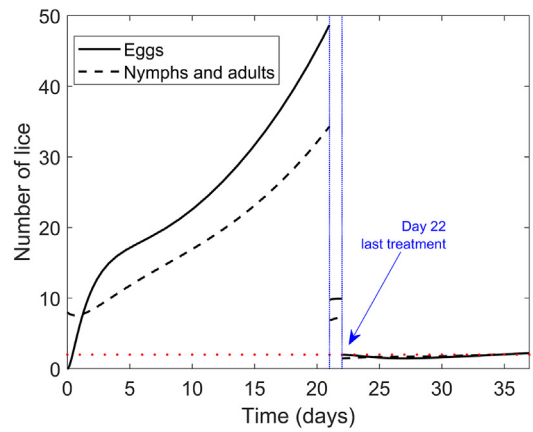
Fig. 3. Strategy nr. 2. Evolution in time of a lice colony which develops from a small group of adults and is treated with conditioners and combs. Starting from day 21 (first treatment) since the beginning of the infection, lice are treated every second day (a,c,e) or every day (b,d,f). Wet combing it is assumed to eliminate (a,b) 20%, (c,d) 50% or (e,f) 80% of lice/eggs.
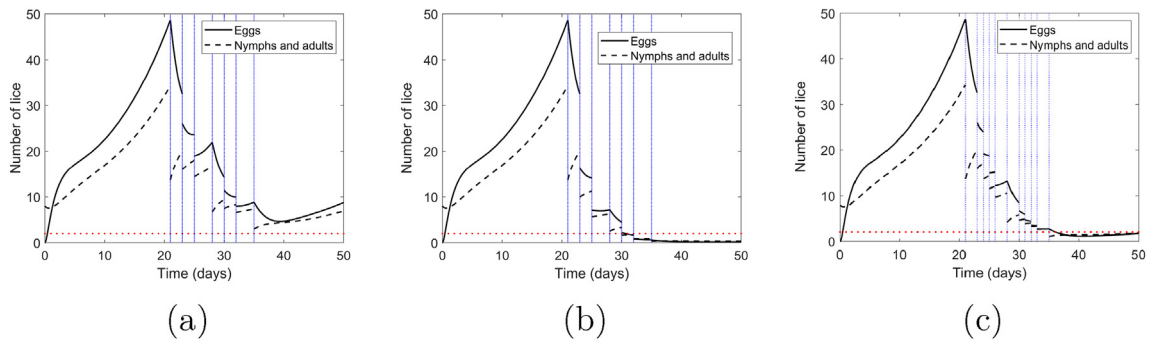
Fig. 4. Strategy nr. 3. Evolution in time of a lice colony which develops from a small group of adults and is treated with non-ovocidal topical treatments alternated to wet combing. Starting from detection lice are treated with shampoo at days 21, 28 and 35 (killing 60% of live lice) in alternation with wet combing (a,b) on days 23, 25, 30 and 32, respectively (c) on days 23, 24, 25, 26, 30, 31, 32, 33. Combing effectiveness was assumed to be (a,c) low (eliminating 20% of live lice/eggs), or (b) moderate (eliminating 50% of live lice/eggs).
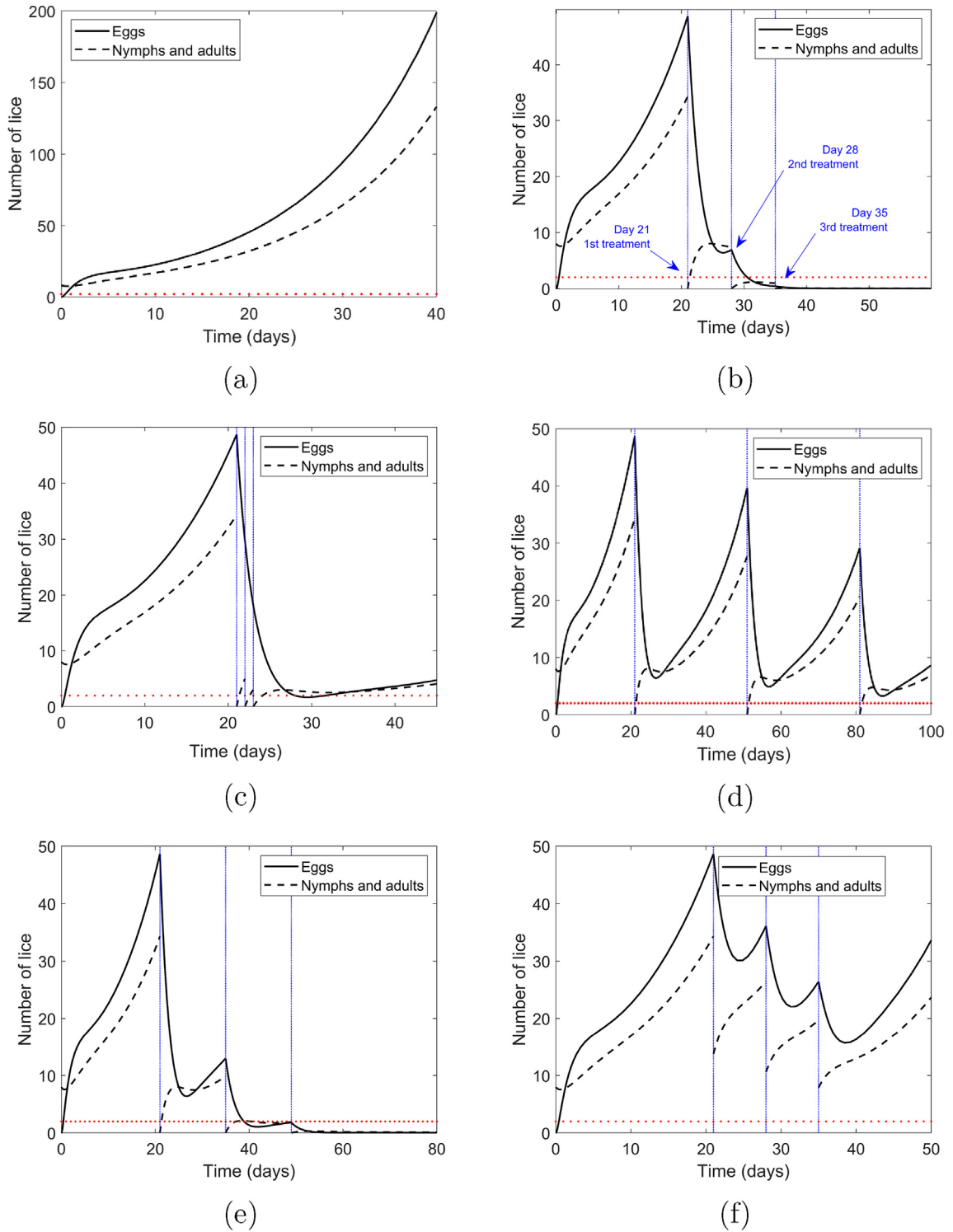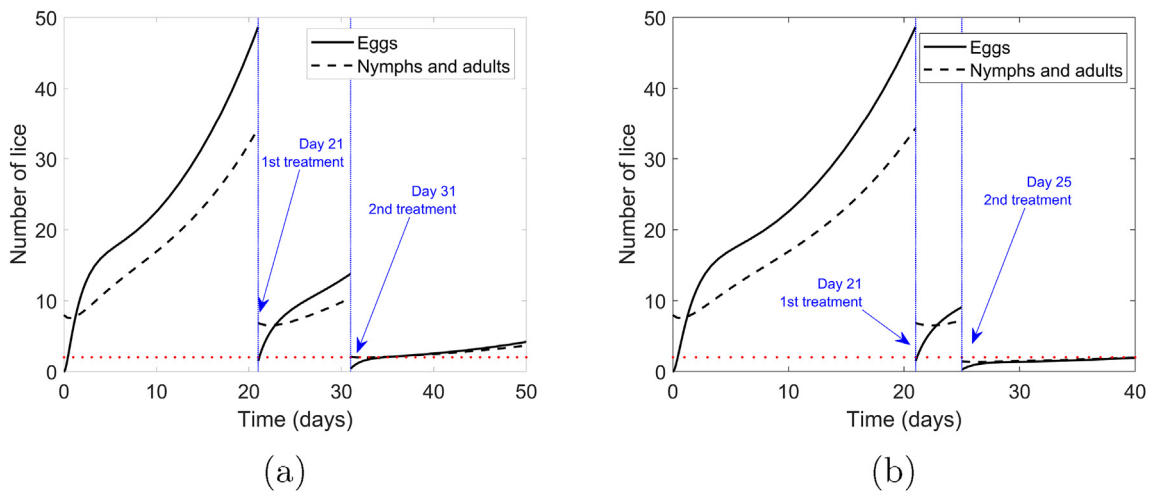

Fig. 5. Strategy nr. 4. Evolution in time of a lice colony which develops from a small group of adults and is treated with dimeticones (NYDA®). At each application, NYDA® is assumed to eliminate 80% of nymphs and adults and 97% of present eggs. Starting from day 21 (first treatment) since the beginning of the infection, NYDA® application is repeated (a) after 10 days (day 31) and (b) after 4 days (day 25).

Strategy nr. 3: Combined treatments (shampoos and combs). In strategies nr.1 and nr.2, shampoos and wet combing were applied separately. Guidelines for head lice treatment have previously suggested to combine different products, applying a shampoo every seven days and a lice comb every two days between one shampoo and the next (Queensland Government, 2019). We simulate (Fig. 4a) the effect of such a combined strategy, assuming that starting from detection lice are treated three times with shampoo (day 21, 28 and 35) and further with low/moderately effective wet combing (killing 20/50% of live lice/eggs) every second day between two shampoos (days 23, 25, 30 and 32). This alternate treatments strategy is effective when combing is removing 50% of live lice and nits, whereas it is not when combing effectiveness is low, compare Fig. 4(a and b). If combing effectiveness is low, but the hair is combed more often, e.g. four times, between two topical treatments, the strategy could also be considered effective as after the last shampoo the lice population remains for two weeks below the detection threshold (Fig. 4c).

Strategy nr. 4: Dimeticones-based treatments. Dimeticones are silicone oils which have been recently employed in anti-head lice compounds. When applied on a louse, dimeticones enter into the spiracles, interrupt oxygen supply and lead to rapid death of the insect (Heukelbach et al., 2008). Two kind of dimeticones have been recently studied see (Feldmeier (2012) and references thereof): (i) Hedrin®, 4% dimeticones solution, which showed 70%–92% efficacy on treating lice infestations, despite being ineffective on eggs, and (ii) NYDA®, a combination of two dimeticones which is also ovocidal (95–100% eggs killed). Being non-ovocidal, treatments with Hedrin® can be associated to the previously simulated strategies nr. 1 and nr. 3 (the latter, if combined with wet combing). In contrast, NYDA® was proposed as a good candidate for a two-application treatment, with a recommended second treatment 8–10 days after the first one (Cummings et al., 2018; Feldmeier, 2012). Assuming that NYDA® eliminates 80% of nymphs and adults and 97% of eggs, we simulate two treatments with NYDA®, the first at detection (day 21) and the second at day 31. However, with this treatment schedule the lice population will grow

beyond the detection threshold in less than one week (Fig. 5a), suggesting that the treatment did not work. The strategy becomes effective when we anticipate the second treatment to day 25 (Fig. 5b) because, nymphs and adults being reduced by NYDA® to 20% of their values, the population growth slows down importantly and lice remain under the detection threshold for two weeks.

One might wonder to what extent our results depend on the timing of the first treatment (assumed to be day 21 in Figs. 2–5), or in other words on the population size of eggs (U_d) or live lice (L_d) at detection. We let now U_d (respectively, L_d) free to vary in the interval [0,200] (respectively, [0,100]), and consider the above presented treatment strategies with variable population size at the time of the first treatment. We shall distinguish regions of the plane (U_d, L_d) indicating weather zero (light yellow), one (dark yellow), two (orange), three (red), or at least four (dark red) treatments are needed to consider the strategy effective. If the initial lice population is very small, because of the local attractiveness property of the lice-free equilibrium (Theorem 2) the lice population dies out without intervention, hence no treatment needs to be applied. When a large amount of eggs and/or live lice is present then at least one treatment is necessary to eradicate the infestation. The number of treatments necessary to define the strategy effective depends on the applied product and on the scheduling. We visualize in Fig. 6 lice treatments with (a) highly effective topical products eliminating 90% of life lice applied once every 7 days; (b) moderately effective topical products eliminating 60% of life lice, applied once every 7 days; (c) moderately effective comb eliminating 50% eggs/lice, applied every second day; (d) NYDA® applied every 9 days and (e) NYDA® applied every 4 days. Whereas at most three applications of topical products would be effective in most cases when the product is killing 90% of nymphs and adult lice (Fig. 6a), four or more treatments become necessary to eradicate the infestation when moderately effective shampoos or combs are used (Fig. 6(b,c)). As NYDA® is assumed to be very effective against eggs, the number of applications necessary to eradicate the infestation depends essentially on the number L_d of nymphs and adult lice at detection. Three applications 9 days apart from each other allow to eliminate lice as long as $L_d < 60$ (Fig. 6d). In considering strategy nr. 4 we found that NYDA® becomes more efficient if applied every 4 days, rather than every 8–10 (Fig. 5b). Fig. 6e

(a)   (b)   (c)

(d)   (e)
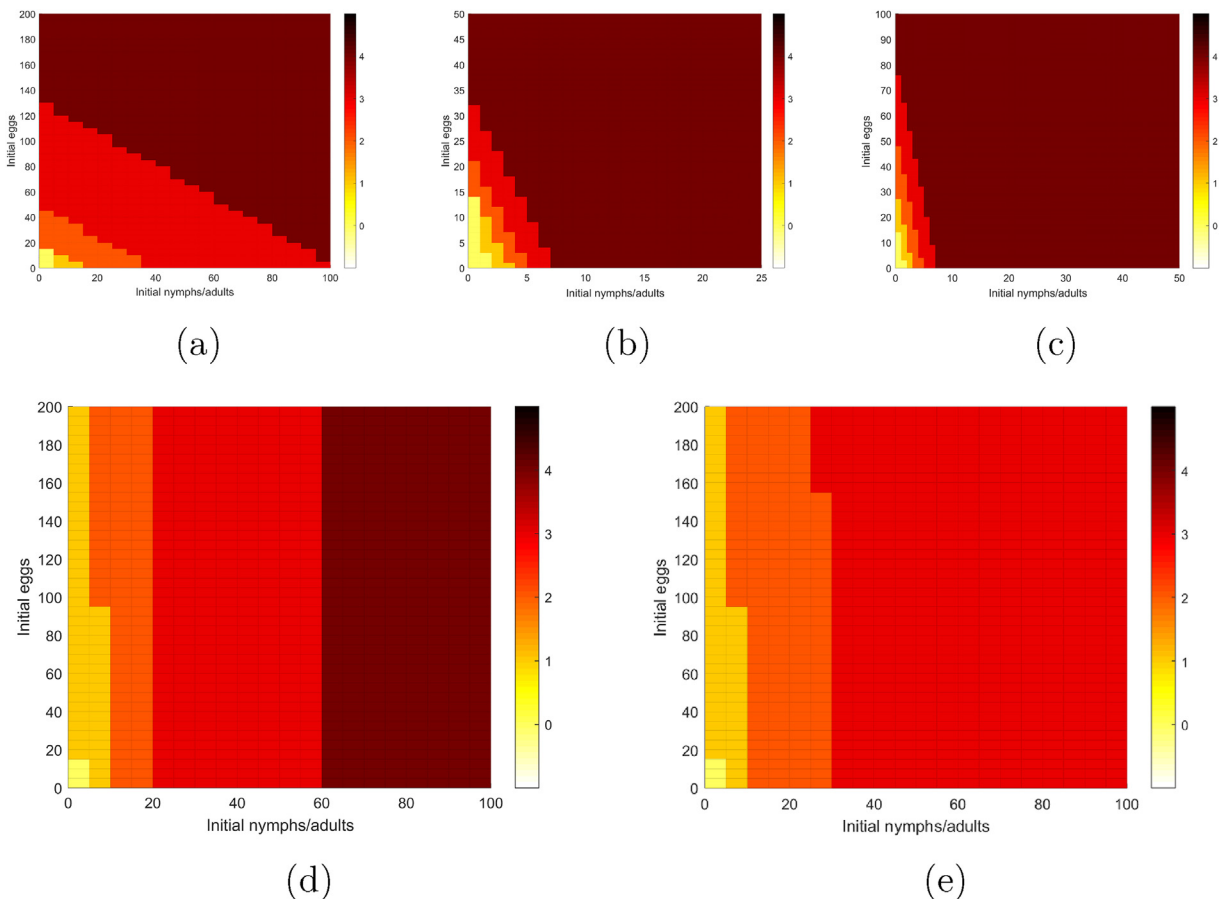
Fig. 6. The severity of a lice infestation at detection affects the number of treatment applications necessary for lice elimination. The panels visualize therapy with: (a) topical treatment eliminating 90% nymphs/adults, applied once every 7 days; (b) topical treatment eliminating 60% nymphs/adults, applied once every 7 days; (c) combing eliminating 50% eggs/lice, applied every second day; (d) NYDA® applied every 9 days; (e) NYDA® applied every 4 days. Color code corresponds to no (yellow), one (dark yellow), two (orange), three (red) and four or more (dark red) applications necessary to eradicate the infestation with the corresponding strategy.
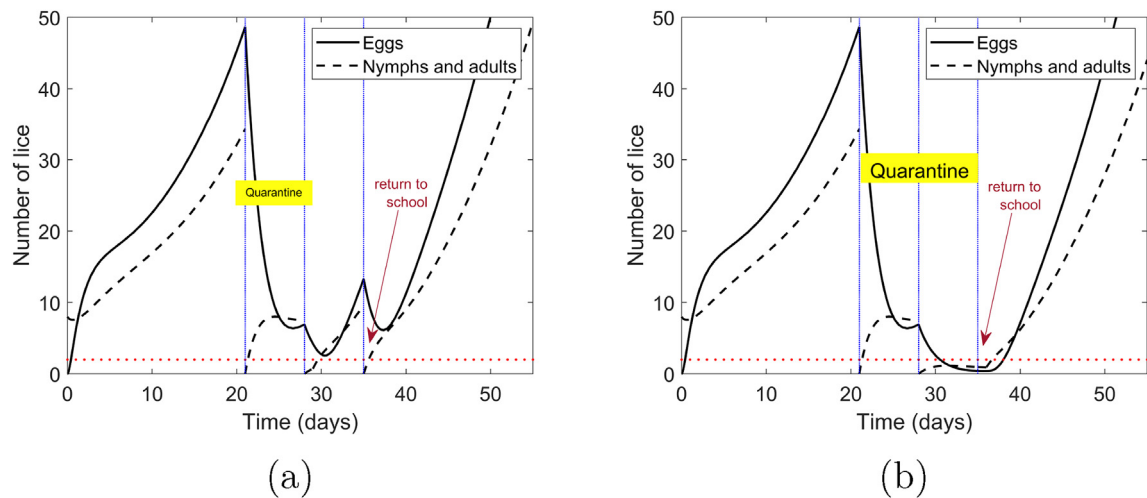
Fig. 7. Evolution in time of a lice colony which develops from a small group of adults in case of a non-isolated infestation. The host is treated with an ideally working shampoo (cf. Fig. 2(b)) applied on day 21,28 and 35. Following detection (day 21) the lice are treated and a the host is quarantined for (a) one week, respectively, (b) two weeks. When the quarantine ends, the host returns to school, where others are infested and lice transmission is possible.

confirms our findings indicating that at most three NYDA® applications 4-days apart are sufficient to eradicate the infestation for $L_d \in [0, 100]$.

5. Discussion

Understanding the life cycle of head lice is an important step in knowing how to treat lice infestations, as the parasite behavior depends considerably on its age and gender. To this purpose we have proposed a mathematical model for a population structured by age and gender formulated as a system of PDEs (1)–(5), which can be reduced to compartmental systems of delay differential equation (10) or ordinary differential equation (13). The latter was used to include treatments against head lice, which are differently eliminating eggs and nymphs/adult lice. To the best of our knowledge, besides the pioneer work by Laguna and Risau-Gusman (2011), this is a quite unique study which proposes a mechanistic mathematical model for understanding the biology of the life cycle of head lice and attesting the efficiency of different treatments in eradicating lice infestations.

Fundamental properties of the ODE model (13) were studied in Section 3. Beside existence, uniqueness and nonnegativity of solutions we have considered existence and stability of equilibria of the dynamical system. Our results show that in case of a quarantined infected host, there might be either no lice (infection free equilibrium P_0) or an heterogeneous population with lice in all life stages. P_0 is locally asymptotically stable, hence small perturbations of this equilibrium might not lead to lice infection, even if untreated (cf. Fig. 6). Further, the analytical results suggest that there is no stationary state in which only juvenile or only adult lice sub-populations survive. Provided that the reproduction, maturation and survival parameters of the lice population satisfy $\mathscr{R}_0^M > 1$ and $\mathscr{R}_0^W > 1$, then the coexistence equilibrium P_1 exists, but it is unstable (Theorem 3) and if not treated, the lice population would grow uncontrolled (Fig. 2a). If the host is not isolated and lice transmission among infected hosts is possible, then there might exist two nontrivial equilibria $P_{2,3}$ (Theorem 4).

By mean of computer experiments and numerical simulations we have studied (Section 4) four possible treatments against head lice, namely topical non-ovocidal treatments (Strategy nr. 1), wet combing (Strategy nr. 2), combination of the two (Strategy nr. 3), and dimeticone-based products (Strategy nr. 4). For all products different efficacy and application schedules were studied. No product was assumed to be 100% successful in removing eggs, nymphs and adult lice, as this is technically not feasible (Speare et al., 2002; Feldmeier, 2012). Of course, if such a product would exist re-treatment would not be required for isolated hosts. If a (almost) perfectly working topical treatment which eliminates at least 90% of live lice is available, then one application every 7 days repeated for three times is sufficient to eradicate moderate to severe infestations (Fig. 6a). Relying on the biology of the lice life-cycle, the time gap between applications should not be too short or too long (Fig. 2(c,d)), but could be relaxed to 14 days. For example, an effective strategy would be to apply a 100% effective insecticide-based shampoo for three times, with two weeks breaks between one application and the next one (Fig. 2e). In case of resistant lice, the duration of the treatment and the number of necessary applications increases (see e.g. for 40% resistance, Figs. 2f and 6b). Combing (Strategy nr. 2) is a useful method for detection, but according to our results, it could not be the method of choice to treat and eradicate a lice infestation. Indeed, unless the lice population at detection is very small and combing is performed very carefully, removing at least half of the present eggs and live lice (Fig. 6c), a high number of treatments could be necessary for the host to be lice free and the infestation could relapse within 2 weeks from the last treatment (Fig. 3).

Combining shampoos and combing (Strategy nr. 3) to treat a moderate to severe infestation could be quite time consuming and uncomfortable for the host due to the high number of applications required. If this method is chosen to treat an infestation, our results suggest to use effective products which can effectively remove eggs/live lice (Fig. 4). Dimeticone-based products, in particular if a new application is repeated 4 days (rather than 8–10 days) after the previous one, allow for a lower number of applications even in case of severe infestations (Figs. 5 and 6). Our results indicate that early detection is crucial for quick and efficient eradication. Indeed, the number of treatment applications necessary to eradicate the infestation population increases with increasing eggs/live lice at the time of first treatment (Fig. 6). In Section 4 we have considered the case of a quarantined host. One might ask if treatments which have been shown to be effective for such hosts do also work when the host is not isolated. Let us consider a perfectly working topical treatment (as in Fig. 2b) and a host, say a pupil, who has been found infested with lice. We assume that upon detection the host is quarantined for one or two weeks and is treated with the perfectly working topical product once a week starting with the detection day (day 21), returning to school the day after the second (day 29, Fig. 7a) or the third treatment (day 36, Fig. 7b). Let us also assume that in the same classroom there is at least another host with undetected or not well treated lice infestation, so that upon returning to school, new lice could be transferred to our initial patient. Fig. 7 shows that the treatment, which was effective for quarantined hosts (Fig. 2b), is failing for hosts who are at risk of reinfection. As long as the treated host goes back to an infectious environment, lice infestation cannot be eradicated. Based on our computational model results it would be advisable to reproduce a lice-free environment and minimize the reinfection risk, treating at the same time not only the first detected host but also his classmates. This is in agreement with the synchronized treatment strategy proposed in Laguna and Risau-Gusman (2011) and Meister and Ochsendorf (2016)). Beyond the scope of the present work, the study of treatments against head lice infestation as we proposed here could be generalized and framed into the context of optimal control theory, where as controls one could take both the time-dependent treatments $T(t)$, $T_U(t)$ and the transmission rates α_j, β_j (thinking of quarantine or reduced contacts as a control measure). Though the model was parametrized based on available literature on the biology of head lice, their life cycle and the estimated efficacy of different treatments against lice, for certain parameters (such as the transferring rates, see Table 1) no data are available. Henceforth, the proposed mathematical model and resulting numerical simulations are not meant for data fitting but rather for understanding the time evolution of an infestation and predicting the performance of a possible treatment strategy. The sharp detection threshold which was used to assess the performance or determining the conclusion of a treatment could be put into question. The choice of a different value for the threshold would quantitatively modify the results presented here, as observed for the model proposed in Laguna and Risau-Gusman (2011). A further limitation of the proposed study lays in the deterministic nature of the model. The deterministic approach used here is appropriate for large populations (such as untreated lice colonies), whereas for populations with very few individuals a stochastic approach would be more suitable. A stochastic model could be adopted to improve the study of borderline cases such as those in Fig. 5b where, though the infestation could be considered eradicated, in the long run the lice population increases again. In a further study we plan to improve the modeling approach proposed here by considering a mixed approach of deterministic and stochastic processes, as it has been proposed in other fields of biology (Kraut and Bovier, 2019).

Declaration of competing interest

None.

Acknowledgment

References

Barbarossa, M. V., Hadeler, K. P., & Kuttler, C. (2014). State-dependent neutral delay equations from population dynamics. *Journal of Mathematical Biology, 69*, 1027–1056.

Bocharov, G. A., & Hadeler, K. P. (2000). Structured population models, conservation laws, and delay equations. *J. Diff. Equations, 168*, 212–237.

Bourgess, I., Maunder, J., & Myint, T. (1983). Maintenance of the crab louse, pthirus pubis, in the laboratory and behavioural studies using volunteers. *Community Medicine*, 238–241.

Boutellis, A., Abi-Rached, L., & Raoult, D. (2014). The origin and distribution of human lice in the world. *Infection, Genetics and Evolution, 23*, 209–217.

Burkhart, C. N. (2003). Fomite transmission with head lice: A continuing controversy. *The Lancet, 361*, 99–100.

Castelletti, N. (2015). *Mathematical modeling of head lice epidemics. Master's thesis.* Faculty for Mathematics, Technical University Munich.

Castillo-Chavez, C., Busenberg, S., & Gerow, K. (1991). Pair formation in structured populations. In J. A. Goldstein, F. Kappel, & W. Schappacher (Eds.), *Differential equations with applications in biology, physics and engineering* (pp. 47–65). New York: Marcel Dekker.

Cummings, C., Finlay, J. C., & MacDonald, N. E. (2018). Head lice infestations: A clinical update. *Paediatrics and Child Health, 23*, e18–e24.

Cushing, J. M. (1998). An introduction to structured population dynamics. In *CMB-NSF Regional Conference Series in Applied Mathematics*. Philadelphia, PA: SIAM.

Department of Health. Healthy living: Treating head lice. https://healthywa.wa.gov.au/Articles/S_T/Treating-head-lice (Last accessed: Sept. 19th, 2019).

Feldmeier, H. (2012). Pediculosis capitis: New insights into epidemiology, diagnosis and treatment. *European Journal of Clinical Microbiology & Infectious Diseases, 31*, 2105–2110.

Feldmeier, H. (2014). Treatment of pediculosis capitis: A critical appraisal of the current literature. *American Journal of Clinical Dermatology, 15*, 401–412.

Gallardo, A., Toloza, A., Vassena, C., Picollo, M. I., & Mougabure-Cueto, G. (2013). Comparative efficacy of commercial combs in removing head lice (pediculus humanus capitis)(phthiraptera: Pediculidae). *Parasitology Research, 112*, 1363—1366.

Hadeler, K. P. (1989). Pair formation in age-structured populations. In *Evolution and control in biological systems* (pp. 91—102). Springer.

Hadeler, K. P. (1993). Pair formation models with maturation period. *Journal of Mathematical Biology, 32*, 1—15.

Heukelbach, J., Pilger, D., Oliveira, F. A., Khakban, A., Ariza, L., & Feldmeier, H. (2008). A highly efficacious pediculicide based on dimeticone: Randomized observer blinded comparative trial. *BMC Infectious Diseases, 8*, 115.

Hoppensteadt, F. (1975). *Mathematical theories of populations: Demographics, genetics, and epidemics*. SIAM.

Kraut, A., & Bovier, A. (2019). From adaptive dynamics to adaptive walks. *Journal of Mathematical Biology, 79*, 1699—1747.

Laguna, M. F., & Risau-Gusman, S. (2011). Of lice and math: Using models to understand and control populations of head lice. *PLoS One, 6*, Article e21848.

Lebwohl, M., Clark, L., & Levitt, J. (2007). Therapy for head lice based on life cycle, resistance, and safety considerations. *Pediatrics, 119*, 965—974.

Li, J. (2004). Simple mathematical models for interacting wild and transgenic mosquito populations. *Mathematical Biosciences, 189*, 39—59.

MacDonald, N. (1978). *Time lags in biological models* (Vol. 27). Berlin: Springer-Verlag (of Lecture notes in biomathematics).

Martcheva, M. (2015). *An introduction to mathematical epidemiology*. Springer.

Maunder, J. W. (1993). An update on headlice. *Health Visitor, 66*, 317—318.

Mehlhorn, H. (2012). *Arthropods as vectors of emerging diseases*. Springer.

Meister, L., & Ochsendorf, F. (2016). Head lice: Epidemiology, biology, diagnosis, and treatment. *Dtsch Arztebl Int, 113*, 763.

Mohr, M., Barbarossa, M. V., & Kuttler, C. (2014). Predator-prey interactions, age structures and delay equations. *Mathematical Modelling of Natural Phenomena, 9*, 92—107.

Perotti, M. A., Catala, S., Ormeno, A., Zelazowska, M., Bilinski, S., & Braig, H. (2004). The sex ratio distortion in the human head louse is conserved over time. *BMC Genetics, 5*, 10. https://doi.org/10.1186/1471-2156-5-10.

Queensland Government. (2019). *Managing Head Lice at Home Package*. https://brayparkss.eq.edu.au/Supportandresources/Formsanddocuments/Documents/Managing-Head-Lice-at-Home.pdf.

Rasmussen, A., Burgess, I., Rozsa, L., & Søholt Larsen, K. (2019). *Liceworld*. http://www.liceworld.com/ (Last accessed: Sept. 19th).

Speare, R., Canyon, D. V., Cahill, C., & Thomas, G. (2007). Comparative efficacy of two nit combs in removing head lice (pediculus humanus var. capitis) and their eggs. *International Journal of Dermatology, 46*, 1275—1278.

Speare, R., Thomas, G., & Cahill, C. (2002). Head lice are not found on floors in primary school classrooms. *Australian & New Zealand Journal of Public Health, 26*, 208—211.

Stone, P., Wilkinson-Herbots, H., & Isham, V. (2008). A stochastic model for head lice infections. *Journal of Mathematical Biology, 56*, 743—763.

Takano-Lee, M., Yoon, K., Edman, J., Mullens, B., & Clark, J. (2003). In vivo and in vitro rearing of pediculus humanus capitis (anoplura: Pediculidae). *Journal of Medical Entomology, 40*, 628—635.

Toloza, A. C., Laguna, M. F., Ortega-Insaurralde, I., Vassena, C., & Risau-Gusman, S. (2018). Insights about head lice transmission from field data and mathematical modeling. *Journal of Medical Entomology, 55*, 929—937.

Webb, G. (2008). *Population models structured by age, size, and spatial position* (Vol. 1936, pp. 1—49). https://doi.org/10.1007/978-3-540-78273-5_1.

Yoon, K., Gao, J., Lee, S., Clark, J., Brown, L., & Taplin, D. (2003). Permethrin-resistant human head lice, pediculus capitis, and their treatment. *Archives of Dermatology, 139*, 994—1000. arXiv:/data/Journals/DERM/11725/DST20220.pdf.

Yuan, Y., & Bélair, J. (2014). Threshold dynamics in an seirs model with latency and temporary immunity. *Journal of Mathematical Biology, 69*, 875—904.

Publication 10:

Risk of lung adenocarcinoma from smoking and radiation arises in distinct molecular pathways

Noemi Castelletti, Jan Christian Kaiser, Cristoforo Simonetto, Kyoji Furukawa, Helmut Küchenhoff, Georgios T Stathopoulos

ORIGINAL ARTICLE

Risk of lung adenocarcinoma from smoking and radiation arises in distinct molecular pathways

Noemi Castelletti[1],[*],[◉], Jan Christian Kaiser[1], Cristoforo Simonetto[1], Kyoji Furukawa[2], Helmut Küchenhoff[3] and Georgios T. Stathopoulos[4],[5]

[1]Institute of Radiation Medicine (IRM), Helmholtz Zentrum München, Ingolstädter Landstraße 1, 85764 Neuherberg, Bavaria, Germany, [2]Biostatistics Center, Kurume University, 67 Asahi-machi, Kurume, Japan, [3]Department of Statistics, Ludwig-Maximilian University (LMU) Munich; Akademiestraße 1, 80799 Munich, Bavaria, Germany, [4]Laboratory for Molecular Respiratory Carcinogenesis, Department of Physiology, Faculty of Medicine; University of Patras; 1 Asklepiou Str., 26504 Rio, Achaia, Greece and [5]Comprehensive Pneumology Center (CPC) and Institute for Lung Biology and Disease (iLBD), University Hospital, Ludwig-Maximilian University (LMU) and Helmholtz Zentrum München, Member of the German Center for Lung Research (DZL), Max-Lebsche-Platz 31, 81377 Munich, Bavaria, Germany

*To whom correspondence should be addressed. Tel: +49 089 31872133; Fax: +49 089 31873363; Email: noemi.castelletti@helmholtz-muenchen.de
Correspondence may also be addressed to Jan Christian Kaiser, Tel: +49 089 31874028; Fax: +49 089 31873363; Email: christian.kaiser@helmholtz-muenchen.de

Abstract

KRAS mutations of lung adenocarcinoma (LADC) are associated with smoking but little is known on other exposure-oncogene associations. Hypothesizing that different inciting agents may cause different driver mutations, we aimed to identify distinct molecular pathways to LADC, applying two entirely different approaches. First, we examined clinicopathologic features and genomic signatures of environmental exposures in the large LADC Campbell data set. Second, we designed a molecular mechanistic risk model of LADC (M_3^{LADC}) that links environmental exposure to incidence risk by mathematically emulating the disease process. This model was applied to incidence data of Japanese atom-bomb survivors which contains information on radiation and smoking exposure. Grouping the clinical data by driver mutations revealed two main distinct molecular pathways to LADC: one unique to transmembrane receptor-mutant patients that displayed robust signatures of radiation exposure and one shared between submembrane transducer-mutant patients and patients with no evident driver mutation that carried the signature of smoking. Consistently, best fit of the incidence data was achieved with a M_3^{LADC} with two pathways: in one LADC risk increased with radiation exposure and in the other with cigarette consumption. We conclude there are two main molecular pathways to LADC associated with different environmental exposures. Future molecular measurements in lung cancer tissue of atom-bomb survivors may allow to further test quantitatively the M_3^{LADC}-predicted link of radiation to transmembrane receptor mutations. Moreover, the developed molecular mechanistic model showed that for low doses, as relevant e.g. for medical imaging, smokers have the same radiation risk compared with never smokers.

Introduction

Lung adenocarcinoma (LADC) is the number one cancer killer worldwide (1,2). LADC is mainly, but not exclusively, caused by tobacco smoke but also occurs in never smokers possibly due to both anthropogenic and environmental radiation exposures (3–5). The comprehensive genomic characterization of LADC from Caucasian and Asian patients has identified mutations in major driver oncogenes such as *KRAS*, epidermal growth factor receptor (*EGFR*) and others, with different frequencies observed in different populations (6,7). However, a biological concept explaining the relative contributions of cigarette smoking and radiation exposures to LADC incidence is still missing.

Abbreviations

3SCE	Three-Stage Clonal Expansion
AIC	Akaike's information criterion
CI	confidence interval
CNA	copy number alteration
EAR	excess absolute rate
EGFR	epidermal growth factor receptor
ERR	excess relative risk
γ-IR	ionizing γ-radiation
MMR	mismatch repair
LADC	lung adenocarcinoma
LSS	Life Span Study
SNV	single nucleotide variant
TSCE	Two-Stage Clonal Expansion

The Life Span Study (LSS) of Japanese atomic bomb survivors is arguably the most important cohort to investigate carcinogenic effects of radiation. Since exposure occurred to the general population, risk estimates from the LSS are applied to assess health effects from environmental and clinical radiation exposure in other populations around the world (8). Recently, a series of studies reported LSS risk estimates for lung cancer (9,10) and its histological types (11) from concomitant exposure to smoking and radiation. These epidomiological studies claim positive, more than multiplicative interaction between smoking and radiation. However, state-of-the-art epidemiological risk models merely establish statistical associations without explicitly considering pathogenic processes or molecular data. Importantly, different molecular pathways with specific age-risk patterns in observational data can lead to the same cancer classification in a given organ. This has been observed for colon cancer, which appears in two main molecular variants with differential growth dynamics (12). Radiation-induced papillary thyroid cancer exhibits a pertinent molecular footprint distinguished from the sporadic variant (13,14). However, when multiple endpoints are analyzed jointly in epidemiology with a state-of-the-art relative risk model, interactions or patterns of risk modifications may arise that are not substantiated by biology and can differ from cohort to cohort.

For lung carcinogenesis molecular biology and epidemiology still lack a common interface. Here, we bridge this gap by applying molecular mechanistic models (M_3) of carcinogenesis as tools to harness molecular data of LADC. M_3 treat carcinogenesis as a progression of cell-based key events on the pathway to malignancy and can detect in cancer incidence imprints from molecular events on recorded hazard or survival rates (15). When developing M_3 for the LSS, we faced the problem that molecular data from lung cancer tissue of LSS patients has not yet been generated. Therefore, we analyze molecular profiles from patients of the USA and China (6,7) to develop a biological concept which guides the design of M_3^{LADC}. The model design is checked in the LSS by means of goodness-of-fit and biological plausibility. It turned out that biological and model-identified pathways can be matched. We provide a comprehensive risk assessment for the LSS which relies on two non-interacting legs of M_3^{LADC} driven by either smoking or radiation. Should genomic data from the LSS become available, M_3^{LADC} is open to direct validation.

Materials and methods

Statistical analysis of molecular data

Mutation rates of 660 patients with LADC from the USA (6) and 101 from China (7) were extracted from the primary publications. For individual patients, clinical, exposure and mutation data from the US cohort were downloaded from the primary publication (6) and manually analyzed. Clinicopathologic and molecular data from (6) and (7) were examined for normality by Kolmogorov–Smirnov test, were found to be not normally distributed and are hence presented as median with Tukey's whiskers (boxes: interquartile range; bars: 50% extreme quartiles) and raw data points (dots). Differences in frequencies were examined by Fisher's exact or χ^2 tests and in medians of non-normally distributed variables by Kruskal–Wallis non-parametric analyses of variance with Dunn's post-tests. Survival was examined by Kaplan–Meier estimates with log-rank tests. Probability (*P*) is two-tailed and *P* < 0.05 was considered significant. Statistics and plots from clinico-pathologic and molecular data were done on Prism v5.0 (GraphPad, La Jolla, CA). Univariate multinomial regression analysis of clinico-pathologic and molecular data from (6) stratified by molecular pathways was done with R* (https://r-project.org/).

The LSS cohort of Japanese atomic bomb survivors

The LSS cohort has been the primary epidemiological basis for evaluating the long-term health effects of radiation, dominated by 0–4 Gy gamma rays of low linear energy transfer. It includes about 94 000 survivors who were in Hiroshima and Nagasaki at the time of bombing and about 27 000 who were temporarily away at that time and whose mortality and cancer incidence have been followed up since 1950 and 1958, respectively (16). As information on smoking is not available for all cohort members, missing data has been imputed (17) and analysis was repeated on 50 different imputed data sets (see Supplementary Material, available at *Carcinogenesis* Online). To put the results of mechanistic modeling into perspective, a descriptive risk model (11) has been applied (see Supplementary Material, available at *Carcinogenesis* Online). Supplementary Table S1, available at *Carcinogenesis* Online, summarizes the LSS cohort data broken down by sex and smoking status.

Mechanistic risk modeling

Mechanistic models have long been applied for the analysis of radio-epidemiological cohorts (15). For the present study, analysis of the LSS cohort was performed independently from the genomic results. But the model concept is motivated by the suggestion of two molecular pathways to LADC.

In a pathway-specific model, cancer develops in the lung epithelium from a large number of *N* healthy cells in homeostasis. Eventually, a very small fraction of healthy cells acquire initial mutations with rate *ν*. Initiated cells may either grow immediately (in the Two-Stage Clonal Expansion model, TSCE) into atypical adenomatous hyperplasia as precursor lesions in invasive LADC with net rate $\gamma = \alpha$-β-μ or only after acquiring a second mutation (Three-Stage Clonal Expansion model, 3SCE). The stem cell division rate α is reduced by a rate β of cell inactivation (i.e. apoptosis) and a transformation rate μ. In the transformation stage after clonal expansion, initiated cells suffer a 'final rare event' often as a mutation in a tumor suppressor gene, which turns them into cancer cells. During a lag time of several years cancer cells grow into a clinically relevant tumor (18). However, in the present LSS data set, inclusion of a lag time had only marginal impact on the results. Therefore, all complex processes after clonal expansion are summarized by a single late event with rate μ. An illustration of such a model but with two pathways can be found in Figure 3A.

For mathematical implementation of the TSCE model, mutation rates and rates of cell division or inactivation are treated as transient Poisson point processes of cell birth and death, which are couched in a set of master equations (19). This set has been transformed into a system of coupled ordinary differential equation of the Ricatti type, which is solved efficiently by a set of backward recursion relations given in Supplementary Table S5, available at *Carcinogenesis* Online. Meza *et al.* (20) present closed analytical forms for the hazard functions of the TSCE model and the 3SCE model. Their mapping of biological stages in cancer development to pertinent stages of age-dependent incidence is very instructive. For the TSCE, the recursion relations are presented in Supplementary Table S5, available at *Carcinogenesis* Online.

In Figure 3A, biological transition rates v, μ, α and β are shown for each pathway. However, the recursion relations for the TSCE model are expressed in terms of the parameter combinations $X = Nv\mu$, $\mu = \alpha$-β-μ and $\delta = \alpha\mu$, which possess the advantage of being identifiable from the
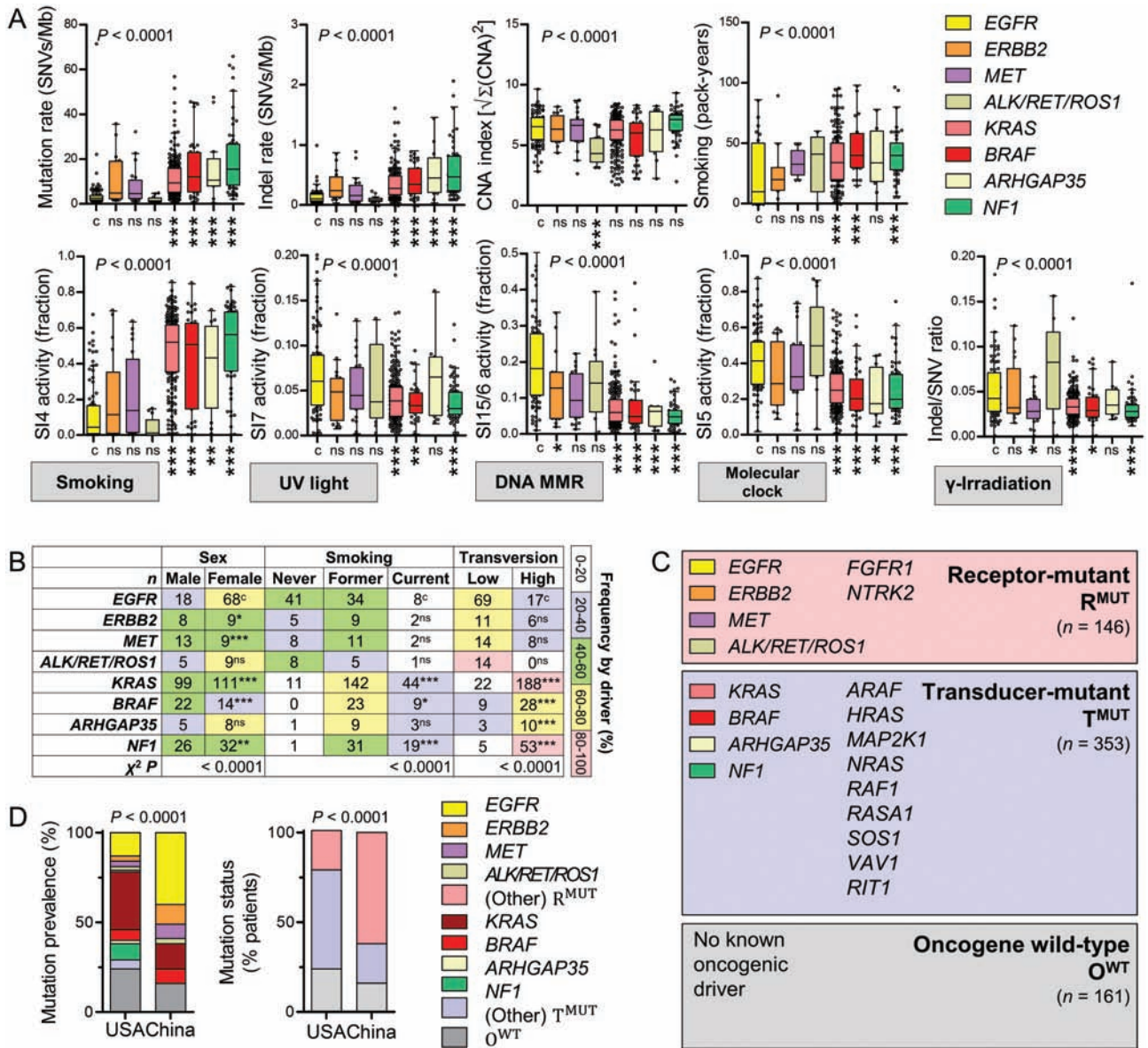
Figure 1. Identification of broad molecular pathways to lung adenocarcinoma. SNV rates, indel rates, CNA indices, smoking exposure, sex, genomic signatures of environmental carcinogen-induced base changes in the trinucleotide context (SI), indel/SNV ratios and transversion status of 660 patients with LADC from the USA (6) grouped by the most frequent driver mutations. **(A)** Data are given as raw data points, median ± Tukey's whiskers (lines: median; boxes: interquartile range; bars: 50% extreme quartiles). *P*, probabilities by Kruskal–Wallis test. Significances for comparison with *EGFR*-mutant control group (c) by Dunn's post-tests. **(B)** Data are given as number of patients (*n*). Color scale indicated frequency per row. *P*, probabilities by χ^2 test. Significances for comparison with *EGFR*-mutant control group (c) by χ^2 or Fischer's exact tests. Sample sizes were *EGFR* (*n* = 86), *ERBB2* (*n* = 17), *MET* (*n* = 22), *ALK/RET/ROS1* (pooled *n* = 14), *KRAS* (*n* = 210), *BRAF* (*n* = 37), *ARHGAP35* (*n* = 13) and *NF1* (*n* = 58). **(C)** Proposed grouping of US LADC patients (6) according to driver mutation into R^{MUT}, T^{MUT} and O^{WT} molecular pathways. **(D)** Mutation rates and molecular pathway classification of 660 US LADC patients (6) and 101 LADC patients from China (7). *P*, probability by χ^2 test. Significances $P \geq 0.05$, $P < 0.05$, $P < 0.01$ and $P < 0.001$ are coded as ns, *, ** and ***, respectively.

incidence data. The identifiability problem follows from the mathematical model structure and cannot be removed by increasing statistical power (12,21). The 3SCE model applies four mathematically identifiable parameters (20). The additional parameter accounts for fluctuations in the first mutational stage at young age but typically is not identifiable in practice due to low case numbers. As a consequence, it can be shown that applying $X = Nv^2\mu \cdot age$ instead of $X = Nv\mu$ in the recursion formulae for the TSCE model, the 3SCE model is approximated with very high accuracy. Exact recursion formulas for the 3SCE model can be used to derive the hazard functions but contain additional non-identifiable parameters (22).

One- and two-path models were tested with TSCE or 3SCE in either pathway (Supplementary Table S2, available at *Carcinogenesis* Online). Exposure to smoking and radiation are assumed to change the biological

parameters in mechanistic risk models. We tested actions on the parameter *X* of initiating mutations and the net clonal expansion rate *γ* using several functional forms but did not test for effects on *δ* since *δ* affects the hazard incidence curve only at high ages. For radiation action, we chose linear, linear-quadratic and linear-exponential responses, which caused either acute or permanent parameter changes. For smoking action, we applied the same functional forms for the response to smoking intensity. The model parameters were increased at the beginning of smoking and remained elevated for current smokers until end of follow-up. Baseline values were retained when smokers ceased cigarette consumption because the implementation of residual effects in model parameters after smoking cessation did not significantly improve the fits. Here, we report only the main effects with optimal functional forms implemented
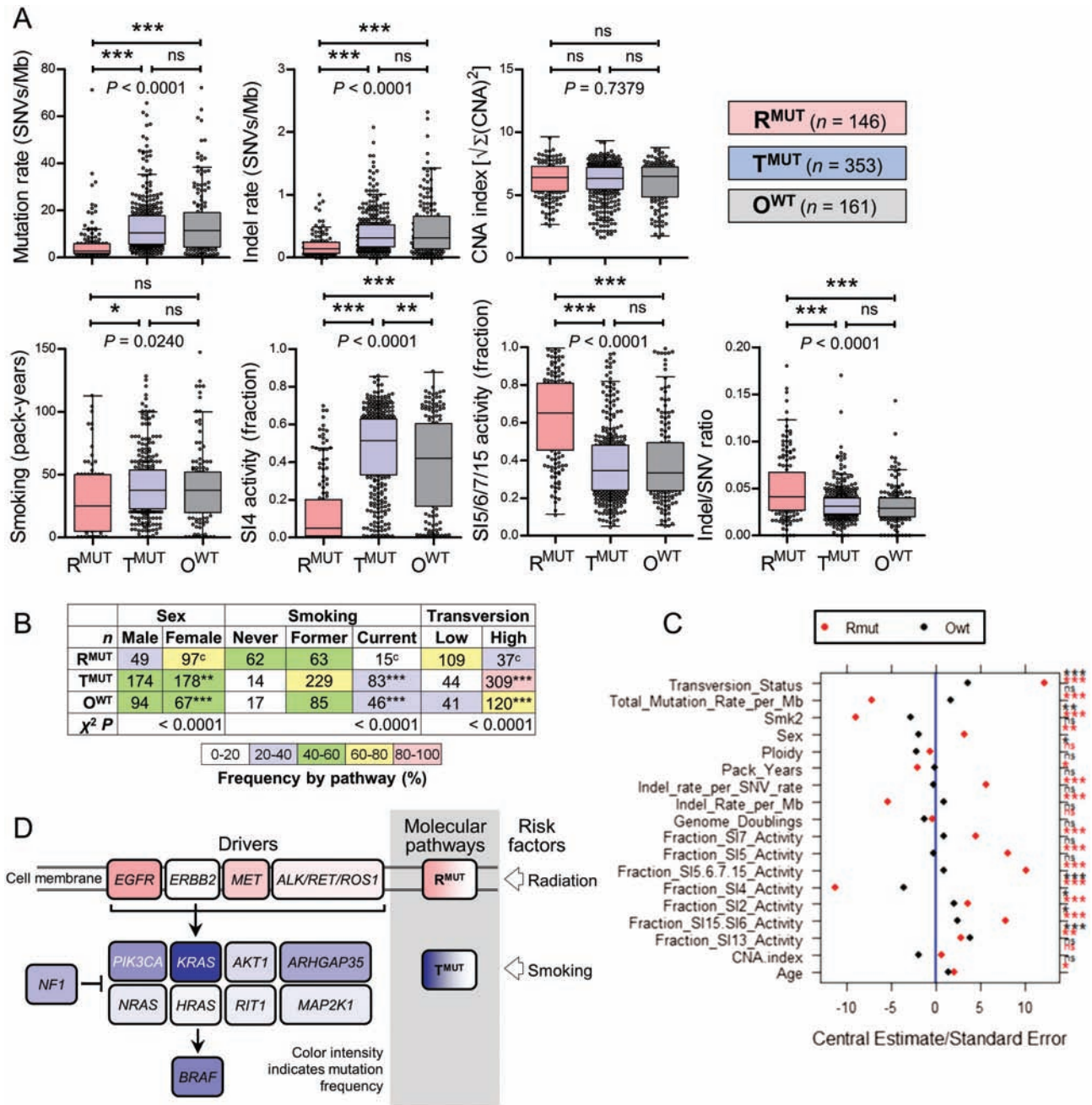
Figure 2. Clinical and molecular characteristics of 660 US LADC patients stratified by molecular pathway. SNV rates, indel rates, CNA indices, smoking exposure, sex, genomic signatures of environmental carcinogen-induced base changes in the trinucleotide context (SI), indel/SNV ratios and transversion status of 660 patients with LADC from the USA (6) grouped by R^{MUT}, T^{MUT} and O^{WT} molecular pathways. **(A)** Data are given as raw data points, median ± Tukey's whiskers (lines: median; boxes: interquartile range; bars: 50% extreme quartiles). P, probabilities by Kruskal–Wallis test. Significances are given for the indicated comparisons by Dunn's post-tests. **(B)** Data are given as number of patients (n). Color scale indicated frequency per row. P, probabilities by χ^2 test. Significances are given for the indicated comparisons by χ^2 or Fischer's exact tests. Sample sizes were EGFR (n = 86), ERBB2 (n = 17), MET (n = 22), ALK/RET/ROS1 (pooled n = 14), KRAS (n = 210), BRAF (n = 37), ARHGAP35 (n = 13) and NF1 (n = 58). **(C)** Points represent regression coefficients divided by their standard errors in univariate multinomial regression. Eighteen clinical and molecular variables of 660 US patients with LADC (6) stratified by molecular pathway were analyzed. Position on x-axis denotes deviation from the estimate in reference group T^{MUT}. Significance of deviation from the reference is color coded (red: R^{MUT}; black: O^{WT}). **(D)** Schematic of the two proposed molecular pathways to LADC and the main risk factors for each pathway. Significances $P \geq 0.05$, $P < 0.05$, $P < 0.01$ and $P < 0.001$ are coded as ns, *, ** and ***, respectively.

in the preferred model. In one pathway, smoking intensity *smkint* linearly enhances the clonal expansion rate

$$\gamma_T = \alpha_T - \beta_T (S) - \mu_T = \gamma_{T0}[1 + g_S \cdot smkint \cdot e^{-\kappa \cdot smkint}]$$

during a period of constant smoking intensity with an attenuated effect for high smoking intensity. In the other pathway, a radiation dose D linearly enhances the clonal expansion rate

$$\gamma_R = \alpha_R - \beta_R (D) - \mu_R = \gamma_{R0}[1 + g_R \cdot D]$$

after exposure for life. Adjustment for differences in the city of residence (Hiroshima or Nagasaki) and drifts in the birth cohort were performed for the mechanistic models with the same factors as in the descriptive model (see Supplementary Material, available at *Carcinogenesis* Online).

For each imputed LSS data set, model parameters were determined by Poisson regression. To limit the work load in the selection phase, candidate models were adjusted to only 10 out of 50 imputed LSS data sets. Model selection was based on goodness-of-fit measured by the cumulative Akaike's information criterion (AIC) = deviance +2 · no. of parameters for 10 data sets. Confidence intervals (CIs) were calculated by extending Rubin's rule (23). The workflow CI calculation is depicted in Supplementary Figure S1, available at *Carcinogenesis* Online.

Results

Identification of two causally and molecularly distinct pathways using molecular data

To identify possible clinical and/or molecular clusters of patients with LADC, we initially analyzed all data available from 660 Caucasian patients with LADC classified by oncogenes (6). In addition to the available clinical information, total single nucleotide variant (SNV) rates, insertion/deletion (indel) rates, copy number alteration (CNA) indices (calculated as the square root of the sum of all CNA squares of each tumor) as well as the contribution of established genomic signatures of environmental exposures were examined. These included a UV-related signature of C>T at TpCpC or CpCpC (COSMIC Signature 7, abbreviated SI7), a smoking-related signature of C>A transversions (SI4), a DNA mismatch repair (MMR) signature of C>T at GpCpG (SI15/SI6), two APOBEC-related signatures of C>G or C>T at TpCpT or TpCpA (SI13 and SI2) and a COSMIC signature 5 (SI5) with putative 'molecular clock' properties (6,24). In addition, we calculated the indel/SNV ratios, since high ratios were found elsewhere to represent a direct molecular imprint of γ-ionizing radiation (γ-IR) from molecular exposure (25).

Grouping of the 660 patients by the most frequent drivers (every driver with $n \geq 10$ patients available was examined) revealed that patients with *EGFR* ($n = 86$), *ERBB2* ($n = 17$), *MET* ($n = 22$) and *ALK/RET/ROS1* (pooled to achieve $n = 14$) mutations [hereafter collectively referred to as receptor-mutant (R^{MUT})] were different from patients with *KRAS* ($n = 210$), *BRAF* ($n = 37$), *ARHGAP35* ($n = 13$) and *NF1* ($n = 58$) mutations [hereafter collectively referred to as transducer-mutant (T^{MUT})]. To this end, R^{MUT} patients displayed lower SNV and indel rates and decreased smoking exposure evident by lower transversion rates and decreased activity of the smoking-related SI4 compared with T^{MUT} patients. At the same time, R^{MUT} patients were more frequently female and displayed increased activities of UV light-related SI7, of DNA MMR-related SI15/SI6 and of SI5 putatively reflecting molecular clock properties compared with T^{MUT} patients. Interestingly, R^{MUT} patients had higher indel/SNV ratios compared with T^{MUT} patients, indicating a molecular signature of γ-IR exposure (25). CNA indices were comparable across patients with different drivers, except from *ALK/RET/ROS1*-fused patients that collectively displayed lower CNA indices compared with all other patients (Figure 1A and B). Based on this finding, we grouped US patients (6) and 101 LADC obtained from Asian patients (7) into R^{MUT}, T^{MUT} and oncogene wild-type (O^{WT}; patient without R^{MUT} or T^{MUT}) groups, hypothesizing that these three groupings may represent distinct molecular pathways to LADC (Figure 1C).

Individual mutation prevalence varied widely between (6) and (7), translating into different frequencies of these pathways in Caucasian and Asian LADC (Figure 1D), a fact that has to be taken into account since the molecular analysis was done with American patients and the model analysis with a Japanese cohort. We next sought to compare the molecular profiles of the three candidate molecular pathways LADC to identify potential similarities and differences.

Interestingly, R^{MUT} LADC appeared distinct, whereas T^{MUT} and O^{WT} LADC were similar by all parameters examined, except SI4 activity (Figure 2A and B). This was also evident from univariate multinomial logistic regression analyses that showed a general pattern of O^{WT} LADC trending with T^{MUT} LADC (Figure 2C). In the case of R^{MUT} LADC, 13 of the 18 analyzed covariables trended different from the reference category T^{MUT} with high significance (Figure 2C). These findings indicated the existence of two distinct molecular pathways to LADC that bear different genomic marks of environmental exposures: one unique to R^{MUT} patients that features robust imprints of γ-IR and the associated DNA MMR (26) and one shared between T^{MUT} and O^{WT} patients (hereafter referred to as T^{MUT}) with genomic marks of smoking exposure (Figure 2D). Interestingly, the R^{MUT} pathway contained patients with ALK/RET/ROS1-fusions, which were recently shown to dose-dependently culminate from γ-IR in thyroid cancer (14).

Identification of two etiologically different pathways from incidence data

The preferred M_3^{LADC} was identified after multiple series of model testing which are summarized below. Models relying on only a single pathway to LADC did not provide a good description of the data with AIC values significantly higher than the preferred tw- path model M_3^{LADC} (Supplementary Table S2, available at *Carcinogenesis* Online). In single path models, interaction between smoking and radiation has been tested by multiplication of both covariables but was rejected based on goodness-of-fit. Smoking significantly increased both initiation and promotion, whereas radiation only enhanced promotion. Informed by these preliminary results, a large number of multi-stage models have been tested in pairs as candidates for preferred pathway-specific models (see Supplementary Table S2, available at *Carcinogenesis* Online). Tomasetti *et al.* (27) argue that two or three driver mutations are involved in LADC development. Thus, we considered only two- and three-stage clonal expansion models (TSCE and 3SCE, respectively) as candidates for both pathways. Whereas the TSCE model starts with one initial mutation, the 3SCE model applies two mutations in the early initiation phase.

After thinning out the set of candidate models we ended up with two almost identical two-path models in terms of goodness-of-fit (Supplementary Table S2, available at *Carcinogenesis* Online). Interestingly, for both models only one pathway turned out to be smoking dependent and the other to depend on radiation. Taking into account the results from the molecular analysis, we label the former T^{MUT} and the latter R^{MUT}. Whereas for the R^{MUT} pathway, a TSCE model yielded better fits than a 3SCE model, in the T^{MUT} pathway, an AIC-based selection of a TSCE model versus a 3SCE model was not possible for the T^{MUT} pathway. For practical reasons, the TSCE model was selected for the T^{MUT} pathway, although a 3SCE model cannot be excluded. The conceptual design of the final preferred two-path LADC model is shown in Figure 3A and the corresponding contributions of the different pathways to the hazard in Figure 3B. Supplementary Table S3, available at *Carcinogenesis* Online, lists the parameters as means over 50 data sets for both pathways. Central risk estimates were calculated with the parameters of Supplementary Table S4, available at *Carcinogenesis* Online. The preferred descriptive model formulated in Supplementary Equations (1)–(4), available at *Carcinogenesis* Online, was also fitted to all 50 imputed data sets and yielded an AIC higher by 7.4 points per data set compared with the preferred M_3^{LADC}.
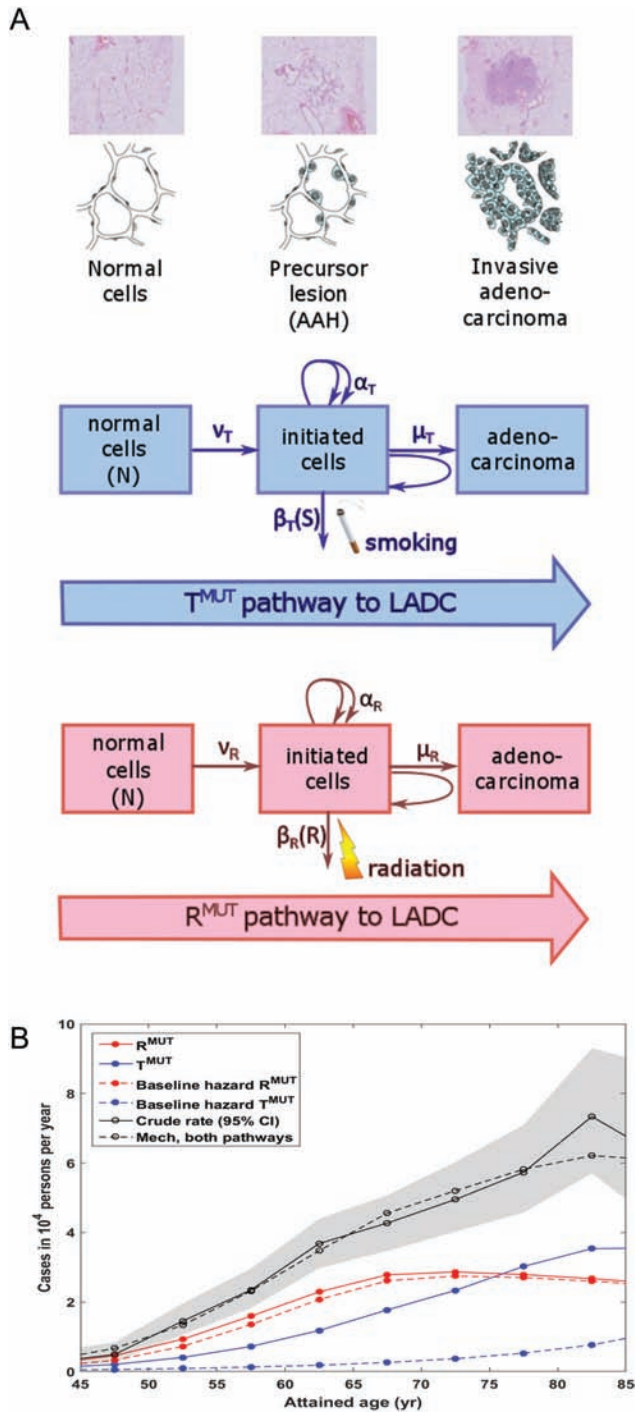
Figure 3. Molecular prediction of LADC risk stratified by molecular pathway. **(A)** Top: Histological progression from normal cells over atypical adenomatous hyperplasia as precursor lesions to invasive LADC [modified figure from Yatabe, Borczuk (40)]. Bottom: Model implementation with two distinct molecular pathways pertaining to either T^{MUT} or R^{MUT} with two versions of the TSCE model. Boxes represent cells in states with defined molecular properties. Arrows represent rates of transition between cell states. In both pathways, a tiny fraction of a large number of N healthy cells incurs early molecular changes with yearly rates ν. Initiated cells may either divide symmetrically with rates α or become inactivated with rates β. The final transformation stage summarizes a sequence of complex processes with effective rate μ. Both agents of smoking and radiation cause the acceleration of clonal expansion by reduced cell inactivation. See model details in Materials and Methods; mathematical model implementation and parameter estimates are given in Supplementary Tables S3–S5, available at

For cigarette smoking, clonal expansion in the T^{MUT} pathway was identified as the main biological target. Sex-specific response curves exhibited markedly different shapes (Supplementary Figure S2, available at *Carcinogenesis* Online). For men, the growth rate increased almost linearly up to a smoking intensity of 20 cigarettes/day and flattened thereafter. Clonal growth in women reacted much stronger to low smoking intensity. The growth reduction after a peak at about 10 cigarettes/day is biologically not plausible (Supplementary Figure S2, available at *Carcinogenesis* Online). But growth models applying a continued increase or plateau were rejected due to markedly inferior goodness-of-fit.

The main radiation effect occurred in the R^{MUT} pathway. An acute radiation pulse yielded a linear permanent increase of the net clonal expansion γ_R consistent with lifelong radiation-induced inflammation caused by genetic damage. Summarizing, the main impact of smoking and radiation took effect in distinct molecular pathways without noticeable synergy. For risk assessment, this particular biological action is better reflected in the excess absolute rate (EAR) compared with the excess relative risk (ERR). Supplementary Figure S3, available at *Carcinogenesis* Online, presents a comparison of baseline hazard rates and hazard rates between the two molecular pathways. Figures 4 and 5 depict the EAR depending on smoking and radiation for pertinent exposure scenarios. In Supplementary Figures S4 and S5, available at *Carcinogenesis* Online, the additive effect from both agents on the EAR is shown. Supplementary Figures S6 and S7, available at *Carcinogenesis* Online, give the sex-specific ERR from smoking and radiation, respectively. Figure 6 presents a pathway-specific breakdown of expected LADC cases in different exposure groups for smoking and radiation.

Discussion

LADC management and outcomes largely rely on tumor genotype (28). However, current risk models of LADC do not provide molecularly stratified risks. We used molecular data from Caucasian and Asian patients with LADC to reveal two broad molecular fingerprints of the disease probably caused by different environmental exposures: one unique to patients with mutations in transmembrane receptors (R^{MUT}) featuring imprints of radiation and another shared by patients with mutations in signal transduction genes and by patients with no known oncogene mutations (T^{MUT}) displaying the molecular signature of tobacco smoking. In addition, we have developed M_3 and have fitted it to observational data of LADC incidence in Japanese atomic bomb survivors with known radiation/smoking exposure but unknown mutation status. This analysis provided independent evidence for the existence of two pathways to LADC, of which one depends on radiation and the other on smoking. Our combined genomic and epidemiologic analyses provide the first mechanistic link between radiation exposure and receptor mutations in LADC, including EGFR mutations and ALK/RET/ROS1 fusions. Importantly, the predictive power of M_3^{LADC} can be subject to rigorous validation by future measurements of the mutation status in LADC tissue of LSS patients.

Carcinogenesis Online. **(B)** Crude rate and predicted hazard (LADC cases in 10 000 persons per year) from the preferred mechanistic model M_3^{LADC} (Mech) for the LSS cohort in 5-year age groups from 40–45 up to 80–85 years. The model clearly distinguishes pathway-specific hazards. The hazard of R^{MUT}-related LADC cases peaks at age 70 years. The hazard in the T^{MUT} pathway becomes dominant at old ages. This is a M_3^{LADC} prediction for the LSS cohort without any genomic data.
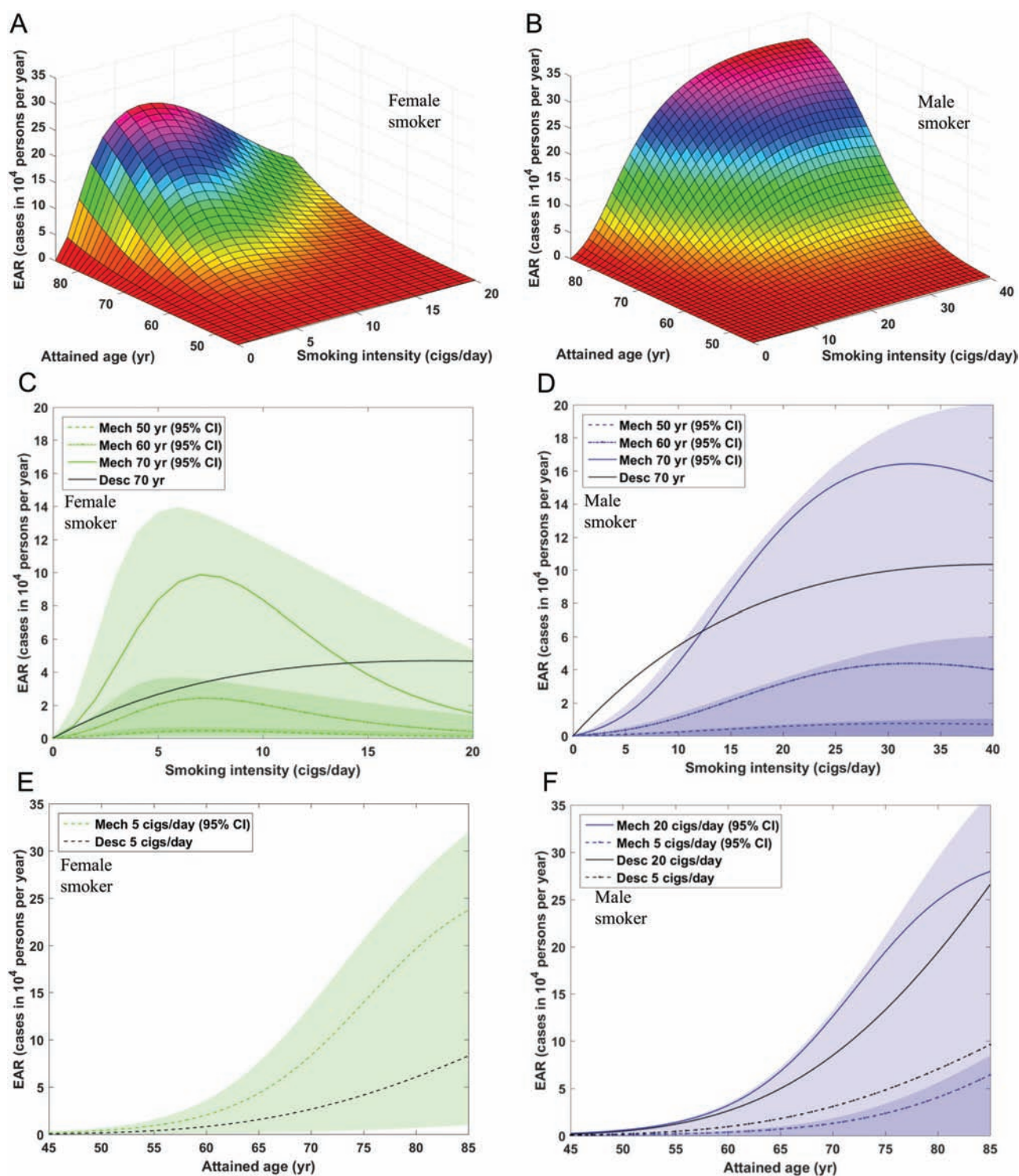
Figure 4. Excess absolute rates (EARs; as cases in 10 000 persons per year) from M_3^{LADC} (Mech) for smoking-induced lung adenocarcinoma in the Japanese LSS cohort for lifelong smokers starting at age 20 years. The EAR is determined by the sex-dependent linear-exponential response to the smoking intensity, which increases the clonal expansion rate in the T^{MUT} pathway independent of radiation (Supplementary Figure S2, top, available at *Carcinogenesis* Online). To eliminate the influence for city of residence, person-year weighted city means are used. Bivariate EAR dependence on attained age and smoking intensity for **(A)** female smokers and **(B)** male smokers. Panels **(C)** and **(D)** depict cross-sectional cuts to panels (A) and (B) for attained ages of 50, 60 and 70 years. Panels **(E)** and **(F)** depict cross-sectional cuts to panels (A) and (B) for 5 cigarettes/day (males and females) and 20 cigarettes/day (males only). Female smokers of 5 cigarettes/day and male smokers of 20 cigarettes/day possess about the same risk. The EAR from a descriptive risk model (Desc) is shown for comparison.

Midha *et al.* (29) provide a comprehensive summary of EGFR prevalence in LADC by ethnicity. In their Table 1, they report for China a prevalence of 48% (range 27–66% in 18 studies). In Japan, a prevalence of 45% (range 21–68% in 33 studies) was found. These shares are notably different from those in the USA of 23% (range 3–42% in 16 studies). The numbers for China comply with about 40% EGFR mutations found by Wu *et al.* (7), which we used to calculate R^{MUT} versus T^{MUT} shares for an Asian
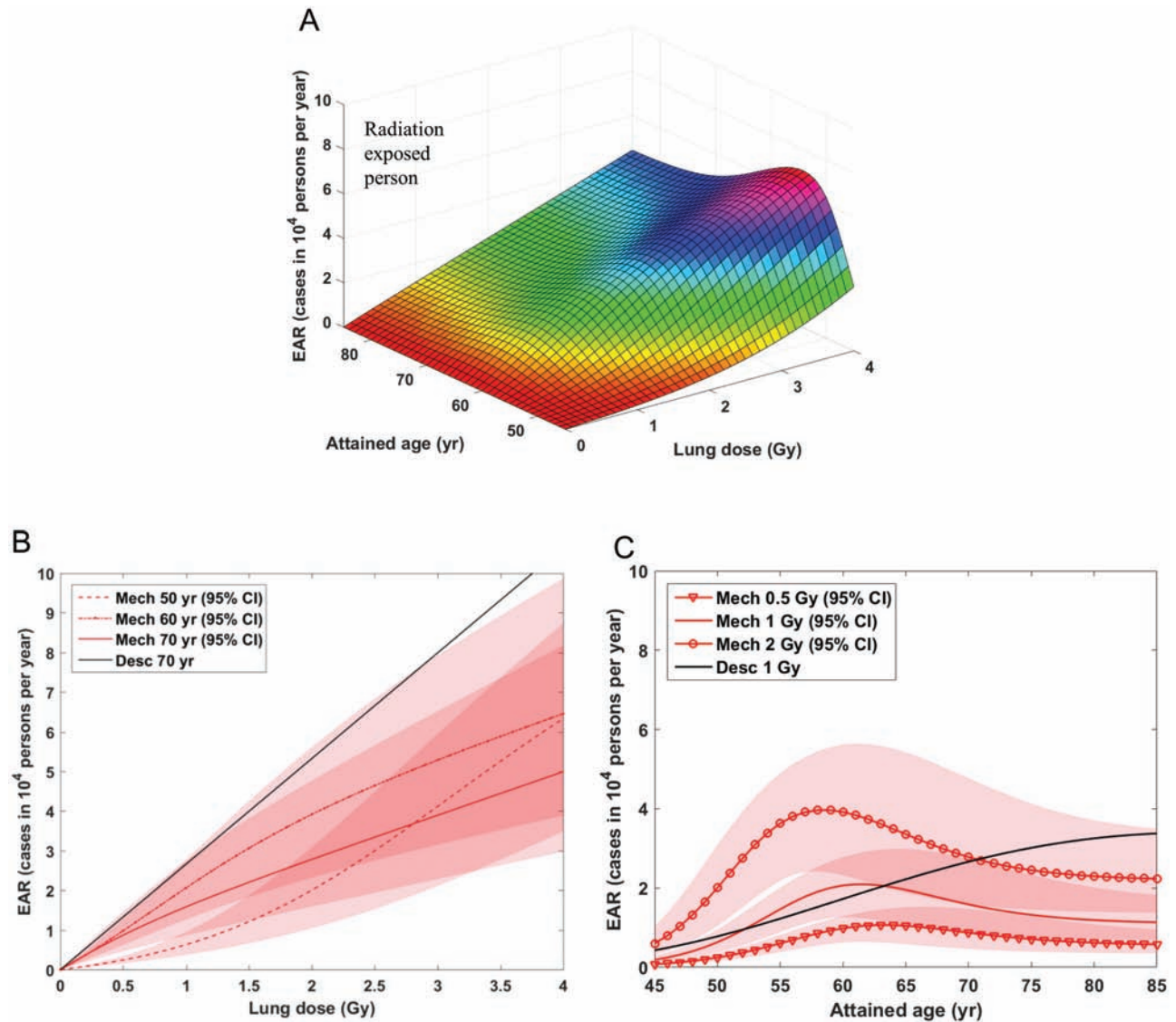
Figure 5. Excess absolute rates (EARs; as cases in 10 000 persons per year) from M_3^{LADC} (Mech) for radiation-induced lung adenocarcinoma in the Japanese LSS cohort for a person exposed at 30 years. The EAR is determined by the linear permanent response to an acute radiation pulse, which increases the clonal expansion rate in the R^{MUT} pathway independent of sex and smoking status (Supplementary Figure S2, bottom, available at *Carcinogenesis* Online). To eliminate the influence for city of residence, person-year weighted city means are used. **(A)** Bivariate EAR dependence on attained age and lung dose. The radiation risk maximizes at about 55 years for high lung dose. **(B)** Cross-sectional cuts to panel (A) for attained ages 50, 60, and 70 years. Over the dose range 0–4 Gy, the EAR responds non-linearly to a lifelong radiation-induced linear response of the clonal expansion rate in the R^{MUT} pathway. **(C)** Cross-sectional cuts to panel (A) for lung doses 0.5, 1 and 2 Gy. The radiation-induced EAR peaks at decreasing age with increasing value. The EAR from a descriptive risk model (Desc) is shown for comparison.

population. Since we performed our main molecular analysis with data from US patients, we considered it important to show the differential prevalence in an Asian (Chinese) data set, which is possibly close to Japanese prevalence in the LSS. Our LSS result for the R^{MUT} pathway predicts a share of 58% (from Figure 6). Since the majority of R^{MUT} cases would carry EGFR mutations, our prediction seems reasonable in view of the large variation in Japanese studies cited by Midha *et al.* (29).

Just like state-of-the-art epidemiological risk models, M_3^{LADC} accurately reproduced LADC incidence in the LSS, albeit with moderately improved goodness-of-fit. Our point estimate of the ERR for an unexposed male smoker starting at 20 years with one pack/day for 50 years of about 3.5 (Supplementary Figure S6, available at *Carcinogenesis* Online) is included in the 95% CI of the estimate 2.4 (1.4, 3,8) from Egawa *et al.* (11). The

difference in point estimates might be related to the use of imputed data in our study compared with including data with unknown smoking status in the study of Egawa *et al.* (11). Lubin and Caporaso (30) analyzed a European lung cancer cohort with detailed smoking information using a generalized linear model in logistic regression. In their Figure 4, the sex-independent exposure response for LADC is measured in units of ERR/pack-year and shows remarkable agreement with our results for current male smokers (Supplementary Figure S6, available at *Carcinogenesis* Online). M_3^{LADC} suggests a higher susceptibility of women to smoke, evident by the current LADC pandemic in women (1). A study of EGFR and KRAS mutations in about 3000 LADC of Caucasian patients revealed a higher susceptibility of women to smoking exposure for KRAS-mutant cancers (31). These findings are in line with a stronger increase of the

Radiation intensity (mGy)	Smoking intensity (cigs/day)	Observed cases (%)	Estimated cases (%)	R^{MUT} estimation (%)	Radiation induced estimated cases (%)	T^{MUT} estimation (%)	Smoking induced estimated cases (%)	Spontaneous estimated cases (%)
0-5	=0	**137 (21)**	**139 (22)**	**120 (19)**	**0 (0)**	**19 (3)**	**0 (0)**	**139 (22)**
5+	=0	**121 (19)**	**116 (18)**	**103 (16)**	**19 (3)**	**13 (2)**	**0 (0)**	**97 (15)**
	5-100	57 (9)	61 (9)	53 (8)	1 (0)	8 (1)	0 (0)	60 (9)
	100+	64 (10)	55 (9)	50 (8)	18 (3)	5 (1)	0 (0)	37 (6)
0-5	>0	**209 (33)**	**209 (33)**	**74 (12)**	**0 (0)**	**135 (21)**	**124 (20)**	**86 (13)**
	1-10	41 (7)	43 (7)	19 (3)	0 (0)	24 (4)	21 (3)	22 (3)
	10-20	109 (17)	105 (16)	37 (6)	0 (0)	68 (11)	63 (10)	42 (7)
	20+	59 (9)	61 (9)	18 (3)	0 (0)	43 (6)	40 (6)	21 (3)
5+	>0	**169 (27)**	**172 (27)**	**71 (11)**	**16 (3)**	**101 (16)**	**93 (14)**	**63 (10)**
	5-100	*87 (14)*	*92 (14)*	*33 (5)*	*1 (0)*	*59 (9)*	*54 (8)*	*37 (6)*
	1-10	24 (4)	20 (3)	9 (1)	0 (0)	11 (2)	9 (1)	11 (2)
	10-20	43 (7)	45 (7)	16 (3)	1 (0)	29 (4)	27 (4)	17 (3)
	20+	20 (3)	27 (4)	8 (1)	0 (0)	19 (3)	18 (3)	9 (1)
	100+	*82 (13)*	*80 (13)*	*38 (6)*	*15 (3)*	*42 (7)*	*39 (6)*	*26 (4)*
	1-10	21 (3)	18 (3)	10 (2)	3 (1)	8 (1)	9 (1)	6 (1)
	10-20	34 (6)	34 (6)	15 (2)	6 (1)	19 (4)	16 (3)	12 (2)
	20+	27 (4)	28 (4)	13 (2)	6 (1)	15 (2)	14 (2)	8 (1)
Total		**636 (100)**	**636 (100)**	**368 (58)**	**35 (6)**	**268 (42)**	**217 (34)**	**384 (60)**

Figure 6. M_3^{LADC} estimates for the breakdown of 636 LADC cases (% of 636 cases) from the LSS cohort in modeled molecular pathways R^{MUT} and T^{MUT} cross tabulated with exposure groups for smoking and radiation. Refined resolution in exposure subgroups of low (5–100 mGy) and moderate (100+ mGy) radiation dose, and light (1–10 cigarettes/day), moderate (11–20 cigarettes/day) and heavy (20+ cigarettes/day) smoking intensity is made. Female smokers fall mostly in the light category. In each subgroup, observed cases are estimated well by the model. Exposure group numbers (bold faced) add up to total numbers (bold faced) in the bottom line. Exposure subgroup numbers add up to group numbers. Note that M_3^{LADC} estimates are derived from LADC incidence data in the LSS without genotyping. Model estimations for numbers and shares of cases in each molecular pathway would be directly accessible to measurements.

smoking risk in the T^{MUT} pathway for female light smokers compared with male light smokers. Our results are concordant to the aforementioned study and can probably be explained by genetic predisposition of women to persistent smoke-induced DNA damage, notwithstanding the possibility for sex-related differences in innate immune responses to tobacco smoke and its carcinogens, as those observed in inbred strains of mice (32). However, for smoking intensities above about 10 cigarettes per day, our model predicts a decrease in risk for females. This biologically implausible trend was already observed using a state-of-the-art epidemiological risk model (11). A possible explanation might be related to reporting bias, as smoking was not socially accepted for females in Japan in former years. As a striking new feature, M_3^{LADC} clearly identified by goodness-of-fit the two molecular pathways that emerged from the molecular analysis. Importantly, the predictive power of M_3^{LADC} can be subject to rigorous validation by future measurements of the mutation status in LADC tissue of LSS patients.

In the M_3^{LADC}, radiation actions are modeled as permanently increased proliferation of pre-neoplastic lesions after acute exposure. This increased clonal expansion rate for life after a single radiation hit best explains the epidemiologic LSS data, based on goodness-of-fit. In addition, this finding is biologically plausible based on multiple recent experimental lines of evidence that indicate that radiation-induced DNA damage exerts perpetual effects by altering intracellular sensing and pro-inflammatory signaling mechanisms (33–36). To this end, it is well known that ionizing radiation causes DNA damage directly and indirectly via reactive oxygen species production (33). This DNA damage was recently shown to be perpetuated by altered splicing and by aberrant regulation of tumor suppressor gene *TP53* (33). In experimental systems where DNA damage is not caused by radiation but by mere abnormal cellular turnover,

caspase 8 was recently shown to mediate epigenetic changes that could very well lead to lifelong inflammation and liver cancer (34). Other groups have linked radiation-induced DNA damage with increased abnormal DNA pattern recognition within micronuclei, providing alternative explanations of how single radiation hits can lead to persistent inflammation (35) and have shown how targeting inflammation can prevent radiation-induced carcinogenesis in the skin (36). Hence, persistent radiation-induced inflammation can be the biological culprit for the lifelong tumor-promoting effects of a single radiation hit observed in the LSS.

Previous molecular studies underpin the biological plausibility of M_3^{LADC}. *KRAS* mutations are more common in smokers (6) and are suspected to confer resistance to radiotherapy (37), which is consistent with the lack of a radiation response in the T^{MUT} pathway in our study. Thus, the main contribution of radiation to LADC incidence is imparted via the R^{MUT} pathway and a possible contribution from the T^{MUT} pathway is too small for quantification. To date, the risk factor that drives LADC development in never smokers is unknown, whereas these patients exhibit higher frequencies of *EGFR* mutations and *EML4/ALK* fusions (3–6). Here, we show that radiation may drive disease development in these patients and provide a risk model for this molecular class of LADC. The genomic signatures of radiation and of MMR for radiation-induced DNA strand breaks were enriched in R^{MUT} tumors (24). R^{MUT} tumors also displayed elevated indel/SNV ratios, shown elsewhere to be a hallmark of secondary cancers induced by γ-IR (25). Moreover, gene fusions such as *EML4/ALK*, *KIF5B/RET* and *CD74/ROS1*, included here in the R^{MUT} pathway, have been linked with radiation in other cancers (14,26). These observations correspond to the radiation response of the R^{MUT} pathway as the most relevant

radiation effect proposed by M_3^{LADC}. Hence, we link for the first time radiation exposure to a molecular subset of LADC using molecular and epidemiologic evidence.

Smoking is linked with *KRAS*-mutant LADC and US patient analysis showed enhanced mutation rates in ever smokers of the T^{MUT} pathway ([6]). This observation should generate an increase of initiating mutations in smokers and was found significant in a one-path model (Supplementary Table S2, available at *Carcinogenesis* Online). However, M_3^{LADC} works without such a plausible smoking effect because improvement in goodness-of-fit was not increased compared with exclusive smoking action on clonal expansion. This result might be caused by insufficient statistical power. Hence, the main biological mechanism of smoking on LADC incidence is associated with enhanced clonal growth as already observed in ([20]) and ([38]). Initiated cells exhibit a growth advantage over healthy cells due to reduced cell death possibly caused by smoking-associated chronic inflammation. Hence our data build on the known linkage between smoking and *KRAS*-mutant LADC by expanding this link to T^{MUT} and O^{WT} LADC and by pinning the effects of smoke in time: at early time-points of smoking exposure. These results are relevant and important for the design of future chemoprevention strategies aimed to halt disease progression in smokers.

Prediction models, which are informed by adequate bioassays in addition to epidemiological variables, can forecast lung cancer occurrence with high accuracy ([39]). They do lack, however, a link between environmental agents and molecular risk stratification, which is provided by M_3^{LADC}. This link suggests no interactively increased LADC risk for heavy smokers in computerized tomography screening. It can be exploited in retrospective assessment to pin down the agent causing LADC based on the molecular profile of diseased tissue, which is highly relevant e.g. for compensation claims in the nuclear industry.

In conclusion, our study answers a longstanding question on the biological origins of age-risk patterns for LADC from concomitant exposure to smoking and radiation. To describe such patterns, standard epidemiological models must inevitably rely on a vague implementation of synergistic effects, which are commonly couched in mathematical terms as either 'additive' or 'multiplicative' sometimes with further generalizations ([9–11]). We have shown here by projecting signatures of environmental exposure into epidemiological cohorts that smoking and radiation drive the development of LADC along different molecular pathways with negligible interaction for doses below 4 Gy. The M_3^{LADC} approach provides a powerful tool for harnessing molecular data to improve studies of risk assessment and prediction in radiation protection and clinical applications. Our approach is of clinical relevance because we solidify cause–effect relationships in LADC development by integrating molecular and epidemiologic data. The cause of LADC can be inferred from their molecular alterations and the share of LADC with specific alterations can be predicted using the M_3^{LADC} model with possibly huge medical and socioeconomic implications'

Supplementary material

Supplementary data are available at *Carcinogenesis* online.

Funding

Acknowledgements

References

1. Fitzmaurice, C. *et al.*; Global Burden of Disease Cancer C (2017) Global, regional, and national cancer incidence, mortality, years of life lost, years lived with disability, and disability-adjusted life-years for 32 Cancer Groups, 1990 to 2015: a systematic analysis for the global burden of disease study. JAMA Oncol., 3, 524–548.
2. Torre, L.A. *et al.* (2015) Global cancer statistics, 2012. CA Cancer J. Clin., 65, 87–108.
3. Hecht, S.S. (1999) Tobacco smoke carcinogens and lung cancer. J. Natl. Cancer Inst., 91, 1194–1210.
4. Alberg, A.J. *et al.* (2013) Epidemiology of lung cancer: Diagnosis and management of lung cancer, 3rd ed: American College of Chest Physicians evidence-based clinical practice guidelines. Chest, 143(5 suppl.), e1S–e29S.
5. Sun, S. *et al.* (2007) Lung cancer in never smokers–a different disease. Nat. Rev. Cancer, 7, 778–790.
6. Campbell, J.D. *et al.*; Cancer Genome Atlas Research Network (2016) Distinct patterns of somatic genome alterations in lung adenocarcinomas and squamous cell carcinomas. Nat. Genet., 48, 607–616.
7. Wu, K. *et al.* (2015) Frequent alterations in cytoskeleton remodelling genes in primary and metastatic lung adenocarcinomas. Nat. Commun., 6, 10131.
8. United Nations Scientific Committee on the Effects of Atomic Radiation (2012) *Sources and Effects of Ionizing Radiation.* UNSCEAR 2012 Report. UNSCEAR.
9. Furukawa, K. *et al.* (2010) Radiation and smoking effects on lung cancer incidence among atomic bomb survivors. *Radiat. Res.*, 174, 72–82.
10. Cahoon, E.K. *et al.* (2017) Lung, laryngeal and other respiratory cancer incidence among Japanese atomic bomb survivors: an updated analysis from 1958 through 2009. Radiat. Res., 187, 538–548.
11. Egawa, H. *et al.* (2012) Radiation and smoking effects on lung cancer incidence by histological types among atomic bomb survivors. Radiat. Res., 178, 191–201.
12. Kaiser, J.C. *et al.* (2014) Genomic instability and radiation risk in molecular pathways to colon cancer. PLoS One, 9, e111024.
13. Kaiser, J.C. *et al.* (2016) Integration of a radiation biomarker into modeling of thyroid carcinogenesis and post-Chernobyl risk assessment. Carcinogenesis, 37, 1152–1160.
14. Efanov, A.A. *et al.* (2018) Investigation of the relationship between radiation dose and gene mutations and fusions in post-Chernobyl thyroid cancer. J. Natl. Cancer Inst., 110, 371–378.
15. Ruhm, W. *et al.* (2017) Biologically-based mechanistic models of radiation-related carcinogenesis applied to epidemiological data. Int. J. Radiat. Biol., 93, 1–25.
16. Ozasa, K. *et al.* (2012) Studies of the mortality of atomic bomb survivors, Report 14, 1950–2003: an overview of cancer and noncancer diseases. Radiat. Res., 177, 229–243.
17. Furukawa, K. *et al.* (2017) Handling incomplete smoking history data in survival analysis. Stat. Methods Med. Res., 26, 707–723.
18. Luebeck, E.G. *et al.* (2013) Impact of tumor progression on cancer incidence curves. Cancer Res., 73, 1086–1096.
19. Feller, W. (1968) An Introduction to Probability Theory and Its Applications. Wiley, New York, NY.
20. Meza, R. *et al.* (2008) Age-specific incidence of cancer: phases, transitions, and biological implications. Proc. Natl. Acad. Sci. USA, 105, 16284–16289.

21. Little, M.P. *et al*. (2010) Parameter identifiability and redundancy: theoretical considerations. PLoS One, 5, e8915.
22. Luebeck, E.G. *et al*. (2008) Does folic acid supplementation prevent or promote colorectal cancer? Results from model-based predictions. Cancer Epidemiol. Biomarkers Prev., 17, 1360–1367.
23. Marshall, A. *et al*. (2009) Combining estimates of interest in prognostic modelling studies after multiple imputation: current practice and guidelines. BMC Med. Res. Methodol., 9, 57.
24. Alexandrov, L.B. *et al*.; Australian Pancreatic Cancer Genome Initiative; ICGC Breast Cancer Consortium; ICGC MMML-Seq Consortium; ICGC PedBrain (2013) Signatures of mutational processes in human cancer. Nature, 500, 415–421.
25. Behjati, S. *et al*.; ICGC Prostate Group (2016) Mutational signatures of ionizing radiation in second malignancies. Nat. Commun., 7, 12605.
26. Seki, Y. *et al*. (2015) Molecular process producing oncogene fusion in lung cancer cells by illegitimate repair of DNA double-strand breaks. Biomolecules, 5, 2464–2476.
27. Tomasetti, C. *et al*. (2015) Only three driver gene mutations are required for the development of lung and colorectal cancers. Proc. Natl. Acad. Sci. USA, 112, 118–123.
28. Reck, M. *et al*. (2013) Management of non-small-cell lung cancer: recent developments. Lancet, 382, 709–719.
29. Midha, A. *et al*. (2015) EGFR mutation incidence in non-small-cell lung cancer of adenocarcinoma histology: a systematic review and global map by ethnicity (mutMapII). Am. J. Cancer Res., 5, 2892–2911.
30. Lubin, J.H. *et al*. (2006) Cigarette smoking and lung cancer: modeling total exposure and intensity. Cancer Epidemiol. Biomarkers Prev., 15, 517–523.
31. Dogan, S. *et al*. (2012) Molecular epidemiology of EGFR and KRAS mutations in 3,026 lung adenocarcinomas: higher susceptibility of women to smoking-related KRAS-mutant cancers. Clin. Cancer Res., 18, 6169–6177.
32. Stathopoulos, G.T. *et al*. (2007) Epithelial NF-kappaB activation promotes urethane-induced lung carcinogenesis. Proc. Natl. Acad. Sci. USA, 104, 18514–18519.
33. Chen, J. *et al*. (2017) Identification of a DNA damage-induced alternative splicing pathway that regulates p53 and cellular senescence markers. Cancer Discov., 7, 766–781.
34. Boege, Y. *et al*. (2017) A dual role of caspase-8 in triggering and sensing proliferation-associated DNA damage, a key determinant of liver cancer development. Cancer Cell, 32, 342–359.e10.
35. Harding, S.M. *et al*. (2017) Mitotic progression following DNA damage enables pattern recognition within micronuclei. Nature, 548, 466–470.
36. Rigby, C.M. *et al*. (2017) Role of p53 in silibinin-mediated inhibition of ultraviolet B radiation-induced DNA damage, inflammation and skin carcinogenesis. Carcinogenesis, 38, 40–50.
37. Wang, M. *et al*. (2014) EGFR-mediated chromatin condensation protects KRAS-mutant cancer cells against ionizing radiation. Cancer Res., 74, 2825–2834.
38. Schöllnberger, H. *et al*. (2006) Analysis of epidemiological cohort data on smoking effects and lung cancer with a multi-stage cancer model. Carcinogenesis, 27, 1432–1444.
39. El-Zein, R.A. *et al*. (2006) Cytokinesis-blocked micronucleus assay as a novel biomarker for lung cancer risk. Cancer Res., 66, 6449–6456.
40. Yatabe, Y. *et al*. (2011) Do all lung adenocarcinomas follow a stepwise progression? Lung Cancer, 74, 7–11.

$$\mathit{IV}$$

Acknowledgments

I would like to begin the acknowledgment section by expressing my gratitude to my supervisors: Professors Michael Hoelscher, Katja Radon, and Helmut Küchenhoff. Without your guidance and support, I would not be here, writing down these words. My collaboration with Michael started in early 2020, and since then, we worked on many topics. I extend my deepest thanks for your mentorship. One of the most valuable ways of thinking I have learned from you is the art of being a visionary and to brighter horizons, and even conceiving plans for what may appear nearly impossible. Additionally, I am grateful for the support and opportunities you have provided within the department(s). Simultaneously, my work with Katja has been also important. She has consistently encouraged me to forge my own path without overthinking. I am thankful for the support you have extended, especially as a woman in the field of science. This perspective is also driving me. Helmut served as my "Doktorvater" during my doctoral studies. Since 2015, we have collaborated, and I owe a significant part of who I am as a scientist to his contributions. I appreciate the considerable time and effort you devoted to me. Your support, even post-doctorate, means a great deal to me.

I would also like to express my gratitude to PD Dr. Andreas Wieser. Our collaborative projects have been invaluable, and I appreciate your willingness to occasionally venture into uncharted territory. This has been an interesting asset.

Dr. Abhishek Bakuli, putting my appreciation into words is a challenge. You stand as one of the finest colleagues I have had the privilege to work alongside. With you, open conversations about work were always possible. Our friendship, which now extends beyond the confines of work, is really meaningful to me. Thank you for remaining a part of my journey, even beyond our professional association.

PD Dr. Elmar Saathoff, thank you for your counsel and the professional knowledge I have gained from you.

Prof Dr. Christina Kuttler, you played a pivotal role in my growth throughout my university journey. We have traversed the research path together, and I sincerely hope this continues in the future.

The initial phase of my research career took place at the Helmholtz Center Munich, specifically at the Institute for Radiation Medicine. I extend my thanks to the entire group, with special appreciation for those who are now at the "Bundesamt für Strahlenschutz." Dr. Christian Kaiser, you laid the foundation for my research, and I thank you for the wealth of knowledge I gained. Thank you for everything!

I would like to extend my gratitude to the entire "Abteilung für Infektions- und Tropenmedizin." The data analysis group has collaborated seamlessly with every team, and I appreciate the support and research opportunities provided here. A special acknowledgment goes to the data analysis group; your support empowers me and keeps me motivated, and I genuinely feel it. THANK YOU.

However, the most profound thanks belong to my husband, Klemens, and my family. They are my pillars of support, my anchors of strength, and the source of my energy and stability. Their love sustains me. For this, I will now express my gratitude in our mother language.

"Caro Klemens, un grazie non basta per tutto quello che sei per me. Ogni giorno sentirti le mie storie, ogni giorno arrivo a casa in ritardo. Ti ringrazio per la pazienza, per il tempo che mi dedichi, per la forza che mi dai. Grazie per il coraggio che mi dimostri nelle scelte. Parte di questo lavoro è dedicato a te

non solo per il posto che hai nella nostra vita, ma anche perché è merito tuo che io ci sia arrivata. Grazie.

Cara famiglia, sono di nuovo qua a scrivere testi scientifici, perché è il mio lavoro e anche gran parte della mia vita. Questa volta voglio ringraziarvi per tutto il supporto che mi date. Cari mamma e papá, mi sostenete sempre, anche da distante. Vi voglio un sacco di bene e vi ringrazio per la famiglia che tenete insieme. Cara sorella, piú diverse non potevamo essere, ma questo ci arricchisce. Grazie per farmi ricordare ogni giorno che la vita è anche altro di quello che faccio. Grazie per la tua pazienza. Cara nonna, la saggezza di determinate decisioni viene da tuo consiglio, grazie per avere sempre un occhio su di me. Piccolo Edo, ormai non piú tanto piccolo… Sei una bomba c'è poco da dire! Di energie e di emozioni. Grazie per ricordarmi ogni giorno del bambino che c'è in me, è una parte fondamentale del mio modo di essere. Un abbraccio a tutti!"